Archvied in Dspace@nitr

Interaction of Flow and Estimation of Discharge in two Stage Meandering Compound Channels

A

Thesis

Submitted to

The Department of Civil Engineering

National Institute of Technology

Rourkela, India

In Partial Fulfillment of the Requirements for the Degree

Doctor of Philosophy in Civil Engineering

K.K. Khatua

October 2007

Declaration

I hereby declare that this submission is my own work and that, to the best of my knowledge and belief, it contains no material previously published or written by another person nor material which to a substantial extent has been accepted for the award of any other degree or diploma of the university or other institute of higher learning, except where due acknowledgement has been made in the text.

(K.K. Khatua)

Date: October 17, 2007

Certificate

This is to certify that the thesis entitled "Interaction of Flow and Estimation of Discharge in Two Stage Meandering Compound Channels" being submitted by Shri Kishanjit Kumar Khatua is a bonafide research carried out by him at Civil Engineering Department, National Institute of Technology, Rourkela, India, under my guidance and supervision. The work incorporated in this thesis has not been, to the best of our knowledge, submitted to any other University or Institute for the award of any degree or diploma.

Prof. K.C. Patra
(Supervisor)

Date: October 17, 2007

Acknowledgements

Dated: 17.10.2007   **(**K.K. Khatua**)**

ABSTRACT

Reliable estimates of discharge capacity are essential for the design, operation, and maintenance of open channels, more importantly for the prediction of flood, water level management, and flood protection measures. In nature, most rivers tend to be of compound sections as well as meandering. For the management of rivers and floodplains, it is important to understand the behavior of flows within compound channels. Cross sections of these compound channels are generally characterized by deep main channel bounded by relatively shallow flood plains at one or both sides. At low depths when the flow is only in the main channel, conventional methods are generally used to assess discharge capacity. When the flow goes over bank, the classical single channel formula gives large error between the estimated and the observed discharge. Standard sub-division and composite roughness methods given in Chow (1959) are essentially flawed when applied to compound channels. The discharge calculation for compound channel is based mainly on refined one dimensional methods of analysis. However, two dimensional (2D) approaches (Shiono & Knight, 1988; Knights & Shiono1996; Knights & Abril1996) and three dimensional analysis (Shiono & Lin 1992; Younis 1996) are more complex and inconvenient to use in practice. The basic idea of one dimensional approach is to subdivide the channel into a number of discrete sub areas, usually the main channel and adjacent flood plains. Discharge for each part is calculated with or without consideration of interaction effect and sum them, possibly with some adjustment to give the total channel discharge. Review of the literature show that investigators propose alternative interface planes to calculate the total discharge carried by a compound channel section. Either including or excluding the interface length with the wetted perimeter does not make sufficient allowance for discharge calculation for all depths of flow over floodplain. It either overestimates or underestimates the discharge result. Investigation is made on the methods for predicting discharge in straight and meandering compound channels. Finally a comparison is made between the different discharge approaches.

Experiments are carried out using new flumes with fabrication of three rigid compound channels: one straight and the other two meandering, in the Fluid Mechanics and Hydraulics Laboratory of the Civil Engineering Department at the National Institute of Technology, Rourkela. All together, 75 series of experimental observations on stage–discharge relationships are made of which, 21 for straight

channels, 27 for mildly meandering channels, and the rest 27 for highly meandering channels. Out of this, detailed velocity and turbulence data are observed for 29 runs of which, 5 for straight compound, 12 for mildly meandering, and the rest 12 for highly meandering simple/compound channels. For each runs, detailed measurements of three-Dimensional velocities are made at one location for straight channels and at two locations (at bend apex and another at geometrical cross over) in the meander path. Using a micro-ADV (Acoustic Doppler Velocity-meter) of 16 MHz, accurate three dimensional point velocities at the defined grid points of the channels are recorded for every run. For each run, the boundary shear distribution along the wetted perimeter of the cross section of the channel is obtained at the defined test section for straight compound channel and at the bend apex test section of the two meandering compound channels for both in-bank and over-bank conditions. The velocity distributions in tangential, radial, and vertical direction are plotted using data from micro- ADV.

With altering its distributional shapes, compound channel flow causes decrease in main channel shear and corresponding increase in the flood plain shear. The reduction of main channel shear is due to the presence of the interaction mechanism that can be explained by the fact that the main channel is loosing energy to its floodplains. The percentage of decrease of main channel shear reduces as the depth of flow over floodplain increases. In the present investigation, boundary shear stress distribution across the periphery is assessed and the results are used to calculate the apparent shear force on the assumed interfaces of separation of compound section to sub-areas. An empirically derived equation relating the geometry parameters and the boundary shear percentages on the floodplain and main channel wetted perimeters of compound channels having high width ratio and high sinuosity are presented. Momentum transfer between main channel and floodplain is quantified in terms of the length of interface and the model results are compared with the experimental results. Basing on the model out put, merits of selection of interface plains for discharge estimation using the divided channel approach is decided.

Four alternative uses of the traditional vertical as well as horizontal interface planes of separation of compound channels are proposed. Investigation is made for the energy losses resulting from the compound response of boundary friction, secondary flow, turbulence, expansions and contractions in straight and meandering channels with over bank flow conditions. Due to flow interaction between the main channel and floodplain, the flow in a compound section consumes more energy than a channel with simple section carrying the same flow and having the same type of

channel surface. The energy loss is manifested in the form of variation of resistance coefficients of the channel with depth of flow. Distribution of energy in compound channel is an important aspect, and is addressed adequately by incorporating the variation of the Manning's roughness coefficient n, Chezy's C, and Darcy – Weisbach's friction factor f and the parameter $\sqrt{S}/n$ with depths of flow ranging from in-bank to the over-bank flow. Stage-discharge curves, channel resistance coefficients, composite Manning's n of straight and meandering compound channels are presented for the present experimental series.

Flow distribution between the sub-sections of a meandering compound channel becomes more complicated due to interaction mechanism as well as with sinuosity. The proposed models predict well the percentage of flow carried by main channel, lower main channel and flood plain. The proposed approaches for discharge prediction in compound channels have also been tested using the experimental data collected from channels at IIT Kharagpur (Patra & Kar,1999), Straight Channels (Knight & Demetriou, 1983), higher sinus channels (Willet & Hard Wick (1993) and the large scale channel of FCF at Wallingford, UK. The models compares well with the reported data of these investigators. Some suggestions for future studies are included at the end of the thesis.

Key Words:

Meander channel, Straight channel, Compound channel, Boundary shear, Energy loss, Apparent shear, Momentum transfer, Discharge estimation, Interface plains, Stage-discharge relationship, Divided channel method, Roughness coefficient, Interface plane, Over-bank flow, In-bank flow Velocity distribution, Flow distribution.

Table of Contents

List of Tables

List of Figures and Photographs

List of Symbols

A_{lmc}	Area of lower main channel
ASSR	Apparent Shear Stress Ratio
A_{mv}	Area of main channel by a vertical interface
A_{fv}	Area of floodplain subsection by a vertical interface
A_i	sub-area
A_*	$N_{fp}A_{fp}/A_{mc}$
ΔA	area that is required to be added to the floodplain area and subtracted from the main channel area
A	Total cross-sectional area of compound channel
AM	*Area* method
A'	One amplitude of a meander channel
A_{mc}	Area of main channel using vertical interface
A_{fp}	Area of floodplain using vertical interface
$(\%A_{mc})$	% of area of main channel using vertical interface
$(\%A_{fp})$	% of area of floodplain using vertical interface
ASF_{IP}	Apparent shear at the interface
%ASF	Percentage of total channel shear force carried by assumed interface planes
$\%ASF_H$	*ASF* on horizontal interface (*od*) as percentage of total shear force
$\%ASF_{ip}$	*ASF* on an interface plane as percentage of total shear force
$\%ASF_V$	*ASF* on vertical interface (*oq*) as percentage of total shear force
$\%ASF_D$	*ASF* on diagonal interface (*oc*) as percentage of total shear force
$\%ASF_{VI}$	*ASF* on variable-inclined interface (aa$_3$) as percentage of total shear force
ADV	Accostic Doppler Velocity Meter
b	Bottom width of main channel
B_w	Width of the meander belt
ENU	East, North and Upward
b'	Top width of main channel
b_1, b_2	Lengths of flood plain bed at left and right sides measured from vertical interface respectively

17

B	Over all width of compound channel
c	Energy loss coefficients based on friction factor
C	Chezy's channel coefficient
C'	A constant given as $= X_{fp} / X_{mc}$
C_x	Factor representing the length of interface $(H-h)$ times that is to be added to the main channel perimeter only from VDM-II
C_{mc}	$[X_{mcv}/(H-h)]$ =Interaction length factors for main channel in VDM-III
C_{fp}	$[X_{fpv}/(H-h)]$ = Interaction length factors for floodplain in VDM-III
C'_{mc}	Interaction length factors for main channel in VDM-IV
C'_{fp}	Interaction length factors for floodplain in VDM-IV
COHM	Coherence Method
COH	Coherence
C_{wd}	Shape coefficient for expansion and contraction losses
C_{sse}	Side slope coefficient for expansion loss
C_{ssc}	Side slope coefficient for contraction loss
C_{sl}	Length coefficient for expansion and contraction losses
DISADF	Discharge adjustment factor
DCM	Divided Channel Method
DDM	Diagonal Division Method
Dee	Diagonal Division Method
d	Depth of flow over floodplain $= (H-h)$
Hee	(HDM-1)
Hie	(HDM-1I)
δ	Aspect ratio of the main channel b/h
(f_{mc})	Resistance coefficient of main channel sub-area
(f_{fp})	Resistance coefficient of floodplain sub-area
F_1, F_2 and F_3	Dependant function of $\%Q_{mc}$ with relative depth, width ratio and sinuosity respectively
F'_1, F'_2 and F'_3	Dependant function of $\%Q_{lmc}$ with relative depth, width ratio and sinuosity respectively
f	Friction factor
F_1	Factor for non friction loss due to main channel geometry
F_2	Factor for non friction loss due to main channel sinuosity
f_*	$N_{fp} f_{fp} / f_{mc}$
f_c	Friction factors of main channel

f_f	Friction factors of floodplain
F_m	Flow resistance in the main channel due to momentum transfer and other factors
g	Acceleration due to gravity
h	Height of main channel up to floodplain bed
h_0	Distance from the channel bottom at which logarithmic law indicates zero velocity
h'	In bank depth
H	Total depth of flow in compound channel
HDM	Horizontal Division Method
Jm	James & Wark method
k	Von Karmans constant;
k_{bf}	Dimensionless energy coefficients in (m^{-1}) due to boundary friction
k_{sf}	Dimensionless energy coefficients in (m^{-1}) due to secondary flow
k_{ex}	Dimensionless energy coefficients in (m^{-1}) due to expansion
k_{co}	Dimensionless energy coefficients in (m^{-1}) due to contraction
m	A exponent
M	Slope of the semi-log plot of velocity distributions
μ	Dynamic viscosity of water
N_r	Reynolds number ratio $(N_r = N_{fp} / N_{mc})$
N_{mc}	Reynolds's number of main channel sub-sections
N_{fp}	Reynolds's number of flood plain sub-sections
N	Reynolds's number of compound section
n	Manning's resistive coefficient
n_{mc}	Manning's roughness factor for main channel
n_{fp}	Manning's roughness factor for floodplain
N_f	Number of floodplains
n	Manning's roughness factor
P_i	Wetted perimeter of each sub-area
P_c	Wetted perimeter of floodplain subsections
P_f	Wetted perimeter of main channel subsections
P_*	$N_f P_f / P_c$
P	Wetted perimeter of the compound channel section
P_{mc}	Wetted perimeter of the main channel

P_{fp}	Wetted perimeter of the floodplain
θ	Angle of interface making an angle with vertical line at junction
(r_C)	Least centerline radius of curvature to its depth
R	Hydraulic radius of the channel cross section
R	Hydraulic mean radius of the channel cross section (A/P)
R	Ratio of the amplitude of e meandering channel to the top width B of compound section
ρ	Density of flowing liquid
R_{mc}	Hydraulic radius of main channel sub-sections
R_{fp}	Hydraulic radius of flood plain sub-sections
SCM	Single Channel Method
S	Channel slope
(τ)	Apparent shear stress in N/m^{2}given by Prinos and Town send (1984) equation
τ_{mc}	Mean boundary shear stress in main channel per its unit length
τ	Boundary shear stress
τ_{fp}	Mean boundary shear stress in floodplain per its unit length
$\int_{mc} \tau dp$	Shear force on surfaces of main channel
u	Shear velocity
u_1, u_2	Time averaged velocities measured at h'_1 and h'_2 heights respectively from boundary
X_{mc}	Interface length for inclusion in the main channel wetted perimeter
X_{fp}	Length of interface to be subtracted from the wetted perimeter of floodplain
$X_{m\theta}$	Interface length for inclusion in the main channel wetted perimeter for an interface at an angle θ with the vertical line at junction
$X_{f\theta}$	Interface length for subtraction from floodplain perimeter for an interface at an angle θ with the vertical line at junction
$Q_1\ Q_2,\ Q_3,\ Q_4$	Flow discharge in the zone-1, zone-2, zone-3, and zone-4 respectively
Q_{basic}	'Basic' discharge
Q_{single}	Discharge estimated by single channel method
Q_{actual}	Actual discharge
$\%Q_{lmc}$	Percentages of flow carried by the lower main channel
$\%Q_{mc}$	Percentages of discharge carried by the main channel

V_{mc} and V_{fp}	Mean velocities of main channel and flood plain sub areas respectively
VDM	Vertical Division Method
ZASIM	Zero Apparent Shear Interface Method
Vee	*(VDM-1)*
Vie	*(VDM-1I)*
Mv^*, Mv	Proposed Vertical method (VDM-III*)
Mh^*, Mh	Proposed horizontal method (HDM-III)
Ma^*, Ma	Proposed area method
*	Represents the methods tested by bank-full Manning's *n* for meandering compound channels only
P_{mcv}	Modified main channel wetted perimeter using vertical subdivisions
P_{mcv}, P_{fpv}	Modified floodplain wetted perimeter using vertical subdivisions
VI	Variable Inclined plain method
Em	Ervine & Ellis method, Mb-Meander belt method
X_{mcv}	Length of vertical interface to be included to the wetted perimeter of main channel sub-area
X_{fpv}	Length of vertical interface to be deducted from the wetted perimeter of floodplain sub-section
τ_v	Apparent shear stress on vertical interface
τ_r	Relative apparent shear stress and is given by Prinos-Townsend empirical formula
ΔV	difference of mean velocity between main channel and floodplain
R_o	Ratio of the amplitude ε of the meandering channel to its top width B
ε	Amplitude of the meandering channel
V_a	sectional mean velocity of this zone
V_x, V_y and V_z	Longitudinal, radial and vertical directions respectively
V_a	Sectional mean velocity of this zone
S_o	Valley slope
r_c	Bend radius
V_b	Sectional mean velocity of this zone
L_w	One wave length of the meander channel
θ '	Mean angle of incidence averaged over the meander wave length calculated from numerical integration
K_c	Given by a third order polynomial fit obtained from the Yen and Yen (1983) data

Q_{bf}	the bank full discharge calculated using in bank method
m	Energy loss coefficients based on geometry
K	Energy loss coefficients based on sinuosity
L	Meander wave length
W_2	Width of zone 2
K_e	Factor for expansion and contraction loss in zone 2
S_s	Cotangent of main channel side slope
K_c	Contraction factor
P_i	Wetted perimeter of each sub-area
$(\%S_{fp})$	Shear force percentages carried by the floodplain perimeter
$(\%S_{mc})$	Shear force percentages carried by the main channel perimeter
S_r	Sinuosity (length along channel center/ straight Valley length)
WSD	West, South and Down ward

List of Symbols

A_{lmc}	Area of lower main channel
ASSR	Apparent Shear Stress Ratio
A_{mv}	Area of main channel by a vertical interface
A_{fv}	Area of floodplain subsection by a vertical interface
A_i	sub-area
A_*	$N_{fp}A_{fp}/A_{mc}$
ΔA	area that is required to be added to the floodplain area and subtracted from the main channel area
A	Total cross-sectional area of compound channel
AM	*Area* method
A'	One amplitude of a meander channel
A_{mc}	Area of main channel using vertical interface
A_{fp}	Area of floodplain using vertical interface
$(\%A_{mc})$	% of area of main channel using vertical interface
$(\%A_{fp})$	% of area of floodplain using vertical interface
ASF_{IP}	Apparent shear at the interface
%ASF	Percentage of total channel shear force carried by assumed interface planes
$\%ASF_H$	*ASF* on horizontal interface (*od*) as percentage of total shear force
$\%ASF_{ip}$	*ASF* on an interface plane as percentage of total shear force
$\%ASF_V$	*ASF* on vertical interface (*oq*) as percentage of total shear force
$\%ASF_D$	*ASF* on diagonal interface (*oc*) as percentage of total shear force
$\%ASF_{VI}$	*ASF* on variable-inclined interface (aa$_3$) as percentage of total shear force
ADV	Accostic Doppler Velocity Meter
b	Bottom width of main channel
B_w	Width of the meander belt
ENU	East, North and Upward
b'	Top width of main channel
b_1, b_2	Lengths of flood plain bed at left and right sides measured from vertical interface respectively

B	Over all width of compound channel
c	Energy loss coefficients based on friction factor
C	Chezy's channel coefficient
C'	A constant given as $= X_{fp} / X_{mc}$
C_x	Factor representing the length of interface $(H{-}h)$ times that is to be added to the main channel perimeter only from VDM-II
C_{mc}	$[X_{mcv}/(H{-}h)]$ =Interaction length factors for main channel in VDM-III
C_{fp}	$[X_{fpv}/(H{-}h)]$ = Interaction length factors for floodplain in VDM-III
C'_{mc}	Interaction length factors for main channel in VDM-IV
C'_{fp}	Interaction length factors for floodplain in VDM-IV
COHM	Coherence Method
COH	Coherence
C_{wd}	Shape coefficient for expansion and contraction losses
C_{sse}	Side slope coefficient for expansion loss
C_{ssc}	Side slope coefficient for contraction loss
C_{sl}	Length coefficient for expansion and contraction losses
DISADF	Discharge adjustment factor
DCM	Divided Channel Method
DDM	Diagonal Division Method
Dee	Diagonal Division Method
d	Depth of flow over floodplain = $(H{-}h)$
Hee	(HDM-1)
Hie	(HDM-1I)
δ	Aspect ratio of the main channel b/h
(f_{mc})	Resistance coefficient of main channel sub-area
(f_{fp})	Resistance coefficient of floodplain sub-area
F_1, F_2 and F_3	Dependant function of $\%Q_{mc}$ with relative depth, width ratio and sinuosity respectively
F'_1, F'_2 and F'_3	Dependant function of $\%Q_{lmc}$ with relative depth, width ratio and sinuosity respectively
f	Friction factor
F_1	Factor for non friction loss due to main channel geometry
F_2	Factor for non friction loss due to main channel sinuosity
f_*	$N_{fp}\, f_{fp}/f_{mc}$
f_c	Friction factors of main channel

f_f	Friction factors of floodplain
F_m	Flow resistance in the main channel due to momentum transfer and other factors
g	Acceleration due to gravity
h	Height of main channel up to floodplain bed
h_0	Distance from the channel bottom at which logarithmic law indicates zero velocity
h'	In bank depth
H	Total depth of flow in compound channel
HDM	Horizontal Division Method
Jm	James & Wark method
k	Von Karmans constant;
k_{bf}	Dimensionless energy coefficients in (m^{-1}) due to boundary friction
k_{sf}	Dimensionless energy coefficients in (m^{-1}) due to secondary flow
k_{ex}	Dimensionless energy coefficients in (m^{-1}) due to expansion
k_{co}	Dimensionless energy coefficients in (m^{-1}) due to contraction
m	A exponent
M	Slope of the semi-log plot of velocity distributions
μ	Dynamic viscosity of water
N_r	Reynolds number ratio ($N_r = N_{fp} / N_{mc}$)
N_{mc}	Reynolds's number of main channel sub-sections
N_{fp}	Reynolds's number of flood plain sub-sections
N	Reynolds's number of compound section
n	Manning's resistive coefficient
n_{mc}	Manning's roughness factor for main channel
n_{fp}	Manning's roughness factor for floodplain
N_f	Number of floodplains
n	Manning's roughness factor
P_i	Wetted perimeter of each sub-area
P_c	Wetted perimeter of floodplain subsections
P_f	Wetted perimeter of main channel subsections
P_*	$N_f P_f / P_c$
P	Wetted perimeter of the compound channel section
P_{mc}	Wetted perimeter of the main channel

P_{fp}	Wetted perimeter of the floodplain
θ	Angle of interface making an angle with vertical line at junction
(r_C)	Least centerline radius of curvature to its depth
R	Hydraulic radius of the channel cross section
R	Hydraulic mean radius of the channel cross section (A/P)
R	Ratio of the amplitude of e meandering channel to the top width B of compound section
ρ	Density of flowing liquid
R_{mc}	Hydraulic radius of main channel sub-sections
R_{fp}	Hydraulic radius of flood plain sub-sections
SCM	Single Channel Method
S	Channel slope
(τ)	Apparent shear stress in N/m^{2}given by Prinos and Town send (1984) equation
τ_{mc}	Mean boundary shear stress in main channel per its unit length
τ	Boundary shear stress
τ_{fp}	Mean boundary shear stress in floodplain per its unit length
$\int_{mc} \tau dp$	Shear force on surfaces of main channel
u	Shear velocity
u_1, u_2	Time averaged velocities measured at h'_1 and h'_2 heights respectively from boundary
X_{mc}	Interface length for inclusion in the main channel wetted perimeter
X_{fp}	Length of interface to be subtracted from the wetted perimeter of floodplain
$X_{m\theta}$	Interface length for inclusion in the main channel wetted perimeter for an interface at an angle θ with the vertical line at junction
$X_{f\theta}$	Interface length for subtraction from floodplain perimeter for an interface at an angle θ with the vertical line at junction
$Q_1\ Q_2, Q_3, Q_4$	Flow discharge in the zone-1, zone-2, zone-3, and zone-4 respectively
Q_{basic}	'Basic' discharge
Q_{single}	Discharge estimated by single channel method
Q_{actual}	Actual discharge
$\%Q_{lmc}$	Percentages of flow carried by the lower main channel
$\%Q_{mc}$	Percentages of discharge carried by the main channel

V_{mc} and V_{fp}	Mean velocities of main channel and flood plain sub areas respectively
VDM	Vertical Division Method
ZASIM	Zero Apparent Shear Interface Method
Vee	*(VDM-1)*
Vie	*(VDM-1I)*
Mv^*, *Mv*	Proposed Vertical method (VDM-III*)*
Mh^*, *Mh*	Proposed horizontal method (HDM-III)
Ma^*, *Ma*	Proposed area method
*	Represents the methods tested by bank-full Manning's *n* for meandering compound channels only
P_{mcv}	Modified main channel wetted perimeter using vertical subdivisions
P_{mcv} ,P_{fpv}	Modified floodplain wetted perimeter using vertical subdivisions
VI	Variable Inclined plain method
Em	Ervine & Ellis method,Mb-Meander belt method
X_{mcv}	Length of vertical interface to be included to the wetted perimeter of main channel sub-area
X_{fpv}	Length of vertical interface to be deducted from the wetted perimeter of floodplain sub-section
τ_v	Apparent shear stress on vertical interface
τ_r	Relative apparent shear stress and is given by Prinos-Townsend empirical formula
ΔV	difference of mean velocity between main channel and floodplain
R_o	Ratio of the amplitude ε of the meandering channel to its top width *B*
ε	Amplitude of the meandering channel
V_a	sectional mean velocity of this zone
V_x, V_y and V_z	Longitudinal, radial and vertical directions respectively
V_a	Sectional mean velocity of this zone
S_o	Valley slope
r_c	Bend radius
V_b	Sectional mean velocity of this zone
L_w	One wave length of the meander channel
θ'	Mean angle of incidence averaged over the meander wave length calculated from numerical integration
K_c	Given by a third order polynomial fit obtained from the Yen and Yen (1983) data

Q_{bf}	the bank full discharge calculated using in bank method
m	Energy loss coefficients based on geometry
K	Energy loss coefficients based on sinuosity
L	Meander wave length
W_2	Width of zone 2
K_e	Factor for expansion and contraction loss in zone 2
S_s	Cotangent of main channel side slope
K_c	Contraction factor
P_i	Wetted perimeter of each sub-area
$(\%S_{fp})$	Shear force percentages carried by the floodplain perimeter
$(\%S_{mc})$	Shear force percentages carried by the main channel perimeter
S_r	Sinuosity (length along channel center/ straight Valley length)
WSD	West, South and Down ward

ABSTRACT

Reliable estimates of discharge capacity are essential for the design, operation, and maintenance of open channels, more importantly for the prediction of flood, water level management, and flood protection measures. In nature, most rivers tend to be of compound sections as well as meandering. For the management of rivers and floodplains, it is important to understand the behaviors of flows within compound channels. Cross sections of these compound channels are generally characterized by deep main channel bounded by one or both sides by a relatively shallow flood plain. At low depths when the flow is only in the main channel, conventional methods are generally used to assess discharge capacity. When the flow goes over bank the classical single channel formula provides large error between the estimated and the observed discharge. Standard sub division and composite roughness methods given in Chow (1959) are essentially flawed when applied to compound channels. The discharge calculation for compound channel is based mainly on refined one dimensional methods of analysis. However two dimensional (2D) approaches (Abril & Knight,1999;Knights& Schino1996; Knights& Abril1996) and three dimensional analysis (Schino & Lin 1992;Younis 1996) are more complex and inconvenient to use in practice. The basic idea of one dimensional approach is to subdivide the channel into a number of discrete sub areas, usually the main channel and adjacent flood plains. Discharge for each part is calculated with or without consideration of interaction effect and sum them, possibly with some adjustment to give the total channel discharge. Review of the literature show that investigators propose alternatives interface planes to calculate the total discharge carried by a compound channel section. Either including or excluding the interface length with the wetted perimeter does not make sufficient allowance for discharge calculation for all depths of flow over floodplain. It either overestimates or underestimates the discharge result. Investigations are made on the different methods for predicting discharge in straight and meandering compound channels. Finally a comparison is made between the different discharge models.

Experiments are carried out using new flumes with fabrication of three rigid compound channels: one straight and the other two meandering, in the Fluid Mechanics and Hydraulics Laboratory of the Civil Engineering Department at the National Institute of Technology, Rourkela. All together 75 series of experimental observations on

stage –discharge relationships are made of which, 21 for straight channels, 27 for mildly meandering channels and the rest 27 for highly meandering channels. Out of this, detailed velocity and turbulence data are observed for 29 runs out of which, 5 for straight compound, 12 for mildly meandering simple/compound and 12 for highly meandering simple/compound channels. For each runs detailed measurement of 3-Dimensional velocities are made at one location for straight channels and at two locations (at bend apex and another at geometrical cross over) in the meander path. Using a micro-ADV (Acoustic Doppler Velocity meter) of 16 MHz, accurate three dimensional point velocities at the defined grid points of the channels are recorded for every run. For each run the boundary shear distribution along the wetted perimeter of the cross section of the channel are obtained at the defined test section for straight compound channel and at the bend apex test section of the two meandering compound channels for both in bank and over bank conditions. The velocity distributions in tangential, radial and vertical direction are plotted in using the data from micro- ADV. and applying software -3-D field.

Compound channel flow causes decrease in main channel shear with altering its distributional shapes and increase in flood plain shear. The reduction of main channel shear is due to the presence of the interaction mechanism that can be explained by the fact that the main channel is loosing energy to floodplain. The percentage of decrease of main channel shear reduces as the depth of flow over floodplain increases. In the investigation the boundary shear stress distribution across the periphery is assessed and the results have been used to calculate the apparent shear forces on the assumed interfaces of separation of compound section to sub areas. An empirically derived equation relating the geometry parameters and the boundary shear percentages on the floodplain and main channel wetted perimeters of a channel having high width ratio and high sinuosity are presented. Momentum transfer between main channel and floodplain is quantified in terms of the length of interface and the model results are compared with the experimental results. Basing on the model out put merits of the selection of the interface plains for discharge estimation using the divided channel approach is decided.

Four alternative uses of the traditional vertical and horizontal interface plane of separation of compound channels are proposed. An investigation has been made for the energy losses resulting from the compound response of boundary friction, secondary flow, turbulence, expansions and contractions in straight and meandering channels with over

bank flow conditions. Due to flow interaction between the main channel and floodplain, the flow in a compound section consumes more energy than a channel with simple section carrying the same flow and having the same type of channel surface. The energy loss is manifested in the form of variation of resistance coefficients of the channel with depth of flow. Distribution of energy in compound channel is an important aspect, and is addressed adequately by incorporating the variation of the Manning's roughness coefficient n, Chezy's C and Darcy – Weisbach's friction factor f and parameter $\sqrt{s}/n$ with depths of flow ranging from in-bank channel to the over-bank flow. Stage-discharge curves, channel resistance coefficients, composite Manning's n of straight and meandering compound channels are presented for the present experimental series. Flow distribution between the sub-sections of a meandering compound channel is complicated due to interaction mechanism as well as sinuosity effect. The proposed models also predict successfully the percentage of flow carried by main channel, lower main channel and flood plain. The proposed approaches of discharge prediction have also been extended to the experimental data collected at channels of IIT, Kharagpur (Patra & Kar,1999), Straight Channels of Knght & Demetriou (1983), a higher sinus channels of Willet & Hard Wick (1993) and the large scale channel of FCF (flood channel facility), Walling ford, UK. All the models compares well with the reported data of these investigators. Some suggestions for future studies are included at the end of the thesis.

Key Words:

Meander Channel, Straight Channel, Compound Channel, Boundary shear, Energy loss, Apparent shear, Momentum transfer, Discharge estimation, Interface plains, Stage discharge relationship, Divided channel method, Roughness coefficient, Interface, Over bank flow, Velocity distribution, Flow distribution.

INTRODUCTION

1.1 MEANDERING

Almost all rivers meander. Straight river reaches longer than 10 to 12 times the channel widths are almost nonexistent in nature. River meandering is a complicated process involving the interaction of flow through channel bends, bank erosion, and sediment transport. Inglis (1947) was probably the first to define meandering and it states "where however, banks are not tough enough to withstand the excess turbulent energy developed during floods, the banks erode and the river widens and shoals. In channels with widely fluctuating discharges and silt charges, there is a tendency for silt to deposit at one bank and for the river to move to the other bank. This is the origin of meandering…" Leliavsky. (1955) summarizes the concept of river meandering in his book which quotes "The centrifugal effect, which causes the super elevation may possibly be visualised as the fundamental principles of the meandering theory, for it represents the main cause of the helicoidal crosscurrents which removes the soil from the concave banks, transport the eroded material across the channel, and deposit it on the convex banks, thus intensifying the tendency towards meandering. It follows therefore that the slightest accidental irregularity in channel formation, turning as it does, the stream lines from their straight course may, under certain circumstances constitute the focal point for the erosion process which leads ultimately to meander".

It is an established fact that meandering represents a degree of adjustment of water and sediment laden river with its geometry and slope. The curvature develops and adjusts itself to transport the water and sediment load supplied from the watershed. The channel geometry, side slope, degree of meandering, roughness and other allied parameters are so adjusted that in course of time the river does the least work in turning, while carrying the loads. With the exception of straight rivers, for most of the natural rivers, the channel slope is usually less than the valley slope. The meander pattern represents a degree of channel adjustment so that a river with flatter slope can exist on a steeper valley slope.

Two parameters are used to classify meandering channels into its categories. Rivers with sinuosity, defined as the ratio of the length of the thalweg (path of deepest flow) to the length of the valley, is classified as straight when the ratio is less than 1.05, and more are classified as sinuous and meandering. The other parameter defining meandering plan form is the ratio of the least centerline radius of curvature (r_c) to the channel width (b) given as (r_c/b).

Meandering channels are also classified as shallow or deep depending on the ratio of the average channel width (b) to its depth (h'). In shallow channels ($b/h' >5$, Rozovskii, 1961) the wall effects are limited to a small zone near the wall which may be called as "wall zone". The central portion called "core zone" is free from the wall effects. In deep channels ($b/h'<5$) the influence of walls are felt throughout the channel width. Meandering and the flow interaction between main channel and its adjoining floodplains are those natural processes that have not been fully understood.

1.2 MEANDERING COMPOUND CHANNEL AND THE DISCHARGE ESTIMATION

It is quite common that during floods the river discharge overtops its bank and spreads to its adjoining floodplains that carry part of the flood load. At this high river stage, the cross sectional geometry of flow undergoes a steep change. The channel section becomes compound. Due to different hydraulic conditions prevailing in the river and floodplain, the flow structure for such section is characterized by large shear layers generated by the difference of mean sub-area velocity between the main channel and the adjoining floodplain flow. Just above the bank-full stage, the velocity of main channel flow is much higher than the floodplain velocity. Therefore, the flow in the main channel exerts a pulling or accelerating force on the floodplain flow, which naturally generates a dragging or retarding force on the flow through the main channel. This leads to the transfer of momentum between the main channel water and that with the floodplain. The interaction effect is very strong at just above bank full stage and decreases with increase in the depth of flow over floodplain. The relative change of "pull" and "drag" of the flow between faster and slower moving sections of a compound section with flow depth complicates the momentum transfer between them. Failure to understand this

process leads to either overestimate or underestimate the discharge leading to the faulty design of a compound channel.

Magnitude of flood prediction is the fundamental for flood warning, determining the development for the present flood-risk areas, and the long-term management of rivers. Discharge estimation methods currently employed in river modeling are based on historic hand calculation formulae proposed by Chezy, Darcy-Weisbatch or Manning. Recent works have provided significant improvements in understanding the flow processes and calculation of channel discharge.

At the junction region between the main channel and that of the floodplain, Sellin (1964) and Knight and Demetriou (1983) indicated the presence of artificial banks made of vortices, which acted as a medium for transfer of momentum. The process of transfer of momentum from main channel to floodplain flow at low floodplain depth and its reversal at high flood plain depths have been reported by Patra and Kar (2000). This momentum transfer complicates the flow process making the flood prediction methods more difficult. During the last decade or so, there has been some research on the topic of flow interaction and the estimation of discharge for straight and meandering compound channels, but a last word on this is still awaited.

The maximum flood levels corresponding discharges depend on the resistance to flow exerted by bed friction and other head loss mechanisms. Researchers have shown that the flow structure is complex even for straight compound channels. For meandering compound channels, the flow mechanisms are complicated due to the three-dimensional (3D) nature of flow and the momentum transfer involved in the system. Prediction of discharge is therefore difficult for over bank flows. The methods that have been proposed so far, are inadequate to meandering channels with over bank floodplain flow. To date, most efforts have been concentrated on straight compound channels. Lotter (1933) proposed a "divided channel method" which is based on separation of the main channel flow from floodplain flow by imaginary fluid boundary. Discharge for each zone is calculated using Manning-Strickler equation and added up to give the section mean discharge. However, the process may lead to an error up to 30% (Greenhill and Sellin, 1993) between the computed and observed discharges. This is mainly due to the neglect of flow interaction or shearing between the deep main channel and the shallow floodplain flow across the plane of separation.

One of the major works of the present research is to propose one-dimensional approaches of estimating discharge in meandering and straight compound channels that can be used as effective tools for future discharge calculations, while taking due care of the effect of flow interaction between river channel and its adjoining floodplains using the "divided channel sections".

1.3 COMMENTS ON CURRENT RESEARCH-OBJECTIVE OF THE STUDY

Estimation of flow for in-bank stages of a channel is simple and straight forward. However, when over bank flow takes place, the classical formula either overestimates or under-estimates the discharge capacity at a river section. Standard sub-division and composite roughness methods given by Chow (1959) are essentially flawed when applied to compound meandering channels. Most of the discharge calculation for compound channel is based mainly on refined one dimensional (1D) method. However, both 2D and 3D approaches are more complex to use in practice. The basic approach in one-dimensional analysis is to subdivide the channel into a number of discrete sub-section areas, usually the main channel and the adjacent flood plains, calculate the discharge for each part with or without consideration of interaction effect and sum them up, possibly with some adjustment so as to give the total channel discharge.

The present study is a step in understanding the flow processes. It is supported by data collected from three experimental channels of different geometry and sinuosity. Experiments conducted using freshly fabricated channels at the Fluid Mechanics and Hydraulics Engineering Laboratory at the National Institute of Technology, Rourkela, on straight, mildly meandering and high meandering, and very wide channels. A rigid boundary channel is considered to be more appropriate to study the basic nature of flow interaction and flow parameters than going for movable bed.

An investigation of energy losses resulting from boundary friction, secondary flow, turbulence, and other factors in meandering compound channels with over bank flow has been presented. Due to flow interaction between the main channel and floodplain, the flow in a compound section consumes more energy than a channel with simple section carrying the same flow and having the same type of channel

surface. The energy loss is manifested in the form of variation of resistance coefficients of the channel with depth of flow. The variations of roughness coefficients with depths of flow ranging from in-bank channel to the over-bank flow are investigated.

In the present study, it is attempted to formulate the models for predicting discharge for compound meandering channel suitable to all types of geometry. The analysis concerning the estimation of discharge in the meandering compound channel have also been extended to an experimental higher sinuous (sinuosity = 1.91) as well as high width ratio ($\alpha = 16.08$) channel. The results of the present analysis are also applied to the experimental channel data reported by Knight and Demetriou (1983), Willets and Hardwick (1993), and to the large scale experimental channel data of FCF (UK).

Boundary shear force results are used to calculate the apparent shear forces on vertical, horizontal, and inclined interfaces. Mathematical models for momentum transfer in terms of apparent shear strength at the assumed interfaces are formulated. Equations are presented giving the quantum of momentum transfer at different interfaces originating from the junction of main channel and floodplain. An empirically derived equation relating the geometry parameters and the boundary shear force on the floodplain bed and walls is presented. A mathematical model quantifying apparent shear force results at the various interface plains are used to assess the channel discharge calculation methods which are based on sub-dividing the flow area.

The main objective of the present study is intended to model the flow interaction for meandering channel with floodplain basing on which a simple but accurate method of calculation of discharge carried by meandering and straight compound geometries is proposed. This should be useful in the solution of many practical problems and better understanding of the mechanism of flow interaction between main channel and the floodplain. The present work is also directed towards understanding the underlying mechanism of flow resistance and flow distribution in the meander and straight compound channel rather than simulating a prototype situation. The experimental channel dimensions are small due to space and other limitations in the laboratory. In view of the above, the research program is taken up with the following objectives:

❖ To collect sufficient literatures on the energy loss aspects, boundary shear distribution, flow distribution in zones/sub-areas, and the existing methods of discharge estimation in straight and meandering compound channels from in-bank to over-bank flow.

❖ To observe the 3-dimensional velocity and the boundary shear distribution of simple meandering, straight compound channel, and meandering compound sections of different geometry and sinuosity.

❖ To study the energy loss aspects of meandering compound channels for the in-bank and over-bank flow situations and the variation of the resistance coefficient with flow depth.

❖ To propose equations to estimate the percentage of shear carried by the main channel and floodplain walls and to extend the models to the channels of high width ratio and sinuosity.

❖ To develop equations for the percentage of discharges carried by various zones of the main channel and flood plain geometries.

❖ To study the nature of momentum transfer between the main channel and floodplain on the basis of apparent shear stress (ASS) results at the assumed interface plains. The interaction is quantified in terms of "Interaction Length" at the interface plains.

❖ To compute the discharge by 'divided channel methods' using number of alternative/ modified / improvement interface planes approaches.

❖ To divide a compound channel into sub-areas by an interface plain of zero shear leading to a "new area method" for discharge prediction.

❖ To validate the developed models using the present experimental channel data collected from three compound channels, high quality FCF channel data at Wallingford UK, meandering channels data of Patra and Kar (2000), and higher sinus channels data of Willet and Hardwick(1993).

❖ To study the flow and velocity parameters for very wide and highly sinuous channels.

*****

LITERATURE REVIEW

2.1 GENERAL

Investigators have studied meander and straight compound channel flows for a fairly long time. The name meander, which probably originated from the river Meanders in Turkey is so frequent in river that it has attracted the interest of investigators from many disciplines. Thomson (1876) was probably the first to point out the existence of spiral motion in curved open channel. Since then, a lot of laboratory and theoretical studies are reported, more so, in the last decade or two. It may be worth while to understand the nature of flow in simple meander channel and straight compound channels before knowing about the flow structure in meander channel-floodplain geometry. There are limited studies available concerning the flow in meandering compound channels.

2.2 SIMPLE MEANDER CHANNELS

Flow in a meandering channel is considerably more complex than flow in straight channels. The flow geometry in meander channel is in the state of either development, decay or both. The following important studies concerning the flow in meandering channels are useful for the present work.

The Soil Conservation Service (1963) proposed a method to account for meander losses by adjusting the basic value of Manning's *n* using sinuosity of the channel only. The adjusted value of Manning's n was proposed for three different ranges of sinuosity.

Toebes and Sooky (1967) conducted experiments in a small laboratory channel with sinuosity 1.09. From the experimental results they concluded that energy loss per unit length for meandering channel was up to 2.5 times as large as those for a uniform channel of same width and for the same hydraulic radius and discharge. They proposed an adjustment to the roughness *f* as a function of hydraulic radius below a critical value of the Froude number.

Chang (1983) investigated energy expenditure and derived an analytical model for obtaining the energy gradient, based on fully developed secondary circulation. By making simplifying assumptions he was able to simplify the model for wide rectangular sections.

Johannesson and Parker (1989 a) presented an analytical model for calculating lateral distribution of depth averaged primary flow velocity in meandering rivers. Using an approximate "moment method" they accounted for the secondary flow in the convective transport of primary flow momentum, yielding satisfactory results of the redistribution of primary flow velocity.

Knight, Yuan and Fares (1992) reported the experimental data of SERC-FCF concerning boundary shear stress distributions in meandering channels throughout the path of one complete wave length. They also reported the experimental data on surface topography, velocity vectors, and turbulence for the two types of meandering channels of sinuosity 1.374 and 2.043 respectively. They examined the effects of secondary currents, channel sinuosity, and cross section geometry on the value of boundary shear in meandering channels and presented a momentum-force balance for the flow.

 James (1994) reviewed the various methods for bend loss in meandering channel proposed by different investigators. He tested the results of the methods using the data of FCF, trapezoidal channel of Willets, at the University of Aberdeen, and the trapezoidal channels measured by the U.S. Army Corps of Engineers at the Waterways Experiment Station, Vicksburg. The results were found to give considerably different. He proposed some new methods accounting for additional resistance due to bend by suitable modifications of previous methods. His modified methods predicted well the stage discharge relationships for meandering channels.

Maria and Silva (1999) expressed the friction factor of rough turbulent meandering flows as the function of sinuosity and position (which is determined by, among other factors, the local channel curvature). They validated the expression by the laboratory data for two meandering channels of different sinuosity. The expression was found to yield the computed vertically averaged flows that are in agreement with the flow pictures measured for both large and small values of sinuosity.

Shiono, Muto, Knight and Hyde (1999) presented the experimental data of secondary flow and turbulence using two components Laser- Doppler Anemometer for both straight and meandering channels to understand the flow mechanism in meandering channels. They developed turbulence models and studied the behavior of secondary flow and centrifugal forces for both in-bank and over-bank flow conditions. They investigated the energy loss due to boundary friction, secondary flow, turbulence, expansion and contraction in meandering channels.

Zarrati, Tamai and Jin (2005) developed a depth averaged model for predicting water surface profiles for meandering channels. They applied the model to three meandering channels (two simple and one compound) data. The model was found to predict well the water surface profile and velocity distribution for simple channels and also for the main channel of compound meandering channel.

2.3   COMPOUND CHANNELS IN STRAIGHT REACHES

While simple channel sections have been studied extensively, compound channels consisting of a deep main channel and one or more floodplains attached to its sides have received relatively less attention. Analysis of these channels is more complicated due to flow interaction taking place between the deep main channel and shallow floodplains. Laboratory channels provide the most effective alternative to investigate the flow processes in compound channels as it is difficult to obtain field data during very high over bank flow situations in natural channels. Therefore, most of the works reported are based on experimental investigations.

Sellin (1964) confirmed the presence of the "kinematics effect" reported by Zheleznyakov (1965) after a series of laboratory studies and presented photographic evidence of the presence of vortices at the junction region of main channel and flood plain. He studied the channel velocities and discharge under both interacting and isolated conditions by introducing a thin impermeable film at the junction. Under isolated condition, velocity in the main channel was observed to be more than interacting condition.

Zheleznyakov (1965) was probably the first to investigate the interaction between the main channel and the adjoining floodplain. He demonstrated under laboratory conditions the effect of momentum transfer mechanism, which was responsible for

decreasing the overall rate of discharge for floodplain depths just above the bank full level. As the floodplain depth increased, the importance of the phenomena diminished. He also carried out field experiments, which confirmed the significance of the momentum transfer phenomenon in the calculation of overall discharge. The relative 'drag' and 'pull' between the faster moving main channel flow and slower moving floodplain flow gave rise to the momentum transfer mechanism, which he termed as "kinematics effect".

Ghosh and Jena (1973) and Ghosh and Mehata (1974) reported studies on boundary shear distribution in straight two stage channels for both smooth and rough boundaries. They related the sharing of the total drag force by different segments of the channel section to the depth of flow and roughness concentration.

Yen and Overton (1973) used isovel plots to locate the interface plane of zero shear. The data showed that the angle of inclination to the horizontal of the interface plane increased with depth of flow over floodplain.

Myers and Elswy (1975) studied the effect of interaction mechanism and shear stress distribution in channels of complex sections. In comparison to the values under isolated condition, the results showed a decrease up to 22 percent in channel shear and increase up to 260 percent in floodplain shear. This indicated the possible regions of erosion and scour of the channel and flow distribution in alluvial compound sections.

Rajaratnam and Ahmadi (1979) studied the flow interaction between straight main channel and symmetrical floodplain with smooth boundaries. The results demonstrated the transport of longitudinal momentum from main channel to flood plain. Due to flow interaction, the bed shear in floodplain near the junction with main channel increased considerably and that in the main channel decreased. The effect of interaction reduced as the flow depth in the floodplain increased.

Wormleaton, Alen, and Hadjipanos (1982) undertook a series of laboratory tests in straight channels with symmetrical floodplains and used "divide channel" method for the assessment of discharge. From the measurement of boundary shear, apparent shear stress at the vertical, horizontal, and diagonal interface plains originating form the main channel-floodplain junction could be evaluated. An apparent shear stress

ratio was proposed which was found to be a useful yardstick in selecting the best method of dividing the channel for calculating discharge. It was found that under general circumstances, the horizontal and diagonal interface method of channel separation gave better discharge results than the vertical interface plain of division at low depths of flow in the floodplains.

Knight and Demetriou (1983) conducted experiments in straight symmetrical compound channels to understand the discharge characteristics, boundary shear stress and boundary shear force distributions in the section. They presented equations for calculating the percentage of shear force carried by floodplain and also the proportions of total flow in various sub-areas of compound section in terms of two dimensionless channel parameters. For vertical interface between main channel and floodplain the apparent shear force was found to be more at low depths of flow and also for high floodplain widths. On account of interaction of flow between floodplain and main channel, it was found that the division of flow between the sub-areas of the compound channel did not follow the simple linear proportion to their respective areas.

Knight and Hamed (1984) extended the work of Knight and Demetriou (1983) to rough floodplains. The floodplains were roughened progressively in six steps to study the influence of different roughness between floodplain and main channel to the process of lateral momentum transfer. Using four dimensionless channel parameters, they presented equations for the shear force percentages carried by floodplains and the apparent shear force in vertical, horizontal, diagonal, and bisector interface plains. The apparent shear force results and discharge data provided the strength and weakness of these four commonly adopted design methods used to predict the discharge capacity of the compound channel.

Wormleaton and Hadjipanos (1985) studied flow distribution in compound channels and showed that even though a calculation method may give satisfactory results of overall discharge in a compound channel, the distribution of flow between floodplain and main channel may be badly modeled. In general, the floodplain flow was found to be underestimated and the main channel flow overestimated.

Myers (1987) presented theoretical considerations of ratios of main channel velocity and discharge to the floodplain values in compound channel. These ratios followed a straight-line relationship with flow depth and were independent of bed slope but dependent on channel geometry only. Equations describing these relationships for smooth compound channel geometry were presented. The findings showed that at low depths, the conventional methods always overestimated the full cross sectional carrying capacity and underestimated at large depths, while floodplain flow capacity was always underestimated at all depths. He underlined the need for methods of compound channel analysis that accurately model proportions of flow in floodplain and main channel as well as full cross-sectional discharge capacity.

Stephenson and Kolovopoulos (1990) discussed four different methods of subdivision of compound channels on the basis of consideration of shear stress between floodplain and main channel to evaluate a method of discharge calculation. Based on the published data, they concluded that their 'area method' was the most promising alternative of discharge computation and that Prinos-Townsend (1984) equation gave better results for apparent shear stress at floodplain and main channel interface. They incorporated channels with fairly wide range of bed roughness and floodplain widths in their computations.

Ackers (1992, 1993) deduced a design formula for straight two stage channels by taking into account the interaction effects between floodplain and main channel. A parameter representing the coherence between the hydraulic condition of floodplain and main channel zones was proposed. The formulations were tested in large-scale experimental channels covering a wide range of geometry.

Myers and Lyness (1997) studied the behavior of two key discharge ratios, namely total to bank full discharge and main channel to floodplain discharge in compound channels for smooth and homogeneously roughened channels of various scales. The total to bank full discharge ratio was shown to be independent of bed slope and scale and was function of cross section geometry only. The other ratio was also independent of bed slope and scale but was influenced by the lateral floodplain bed slope. They evaluated the coefficients and exponents in the equations relating to flow ratios to flow depths.

Pang (1998) conducted experiments on compound channel in straight reaches under isolated and interacting conditions. It was found that the distribution of discharge between the main channel and floodplain was in accordance with the flow energy loss, which can be expressed in the form of flow resistance coefficient. In general, Manning's roughness coefficient n not only denoted the characteristics of channel roughness, but also influenced the energy loss in the flow. The value of n with the same surface in the main channel and floodplain possessed different values when the water depth in the section varied.

Bousmar and Zech (1999) presented a theoretical 1D model of compound channel flow known as the exchange-discharge model (EDM) which is suitable for stage-discharge computation as well as practical water-profile simulations. The momentum transfer is estimated as the product of velocity gradient at the interface by the mass discharge exchanged through this interface resulting from the turbulence. Similarly, the turbulent exchange discharge is estimated by a model analogous to the mixing length model including a proportionality factor ψ that is found to be reasonably constant. They summarised that the model predicts well the stage-discharge both for the experimental data and natural data. They applied their models successfully for flow prediction in a prototype River Sambre in Belgium.

Christopher, Thrnton, Steven, Morris and Fischenich (2000) performed series of eight experiments in a physical model of a compound channel to quantify the apparent shear stress at the interface between main channel and both vegetated and unvegetated floodplain. They analyzed the data by using a turbulence-based method to calculate the apparent shear stress as a function of the fluctuation in channel velocities. They presented an empirical relationship for the estimation of the apparent shear stress at the main channel-floodplain interface which was found to be the function of the bed shear stress, average velocity, flow depth, and the blockage caused by floodplain vegetation. They also presented an empirical relationship to incorporate a quantitative measure of the density of vegetation within a floodplain.

Myers, Lyness and Cassells (2001) presented the experimental results of both fixed and mobile main channel boundaries together with two types of flood plain roughness compound channel using FCF data. On the basis of mathematical modeling, they proposed the velocity and discharge ratio relationships which was

helpful for discharge assessment in over-bank flows and compared their results well with the data from a prototype natural compound river channel. They found that the ratios of main channel to floodplain average velocities and discharge plot logarithmically for the laboratory data, and linearity with the natural river data. The "divided channel method"(DCM) of discharge estimation overestimated the discharge in all cases and exhibited reasonable accuracy when applied to laboratory data with smooth floodplains, but showed significant errors up to 35% for rough floodplain data, and up to 27% for river data. The single channel method (SCM) significantly underestimated compound discharge for all cases for low flow depths, but became more accurate at larger depths for the smooth boundary laboratory data as well as the river data.

Atabay and Knight (2002) presented some stage discharge relationship of symmetrical compound channel section using the experimental results of the Flood Channel Facility (FCF). They examined the influence of flood plain width and main channel aspect ratio to the stage discharge relationship. They derived simple empirical relationships between stage and total discharge, and stage and zonal discharge for uniform roughness and varying flood plain width ratio. The broad effects on the stage –discharge relationship due to flood plain width ratio were examined.

Ozbek, Kocyigit and Cebe (2003) used limited experimental results from the FCF at Wallingford, for computing apparent shear stress and discharge in symmetrical compound channels with varying floodplain widths. They considered three assumed interface planes (vertical, horizontal, and diagonal) between the main channel and the floodplain sub-sections for computation of apparent shear stresses across the interfaces. They evaluated the discharge values for each sub-section and for the whole cross-section. They showed that the performance of these computation methods depend on their ability to accurately predict apparent shear stress. The diagonal and horizontal division methods provided better results than the vertical division method, with the diagonal method giving the most satisfactory results.

Tominaga and Knight (2004) conducted numerical simulation to understand the secondary flow effect on the lateral momentum transfer with a standard k-ϵ model

linked artificially with a given secondary flow. This simulation reproduced the typical linear distribution of momentum transfer term. The simulated secondary flow decreased the bed shear in main channel and increased the flood plain shear.

Proust, Riviere, Bousmar, Paquier, Zech, Morel (2006) Investigated experimentally the flow in a asymmetrically compound channel transition reach in an abrupt floodplain contraction (mean angle 22°). They compared three 1D models and one 2D simulation to their experimental data to know whether the models, developed for straight and slightly converging channels, are equally valid to their geometry. They showed that the error on the level of water is moderated due to lateral mass transfer but increased error of discharge distribution in the sub-areas. They suggested for further work to understand the phenomena of severe mass transfers in non-prismatic compound channels.

2.4 MEANDERING COMPOUND CHANNELS

There are limited reports available in literature concerning the flow, velocity, shear stress and energy distribution in meandering compound sections.

A study by United States Water Ways Experimental Station (1956) related the channel and floodplain conveyance to geometry and flow depth, concerning, in particular, the significance of the ratios of channel width to floodplain width and meander belt width to floodplain width in the meandering two stage channels.

Toebes and Sooky (1967) were probably the first to investigate under laboratory conditions the hydraulics of meandering rivers with floodplains. They attempted to relate the energy loss of the observed internal flow structure associated with interaction between channel and floodplain flows. The significance of helicoidal channel flow and shear at the horizontal interface between main channel and floodplain flows were investigated. It was found that energy loss in compound meandering channel was more than the sum of simple meandering and uniform channel carrying the same total discharge and same wetted perimeter. The interaction loss increased with decreasing mean velocities and exhibited a maximum when the depth of flow over the floodplain was less. For the purpose of analysis, a horizontal fluid boundary located at the level of main channel bank full stage was proposed as the best alternative to divide the compound channel into hydraulic

homogeneous sections. Helicoidal currents in meander floodplain geometry were observed to be different and more pronounced than those occurring in a meander channel carrying in bank flow. It was reported that Reynold's number (R) and Froude number (F) had significant influence on the meandering channel flow.

Ghosh and Kar (1975) reported the evaluation of interaction effect and the distribution of boundary shear stress in meander channel with floodplain. Using the relationship proposed by Toebes and Sooky (1967) they evaluated the interaction effect by a parameter (W). The interaction loss increased up to a certain floodplain depth and there after it decreased. They concluded that the channel geometry and roughness distribution did not have any influence on the interaction loss.

Ervine and Ellis (1987) carried out experimental investigation for the different sources of losses of energy in the meandering compound channel. They divided the compound channel into three sub areas, namely (i) the main channel below the horizontal interface from the junction, (ii) the meander belt above the interface, and (iii) the area out side the meander belt of the flood plain. They identified the different sources of losses of energy in each sub-area and proposed a discharge estimation method.

Kiely (1989), and McKeogh and Kiely (1989) studied the discharges, velocities, and turbulence characteristics for a meandering and straight main channel with floodplains in small laboratory flumes. Kiely observed that (1) the longitudinal turbulence intensities were higher in magnitude for meandering channels than straight channels, (2) the maximum turbulence intensity was observed to occur on the floodplains, adjacent to the downstream interface of the crossover sections and at the inner bend of the main channel, (3) turbulence transfer from the floodplain to the main channel was observed in straight and meandering channels, and (4) floodplains of meander channels may convey more flow than the floodplains of straight channels, and (5) the flow is approximately parallel to the floodplain valley slope for higher depth ratios.

Ervine, Willetts, Sellin and Lorena (1993) reported the influence of parameters like sinuosity, boundary roughness, main channel aspect ratio, width of meander belt, flow depth above bank full level, and cross sectional shape of main channel

affecting the conveyance in the meandering channel. They quantified the effect of each parameter through a non-dimensional discharge coefficient F^* and reported the possible scale effects in modelling such flows.

Sellin, Ervine and Willetts (1993) studied the influence of channel geometry, floodplain widths and roughness on the stage-discharge relationship. They found that the interaction mechanism associated with over bank flow in straight channels had very little influence on meandering two stage channels. For compound channel with smooth boundary, the loss of energy at various flow depths was expressed in terms of the variation of Manning's n and Darcy -Weisbach friction factor f. They suggested that considerably more work is needed to establish a sufficiently robust calculation method to reflect adequately the range of circumstances found in the field. The influence of floodplain roughness, main channel cross section, and sinuosity on the flow structures required further studies.

Greenhill and Sellin (1993) presented a method to design compound meandering channels based on the Manning–Strickler equation and found that the method predicted successfully the stage–discharge relationship for the tests carried out using FCF at UK and the data of other research projects. They suggested that their work be tested against field measurements.

Willetts and Hardwick (1993) reported the measurement of stage–discharge relationship and observation of velocity fields in small laboratory two stage channels. It was found that the zones of interaction between the channel and floodplain flows occupied the whole or at least very large portion of the main channel. The water, which approached the channel by way of floodplain, penetrated to its full depth and there was a vigorous exchange of water between the inner channel and floodplain in and beyond the down stream half of each bend. This led to consequent circulation in the channel in the whole section. The energy dissipation mechanism of the trapezoidal section was found to be quite different from the rectangular section and they suggested for further study in this respect. They also suggested for further investigation to quantify the influence of floodplain roughness on flow parameters.

Wark and James (1994) developed a procedure to calculate conveyance in meandering channels with over bank flow based on the horizontal division of the

cross section. It represented a significant change to the current practice of using vertical division of separating the floodplain from main channel. The non-friction energy losses were shown to be less important as the floodplain was roughened. The bed friction remained the most significant source of energy loss in the channels with over bank flow. The work was tested against the field data collected from the river Roding at Abridge in Essex and found to predict the measured stage – discharge relations reasonably well.

Shiono, Al-Romaih, and Knight (1999) reported the effect of bed slope and sinuosity on discharge of two stage meandering channel. Basing on dimensional analysis, an equation for the conveyance capacity was derived, which was subsequently used to obtain the stage-discharge relationship for meandering channel with over bank flow. It was found that the channel discharge increased with an increase in bed slope and it decreased with increase in sinuosity for the same channel. An error of 10% in discharge estimation was reported for relative depths exceeding 0.01.

Shiono, Muto, Knight, and Hyde (1999) presented the secondary flow and turbulence data using two components Laser- Doppler anemometer. They developed the turbulence models, and studied the behaviour of secondary flow for both in bank and over bank flow conditions. They divided the channel into three sub areas, namely (i) the main channel below the horizontal interface (ii) the meander belt above the interfaces and (iii) the area out side the meander belt of the flood plain. They investigated the energy losses for compound meandering channels resulting from boundary friction, secondary flow, turbulence, expansion and contraction. They reported that the energy loss at the horizontal interface due to shear layer, the energy loss due to bed friction and energy loss due to secondary flow in lower main channel have the significant contribution to the shallow over-bank flow. They also concluded that the energy loss due to expansion and contraction in meander belt have the significant contribution to the high over-bank flow.

Ervine, Alan, Koopaei, and Sellin (2000) presented a practical method to predict depth-averaged velocity and shear stress for straight and meandering over bank flows. They also presented an analytical solution to the depth-integrated turbulent form of the Navier-Stokes equation that includes lateral shear and secondary flows in addition to bed friction. They applied this analytical solution to a number of

channels, at model, and field scales, and compared with other available methods such as that of Shiono and Knight and the lateral distribution method (LDM).

Patra and Kar (2000) reported the test results concerning the boundary shear stress, shear force, and discharge characteristics of compound meandering river sections composed of a rectangular main channel and one or two floodplains disposed off to its sides. They used five dimensionless channel parameters to form equations representing the total shear force percentage carried by floodplains. A set of smooth and rough sections were studied with aspect ratio varying from 2 to 5. Apparent shear forces on the assumed vertical, diagonal, and horizontal interface plains were found to be different from zero at low depths of flow and changed sign with increase in depth over floodplain. They proposed a variable-inclined interface for which apparent shear force was calculated as zero. They presented empirical equations predicting proportion of discharge carried by the main channel and floodplain.

Morvan, Pender, Wright, and Ervine (2003) investigated the velocity field in meandering compound channels with over bank flow using the Flood Channel Facility (FCF) data, and simulated the flow field using computational fluid dynamics. They predicted the velocities, secondary velocities and t he helical motion of the water flowing within the main channel and compared their results with the experimental data.

Patra and Kar (2004) reported the test results concerning the flow and velocity distribution in meandering compound river sections. Using power law they presented equations concerning the three-dimensional variation of longitudinal, transverse, and vertical velocity in the main channel and floodplain of meandering compound sections in terms of channel parameters. The results of formulations compared well with their respective experimental channel data obtained from a series of symmetrical and unsymmetrical test channels with smooth and rough surfaces. They also verified the formulations against the natural river and other meandering compound channel data.

*****

EXPERIMENTAL SETUP AND PROCEDURE

3.1 EXPERIMENTAL SETUP

For the purpose of present research, two meandering and one straight experimental compound channels are fabricated inside separate tilting flumes in the Fluid Mechanics and Hydraulics Engineering Laboratory of the Civil Engineering Department, at the National Institute of Technology, Rourkela, India. The straight compound channel (Type-I) has equal flood plain at both sides of the main channel (Fig.3.1 a and b). The other two are compound meandering channels of Type-II (Figs.3.2) and Type-III (Figs.3.3) respectively, consisting of meandering main channel with unequal flood plains at both sides. The Plan forms of the Type-I, II and III experimental compound channels with measuring equipments taken from the up stream side are shown in photos P 3.1, 3.2, and 3.3 respectively, while the photo graphs of the same channels with measuring equipments taken from the down stream side end are shown in photos P 3.4, 3.5, and 3.6 respectively. The three different rectangular tilting flumes are made out of metal frame with glass walls. The geometrical features of the experimental channels are given in Table-3.1.
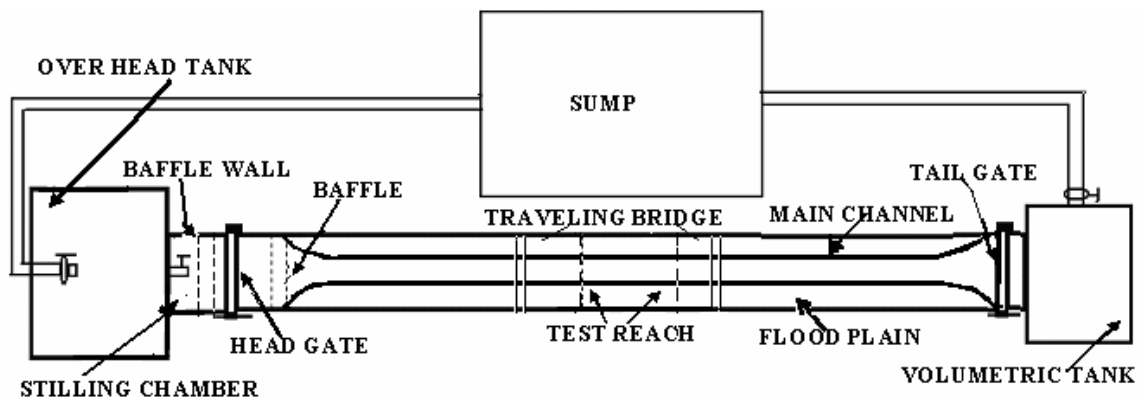
Fig. 3.1 (a) Plan view of experimental set up of the Type-I channel
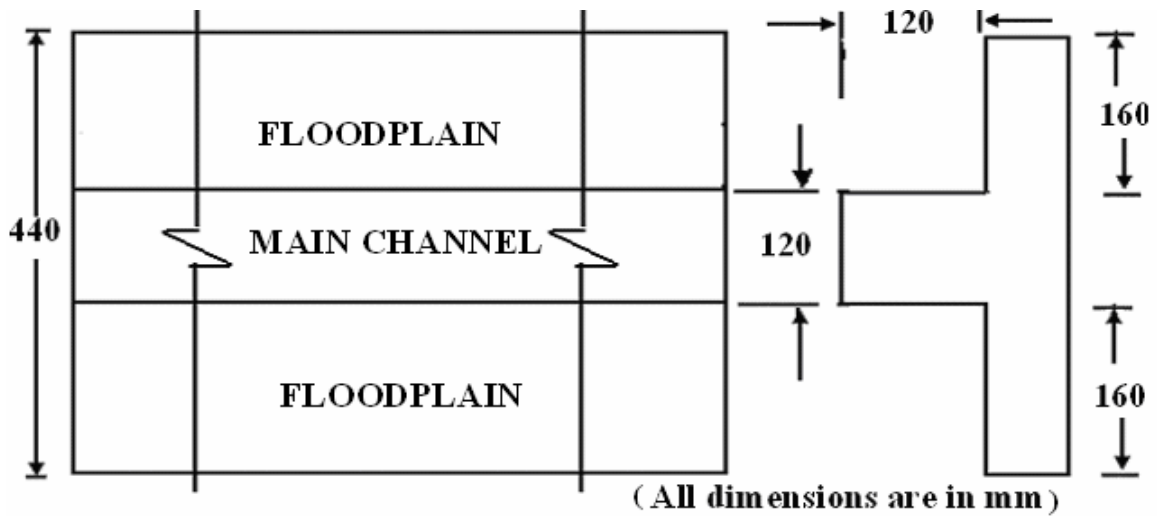
Fig. 3.1(b) Geometrical Parameter of the Type-I channel
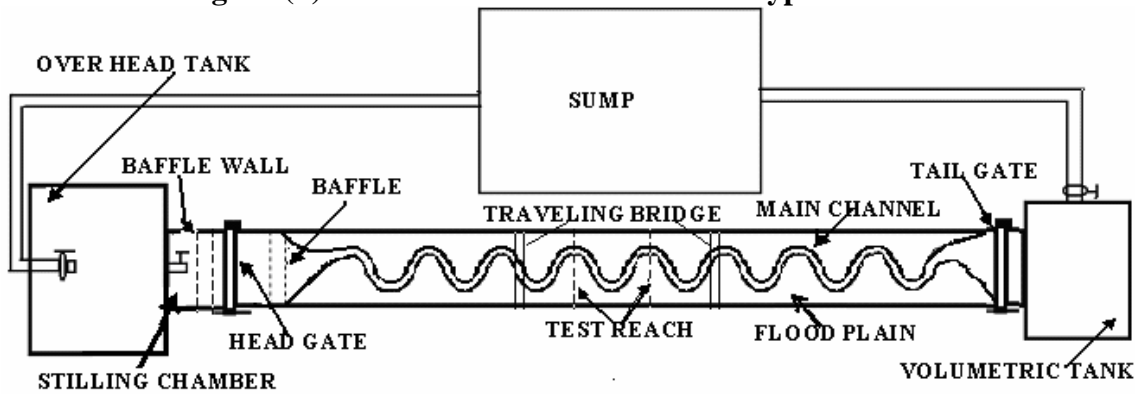
Fig. 3.2 (a) Plan form of Type-II channel
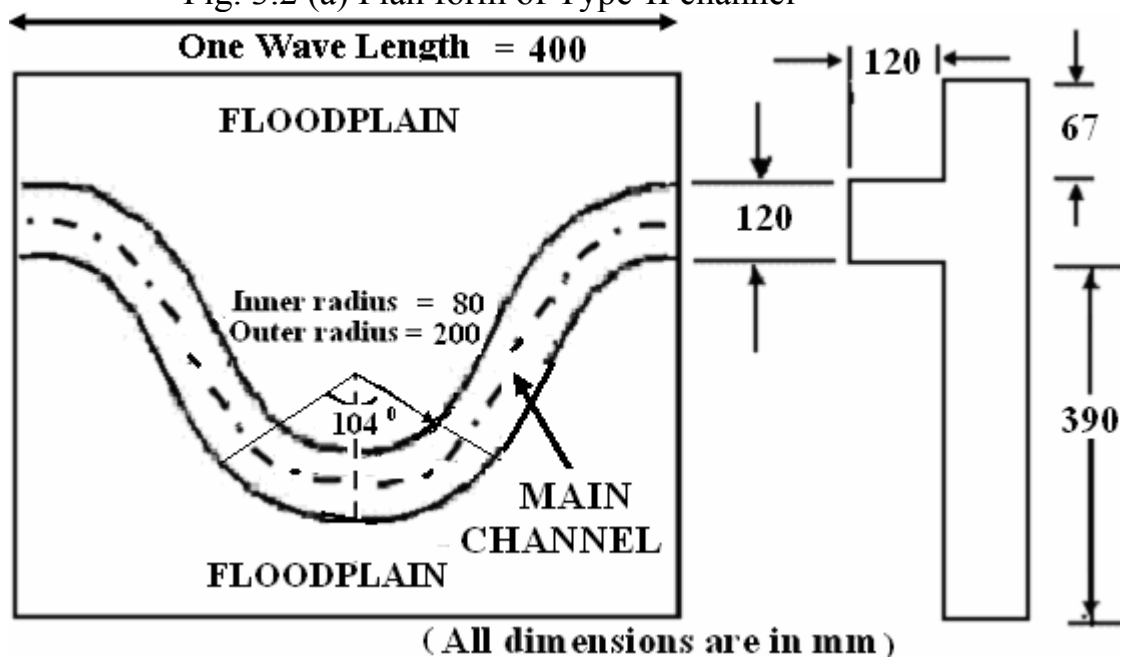
Fig. 3.2 (b) Details of one wave length of Type-II channel
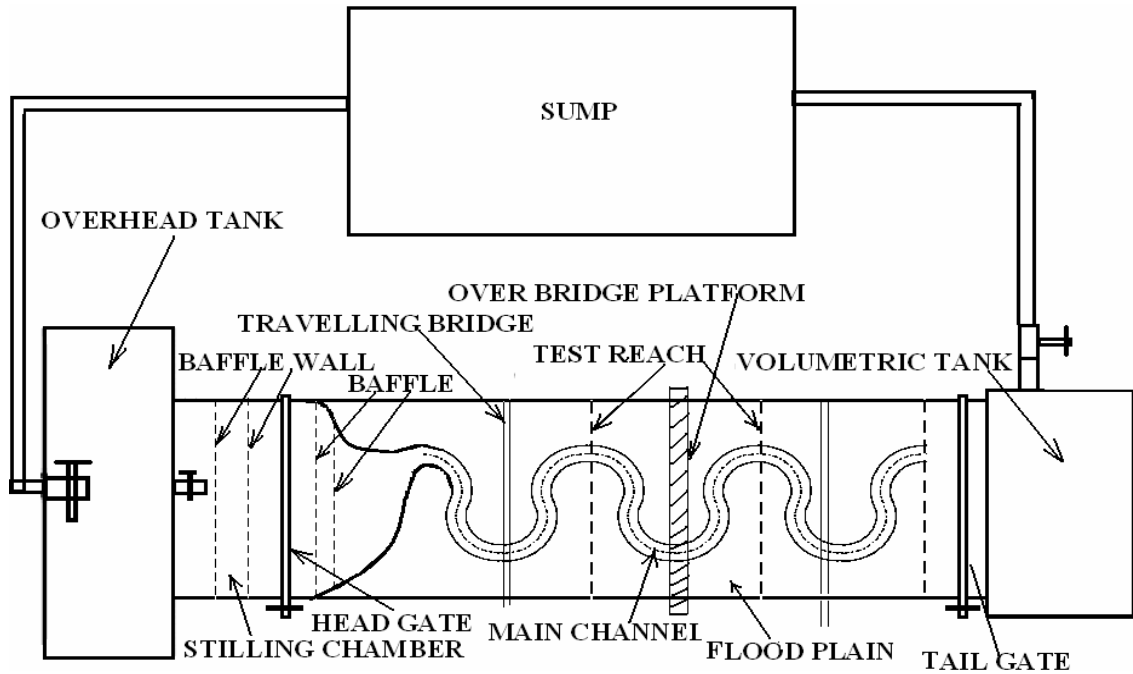
Fig. 3.3 (a) Plan form of Type-III channel
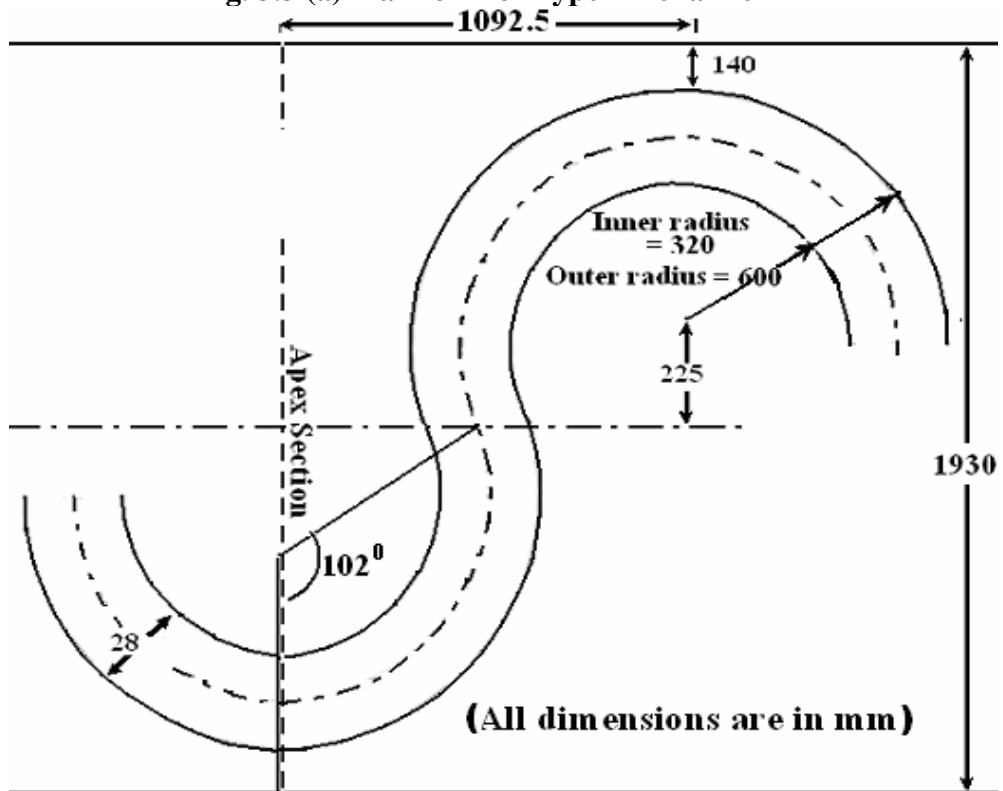
Fig. 3.3 (b) Details of one wave length of Type-III channel

The flumes are made tilting by hydraulic jack arrangement. Inside each flume, separate meandering/straight channels are cast using 50-mm-thick Perspex sheets. To facilitate fabrication, the whole channel length has been made in blocks of 1.20 m length each. The models thus fabricated have details given below:

Type-I channel: The straight compound section has the main channel dimension of 120 mm×120 mm, and flood plain width B = 440 mm (Fig.3.1 b). The channel is cast inside a tilting flume of 12m long, 450 mm wide, and 400 mm deep. The bed slope of the channel is kept at 0.0019.

Type-II channel: The meandering main channel has the dimensions of 120 mm×120 mm in cross section with floodplains at both sides. It has over all width of B = 577 mm, wavelength L = 400 mm, double amplitude $2A'$ = 323 mm giving rise to sinuosity of 1.44 (Fig.3.2 and photo P 3.7). This mildly meandering channel is placed inside a tilting flume of 12 m long, 600 mm wide, and 600 mm deep.

Type-III channel: This meandering compound channel is trapezoidal in cross section of the main channel of 120 mm wide at bottom, 280 mm at top having bank-full depth of 80 mm, and side slopes of 1:1. The flood plain width B is measured as 1930 mm. The main channel has wavelength L = 2185 mm and double amplitude $2A'$ = 1370 mm. Sinuosity for this channel is scaled as 1.91 (Fig.3.3 and Photo P 3.8).

Table 3.1 Details of geometrical parameters of the experimental channels

Sl.No	Item Description	Straight Type-I	Mildly Meander -Type-II	Highly Meander - -Type-III
1.	Wave length in down valley direction	-------	400 mm	2185 mm
2.	Amplitude (ε)	------	162 mm	685 mm
3.	Geometry of Main channel section	Rectangular	Rectangular	Trapezoidal (side slope 1:1)
4.	Main channel width(b)	120 mm	120 mm	120mm at bottom
5.	Bank full depth of main channel	120 mm	120 mm	80 mm
6.	Top width of compound channel (B)	440 mm	577 mm	1930 mm
7.	Slope of the channel	0.0019	0.0031	0.0053
8.	Meander belt width	-------	443 mm	1650 mm
9.	Minimum radius of curvature of channel centerline at bend apex	-------	140 mm	460 mm
10.	(α) =Ratio of top width (B) to channel width (b)	3.667	4.808	16.083
11.	Sinuosity	1.00	1.44	1.91
12.	Cross over angle in degree	---------	104	102
13.	Flume size	0.45m×0.4m ×12m long	0.6m×0.6m ×12m long	2.0m×0.6m ×12m long

Photo P-3.1

Photo P-3.2

Photo P-3.3

Photo P-3.4

Photo P-3.5

Photo P-3.6

Photo P-3.7

Photo P-3.8

Details of flow parameter of the experimental channels and the associated experimental runs are given in Table-3.2. Using the downstream tailgate, uniform flow is maintained for each experimental runs and for each channel by maintaining the water surface slope parallel to the valley bed slope. All the observations are recorded in the central test reach for straight channel of Type-I and one wave length in central reach of Type-II and Type-III meandering channels.

Table3.2   Hydraulics details of the experimental runs

Sl.No	Item description		Straight (Type I)	Meander (Type II)	Meander (Type III)
1.	Number of runs for stage-discharge data	Simple channel	Inbank 11	Inbank 15	Inbank 15
		Compound channel	overbank 10	overbank 12	overbank 12
2.	Discharges (cm^3/s)	Inbank flow	1061, 1280, 2148, 2307, 2902, 3249, 4117, 4548, 5058, 5947, 6312	316, 426, 1347, 1669, 2200, 2357, 2619, 2757, 2946, 3338, 3698, 4191, 4656, 5596, 5680	287, 484, 987, 1742, 2048, 2757, 3224, 3338, 3698, 4191, 4656, 5122, 5515, 6396, 7545
		Overbank flow	8726, 10007, 12245, 13004, 16706, 19861, 25329, 30844, 36275, 39071	9006, 10107 10898, 12245 13005, 15289 15998, 16762 19866, 20523 25661, 31358	12757, 13974, 24487, 27185, 31299, 33817, 37173, 39048, 41416, 44412, 46014, 48474
3.	Depth of flow (cm) corresponding to flow discharge of runs (2)	Inbank flow	3.02, 3.44, 4.98, 5.24, 6.21, 6.80, 8.15, 8.82, 9.55, 10.92, 11.48	1.29, 1.57, 3.44, 4.05, 4.98, 5.31, 5.78, 6.08, 6.41, 7.11, 7.7, 8.55, 9.34, 10.9, 11.01	1.05, 1.44, 2.22, 3.13, 3.44, 4.1, 4.55, 4.65, 4.93, 5.3, 5.62, 5.93, 6.18, 6.71, 7.33
	Relative depth β [(Ratio of depth over main channel *(H-h)* to total depth *(H)*]	Overbank flow	*0.12, 0.15, 0.19, 0.21,0.26,0.30, 0.36,* 0.41, *0.44, 0.46*	*13.32, 13.68,* 13.89, 14.23, 14.42, 14.95, 15.11, 15.28, *15.94, 16.08,* 17.1, 18.15	8.74, 8.86, 9.74, 9.92, 10.17, 10.33, 10.53,10.65,*10.76, * 10.93,11.01,*11.11*
4.	Maximum design depth of flow over floodplain		206.5 mm	203.2 mm	118 mm
5.	Ratio of top width (*B*) to channel width (*b*) i.e. relative width (*α*)		3.667	4.808	16.083
6.	Nature of the surface of bed		smooth and rigid bed	smooth and rigid bed	smooth and rigid bed
7.	No. of runs for detailed measurement of 3 dimensional point Inbank/Over bank		Inbank 0 overbank 5	Inbank 6 overbank 6	Inbank 6 overbank 6

A recirculating system of water supply is established. Two parallel pumps (Photo p 3.9) are used pump water from an underground sump to the overhead tank. The overhead tank has an over flow arrangement to spill excess water to the sump and thus maintain a constant head**.** From the over head tank, water is led to a stilling tank

located at the upstream of the channel. A series of baffle walls between the stilling tank and channels are kept to reduce turbulence of the incoming water. At the end of the experimental channel, water is allowed to flow through a tailgate and is collected in a masonry volumetric tank from where it is allowed to flow back to the underground sump. From the sump water is pumped back to the overhead tank, thus setting a complete re-circulating system of water supply for the experimental channel. The tailgate helps to establish uniform flow in the channel. It should be noted that the establishment of a flow that has its water surface parallel to the valley slope (where the energy losses are equal to potential energy input) may become a standard whereby the conveyance capacity of a meandering channel configuration is assessed.

Water surface slope measurement is carried out using a pointer gauge fitted to the traveling bridge (photo P.3.10 and photo P.3.13) operated manually having least count of 0.1 mm. Point velocities are measured with a 16-Mhz Micro ADV (Acoustic Doppler Velocity-meter) at a number of locations across the predefined channel section. Guide rails are provided at the top of the experimental flume on which a traveling bridge is moved in the longitudinal direction of the entire experimental channel. The point gauge and the micro-ADV attached to the traveling bridge can also move in both longitudinal and the transverse direction of the experimental channel at the bridge position. The micro-ADV readings are recorded in a computer placed besides the bridge (photo P.3.11a and photo P.3.11 b). As the ADV is unable to read the data of upper most layer (up to 5cm from free surface), a micro -Pitot tube (photo P.3.12a and photo P.3.12 b) of 4 mm external diameter in conjunction with suitable inclined manometer are used to measure velocity and its direction of flow at the pre defined points of the flow-grid. A flow direction finder (photo P. 3.12a and photo P. 3.13) is also used to get the direction of maximum velocity with respect to the longitudinal flow direction. The Pitot tube is physically rotated normal to the main stream direction till it gives maximum deflection of manometer reading. The angle of limb of Pitot tube with longitudinal direction of the channel is noted by the circular scale and pointer arrangements attached to the flow direction meter.

Discharge in the channel is measured by the time rise method. The water flowing out at the down stream end of the experimental channel is led to a rectangular

measuring tank of 1690 mm long × 1030 mm wide for Type-I channel, 1985 mm long ×1900 mm wide for the Type-II channel, and 2112 mm long × 3938.92 mm wide tank for Type-III channel. The change in the depth of water with time is measured by a glass tube indicator (photo P.3.14) with a scale having least count of 0.01mm.

3.2   EXPERIMENTAL PROCEDURE

3.2.1   DETERMINATION OF CHANNEL SLOPE

By blocking the tail end, the impounded water in the channel is allowed to remain standstill. The level difference between channel bed and water surface are recorded at a distance of one wavelength along its centerline for Type-II and Type-III channels. The mean slopes for Type-II and Type-III channels is obtained by dividing the level difference between these two points by the length of meander wave along the centerline. For Type-I channel, the mean slope is obtained by dividing the level difference between the two end points of the test reach of 1m along the centerline.

3.2.2 MEASUREMENT OF DISCHARGE AND WATER SURFACE ELEVATION

A point gauge with least count of 0.1 mm is used to measure the water surface elevation above the bed of the main channel or flood plain. As mentioned before, a measuring tank located at the end of each test channel receives water flowing through the channels. Depending on the flow rate, the time of collection of water in the measuring tanks vary between 50 to 262 seconds, lower one for higher rate of discharge. Change in the mean water level in the tank over the time interval is recorded. From the knowledge of the volume of water collected in the measuring tank and the corresponding time of collection, the discharge flowing in the experimental channel for each run of each channel is obtained.

Photo P-3.9

Photo P-3.10

Photo P-3.11(a)

Photo P-3.11(b)

Photo P-3.12(a and b)

Photo P-3.13

Photo P-3.14

3.2.3   MEASUREMENT OF VELOCITY AND ITS DIRECTION

A 16-MHz Micro ADV (Acoustic Doppler Velocity-meter) from M/s Son-Tek, San Diego, Canada is used for 3-axis (3D) velocity measurement at each grid point of the channel sections. The higher acoustical frequency of 16 MHz makes the Micro-ADV the optimal instrument for laboratory study. The Micro ADV with the software package is used for taking high-quality three dimensional velocity data at different points. The data is received at the ADV-processor. A computer attached with the processor shows the 3-dimensional velocity data after compiling with the software package. At every point, the instrument records a number of velocity data per minute. With the statistical analysis using the installed software, mean values of 3D point velocities are recorded for each flow depth. The Micro-ADV uses the Doppler shift principle to measure the velocity of small particles, assuming to be moving at velocities similar to the fluid. Velocities is resolved into three orthogonal components (tangential, radial, and vertical) and are measured at 5 cm below the sensor head, minimizing interference of the flow field, and allowing measurements to be made close to the bed. The Micro ADV has excellent features such as

- Three-axis velocity measurement
- High sampling rates - up to 50 Hz
- Small sampling volume - less than 0.1 cm^3
- Small optimal scatterer - excellent for low flows
- High accuracy upto1% of measured range
- Large velocity ranges between 1 mm/s to 2.5 m/s
- Excellent low-flow performance
- No recalibration needed
- Comprehensive software

The ADV is unable to read the upper layer velocity, that is, up to 50 mm from free surface. To overcome the short, a standard Prandtl type micro-Pitot tube in conjunction with a manometer of accuracy 0.12 mm is used for the measurement of point velocity readings at the specified location for the upper 50 mm region from free surface across the channel. The results from the observations have been discussed in the next chapter.

A flow direction meter is used to find the direction of the velocity readings taken by micro Pitot tube in the experimental channel. It essentially consists of a copper tube at lower end of which a metal pointer rod tied with a thread is attached, while another pointer at the upper end of the tube moves over a circular metallic protractor. The copper tube is fixed with the protractor through a ball bearing arrangement. The thread tied to the pointer rod is lowered into water that moves along the resultant direction of flow. The copper tube with the metal pointer rod at upper end is made to rotate till the pointer and thread are in a vertical straight line parallel to each other. The angle of rotation by upper pointer with the metallic protractor gives the direction of flow. The deviation of the angle of flow shown by the pointer with respect to the zero position of the metallic protractor (tangential direction) is taken as the local direction of the total velocity vector in the channel. For flow confined to simple meander channel, two predefined sections, that is, AA and BB (Fig.4.2) along the meander path is selected for velocity measurements so as to get a broad picture of flow parameters covering half the meander wave length. For straight compound channels, the measurement section is taken at one section in the central test reach. While taking velocity readings using, Pitot tube, the tube is placed facing the direction of flow and then is rotated along a plane parallel to the bed and till it registers relatively a maximum head difference in the attached manometer. The deviation angle between the reference axis and the total velocity vector is considered positive, when the velocity vector is directed away from the outer bank. The total head h reading by the Pitot tube at the location in the channel is used to give the magnitude of the total velocity as $U = (2gh)^{0.5}$, where g is the acceleration due to gravity. Resolving U into the tangential and radial directions, the local velocity components are determined. While doing so, the tube coefficient is taken as unit and the error due to turbulence in the computation of U is considered negligible. Using the data of velocities by Pitot tube and micro-ADV close to the surface of the channels, the boundary shear at various points on the channel bed at the predefined channel sections are evaluated from the logarithmic velocity distribution relationship which is described in the next chapter.

*****

4.1 GENERAL

The results of experiments concerning the distribution of velocity, flow, and boundary shear stress are presented in this chapter. The discharge against the stage from in-bank to over-bank flow situations for straight symmetrical compound channel (Type-I), meandering compound channels (Type-II and Type-III) are presented in Fig.4.1 (a), Fig. 4.1 (b), and Fig. 4.1 (c) respectively.

4.2 NORMAL DEPTH OF FLOW

In the present investigation involving the flow in simple meandering channels, straight compound channel, and meandering channels with floodplains, achieving steady and uniform flow may be difficult due to the effect of curvature and the influence of a number of geometrical parameters. However, for the purpose of analysis, an overall uniform flow is assumed to exist in the channels. Flow depths in the experimental channel runs are so maintained that the water surface slope becomes parallel to the valley slope. At this stage, the energy losses are taken as equal to potential energy input. This has become a standard whereby the conveyance capacity of a meandering channel configuration can be assessed (Shiono, Al-Romaih, and Knight 1999). Under such conditions, the depths of flow at the channel centerline separated by one wavelength distance must be the same. In all the experimental runs this simplified approach has been tried to achieve. This stage of flow is taken as normal depth, which can carry a particular flow only under steady and uniform conditions.
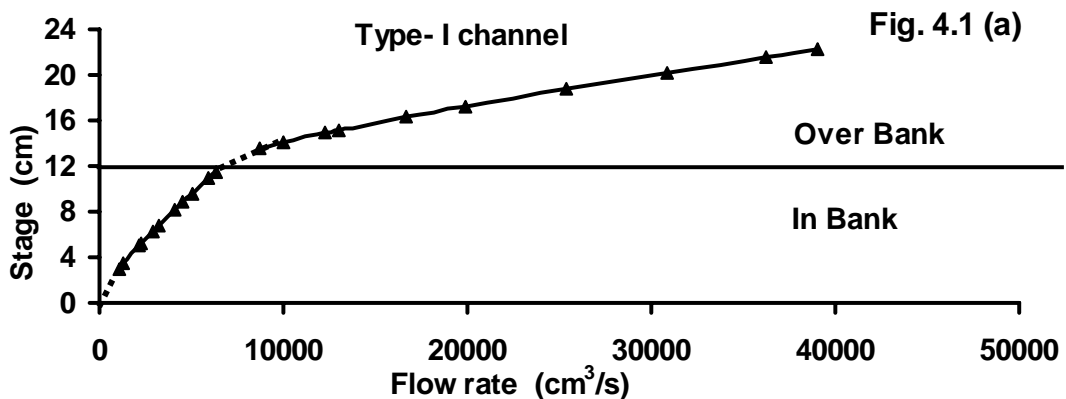
Fig. 4.1 (a)
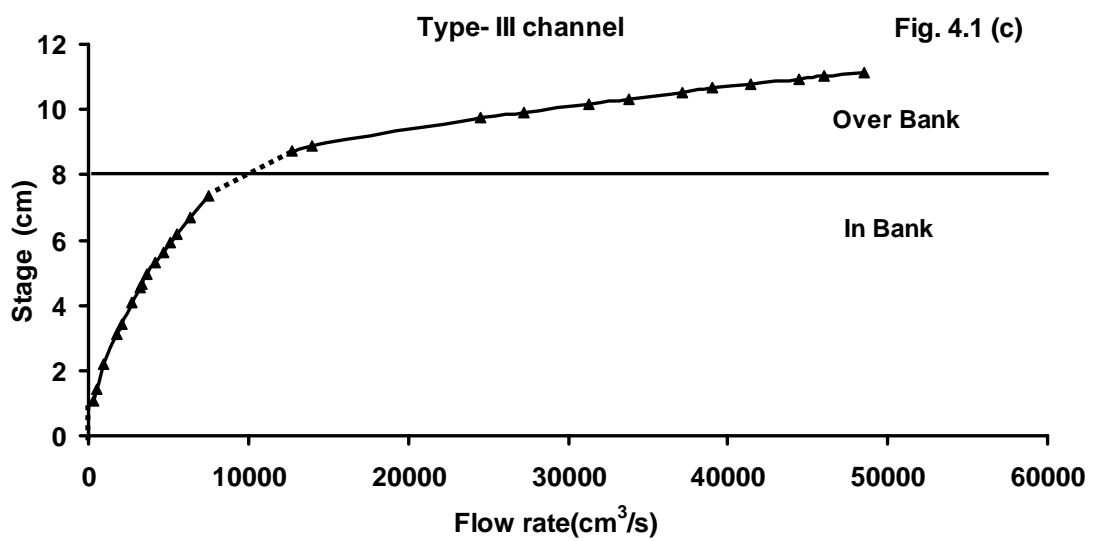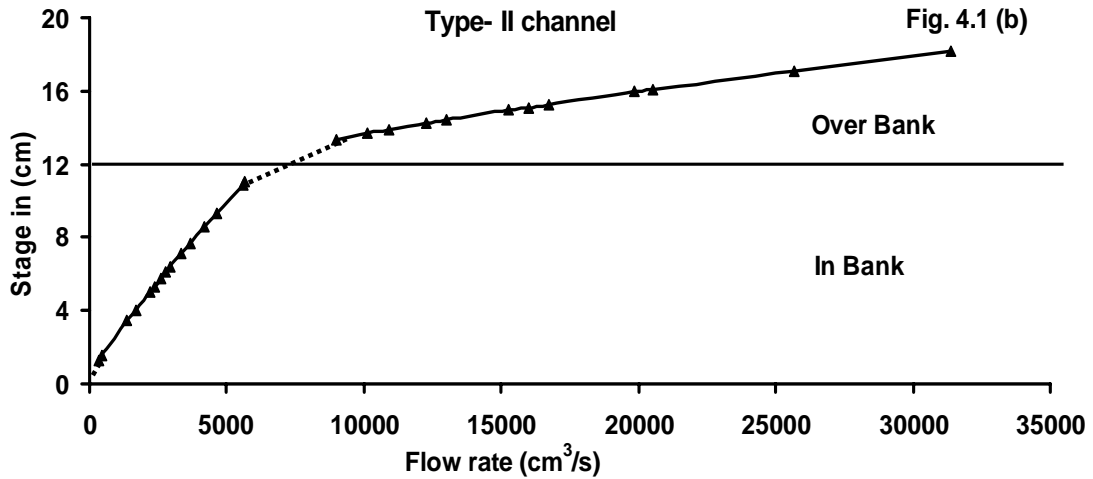
Fig.4.1 (a, b and c) Stage discharge relationships for the experimental channels

4.3 DISTRIBUTION OF TANGENTIAL (LONGITUDINAL) VELOCITY

Measurement of velocity for the experimental channels is mostly recorded by a micro-ADV. The instrument uses the sign convention for 3-dimensional velocity as positive for ENU (east, north and upward) and negative for WSD (west, south and down ward) directions respectively for the longitudinal (V_x), radial (V_y) and vertical components (V_z). For the experimental channel position, east refers to the direction of longitudinal velocity. The east probe of ADV is kept in the longitudinal flow direction. Accordingly the other two flow directions are referred. In the experiments for meandering simple and compound channels, the readings are taken at the bend apex with tangential velocity direction taken as east. For radial velocity, positive stands for outward and negative stands for inward radial velocity direction. Similarly

for vertical component of velocity when the ADV readings shows positive, then the velocity component is upward and if negative, it is in the down-ward direction.
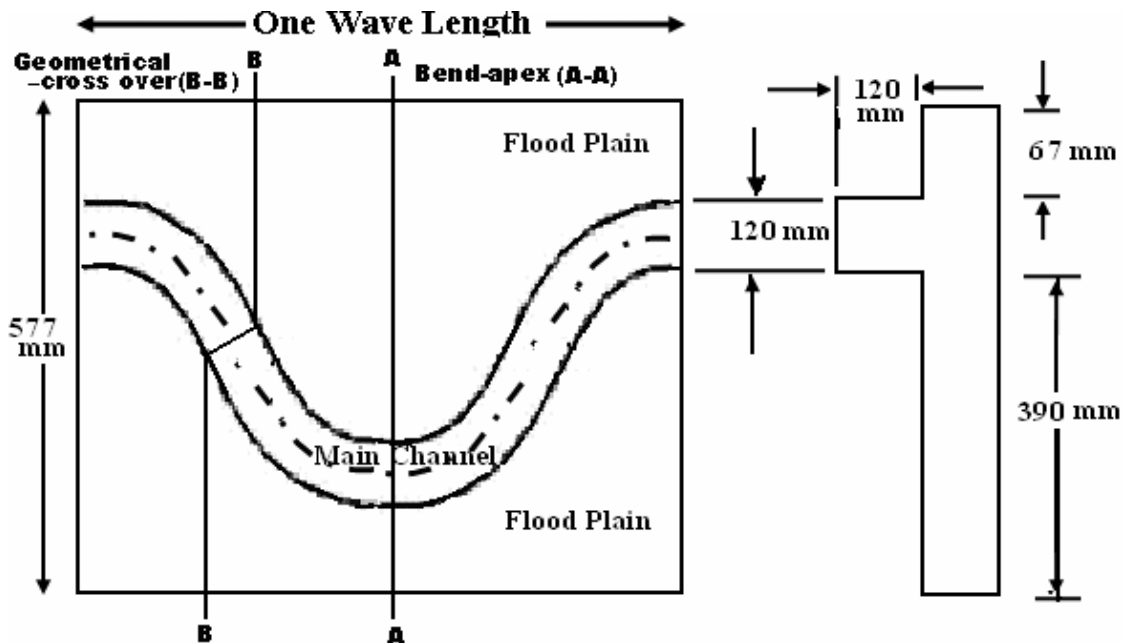
Fig. 4.2 Location of bend apex AA and geometrical cross over BB (both for in-bank and over bank conditions) of Type-II meandering channel

For simple meander channels, the radial distribution of tangential velocity in contour form for the runs of meandering channels of Type-II at locations AA (bend apex) and BB (geometrical cross over) are shown in Figs. 4.3.1 through Fig. 4.3.6 and Figs. 4.3.7 through Fig. 4.3.12 respectively. Similarly for Type-III channels the radial distributions of tangential velocity at bend apex location AA are shown in Figs.4.4.1-4.4.6 and at geometrical cross over location BB it is shown in Figs. 4.4.7 to 4.4.12 respectively. For the meander channel with floodplains (Type-II and Type-III series) at locations AA and BB, the corresponding longitudinal velocity contours are shown in Figs. 4.5.1-4.5.12 and 4.6.1-4.6.12 respectively. Figs.4.3.1-4.3.6 and Figs.4.4.1-4.4.6 also show the boundary shear distribution for simple meandering channels of Type-II and Type-III respectively. For meandering channels with floodplain of Type-II and Type-III channels the boundary shear distribution are shown in Figs.4.5.1- Fig.4.5.6 and Figs.4.6.1- Fig.4.6.6 respectively. For the straight compound channels of Type-I the radial distribution of tangential velocity with the boundary shear distribution are shown in Figs.4.7.1- Fig.4.7.5.
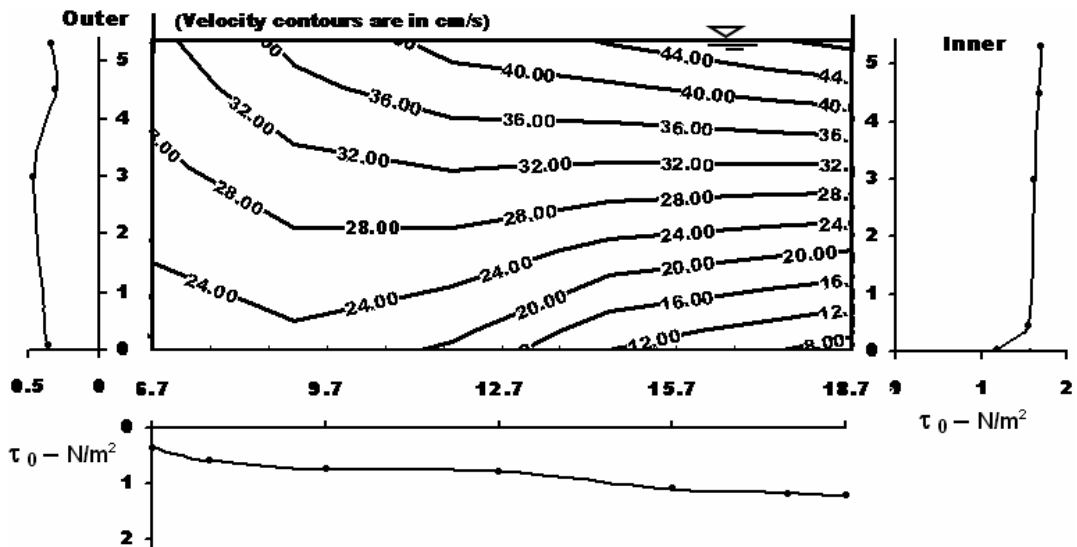
Fig. 4.3.1- In bank depth *h'* = 5.31cm (Type-II channel at bend apex AA)
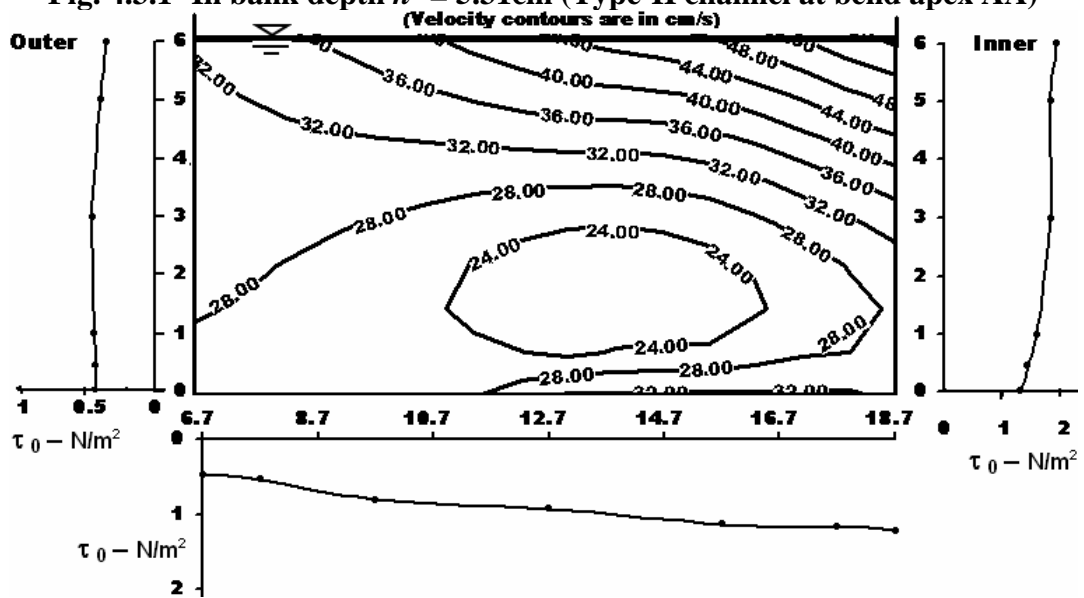
Fig 4.3.2- In bank depth *h'* = 6.08 cm (Type-II channel at bend apex AA)
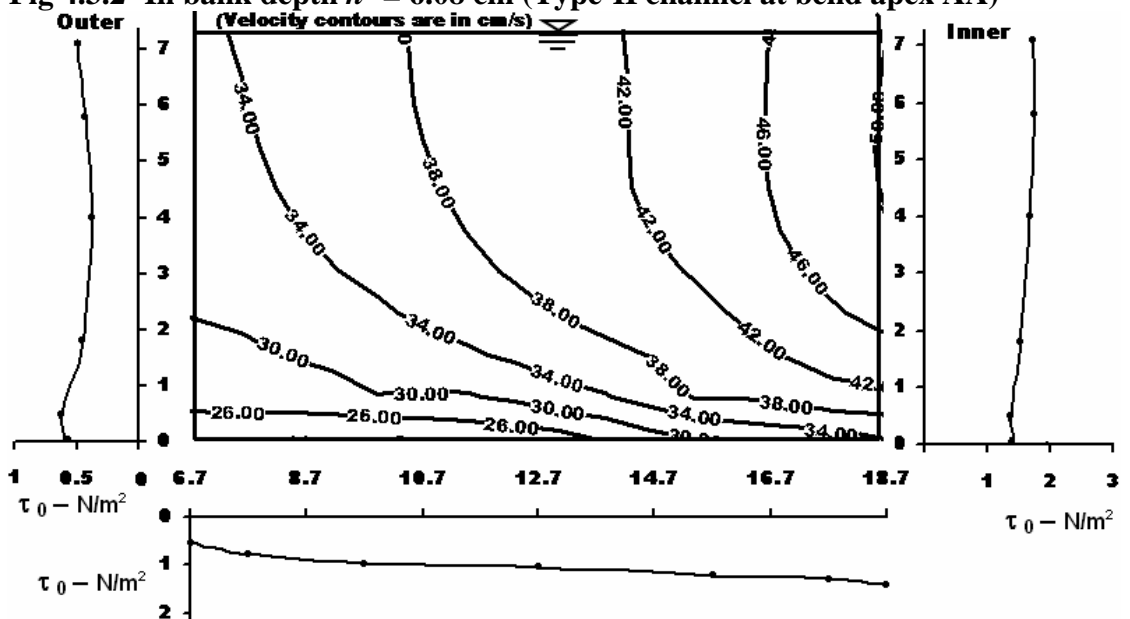
Fig. 4.3.3- In bank depth *h'* = 7.11 cm (Type-II channel at bend apex AA)
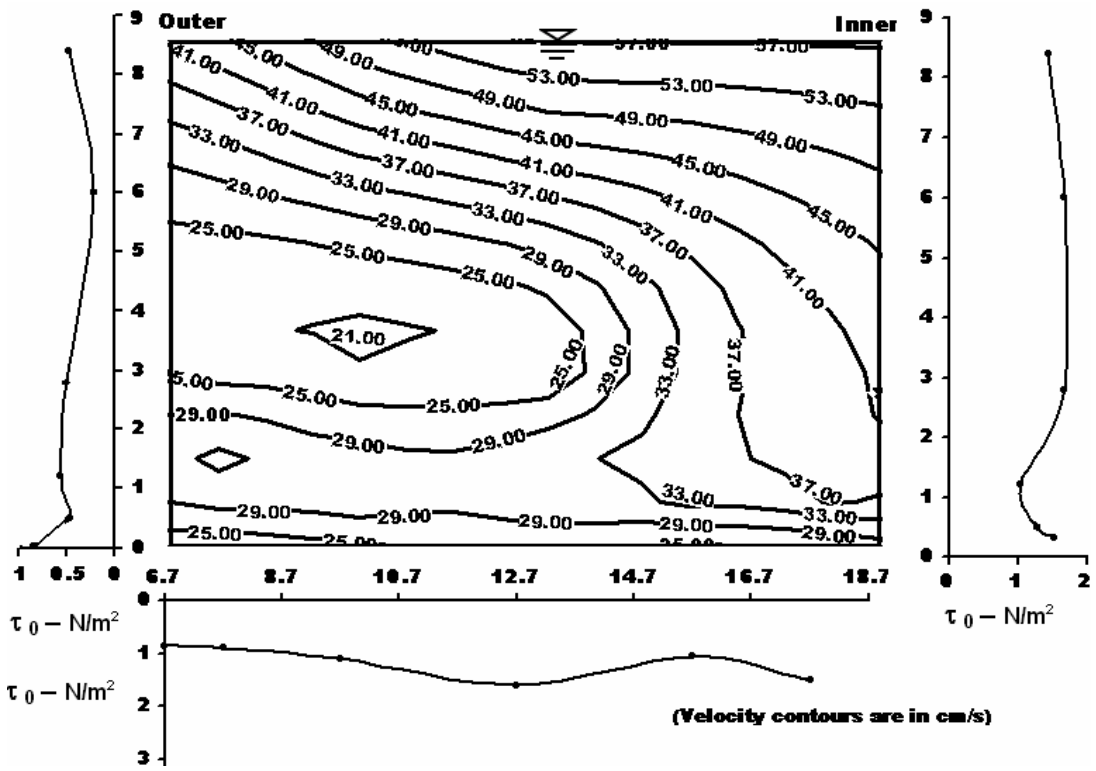
Fig. 4.3.4- In bank depth *h' = 8.55 cm (Type-II channel at bend apex AA)
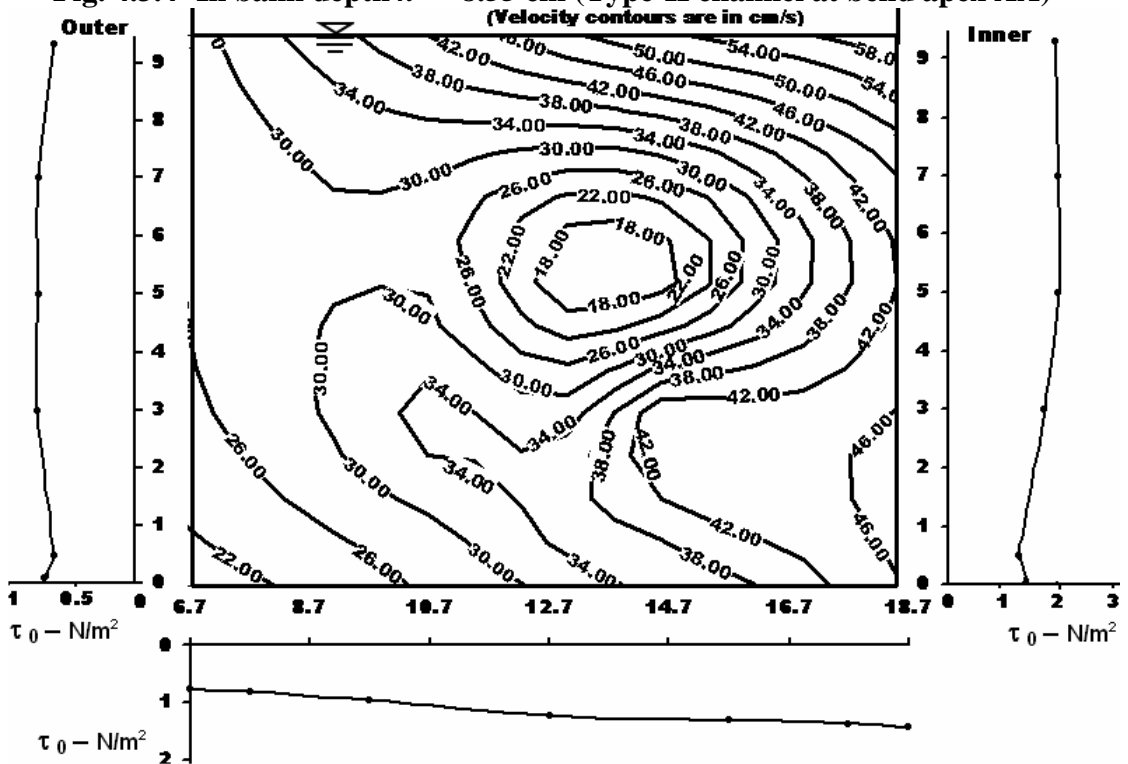
Fig. 4.3.5- In bank depth *h' = 9.34 cm (Type-II channel at bend apex AA)

Fig. 4.3.6- In bank depth $h' = 11.01$ cm (Type-II channel at bend apex AA)

Figs.4.3.1-4.3.6 Contours showing the distribution of tangential velocity and boundary shear distribution at bend apex (section AA) of simple meandering (Type-II) channels.

Fig. 4.3.7- In bank depth $h' = 5.31$ cm (Type-II channel at cross-over BB)
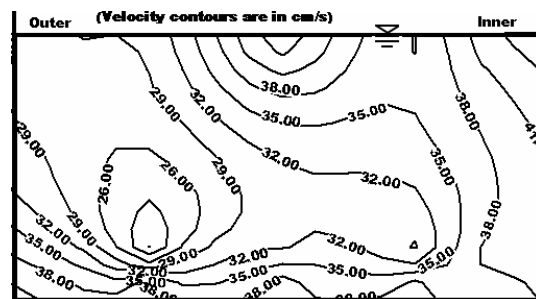
Fig. 4.3.8- In bank depth $h' = 6.08$ cm (Type-II channel at cross-over BB)
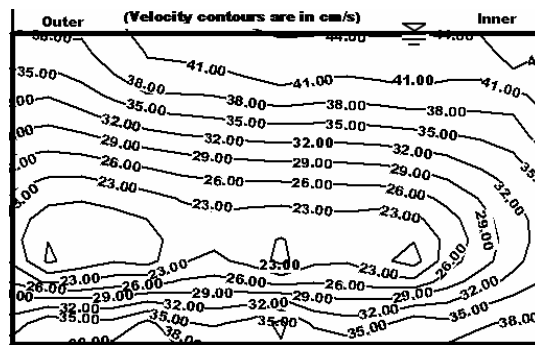
Fig. 4.3.9- In bank depth $h' = 7.11$ cm (Type-II channel at cross-over BB)
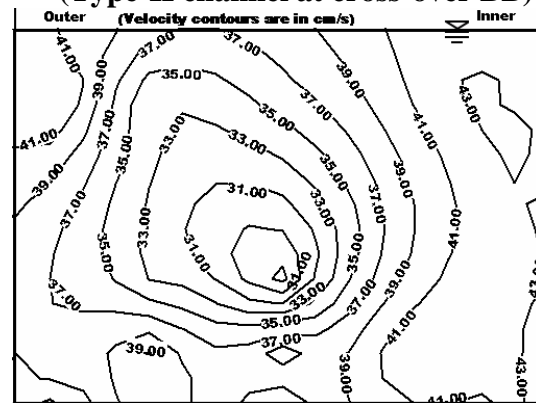
Fig. 4.3.10- In bank depth $h' = 8.55$ cm (Type-II channel at cross-over BB)

- 41 -
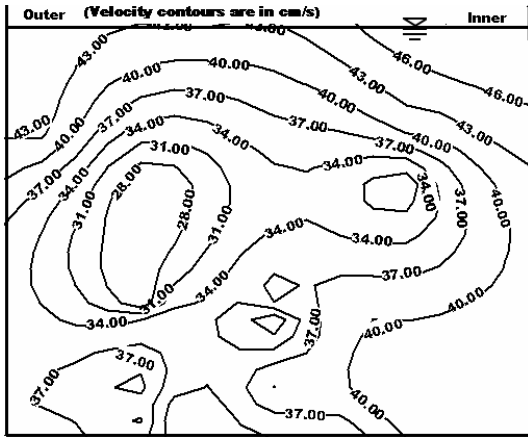
Fig. 4.3.11- In bank depth *h'* =9.34 cm **Fig. 4.3.12- In bank depth *h'* = 11.01 cm**
(Type-II channel at cross-over BB) **(Type-II channel at cross-over BB)**
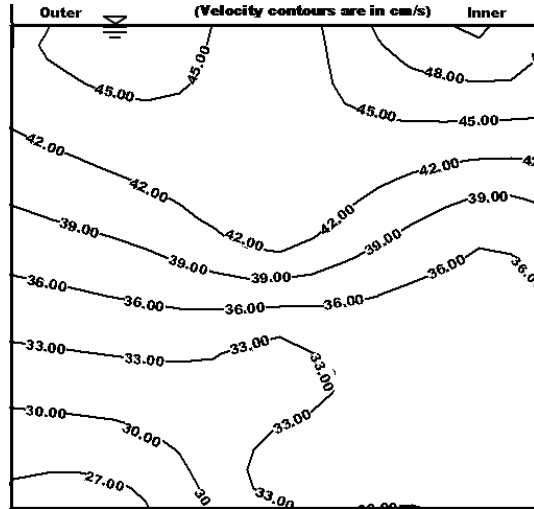
Figs.4.3.7-4.3.12 Contours showing the distribution of tangential velocity at geometrical cross-over (section BB) of simple meandering (Type-II) channels.
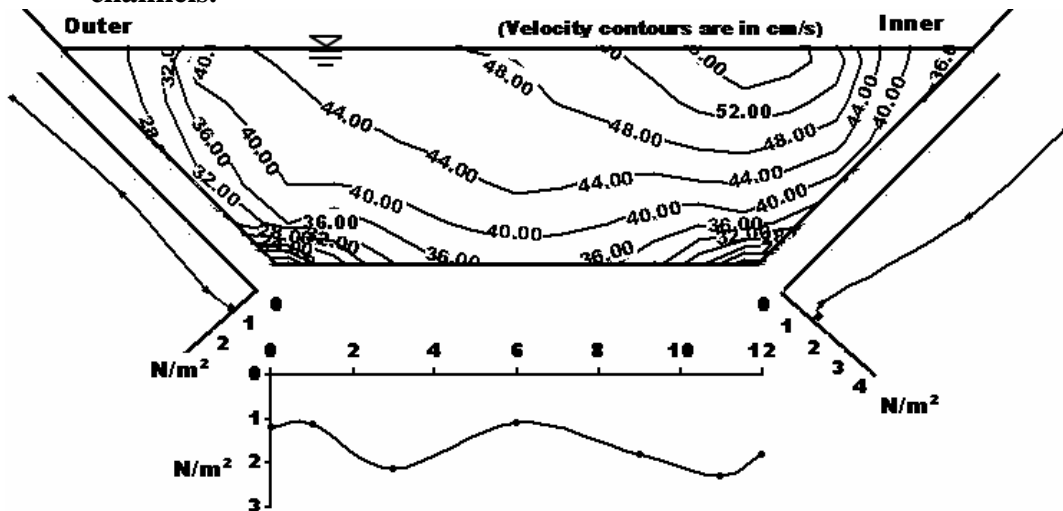
Fig. 4.4.1- In bank depth *h'* = 5.3 cm (Type-III channel at bend apex AA)

Fig. 4.4.2- In bank depth *h'* =5.62 cm (Type-III channel at bend apex AA)

Fig. 4.4.3- In bank depth *h'* =5.93 cm (Type-III channel at bend apex AA)

Fig. 4.4.4- In bank depth *h'* =6.18 cm (Type-III channel at bend apex AA)
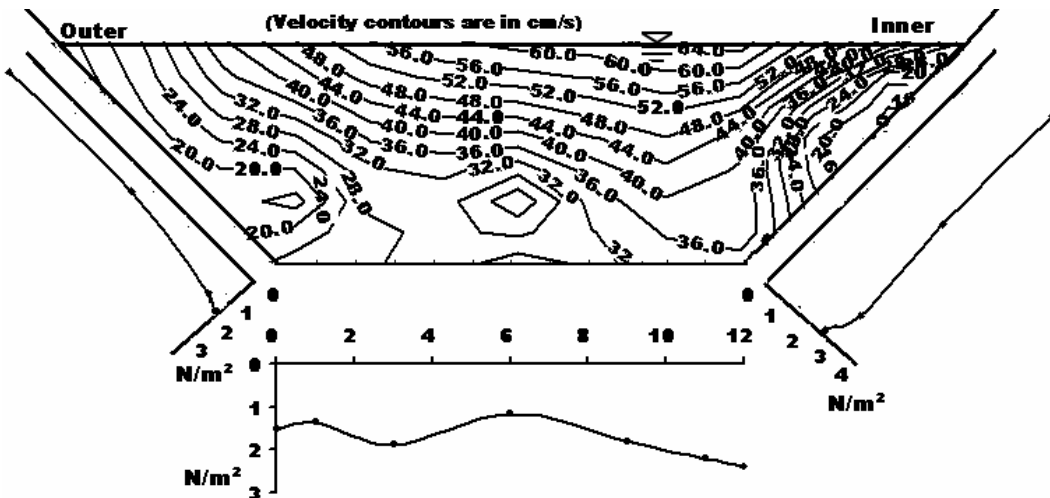
Fig. 4.4.5- In bank depth *h'* =6.71 cm (Type-III channel at bend apex AA)
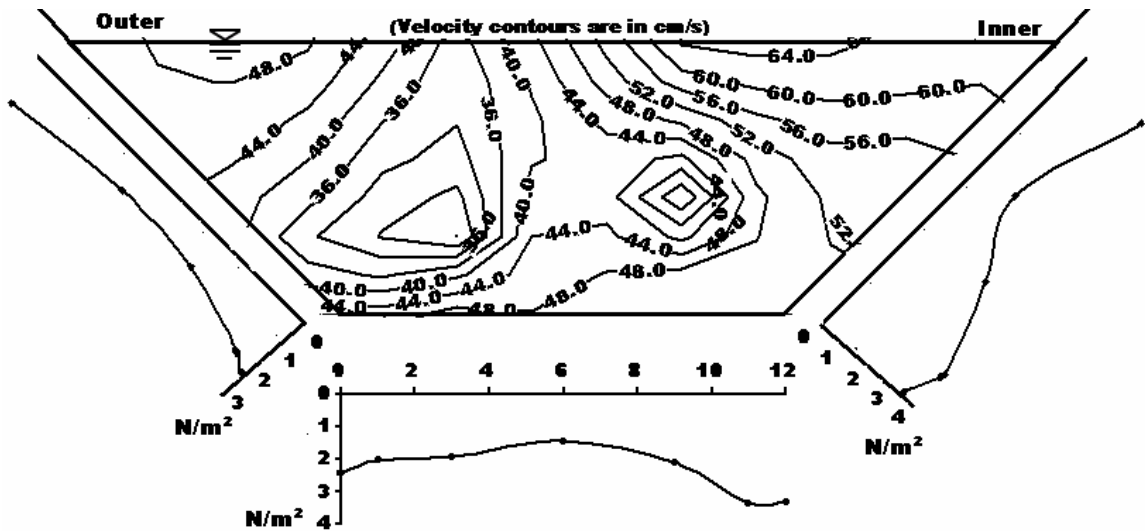
Fig. 4.4.6- In bank depth *h'* =7.33 cm (Type-III channel at bend apex AA)

Figs.4.4.1-4.4.6 Contours showing the distribution of tangential velocity and boundary shear distribution at bend apex (section AA) of simple meandering (Type-III) channels.
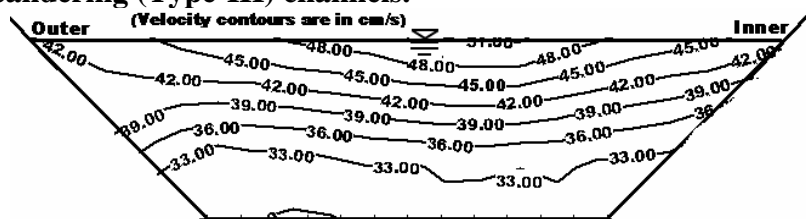
Fig. 4.4.7- In bank depth *h'* = 5.3 cm (Type-III channel at cross-over BB)
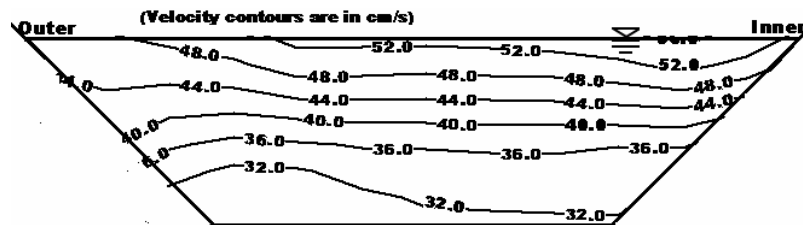
Fig. 4.4.8- In bank depth *h'* = 5.62 cm (Type-III channel at cross-over BB)
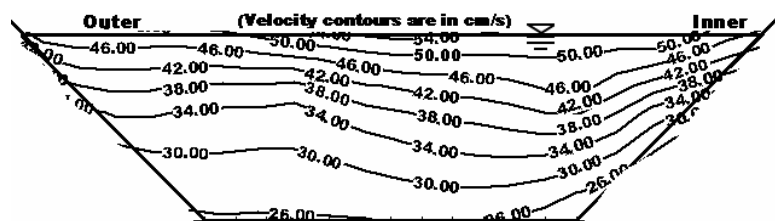
Fig. 4.4.9- In bank depth *h'* = 5.93 cm (Type-III channel at cross-over BB)
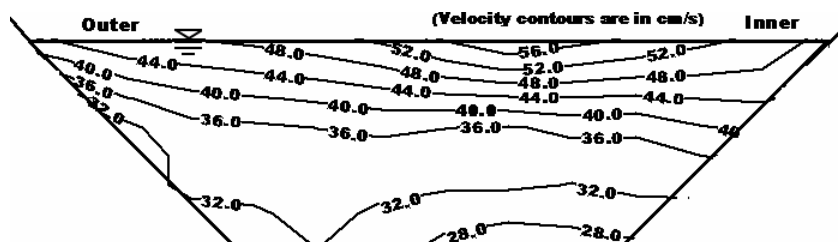
Fig. 4.4.10- In bank depth *h'* = 6.18 cm (Type-III channel at cross-over BB)
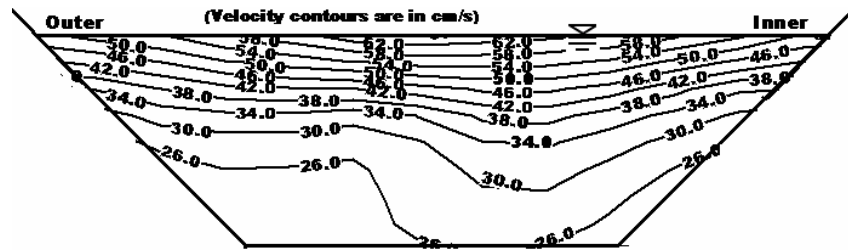
Fig. 4.4.11- In bank depth *h' = 6.71 cm (Type-III channel at cross-over BB)
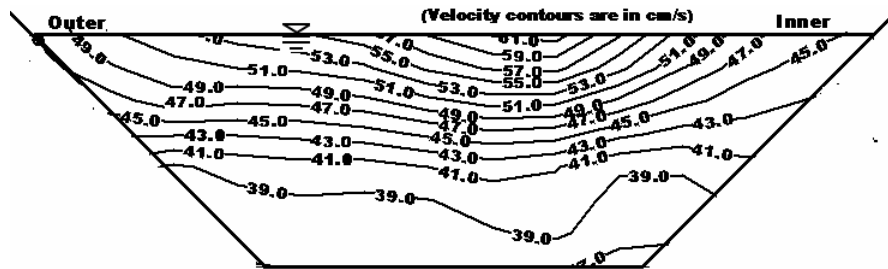
Fig. 4.4.12- In bank depth *h' =7.33 cm (Type-III channel at cross-over BB)

Figs.4.4.7-4.4.12 Contours showing the distribution of tangential velocity at geometrical crossover (section BB) of simple meandering (Type-III) channels.

4.3.1   SIMPLE MEANDER CHANNEL

From the distribution of tangential velocity in simple meander channel sections in contour form (Figs. 4.3.1 to Fig.4.3.12 and Figs. 4.4.1 to Fig.4.4.12) at the locations AA and BB the following features can be noted.

(i)   The contours of tangential velocity distribution indicate that the velocity patterns are skewed with curvature. At the geometrical cross over BB there, is minimum skewing of the velocity. Higher velocity contours are found to concentrate gradually at the inner bank between geometrical cross over to bend apex. Maximum skewing of the longitudinal velocity can be observed at the point close to the minimum radius of curvature (bend apex AA).

(ii)   Another feature is the location of the thread of maximum velocity along the meander channel. In all the channels, the thread of maximum velocity is found to occur near the inner wall of the channel section, where the radius of curvature is the minimum, i.e., at section AA. At the cross over location BB (location of reversal curvature), the thread of maximum velocity gradually shifts to the channel center confirming the findings of Kar (1977), Bhattacharya (1995), and Patra and Kar (2004), whose experiments were conducted in the deep, strongly meandering channels with rigid boundary. This is strikingly different from the findings of other investigators on

- 45 -

shallow meandering channels. For shallow meandering channels the thread of maximum velocity is located near the outer bank at the bend apex. It indicates that the effect of secondary circulation is predominant in shallow channels and is less effective in deep channels.

(iii) From the contours of tangential velocity at these sections, it can be observed that the distribution of tangential velocity does not follow the power law or the logarithmic law. Under ideal conditions these theoretical velocity distribution laws gives the maximum velocity at the free water surface, where as the flow in any type of natural or laboratory channels do not show such a distribution.

(iv) Sinuosity of the meander channel is found to affect the distribution of tangential velocity considerably. The results of channel Type-II and Type-III (with sinuosity = 1.44 and 1.91 respectively) show irregular tangential velocity distribution. The magnitude and the concentration of velocity distribution are affected by the curvature of the meander channel. Similar reports are also seen for deep channels of Kar (1977) and Das (1984), the distribution of tangential velocity as erratic.
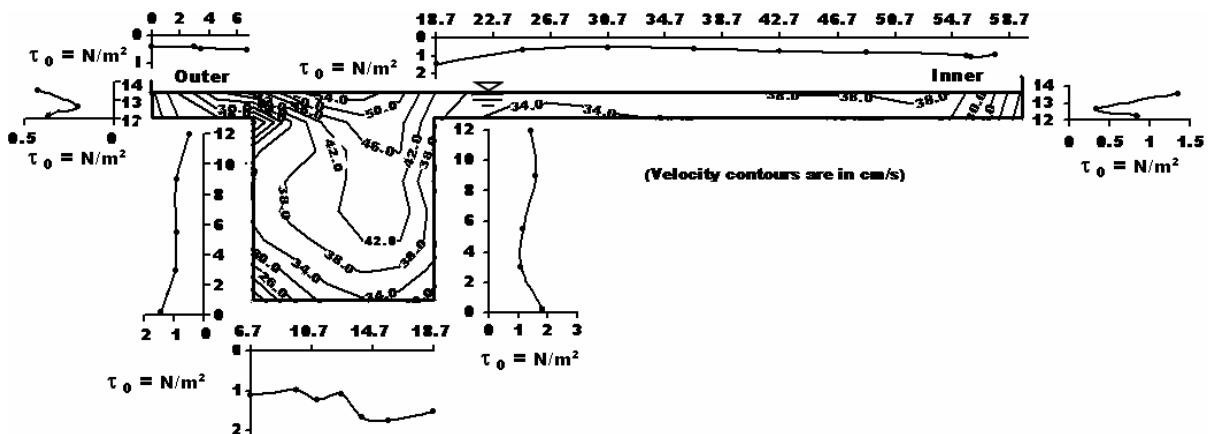
Fig. 4.5.1 Over-bank depth *(H- h)* = 1.68 cm (Type-II channel at bend apex AA)
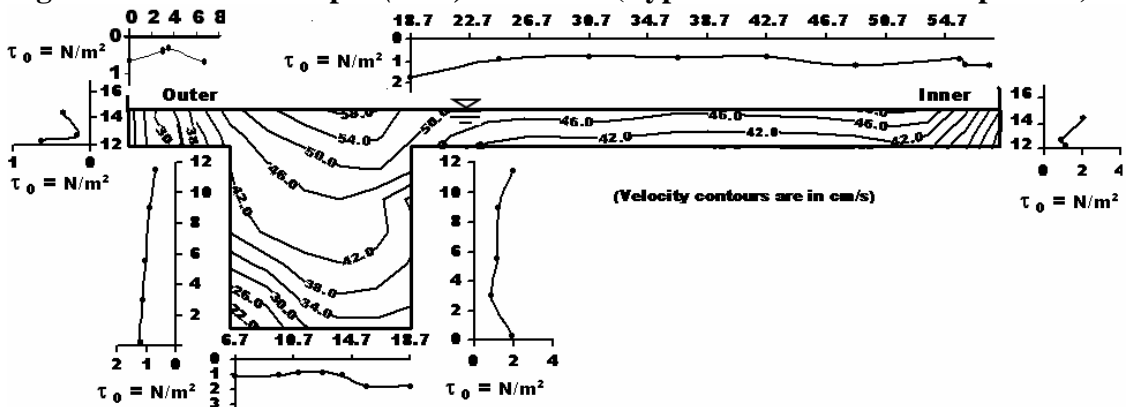
Fig. 4.5.2 Over-bank depth (*H- h*) = 2.42 cm (Type-II channel at bend apex AA)

- 46 -
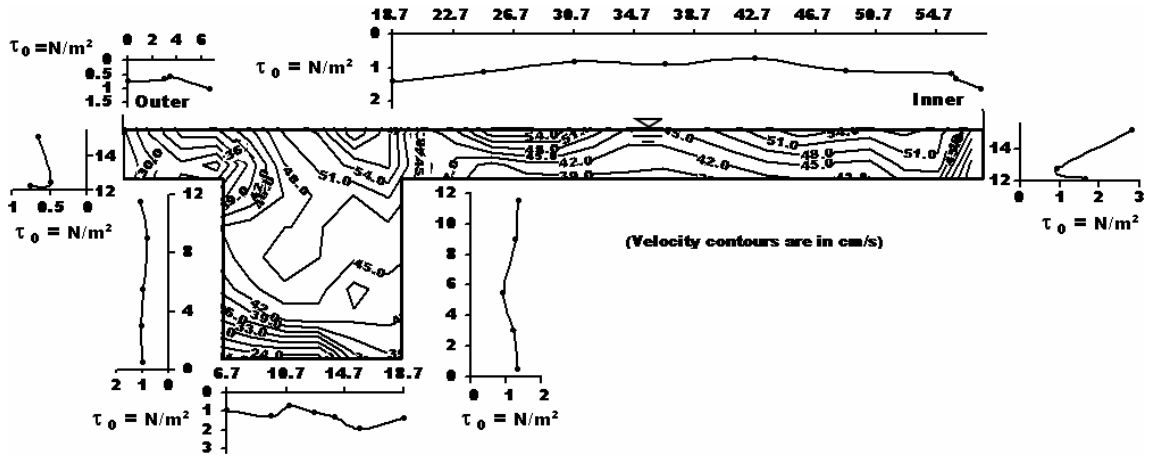
Fig. 4.5.3 Over-bank depth (*H- h*) = 3.28 cm (Type-II channel at bend apex AA)
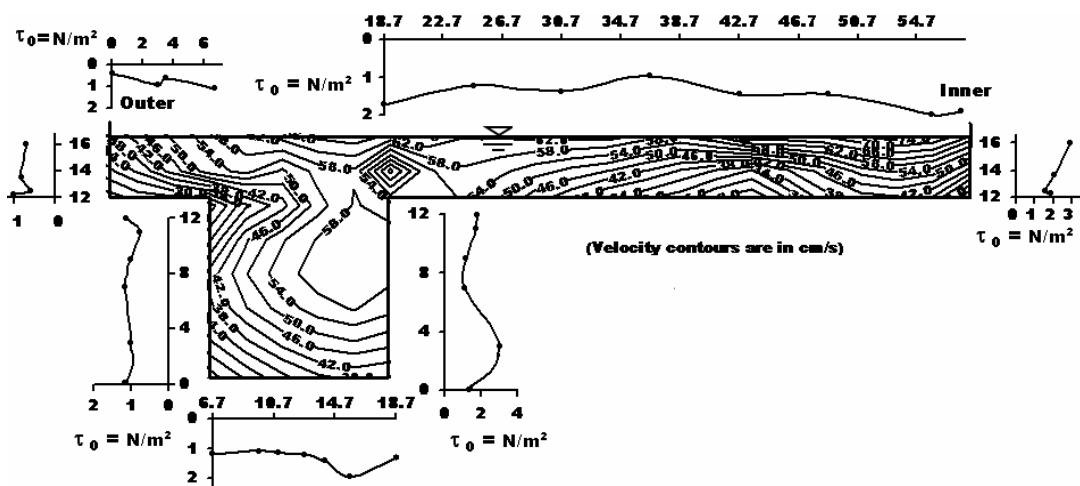
Fig. 4.5.4 Over-bank depth (*H- h*) = 4.08 cm (Type-II channel at bend apex AA)
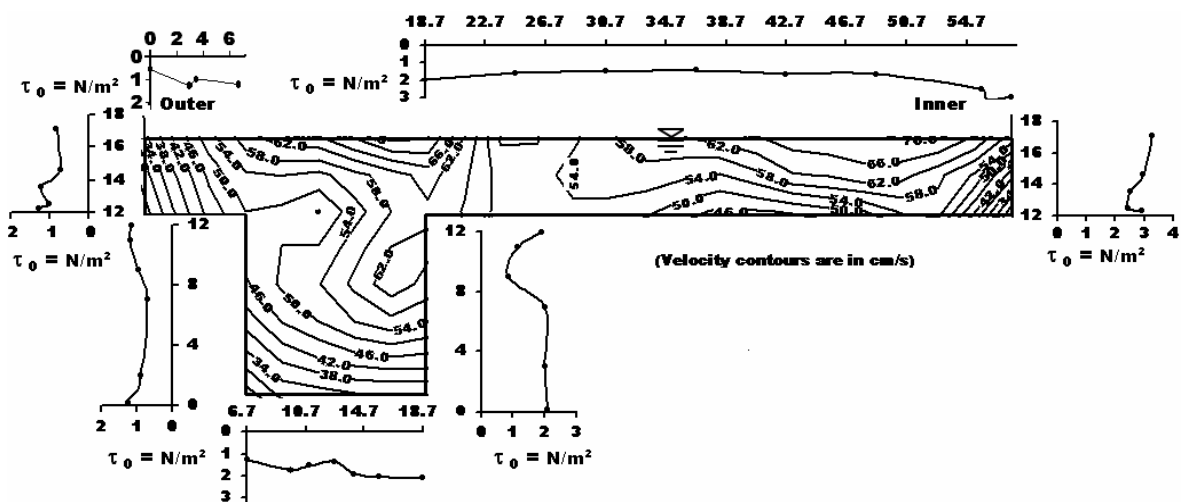
Fig. 4.5.5 Over-bank depth (*H- h*) = 5.10 cm (Type-II channel at bend apex AA)
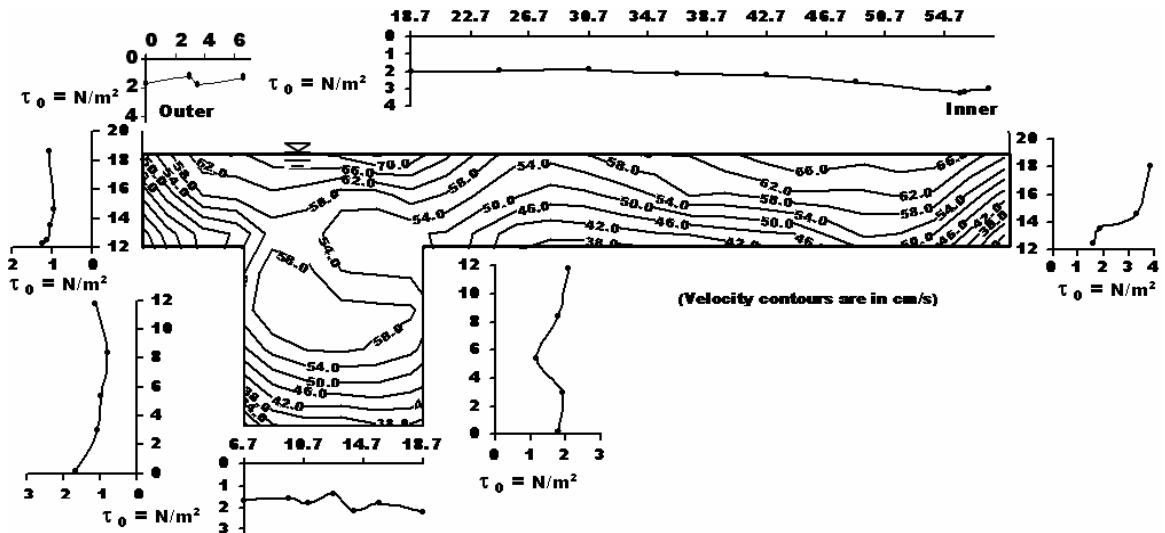
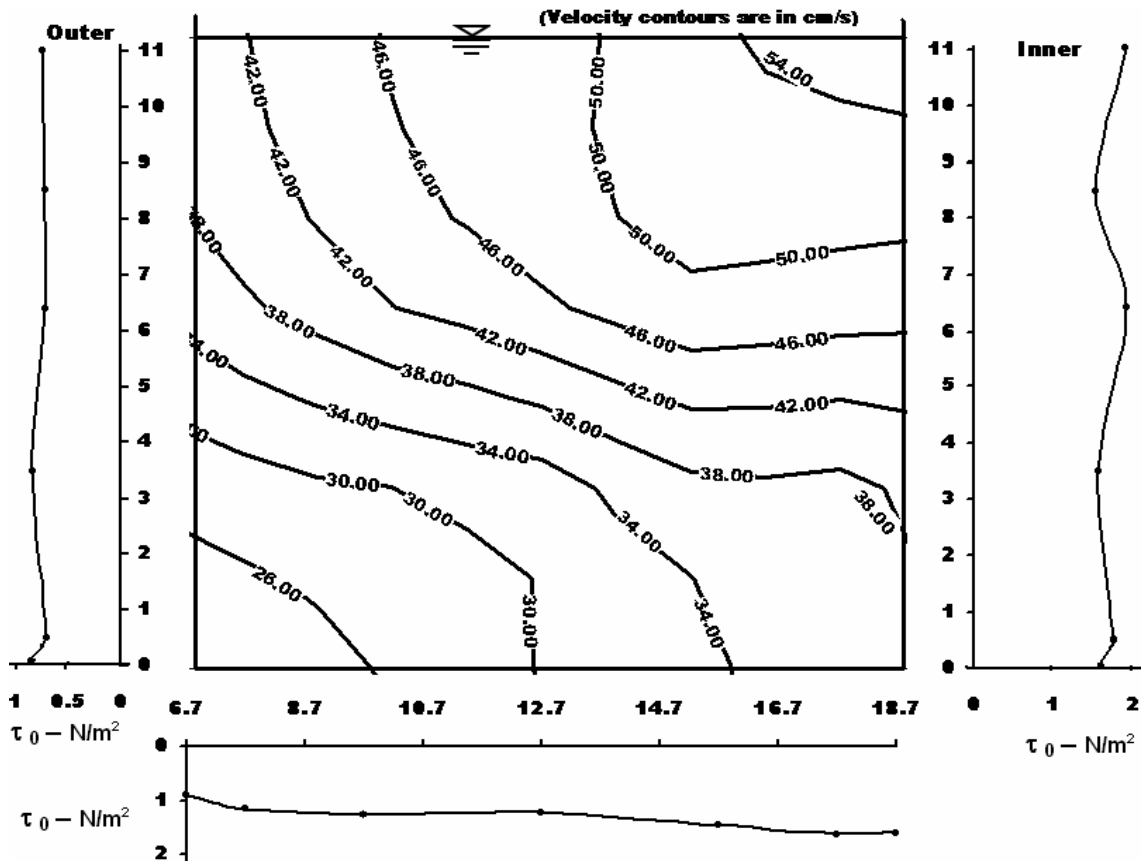**Fig. 4.5.6 Over-bank depth (*H- h*) = 6.15 cm (Type-II channel at bend apex AA)**

Fig.4.5.1-4.5.6 Contours showing the distribution of tangential velocity and boundary shear distribution at bend apex (section AA) of compound meandering (Type-II) channels.
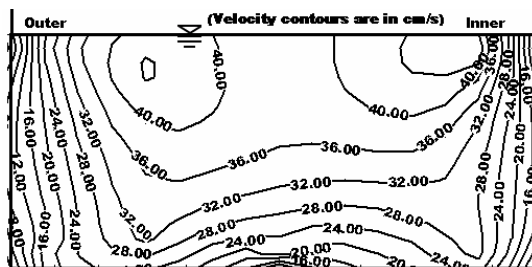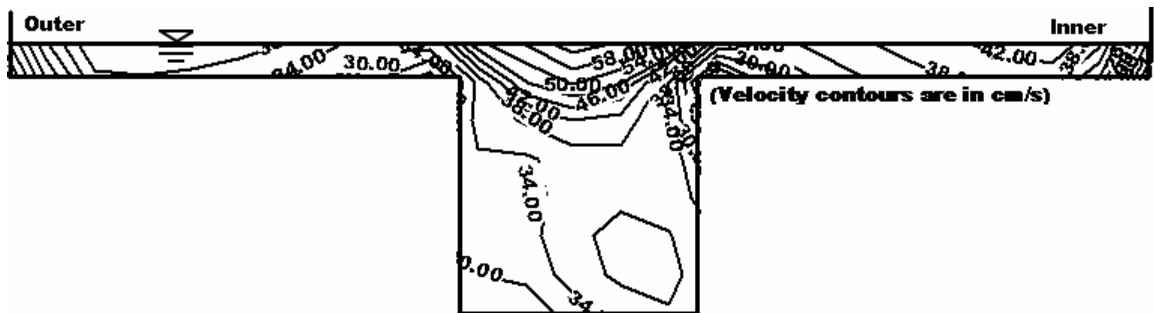

Fig. 4.5.7 Over-bank depth (*H- h*) = 1.68 cm (Type-II channel at cross over BB)
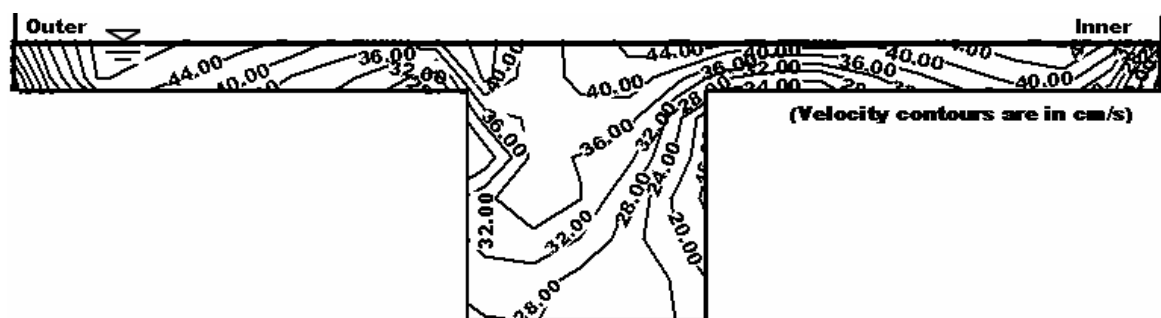
Fig. 4.5.8 Over-bank depth (*H- h*) = 2.42 cm (Type-II channel at cross over BB)
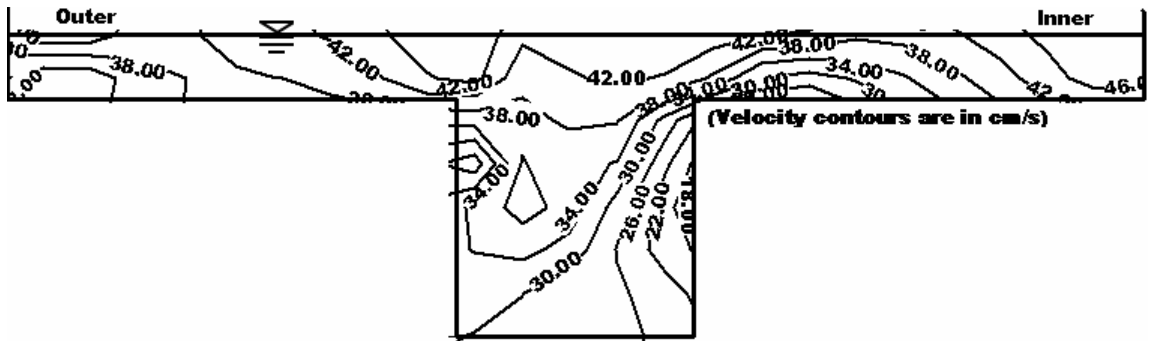
Fig. 4.5.9 Over-bank depth (*H- h*) = 3.28 cm (Type-II channel at cross over BB)
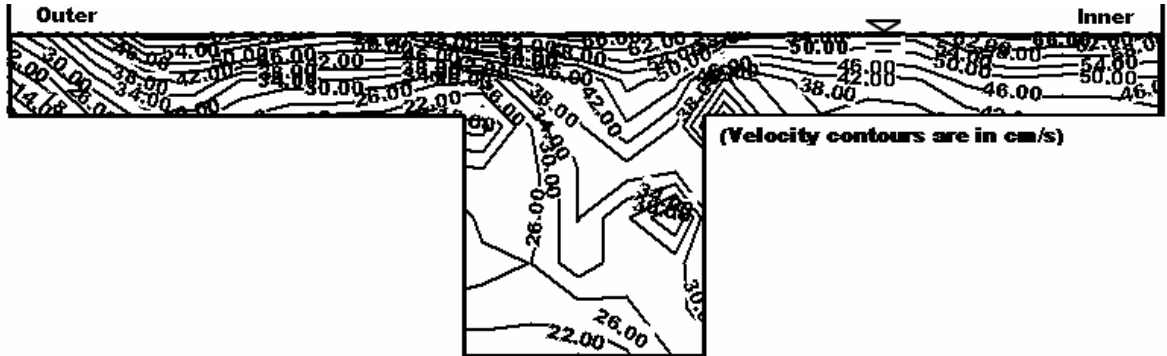
Fig. 4.5.10 Over-bank depth (*H- h*) = 4.08 cm (Type-II channel at cross over BB)
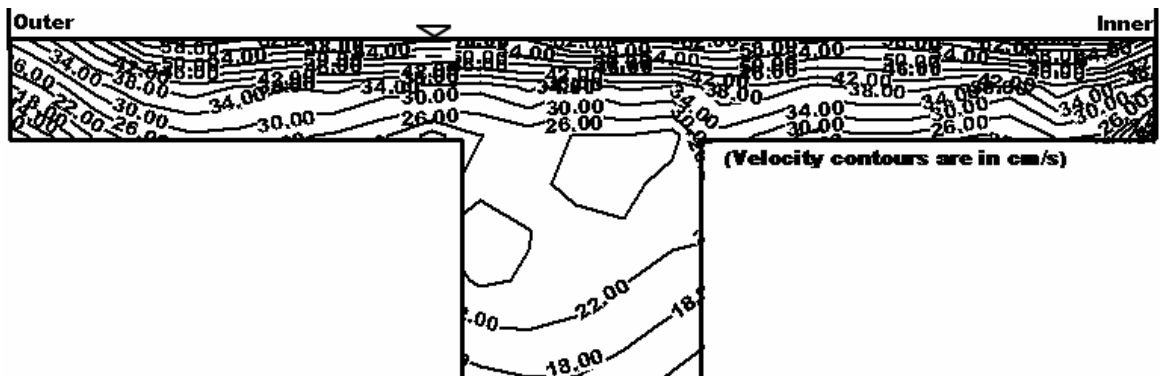
Fig. 4.5.11 Over-bank depth *(H- h)* = 5.10 cm (Type-II channel at cross over BB)

Fig. 4.5.12 Over-bank depth (*H- h*) = 6.15 cm (Type-II channel at cross over BB)

Fig.4.5.7-4.5.12 Contours showing the distribution of tangential velocity at geometrical cross over (section BB) of compound meandering (Type-II) channels.
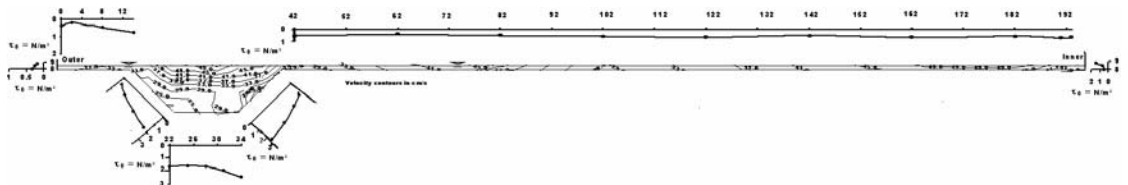
Fig. 4.6.1 Over-bank depth (*H- h*) = 0.74 cm (Type-III channel at bend apex AA)
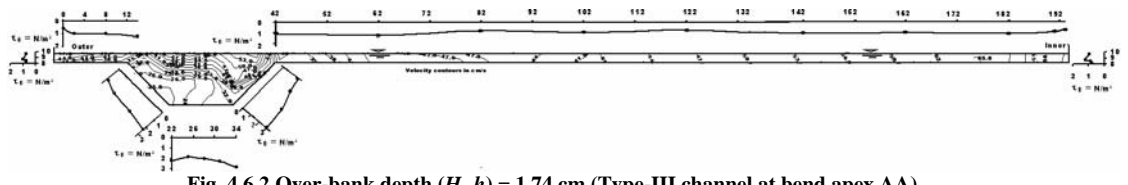
Fig. 4.6.2 Over-bank depth (*H- h*) = 1.74 cm (Type-III channel at bend apex AA)
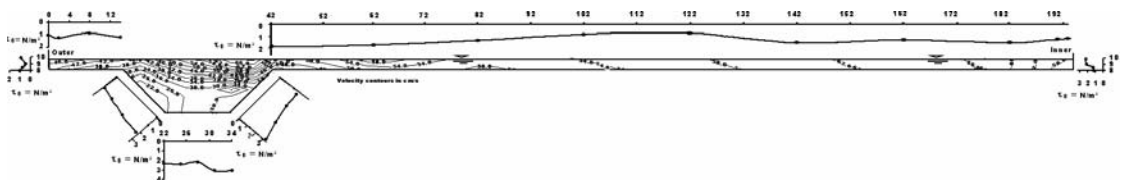
Fig. 4.6.3 Over-bank depth (*H- h*) = 1.92 cm (Type-III channel at bend apex AA)
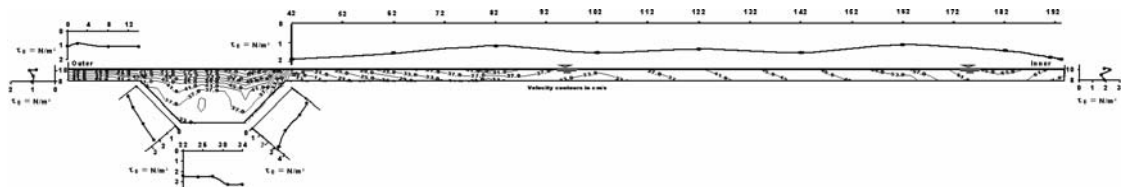
Fig. 4.6.4 Over-bank depth (*H- h*) = 2.17 cm (Type-III channel at bend apex AA)
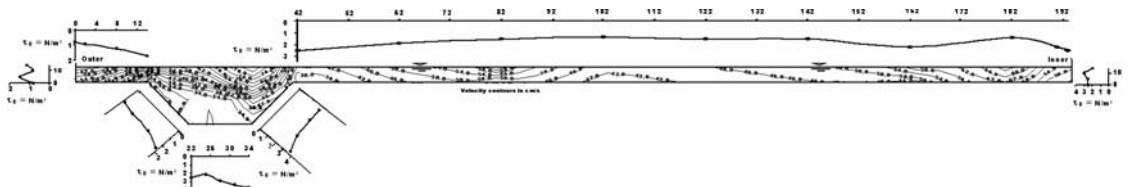
Fig. 4.6.5 Over-bank depth (*H- h*) = 2.93 cm (Type-III channel at bend apex AA)
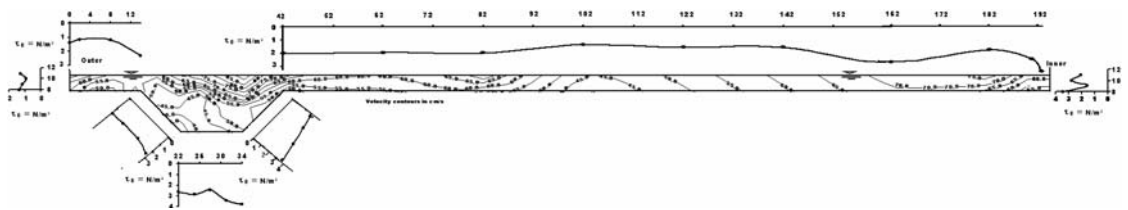
Fig. 4.6.6 Over-bank depth (*H- h*) = 3.01 cm (Type-III channel at bend apex AA)

Fig.4.6.1-4.6.6 Contours showing the distribution of tangential velocity and boundary shear distribution at bend apex (section AA) of compound meandering (Type-III) channels.

Fig. 4.6.7 Over-bank depth (*H- h*) = 0.74 cm (Type-III channel at cross over BB)

Fig. 4.6.8 Over-bank depth (*H- h*) = 1.74 cm (Type-III channel at cross over BB)

Fig. 4.6.9 Over-bank depth (*H- h*) = 1.92 cm (Type-III channel at cross over BB)

Fig. 4.6.10 Over-bank depth (*H- h*) = 2.17 cm (Type-III channel at cross over BB)
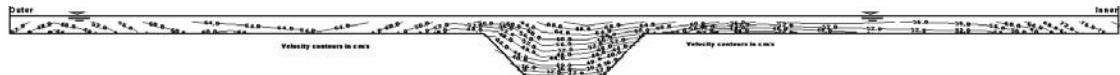
Fig. 4.6.11 Over-bank depth (*H- h*) =2.93 cm (Type-III channel at cross over BB)

Fig. 4.6.12 Over-bank depth (*H- h*) = 3.01 cm (Type-III channel at cross over BB)

Fig.4.6.7-4.6.12 Contours showing the distribution of tangential velocity at geometrical cross over (section BB) of compound meandering (Type-III) channels.

4.3.2 MEANDER CHANNEL WITH FLOODPLAIN

From the isovels of tangential velocity (Figs. 4.5.1.to Figs. 4.5.12 and Figs. 4.6.1.to 4.6.12) for the meander channel - floodplain geometry of Type-II and Type-III channels respectively, the following features are noted.

(i)   Distribution of tangential velocity in the main channel portion is somewhat similar to the patterns observed in the simple meander channels except at the main channel-floodplain junction regions. This is mainly due to the flow interaction between the main channel and floodplain.

(ii)   At the bend apex of both Type-II and Type-III meandering compound channels, the maximum velocity contours are found near the inner wall junction for low over bank depth. For higher over bank depths the maximum velocity contours are found at the inner wall of flood plain.

(iii)   At the section of geometrical cross over region where the radius of curvature is the minimum, the thread of maximum velocity is found to deviate from near the channel centerline to the inner bank. For higher over bank depths at this location, one region of maximum tangential velocity is found near the inner bank of the floodplain.

(iv)   Beginning with the section of geometrical cross over, higher velocity contours are found to concentrate gradually at the inner bank. The tangential velocity is therefore skewed and the maximum skewing is observed at the section of minimum curvature confirming the findings of Kar (1977), Bhattacharya (1995), and Patra and Kar (2004), whose experiments are conducted in the deep, strongly meandering channels with rigid boundary.

(v)   There is significant difference in the mean value of tangential velocity of the main channel when compared to flood plains sub-areas.

(vi)   When the flow overtops the main channel and spreads to the adjoining floodplains, the section mean velocity in the main channel reduces. At low over bank depths, the section mean velocity in the floodplain is found to be less than the main channel. As the depth of flow in the floodplain increases, the section mean velocity in the floodplain also increases. At still higher depths of flow in the floodplain, the section mean velocity of the floodplain is found to be higher than the section mean velocity of the main channel. Again the mean velocity in the inner floodplain is observed to be higher than the outer floodplain at all depths at the bend apex.
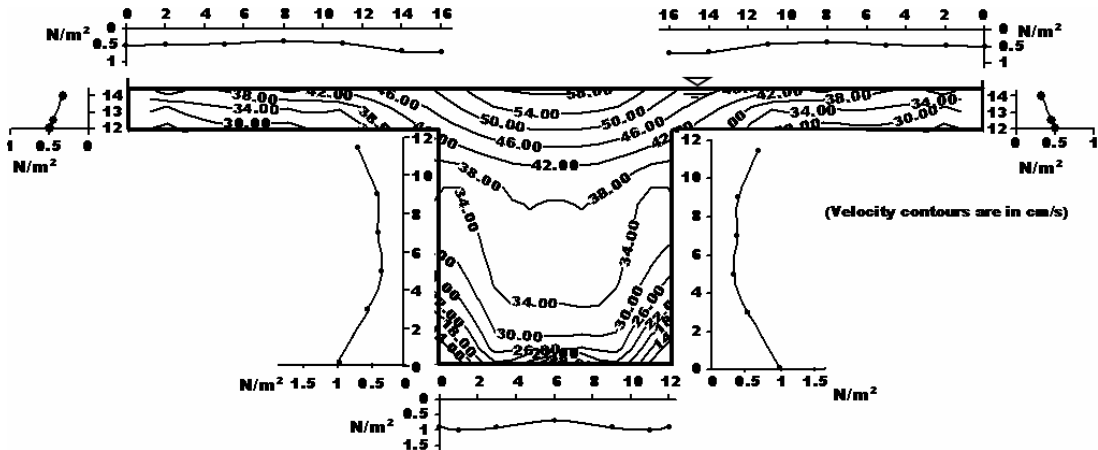
Fig. 4.7.1 Over-bank depth (*H- h*) = 2.12 cm (Type-I channel)
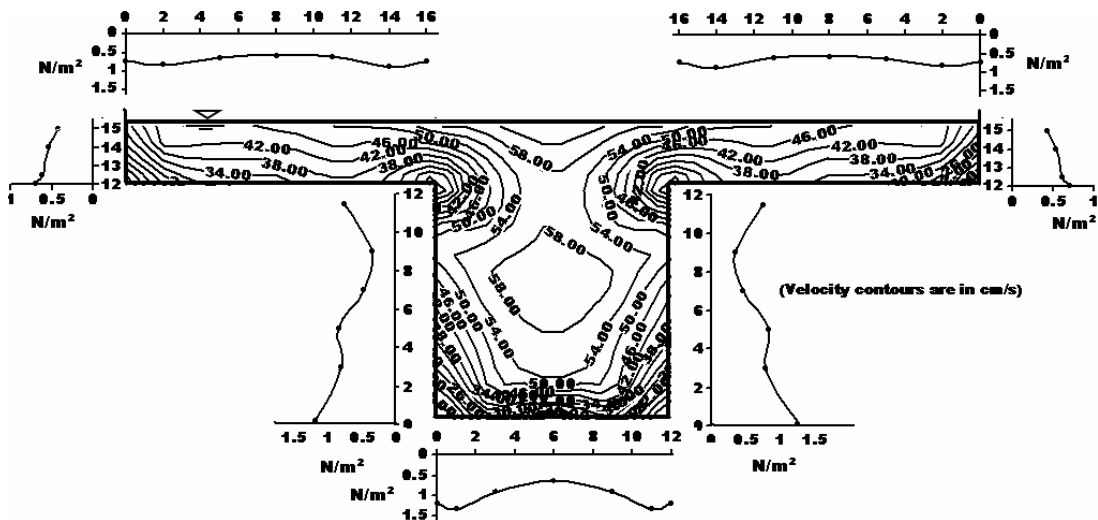
Fig. 4.7.2 Over-bank depth (*H- h*) = 3.15 cm (Type-I channel)
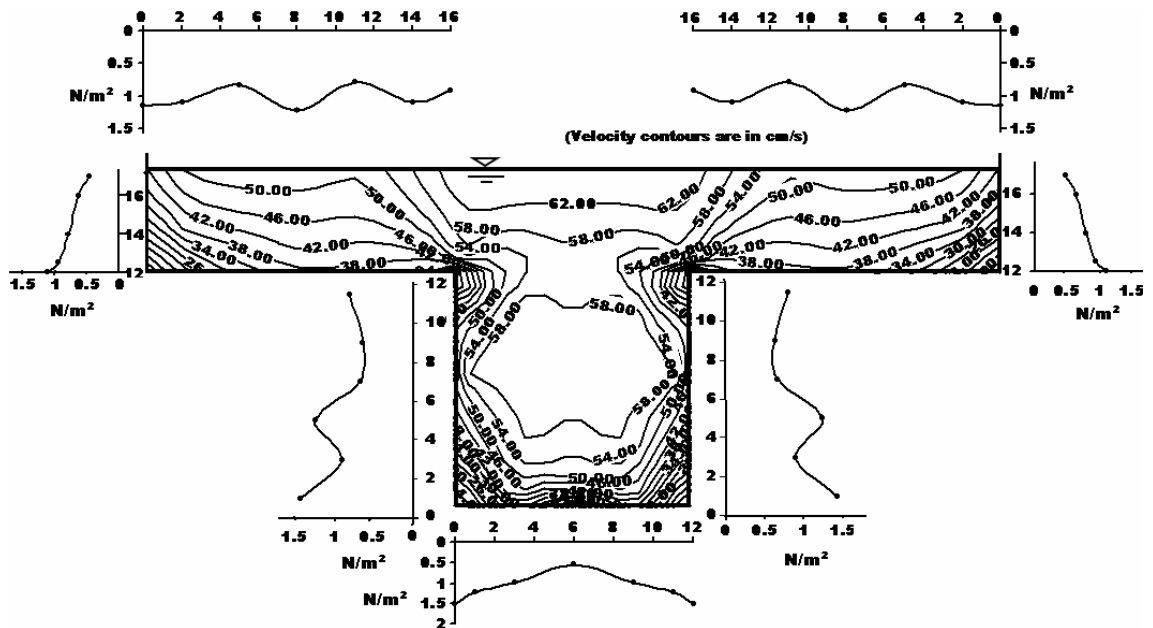
Fig. 4.7.3 Over-bank depth (*H- h*) = 5.25 cm (Type-I channel)
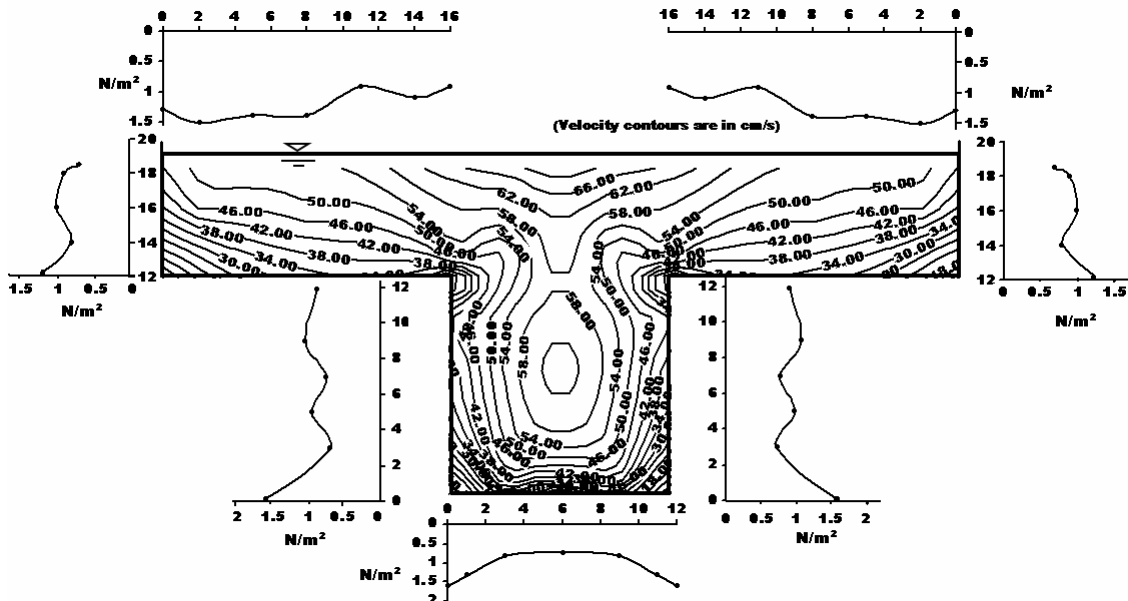
Fig. 4.7.4 Over-bank depth (*H- h*) = 6.75 cm (Type-I channel)
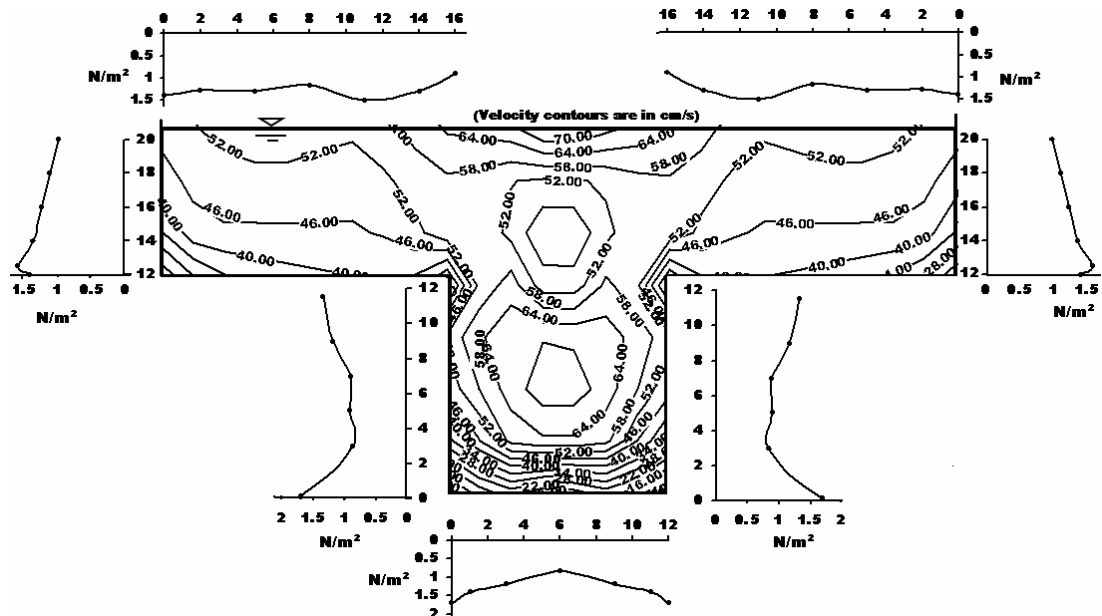
Fig. 4.7.5 Over-bank depth (*H- h*) = 8.21 cm (Type-I channel)

Fig.4.7.1-4.7.5 Contours showing the distribution of tangential velocity and boundary shear distribution of straight compound channels (Type-I). Longitudinal velocity contours are in cm/s

4.3.3 STRAIGHT COMPOUND CHANNEL

The Type-I straight compound channel and meandering compound channel Type-II are classified as deep main channel (*b/h'*<5) where wall effects are felt throughout the section when compared to shallow channels. From the isovels of tangential

- 55 -

velocity for the straight compound channel geometry, the following features can be noted (Figs. 4.7.1. through Fig. 4.7.5).

(i) For low over bank depths, the thread of maximum velocity contours lies in the upper main channel layer near the free surface.

(ii) For higher over bank depths, the thread of maximum velocity occurs at two regions of main channel (Fig.4.7.5). The longitudinal velocity components gradually decrease towards both sides of flood plain.

4.4 MEASUREMENTS OF BOUNDARY SHEAR STRESS

Information regarding the nature of boundary shear stress distribution in simple and compound channels is needed to solve a variety of river hydraulics and engineering problems such as to give a basic understanding of the resistance relationship, to understand the mechanism of sediment transport, and to design stable channels. The most commonly used methods for boundary shear determination are based on the measurement of velocity variation near the walls.

It is well established that for a regular prismatic channel under uniform flow conditions the sum of retarding boundary shear forces acting on the wetted perimeter must be equal to the resolved weight force along the direction of flow. Assuming the boundary shear stress τ_0 to be constant over the entire boundary of the channel we can express τ_0 as.

$$\tau_0 = \rho g R S \tag{4.1}$$

where g = gravitational acceleration, ρ = density of flowing fluid, S = slope of the energy line, R = hydraulic radius of the channel cross section (A/P), A = area of channel cross section, and P = wetted perimeter of the channel section.

The local shear velocity $u_* = (\tau_0/\rho)^{0.5}$ is used as the velocity scale in the study of velocity distribution close to the walls in open channels. From the mixing length theory, the shear stress for the turbulent flow is given as

$$\tau_0 = \rho k^2 h'^2 \left(\frac{du}{dh}\right)^2 \tag{4.2}$$

where u = the velocity at location h' from the wall, k = Von Karman's constant which has a value of approximately 0.40 for most of the flows. The shear stress τ close to the boundary can be assumed to be equal to that at the boundary (τ_0), as is

indeed shown to be reasonably true by measurements. Substituting $u_* = (\tau_0/\rho)^{0.5}$ in equation 4.2, integrating and taking $u = 0$ at $h' = h_0$ (that is h_0 is the distance from the channel bottom at which logarithmic law indicates zero velocity) the following equation results.

$$\frac{u}{u_*} = \frac{1}{k}\ln\left(\frac{h'}{h_0}\right) = \frac{2.3}{k}\log\left(\frac{h'}{h_0}\right) = 5.75\log\left(\frac{h'}{h_0}\right) \qquad (4.3a)$$

$$\text{or} \quad u = 5.75u_*\log\left(\frac{h'}{h_0}\right) \qquad (4.3b)$$

Equation (4.3) is known as Prandtl-Karman law of velocity distribution and is generally found applicable over the entire depth of flow. In a curved channel, there is variation of the retarding shear force in the longitudinal and transverse direction and the variation is dependent on the location at the bend and the radius of curvature. Shear stress is related to velocity distribution near the boundary. Shear stress measurement carried out in the experimental channels help to derive information on the possible erosion and depositional patterns in the natural alluvial channels. There are several methods used to evaluate boundary shear in an open channel. The velocity profile method of shear stress distribution is popularly used for experimental channels and is described here.

4.4.1 VELOCITY PROFILE METHOD

One indirect method uses the graphical plotting of velocity distribution based on the work of Karman and Prandtl. Let u_1 and u_2 are the time averaged velocities measured at h'_1 and h'_2 heights respectively from the boundary From the closely spaced velocity distribution observed at the vicinity of the channel bed and the wall we can take a difference of u' and h' between two points 1 and 2 close to each other. Substituting u_1, h'_1, u_2, and h'_2 in equation (4.3b), taking a finite difference and by taking $u_* = (\tau_0/\rho)^{0.5}$ we can write (4.3b) as

$$u_* = \frac{1}{5.75}\frac{u_2 - u_1}{\log_{10}(h'_2/h'_1)} = \frac{M}{5.75} \qquad (4.4)$$

again by substituting $u_* = (\tau_0/\rho)^{0.5}$ in equation (4.4) we can rewrite it as

$$\tau_0 = \rho\left[\frac{M}{5.75}\right]^2 \qquad (4.5)$$

where $M = \dfrac{u_2 - u_1}{\log_{10}(h'_2 / h'_1)} = \dfrac{u_2 - u_1}{\log_{10}(h'_2) - \log_{10}(h'_1)} =$ the slope of the semi-log

plot of velocity distributions near the channel bed and the wall. Using the Micro-ADV, velocities readings close to boundary for each flow is recorded for boundary shear evaluation. Knowing the value of M (slope of the semi-logarithmic plot between distances from boundary *h'* against the corresponding velocity values and using equation (4.5), the local shear stress very close to the boundary are estimated.
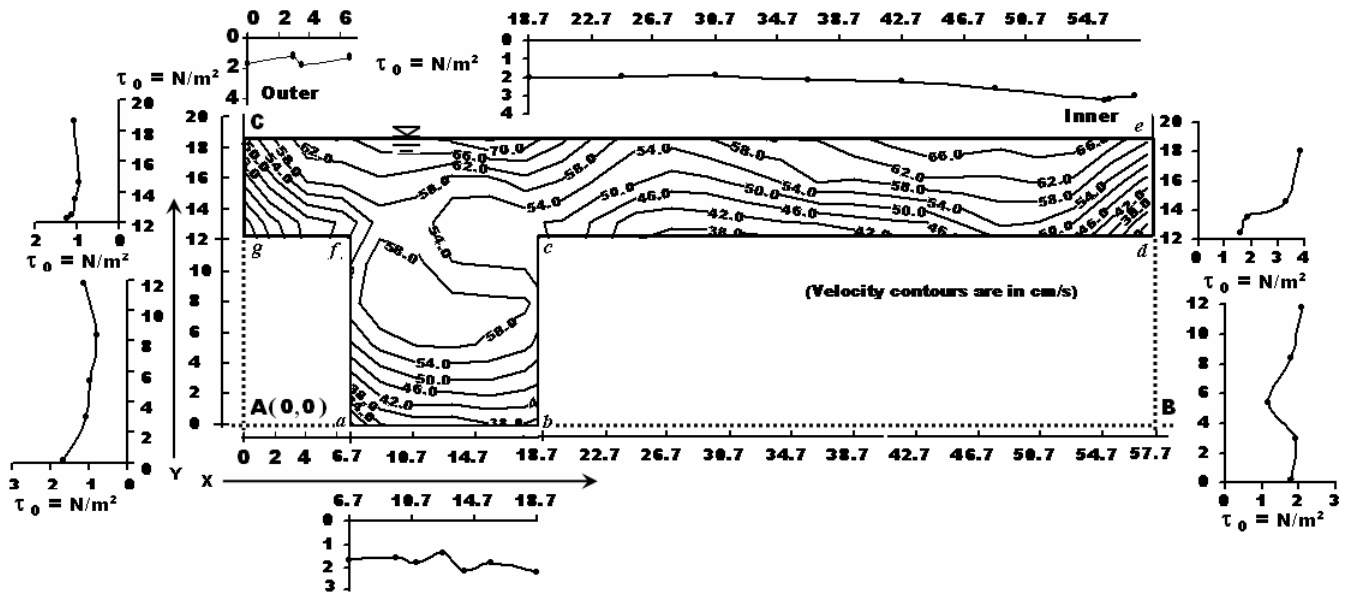
Fig.4.8 Details of the co-ordinates and boundary shear distribution from velocity contours for the run MM27 of Type-II Compound meandering channel.

A sample calculation of shear stress for the run MM27 of Type-II compound meandering channel is given in Table.4.1. In Fig.4.8 the point (A) is taken as origin with co-ordinate (0, 0). The total perimeter of the compound channel for the run *MM27* in Fig.4.8 is marked as [C *g f a b c d e*] with the respective co-ordinates with reference to the origin A (0,0) are C (0,18.15), *g* (0,12), *f* (6.7,12), *a* (6.7,0), *b* (18.7,0), *c* (18.7,12), *d* (57.7,12), and *e* (57.7,18.15) respectively. The slope of the semi log-plot (*M*) close to the boundary at different points along the wetted perimeter of channels and using equation (4.5) the shear stress is calculated and given in Table.4.1.

Table 4.1 Computation of non-uniform shear distribution from velocity contours close to boundary for the run MM27 of Type-II Compound meandering channel

Location of station as co-ordinate (x,y)	Row-1	a (6.7,0)	(9.7,0)	(11,0)	(12.7,0)	(14,0)	15.7,0)	b(18.7,0)	(18.7,3)	(18.7,5.4)	18.7,8.4)
Slope of semi-log plot $M = \dfrac{u_2 - u_1}{\log_{10}(h'_2) - \log_{10}(h'_1)}$	Row-2	23.09	22.53	24.15	20.97	26.33	24.14	24.26	24.82	19.44	24.03
Local shear stress in N/m^2	Row-3	1.64	1.56	1.80	1.35	2.14	1.79	1.81	1.90	1.16	1.78

Table 4.1-continued

Row-1	c (18.7,12)	(24.7,12)	(30.7,12)	(36.7,12)	(42.7,12)	(48.7,12)	(55.7,12)	d (57.7,12)	(57.7,12.5)	(57.7,13.6)	(57.7,14.6)
Row-2	25.86	25.20	24.59	26.32	26.69	28.96	32.19	32.08	22.80	24.52	32.69
Row-3	2.06	1.96	1.87	2.14	2.20	2.59	3.20	3.18	1.60	1.86	3.30

Table 4.1-continued

Row-1	e(57.7,18.1)	C(0,18.1)	(0,14.6)	(0,13.6)	(0,12.5)	g (0,12	(3,12)	(6.5,12)	f (6.7,12)	(6.7,8.4)	(6.7,5.4)	(6.7,3)	a(6.7,0)
Row-2	35.24	18.7	17.5	18.4	19.00	20.1	19.56	23.58	19.05	16.11	17.77	18.74	23.09
Row-3	3.83	1.08	0.94	1.05	1.11	1.25	1.18	1.72	1.12	0.80	0.97	1.08	1.64

4.5 DISTRIBUTION OF BOUNDARY SHEAR

Most of hydraulic formulae assume that the boundary shear stress distribution is uniform over the wetted perimeter. However, for meander channel - floodplain geometry, there is a wide variation in the local shear stress distribution from point to point in the wetted perimeter. Therefore, there is a need to evaluate the shear stress carried by the channel and floodplain boundary at various locations of meander path. Boundary shear stress measurements at the bend apex of a meander path covering a number of points in the wetted perimeter have been obtained from the semi-log relationship of velocity distribution. For each run of the experiment, shear stress distributions are found. For simple meander channels of Type-II and Type-III, the distribution of boundary shear along the channel perimeter at bend apex section AA of the meander path is shown in Figs.4.3.1-Fig.4.3.6 and Fig.4.4.1-Fig.4.4.6 respectively. For comparison, the mean shear stresses obtained by the velocity distribution approach and energy gradient methods for the simple meander channel are given in Table 4.2.

For meandering channels with floodplain of Type-II and Type-III channels, the boundary shear distributions are shown in Figs.4.5.1-Fig.4.5.6 and Figs.4.6.1-Fig.4.6.6 respectively. For the straight compound channels of Type-I these are shown in Figs.4.7.1 to Fig.4.7.5. For these channels also, the mean shear found from the velocity distribution agrees well with the mean value computed from energy gradient approach. These are given in Table 4.3. The following features can be noted from the figures of boundary shear distribution.

Table 4.2 Summary of boundary shear results for the experimental simple meandering channels observed at bend apex-AA

Channel Type	Run No	Flow depth (cm)	Discharge (cm^3/s)	Cross Section Area (cm^2)	Wetted perimeter (cm)	Overall mean shear stress by energy gradient approach (N/m^2)	Overall mean shear stress by velocity distribution approach (N/m^2)	Overall shear force by energy gradient approach (N/m)	Overall shear force by velocity distribution approach (N/m)
(1)	(2)	(3)	(4)	(5)	(6)	(7)	(8)	(9)	(10)
Type-II Mildly Meandering Channel	MM6	5.31	2357	63.72	22.62	0.897	0.857	0.194	0.203
	MM8	6.08	2757	72.96	24.16	0.969	0.918	0.222	0.234
	MM10	7.11	3338	85.32	26.22	1.041	0.989	0.260	0.273
	MM12	8.55	4191	102.60	29.10	1.065	1.072	0.312	0.310
	MM13	9.34	4656	112.08	30.68	1.209	1.136	0.362	0.371
	MM15	11.01	5680	132.12	34.02	1.264	1.181	0.402	0.430
Type-III Highly Meandering channel	HM10	5.3	4191	91.69	26.99	1.790	1.766	0.477	0.483
	HM11	5.62	4656	99.02	27.89	1.951	1.844	0.515	0.544
	HM12	5.93	5122	106.32	28.77	2.037	1.919	0.553	0.586
	HM13	6.18	5515	112.35	29.48	2.069	1.981	0.584	0.610
	HM14	6.71	6396	125.54	30.98	2.282	2.107	0.653	0.707
	HM15	7.33	7545	141.69	32.73	2.426	2.250	0.737	0.794

Table 4.3 Summary of boundary shear results for over bank flow condition for the experimental channels observed at bend apex-AA

Channel Type	Run No	Relative depth (β)	Discharge (cm^3/s)	Total Area (cm^2)	Total Wetted Perimeter (cm)	Observed total shear force in main channel perimeter (N/m)	Observed total shear force in floodplain perimeter (N/m)	Observed % of shear force in floodplain perimeter (%S_{fp})	Overall shear stress by energy gradient approach (N/m^2)	Overall shear stress by velocity distribution approach (N/m^2)
(1)	(2)	(3)	(4)	(5)	(6)	(7)	(8)	(9)	(10)	(11)
Type-I Straight compound channel ($\alpha = 3.666$)	S13	0.15	10007	237.3	72.24	0.240	0.174	42.10	0.442	0.414
	S15	0.21	13004	282.6	74.30	0.292	0.265	47.64	0.527	0.557
	S17	0.30	19861	375.1	78.50	0.339	0.393	53.70	0.699	0.732
	S18	0.36	25329	440.9	81.50	0.357	0.529	59.70	0.822	0.886
	S19	0.41	30844	505.2	84.42	0.403	0.632	61.10	0.942	1.035
Type-II Sinuous compound channel ($\alpha = 4.808$)	MM17	0.12	10107	240.9	85.06	0.427	0.360	45.73	0.733	0.787
	MM20	0.17	13005	283.6	86.54	0.418	0.468	52.80	0.863	0.886
	MM23	0.21	16762	333.2	88.26	0.372	0.554	59.80	1.013	0.926
	MM25	0.25	20523	379.4	89.86	0.441	0.771	63.63	1.154	1.212
	MM26	0.30	25661	438.2	91.91	0.487	0.999	67.25	1.333	1.486
	MM27	0.34	31358	498.8	94.04	0.515	1.215	70.21	1.517	1.73
Type-III Highly Sinuous & Trapezoidal compound channel ($\alpha = 16.08$)	HM16	0.08	12757	302.8	201.10	0.627	0.751	54.47	1.574	1.378
	HM18	0.18	24487	495.8	203.10	0.699	1.756	71.52	2.577	2.455
	HM19	0.19	27185	530.5	203.46	0.797	2.144	72.89	2.76	2.941
	HM20	0.21	31299	578.8	203.96	0.795	2.372	74.91	3.01	3.167
	HM25	0.27	44412	725.4	205.48	0.819	3.081	78.99	3.77	3.9
	HM27	0.28	48474	760.2	205.84	0.814	3.206	79.76	3.95	4.02

4.5.1 SIMPLE MEANDER CHANNELS

(i)   On comparison of the results with straight uniform channel, it can be seen that there is asymmetrical nature of shear distribution especially where there is predominant curvature effect.

- 60 -

(ii)   The over all mean value of boundary shear stress obtained through the velocity distribution approach compares well with that obtained from energy gradient approach.

(iii)   Maximum value of wall shear occurs significantly below the free surface and is located at the inner walls.

4.5.2   MEANDER CHANNELS WITH FLOODPLAIN

(i)   For meander channel with floodplain there is also good agreement between the measured mean boundary shear from experiments with that of energy gradient approach.

(ii)   The local variation of shear is probably due to the assumption of constant value of k (Von Karman turbulent coefficient) in fitting the logarithmic velocity profile.

(iii)   The asymmetrical nature of shear stress distribution is very much evident at the sections of bend apex, confirming the findings of Kar (1977), Bhattacharya (1995) and Patra and Kar (2000).

(iv)   For low over bank depths, it can be seen that the maximum value of wall shear stress occurs along the inner side wall of main channel. For higher over-bank depths, the maximum value of wall shear stress occurs along the inner side wall of floodplain.

(v)   For higher depths of flow over floodplain, the maximum bed shears is located in the floodplain region and for low over-bank depth the maximum bed shear lies near the inner bed of main channel. Though a general pattern of shear distribution is rather unaffected by the over bank flow depth, the width of floodplain and sinuosity are found to affect the nature of distribution to some extent.

(vi)   The percentage of shear carried by flood plain region is found to be more for meandering compound channel when compared to that for straight compound channel.

(vii)   Low magnitude of boundary shear is found at the outer walls when compared to that at the inner wall.

4.5.3 STRAIGHT COMPOUND CHANNEL

(i)   Symmetrical and uniform nature of boundary shear stress distribution is found for straight compound channel of Type-I when compared to the meandering compound channels of Type-II and Type-III.

(ii)   The boundary shear at the main channel junctions are generally found to be more than that compared to other points of the wetted perimeter.

(iii)   The total shear carried by flood plain is found to be larger than that of the main channel.

(iv)   Boundary shear in the main channel and floodplain regions increases proportionately with the over bank flow depth.

(v)   Total shear carried by the wetted perimeter of the compound channel compares well with the energy gradient approach.

4.6 DISTRIBUTION OF RADIAL (TRANSVERSE) VELOCITY

For simple meander channels, the radial velocity components in contour form for the runs of Type-II channels at locations AA (bend apex) and BB (cross over) are shown in Figs. 4.9.1 through Fig. 4.9.6 and Figs. 4.9.7 through Fig. 4.9.12 respectively. Similarly for Type-III channels the velocity distributions at location AA and BB are shown in Figs.4.10.1-Fig.4.10.6 and Figs.4.10.7- Fig.4.10.12 respectively. For the meander channel with floodplains (Type-II) at locations AA, and BB the radial velocity contours are shown in Figs. 4.11.1- Fig. 4.11.6 and Figs.4.11.7- Fig.4.11.12 respectively. For the meandering compound channel (Type-III) at locations AA, and BB the radial velocity contours are shown in Figs. 4.12.1- Fig.4.12.6 and Fig.4.12.7- Fig.4.12.12 respectively. For the straight compound channels of Type-I, the distribution of radial velocity are shown in Figs.4.13.1 to Fig.4.13.10. According to the sign convention by the micro-ADV, the positive radial component shows outward direction and negative radial component shows in-ward direction
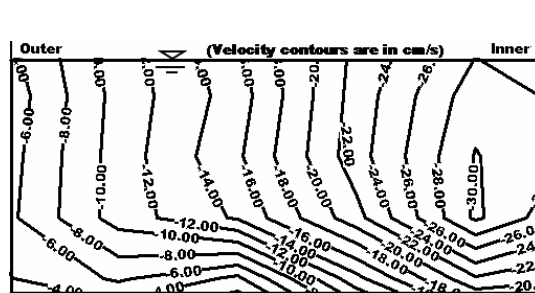
Fig.4.9.1 in-bank depth *h' = 5.31* cm   **Fig.4.9.2 in-bank depth *h' = 6.08* cm**
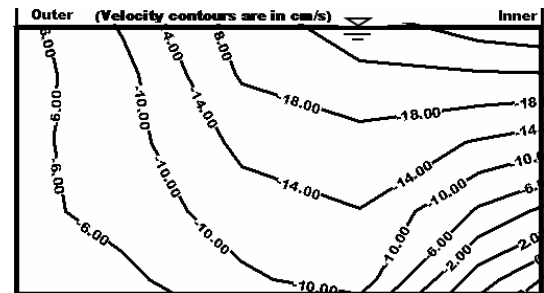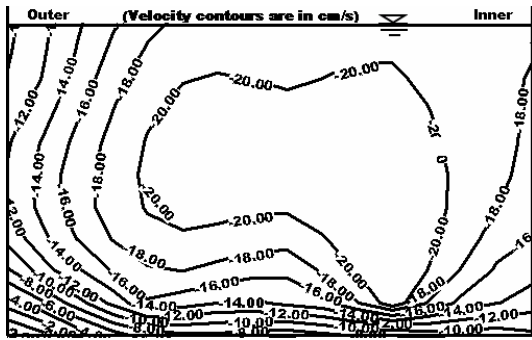
Fig.4.9.3 in-bank depth *h' = 7.11 cm*
(Type-II channel at bend apex AA)
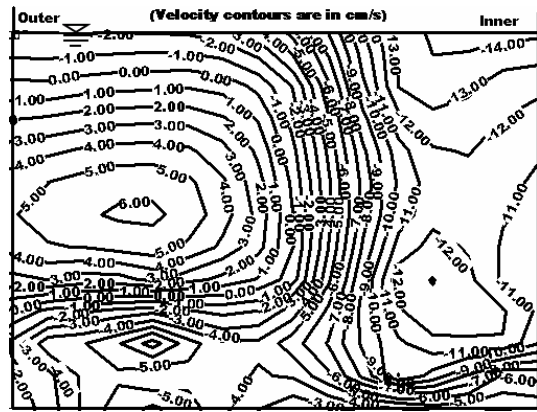
Fig.4.9.4 in-bank depth *h' = 8.55 cm*
(Type-II channel at bend apex AA)
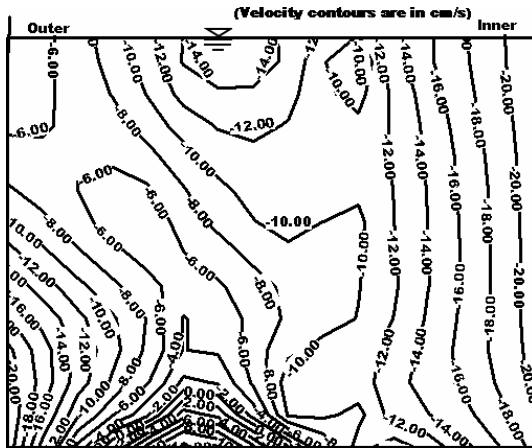
Fig. 4.9.5 in-bank depth *h' = 9.34 cm*
(Type-II channel at bend apex AA)
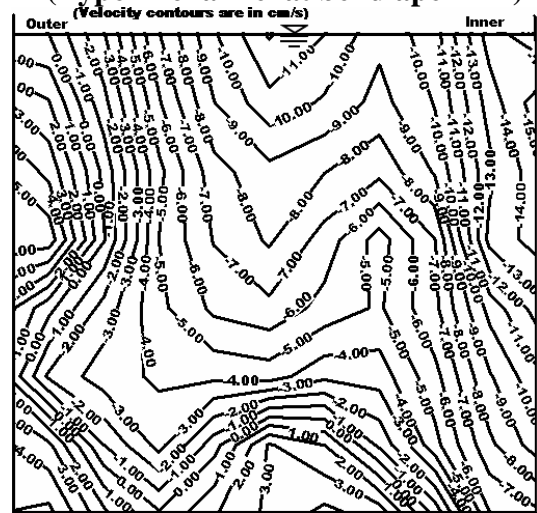
Fig.4.9.6 in-bank depth *h' = 11.01 cm*
(Type-II channel at bend apex AA)

Figs.4.9.1-Fig.4.9.6 Contours showing the distribution of radial velocity at bend-apex (Section AA) of simple meandering (Type-II) channels.
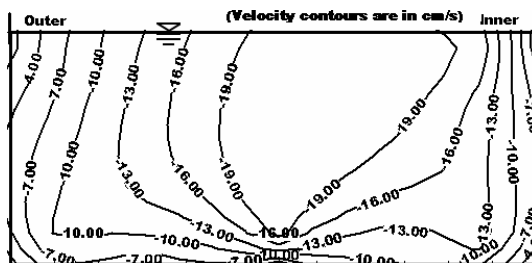
Fig.4.9.7 in-bank depth h' = 5.31 cm
(Type-II channel at cross-over BB)
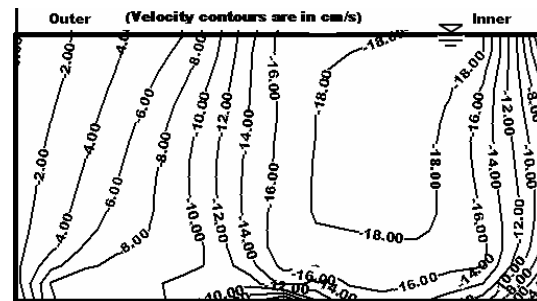
Fig.4.9.8 in-bank depth h' = 6.08 cm
(Type-II channel at cross-over BB)
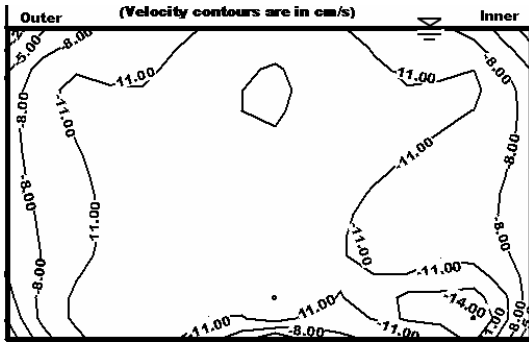
Fig.4.9.9 in-bank depth h = 7.11 cm
(Type-II channel at cross-over BB)
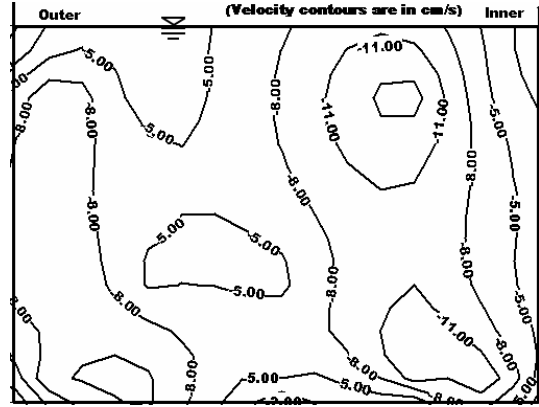
Fig.4.9.10 in-bank depth h = 8.55 cm
(Type-II channel at cross-over BB)
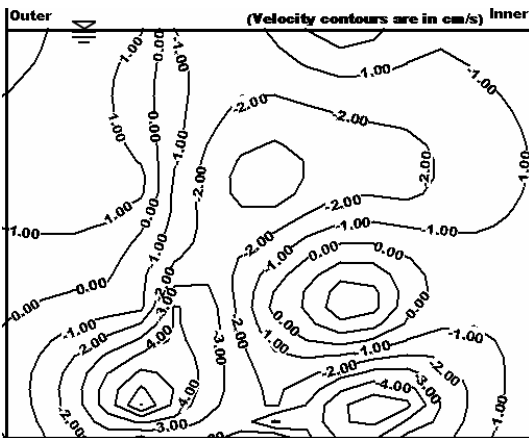
Fig.4.9.11 in-bank depth h ,= 9.34 cm
(Type-II channel at cross-over BB)
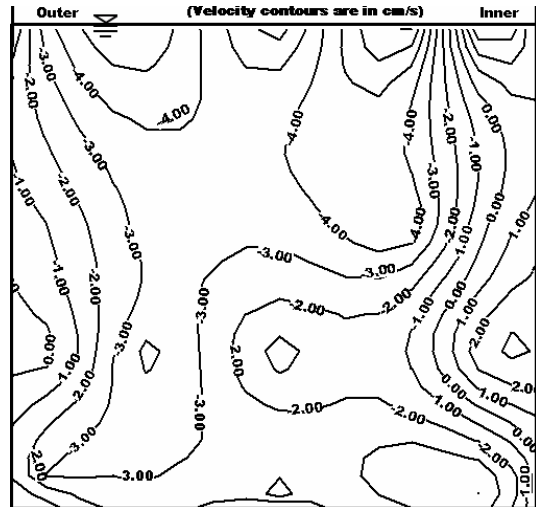
Fig. 4.9.12 in-bank depth h' = 11.01 cm
(Type-II channel at cross-over BB)

Figs.4.9.7-Fig.4.9.12 Contours showing the distribution of radial velocity at geometrical-crossover of simple meandering (Type-II) channels.
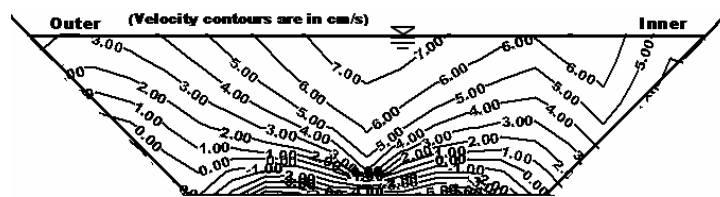
Fig. 4.10.1- In bank depth h' = 5.3 cm
(Type-III channel at bend apex AA)
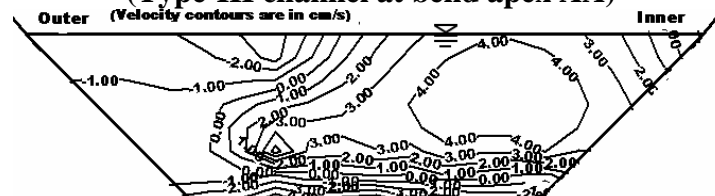
Fig. 4.10.2- In bank depth h' = 5.62 cm
(Type-III channel at bend apex AA)

- 64 -
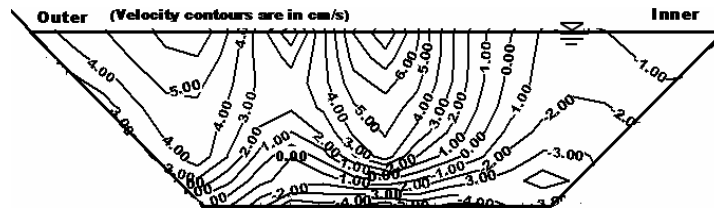
Fig. 4.10.3- In bank depth h' = 5.92 cm
(Type-III channel at bend apex AA)

Fig. 4.10.4- In bank depth *h'* = 6.18 cm
(Type-III channel at bend apex AA)

Fig. 4.10.5- In bank depth *h'* = 6.71cm
(Type-III channel at bend apex AA)

Fig. 4.10.6- In bank depth *h'* = 7.33 cm
(Type-III channel at bend apex AA)

Fig.4.10.1-Fig.4.10.6 Contours showing the distribution of radial velocity at bend apex (Section AA) of simple meandering (Type-III) trapezoidal channels.

Fig. 4.10.7- In bank depth *h'* = 5.3 cm
(Type-III channel at cross-over BB)

Fig. 4.10.8- In bank depth *h'* = 5.62 cm
(Type-III channel at cross-over BB)

Fig. 4.10.9- In bank depth *h' = 5.92 cm*
(Type-III channel at cross-over BB)

Fig. 4.10.10- In bank depth *h' = 6.18 cm*
(Type-III channel at cross-over BB)
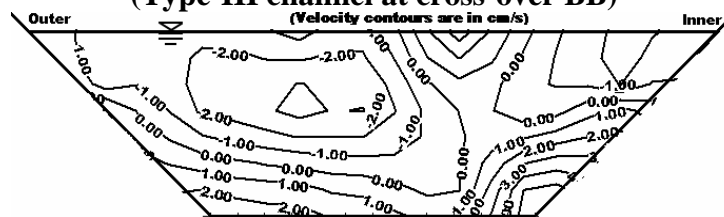
Fig. 4.10.11 In bank depth *h' = 6.71 cm*
(Type-III channel at cross-over BB)
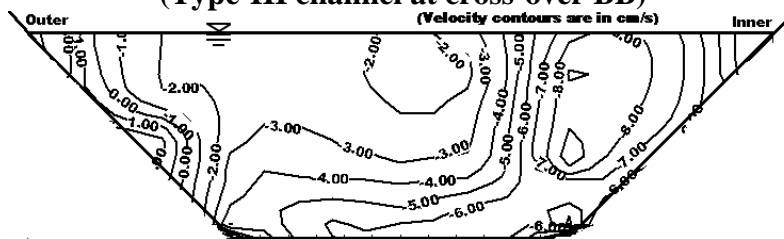
Fig. 4.10.12- In bank depth *h' = 7.33cm*
(Type-III channel at cross-over BB)

Fig.4.10.7-Fig.4.10.12 Contours showing the distribution of radial velocity at geometrical cross-over (Section BB) of simple meandering (Type-III) trapezoidal channels.

4.6.1 SIMPLE MEANDER CHANNEL

From the distribution of radial velocity in contour form for the flow confined within the meander section only for Type-II and Type-III channels (Figs. 4.9.1-Fig. 4.9.6 and Figs. 4.10.1-Fig. 4.10.6), the following information can be drawn.

(i)   The radial velocity is observed to be smaller than tangential velocity. For the trapezoidal Type-III channels, the radial velocity is observed to be around 10 % of the longitudinal velocity (Fig.4.10.3 and Fig.4.4.3).

(ii)   Higher radial components are found for Type-II rectangular main channel section of the order of 67 % of longitudinal velocity (Fig.4.9.1 and Fig.4.3.1).

(iii)   At the bend-apex, the micro-ADV readings for radial velocity directions are found to be mostly negative indicating that it is pointing inward direction. Higher velocity contours are seen near the inner bank and lower contours at the outer banks.

(iv)   At the geometrical cross-over region, the radial components are towards inward direction having lesser magnitudes when compared to that at the bend-apex, indicating a phase lag between channel cross-over and flow cross over.

Fig. 4.11.1 Over-bank depth (*H- h*) = 1.68 cm (Type-II channel at bend apex AA)

Fig. 4.11.2 Over-bank depth (*H- h*) = 2.42 cm (Type-II channel at bend apex AA)

Fig. 4.11.3 Over-bank depth (*H- h*) = 3.28 cm (Type-II channel at bend apex AA)

Fig. 4.11.4 Over-bank depth (*H- h*) = 4.08 cm (Type-II channel at bend apex AA)

Fig. 4.11.5 Over-bank depth (*H- h*) = 5.10 cm (Type-II channel at bend apex AA)

Fig. 4.11.6 Over-bank depth (*H- h*) = 6.15 cm (Type-II channel at bend apex AA)

Figs.4.11.1- Fig.4.11.6 Contours showing the distribution of radial velocity at bend-apex (Section AA) of compound meandering (Type-II) channels.

Fig. 4.11.7 Over-bank depth (*H- h*) =1.68 cm (Type-II channel at cross over BB)

Fig. 4.11.8 Over-bank depth (*H- h*) = 2.42 cm (Type-II channel at cross over BB)

Fig. 4.11.9 Over-bank depth (*H- h*) = 3.28 cm (Type-II channel at cross over BB)

Fig. 4.11.10 Over-bank depth (*H- h*) = 4.08 cm (Type-II channel at cross over BB)

Fig. 4.11.11 Over-bank depth (*H- h*) = 5.10 cm (Type-II channel at cross over BB)

Fig. 4.11.12 Over-bank depth (*H- h*) = 6.15 cm (Type-II channel at cross over BB)

Figs.4.11.7- Fig.4.11.12 Contours showing the distribution of radial velocity at geometrical cross-over (Section BB) of compound meandering (Type-II) channels.

Fig. 4.12.1 Over-bank depth (*H- h*) = 0.74 cm (Type-III meandering compound channel at bend apex AA)

Fig. 4.12.2 Over-bank depth (*H- h*) = 1.74 cm (Type-III meandering compound channel at bend apex AA)

Fig. 4.12.3 Over-bank depth (*H- h*) = 9.92 cm (Type-III meandering compound channel at bend apex AA)

Fig. 4.12.4 Over-bank depth (*H- h*) = 2.17 cm (Type-III meandering compound channel at bend apex AA)

Fig. 4.12.5 Over-bank depth (*H- h*) =2.93 cm (Type-III meandering compound channel at bend apex AA)

Fig. 4.12.6 Over-bank depth (*H- h*) = 3.01 cm (Type-III meandering compound channel at bend apex AA)

Figs.4.12.1-Fig.4.12.6 Contours showing the distribution of radial velocity components at bend-apex (Section AA) of compound meandering (Type-III) channels.

Fig. 4.12.7 Over-bank depth (*H- h*) = 0.74 cm (Type-III meandering compound channel at cross-over BB)

Fig. 4.12.8 Over-bank depth (*H- h*) =10.74 cm (Type-III meandering compound channel at cross-over BB)

Fig. 4.12.9 Over-bank depth *(H- h)* = 1.92 cm (Type-III meandering compound channel at cross-over BB)

Fig. 4.12.10 Over-bank depth (*H- h*) = 2.17 cm (Type-III meandering compound channel at cross-over BB)

Fig. 4.12.11 Over-bank depth(*H- h*) = 2.93 cm (Type-III meandering compound channel at cross-over BB)

Fig. 4.12.12 Over-bank depth (*H- h*) = 3.01 cm (Type-III meandering compound channel at cross-over BB)

Figs.4.12.7-Fig.4.12.12 Contours showing the distribution of radial velocity components at geometrical cross-over (Section BB) of compound meandering (Type-III) channels.

4.6.2   MEANDER CHANNEL WITH FLOODPLAIN

From the distribution of radial velocity for Type-II and Type-III meander channel with floodplains, the following interesting features can be observed (Figs. 4.11.1 through Fig. 4.11.12 and Figs. 4.12.1 through Fig. 4.12.12).

(i)   At the bend apex (AA) of meandering compound channel of Type-II, the micro-ADV reading shows negative signs of the radial velocity indicating the flow direction is towards inner flood plain.

(ii)   At both the bend-apex (AA) and cross-over regions (BB) of Type-III meandering compound channels, negative contours are found in flood plain regions and positive contours are found in the main channel regions. At the bend apex, the higher positive velocity contours concentrate near the inner wall of main channel.

(iii) The radial velocity at geometrical cross over region is found to be more than that at bend-apex showing almost 90^0 phase lag between channel geometry and flow geometry.

(iv)   At the bend apex AA, the thread of larger in-ward radial components are found just above the bed of the main channel.

(v)   At higher over-bank depth, higher magnitude of inward radial velocity is observed near the inner side of floodplains for both Type-II and Type-III channels.

(vi)   At the cross-over regions (BB) for Type-III channel, for higher over bank depths the large magnitude of inward radial velocity is observed at both sides of flood plain and the out-ward velocity components in main channel area.

Fig. 4.13.1 Over-bank depth (H-h) = 2.12 cm (Type-I compound channel)

Fig. 4.13.2 Over-bank depth (H- h) = 3.15 cm (Type-I compound channel)

(Velocity contours are in cm/s)

Fig. 4.13.3 Over-bank depth (H- h) = 5.25 cm (Type-I compound channel)

(Velocity contours are in cm/s)

Fig. 4.13.4 Over-bank depth (H- h) =6.75 cm (Type-I compound channel)

Fig. 4.13.5 Over-bank depth (*H- h*) = 8.21 cm (Type-I compound channel)

Fig.4.13.1-4.13.5 Contours showing the distribution of radial velocity of Type-I straight compound channels. Radial velocity contours in cm/s.

4.6.3 STRAIGHT COMPOUND CHANNEL

The present Type-I experimental compound channel is classified as deep as the width to depth ratio is less than five. For this channel, the wall effects are felt through out the cross section when compared to a shallow channel. The following features are noted from the isovel plots of radial velocity for straight compound channel geometry of Type-I (Figs. 4.13.1. through Fig. 4.13.5)

    (i)   The radial component of velocity for straight compound channel is observed to be of smaller magnitude when compared to that of meandering over bank flow of about same depth ratio.

    (ii)   At low over bank depths, the radial velocity component is towards the direction of floodplain. For higher over bank depths, the direction of radial velocity component is from floodplain to the main channel, showing of reversal of its behaviors with depth over floodplain.

    (iii)   Higher radial velocity contours are seen near the junction of main channel and floodplain showing the higher momentum transfer at these regions.

4.7 DISTRIBUTION OF VERTICAL VELOCITY

For simple meander channels, the vertical velocity in contour form for Type-II channels at locations AA (bend apex) and at BB (geometrical cross over) are shown in Figs. 4.14.1- Fig.4.14.6 and Figs. 4.14.7- Fig.4.14.12 respectively. Similarly for

Type-III channels the vertical velocity distribution at location AA and BB are shown in Figs. 4.15.1- Fig.4.15.6 and Figs. 4.15.7- Fig. 4.15.12. For the meander channel with floodplains (Type-II) at locations AA and BB the vertical velocity distributions of the channels are shown in Figs. 4.16.1- Fig. 4.16.6 and Figs. 4.16.7- Fig. 4.16.12 respectively. For the meander channel with floodplains (Type-III), the vertical velocity distributions in contour form at bend apex is shown in Figs. 4.17.1- Fig. 4.17.6 and at the geometrical cross over the corresponding contours are shown in Figs. 4.17.7- Fig. 4.17.12 respectively. For the straight compound channels of Type-I, the radial distribution of vertical velocity are shown in contours forms in Figs.4.18.1-Fig. 4.18.5. According to the sign convention by the micro-ADV upward vertical velocity shows positive sign and down-ward vertical velocity shows negative sign.
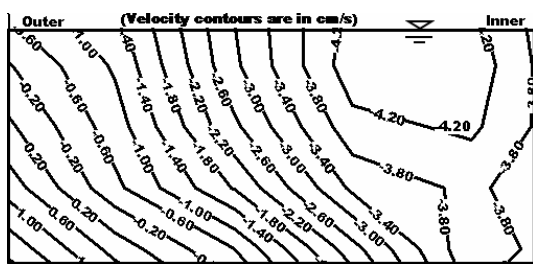
Fig.4.14.1 In-bank depth $h' = 5.31$ cm (Type-II channel at bend apex AA)
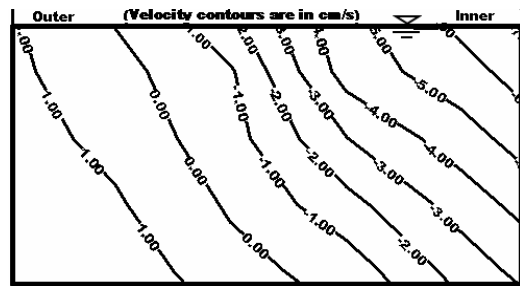
Fig.4.14.2 In-bank depth $h' = 6.08$cm (Type-II channel at bend apex AA)
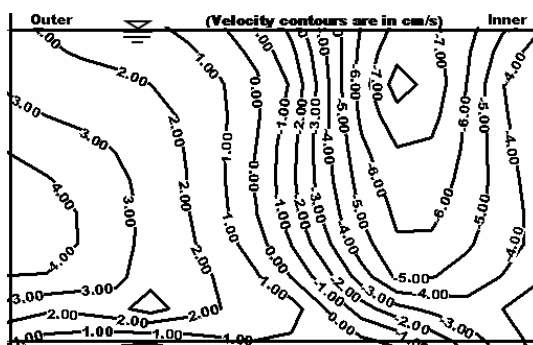
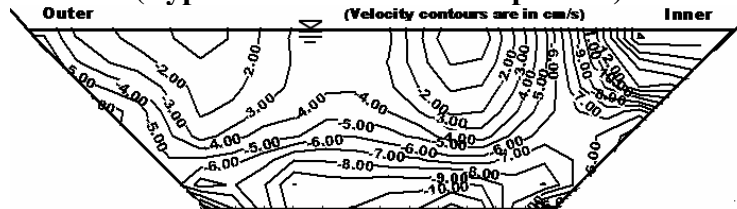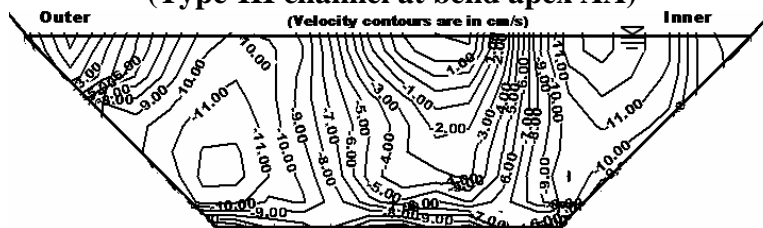**Fig.4.14.3 In-bank depth $h' = 7.11$cm (Type-II channel at bend apex AA)**
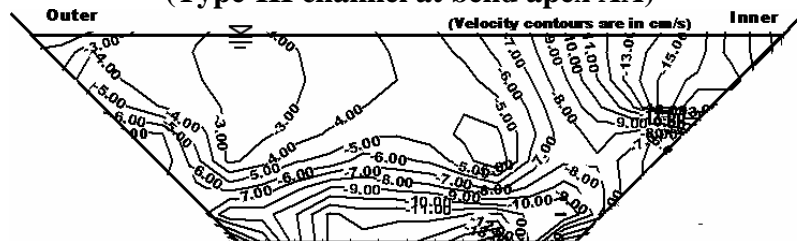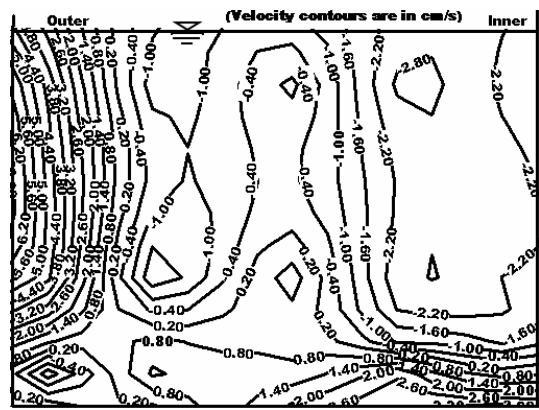

Fig. 4.14.4 In-bank depth $h' = 8.55$cm (Type-II channel at bend apex AA)
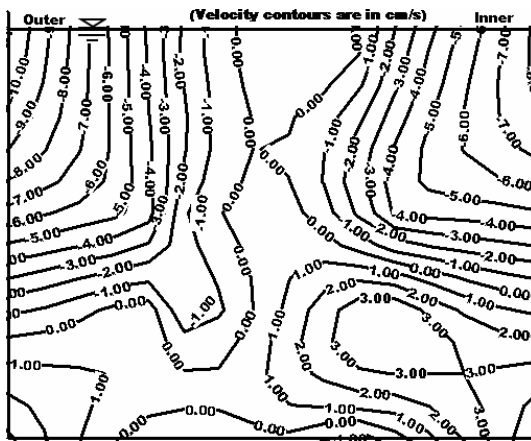
Fig.4.14.5 In-bank depth *h' = 9.34 cm*
(Type-II channel at bend apex AA)
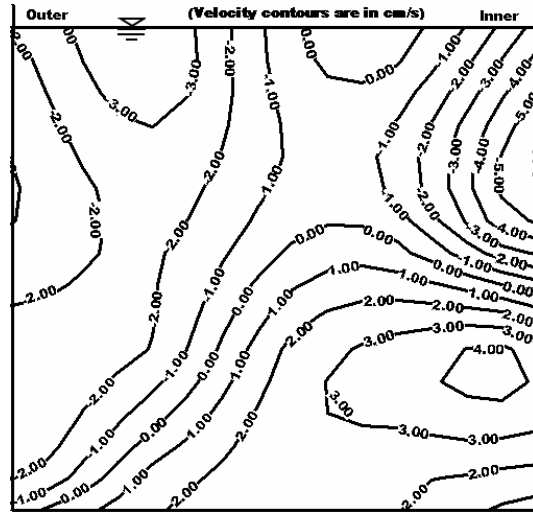
Fig.4.14.6 In-bank depth *h' = 11.01cm*
(Type-II channel at bend apex AA)

Fig.4.14.1-4.14.6 Contours showing the distribution of vertical velocity components at bend-apex (Section AA) of simple meandering (Type-II) channels.
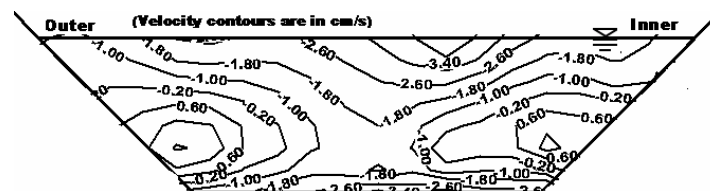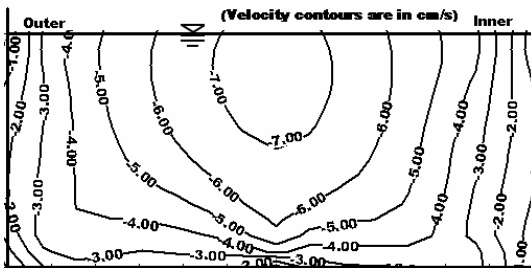
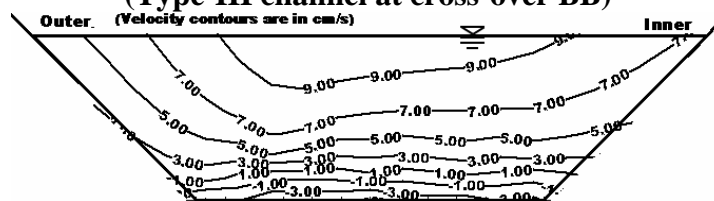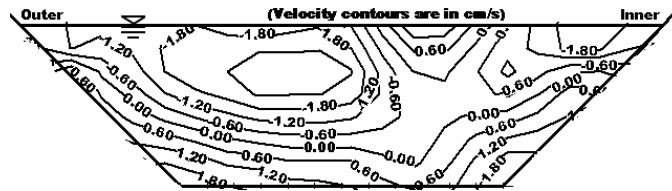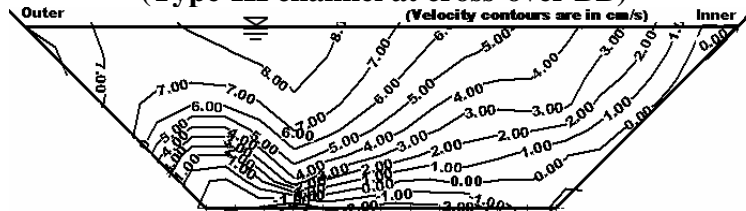**Fig.4.14.7 In-bank depth *h' = 5.31 cm***
(Type-II channel at cross over BB)
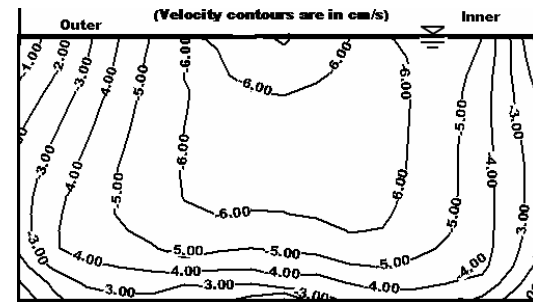
Fig.4.14.8 In-bank depth *h' = 6.08cm*
(Type-II channel at cross over BB)
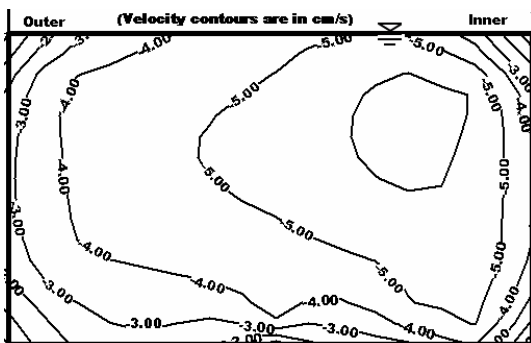
Fig.4.14.9 In-bank depth *h' = 7.11cm*
(Type-II channel at cross over BB)
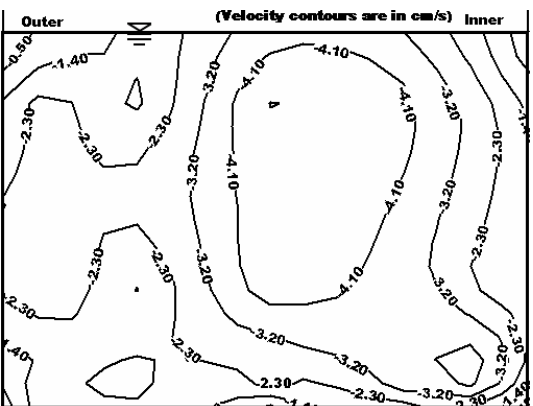
Fig.4.14.10 In-bank depth *h' = 8.55cm*
(Type-II channel at cross over BB)
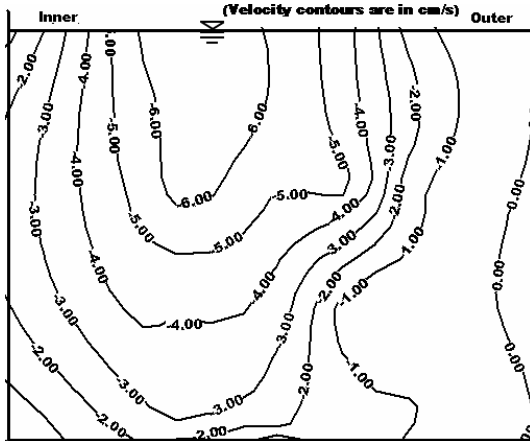
Fig.4.14.11 In-bank depth *h'* = 9.34 cm
(Type-II channel at cross over BB)
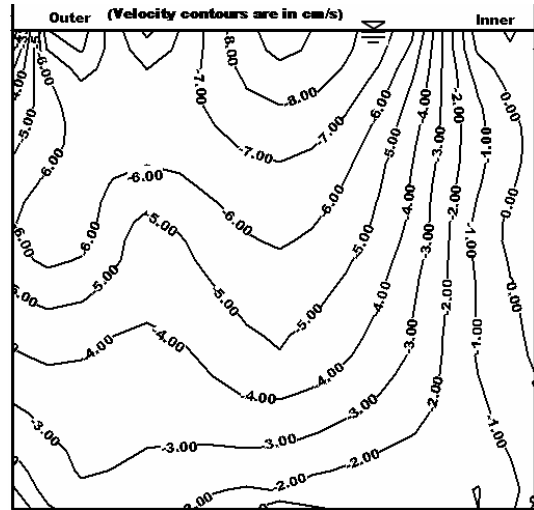
Fig.4.14.12 In-bank depth *h'* = 11.01cm
(Type-II channel at cross over BB)

Fig.4.14.7 Fig.4.14.12 Contours showing the distribution of vertical velocity at geometrical cross-over (Section BB) of simple meandering (Type-II) channels.
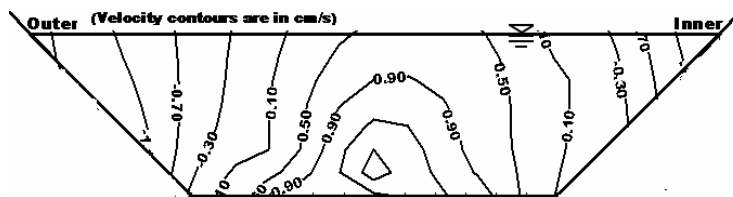
Fig. 4.15.1 In bank depth *h'* = 5.3cm (Type-III channel at bend apex AA)
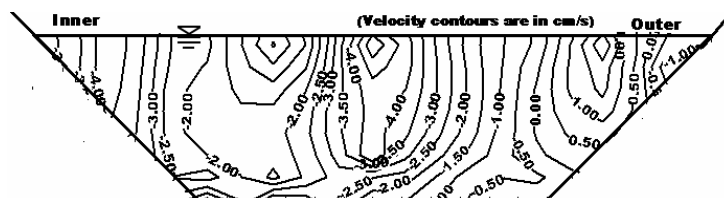
Fig. 4.15.2 In bank depth *h'* = 5.62 cm (Type-III channel at bend apex AA)
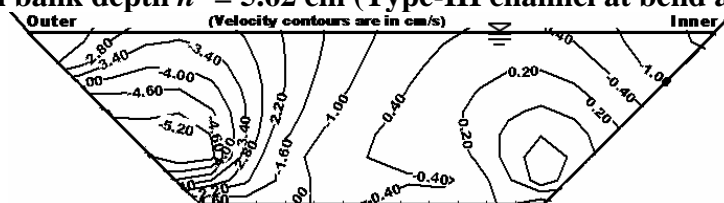
Fig. 4.15.3 In bank depth *h'* = 5.93 cm (Type-III channel at bend apex AA)
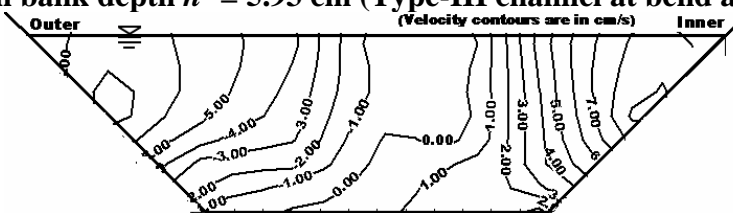
Fig. 4.15.4 In bank depth *h'* = 6.18 cm (Type-III channel at bend apex AA)
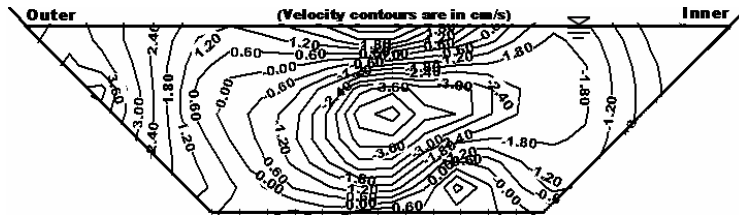
Fig. 4.15.5 In bank depth *h' = 6.71 cm* (Type-III channel at bend apex AA)
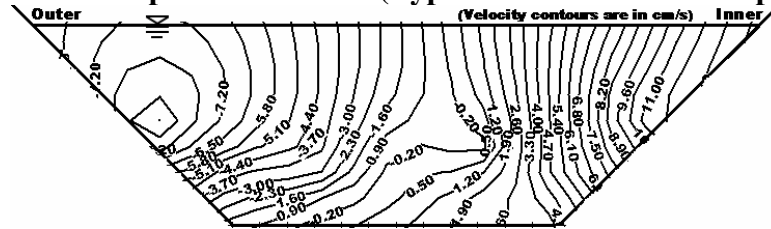
Fig. 4.15.6 In bank depth *h' = 7.33 cm* (Type-III channel at bend apex AA)

Fig.4.15.1-Fig.4.15.6 Contours showing the distribution of vertical velocity components at bend apex (Section AA) of simple meandering (Type-III) channels.
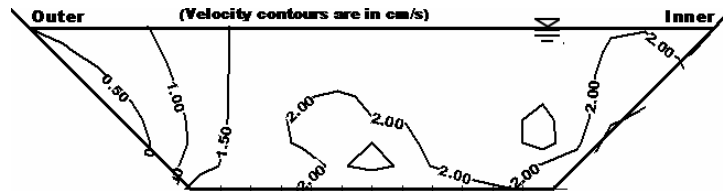
Fig. 4.15.7 In bank depth *h' = 5.3 cm* (Type-III channel at cross over BB)
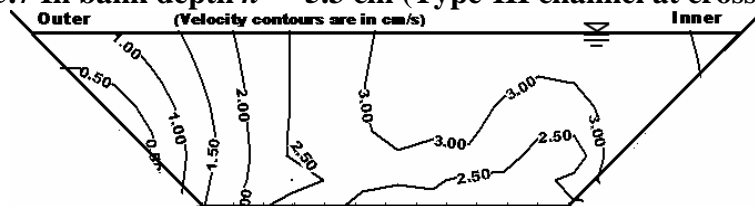
Fig. 4.15.8 In bank depth *h' = 5.62 cm* (Type-III channel at cross over BB)
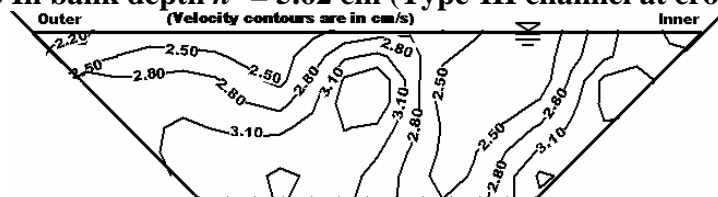
Fig. 4.15.9 In bank depth *h' = 5.93 cm* (Type-III channel at cross over BB)
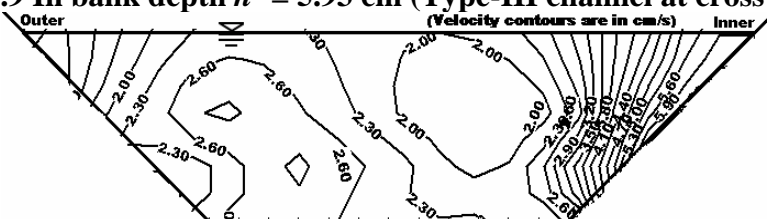
Fig. 4.15.10 In bank depth *h' = 6.18cm* (Type-III channel at cross over BB)
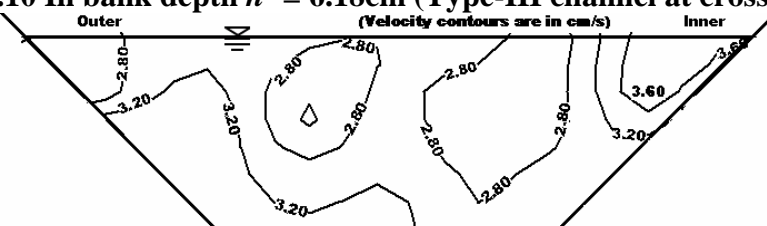
Fig. 4.15.11 In bank depth *h' =* 6.71 cm (Type-III channel at cross over BB)
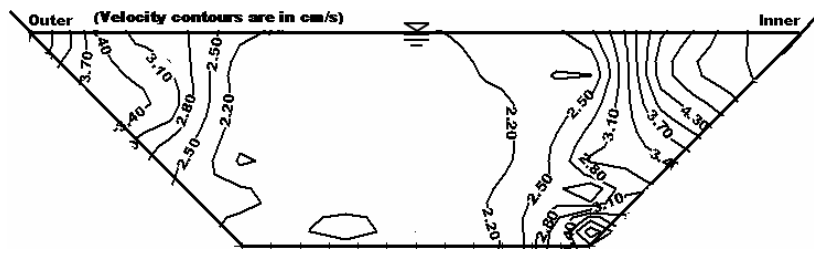
Fig. 4.15.12 In bank depth *h' =* 7.33cm (Type-III channel at cross over BB)

Fig.4.15.7-Fig.4.15.12 Contours showing the distribution of vertical velocity at cross-over (Section BB) of simple meandering (Type-III) channels.

4.7.1   SIMPLE MEANDER CHANNEL

From the distribution of vertical velocity components in Type-II and Type-III simple meander channel sections in contour form at the locations AA and BB, the following features are noted.

(i)   For in-bank flow, the maximum upward components are found at outer wall and maximum down-ward components are found at inner wall. With increase in flow depths, the values of vertical velocity are found to decrease.

(ii)   At the geometrical cross-over region, the vertical components of velocity are mostly towards down-ward direction. With increase in flow depth the magnitude of vertical velocity decreases.

(iii)   At geometrical cross-over section the vertical components of velocity at the water surface is observed to be higher than that at the bottom of the meandering channel.

(iv)   At cross-over section of Type-III trapezoidal meandering channels, up-ward components are also observed. This is due to the phase lag of the channel geometry with the flow geometry.

(v)   Magnitudes of vertical velocity components for meandering channels are found to be less when compared to the magnitude of radial component of velocity.

(vi) Magnitude of vertical velocity component is found to be the order of around 1.4% of longitudinal velocity for type-III channel and as high as 14% for type-II channel of the corresponding longitudinal velocity.
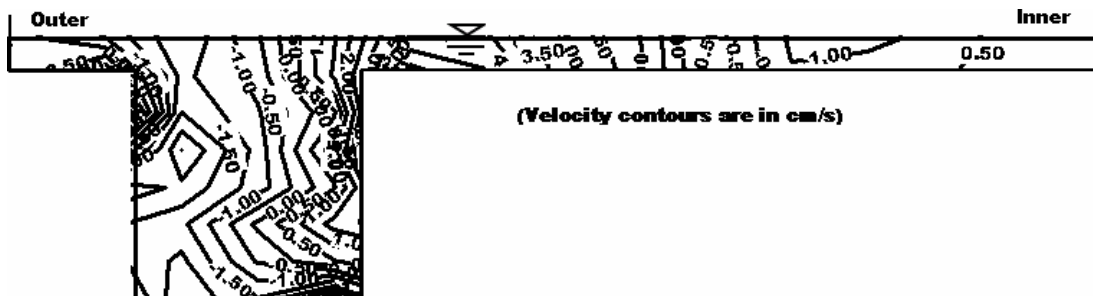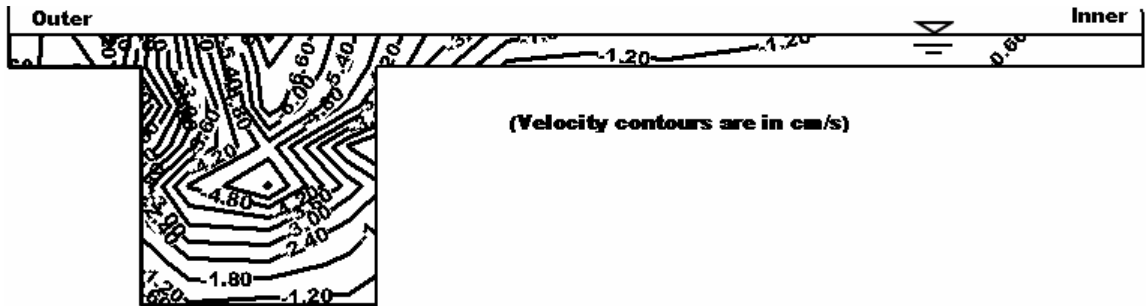
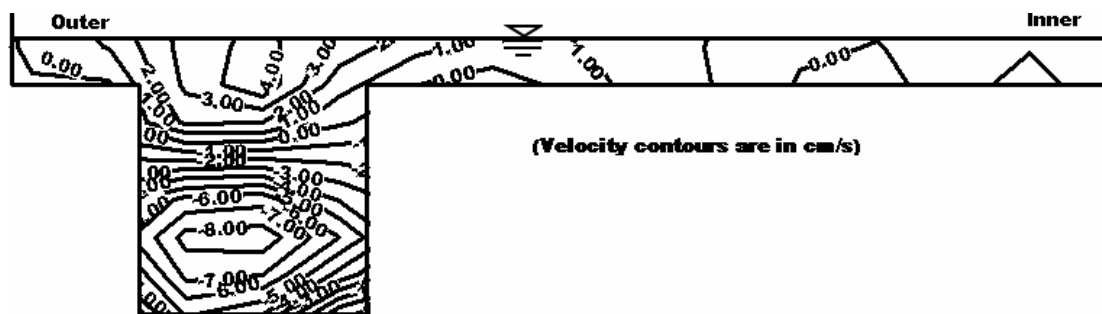**Fig. 4.16.1 Over-bank depth (*H- h*) = 1.68 cm (Type-II channel at bend apex AA)**
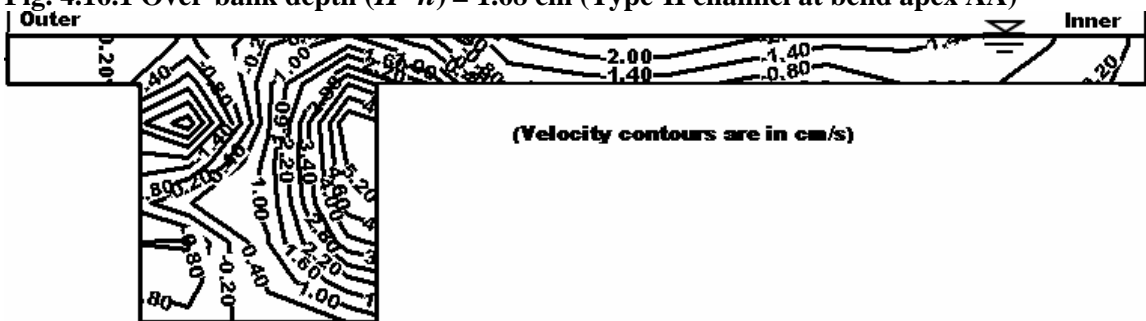
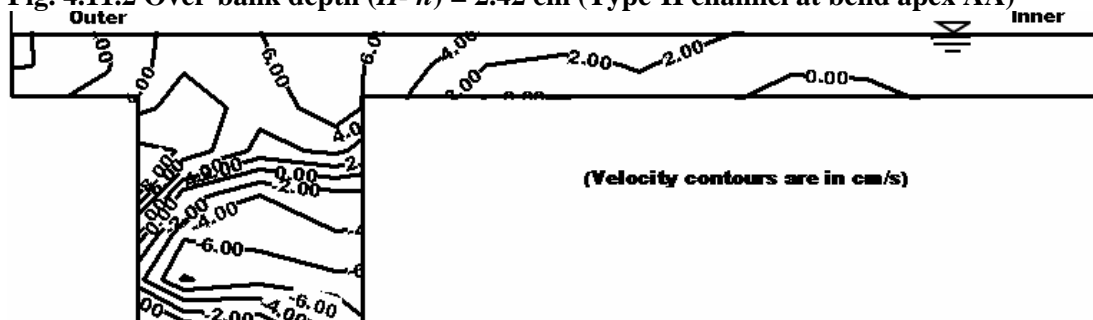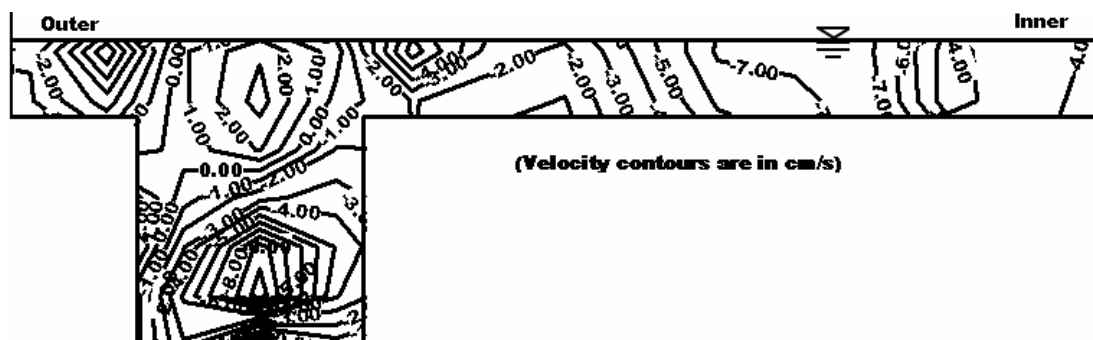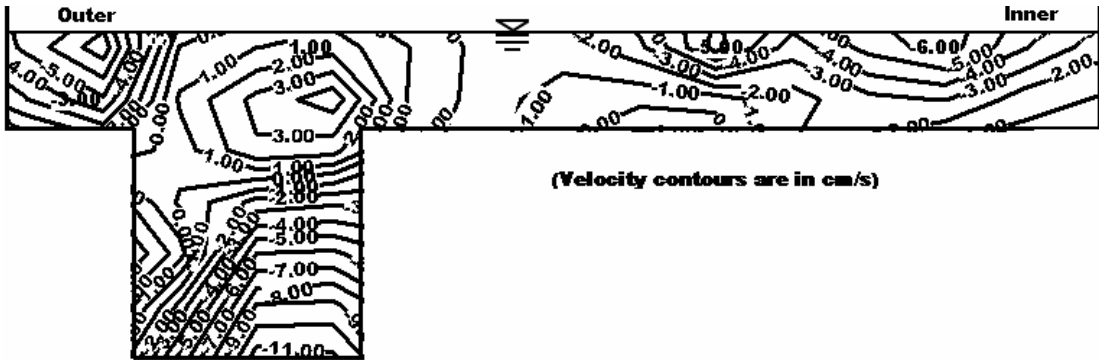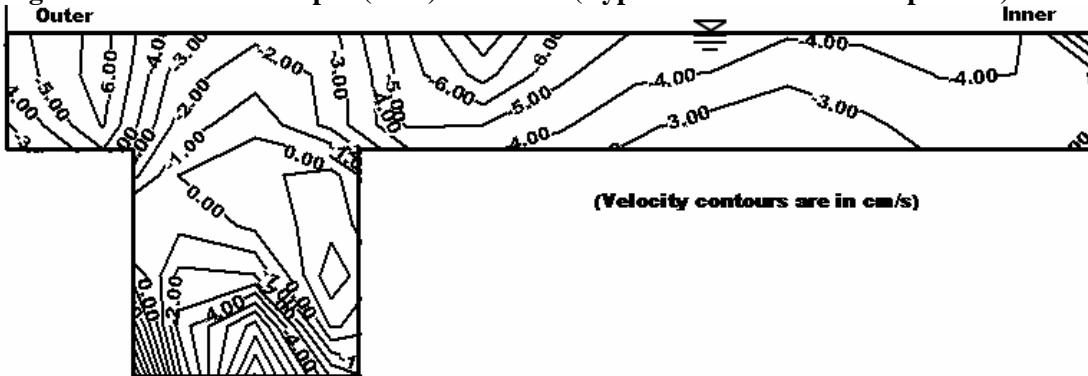**Fig. 4.16.2 Over-bank depth (*H- h*) = 2.42 cm (Type-II channel at bend apex AA)**
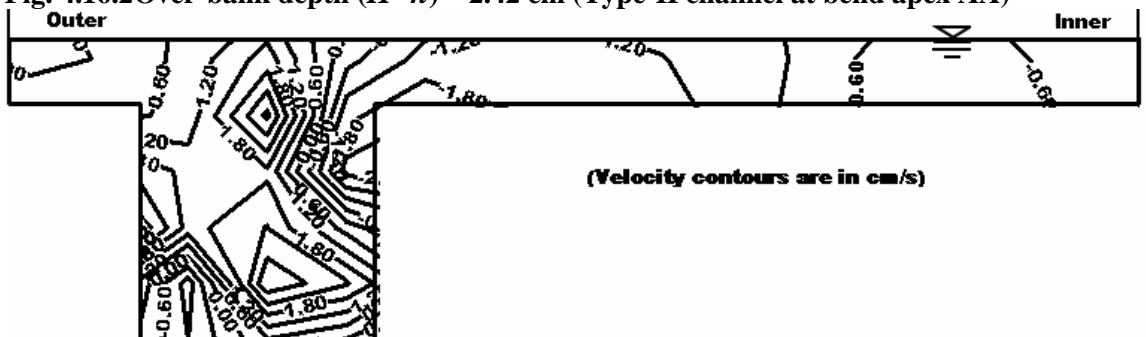
Fig. 4.16.3 Over-bank depth (*H- h*) = 3.28 cm (Type-II channel at bend apex AA)
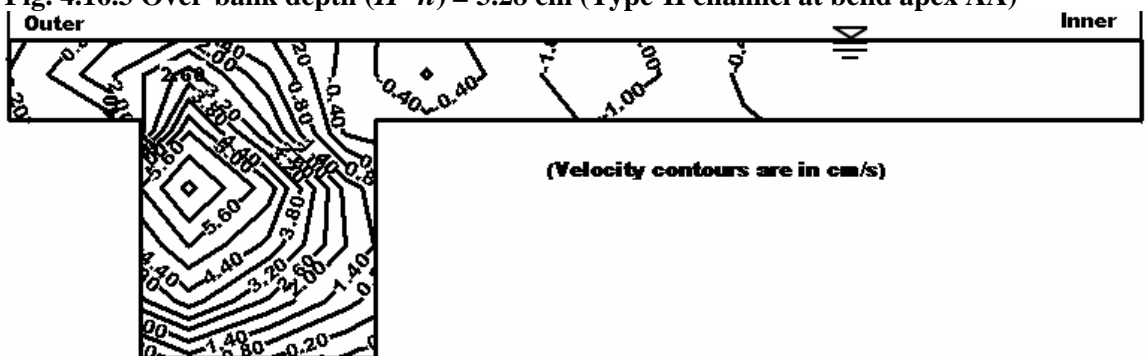
Fig. 4.16.4 Over-bank depth (*H- h*) = 4.08 cm (Type-II channel at bend apex AA)
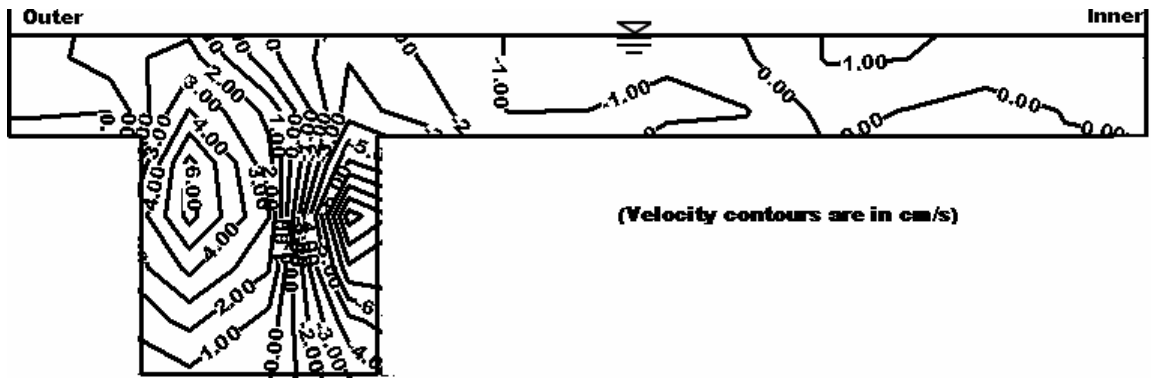
Fig. 4.16.5 Over-bank depth (*H- h*) = 5.10 cm (Type-II channel at bend apex AA)
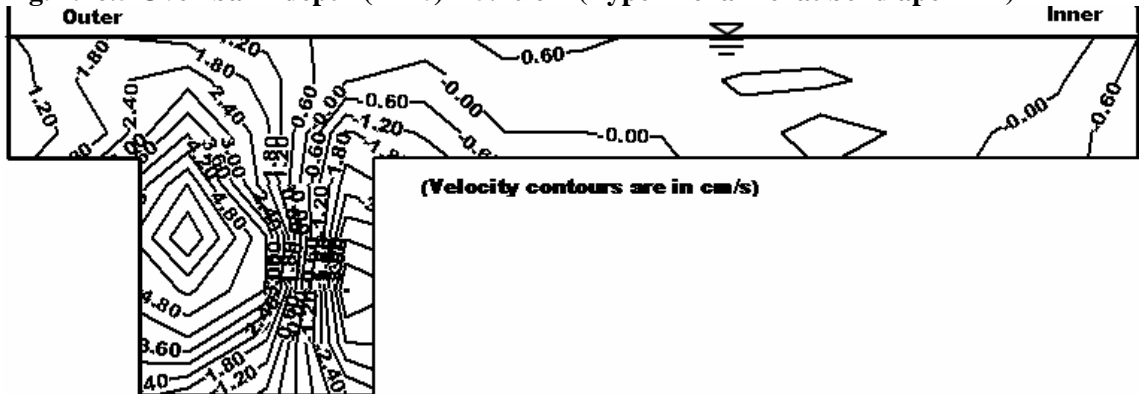
Fig. 4.16.6Over-bank depth (*H- h*) = 6.15 cm (Type-II channel at bend apex AA)

Fig.4.16.1-Fig. 4.16.6 Contours showing the distribution of vertical velocity at bend apex (Section AA) of meandering compound (Type-II) channels.
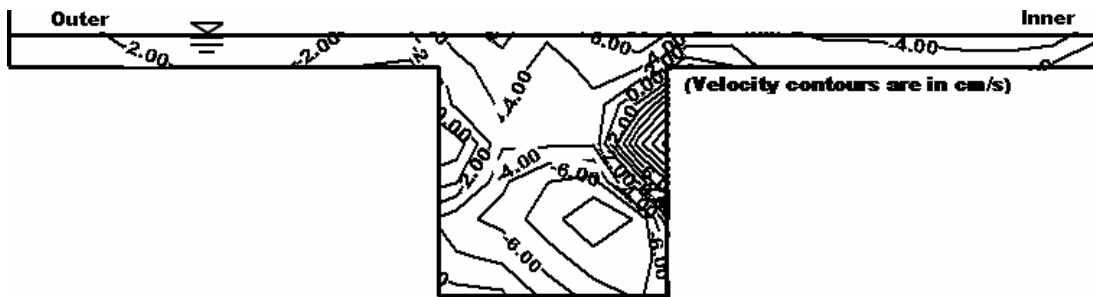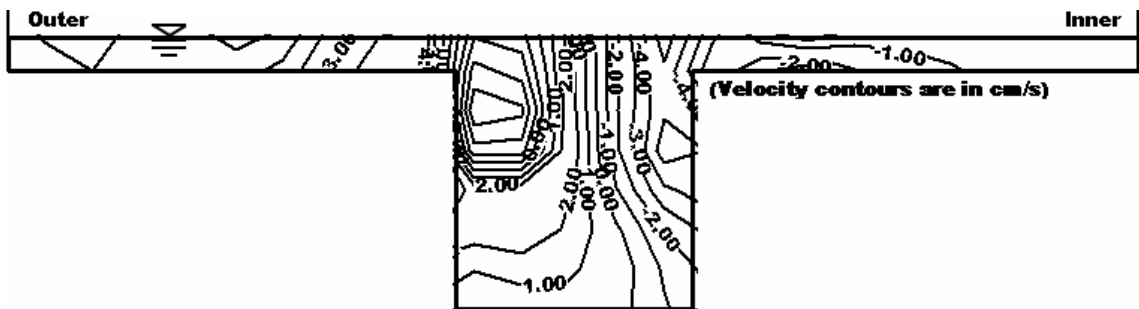
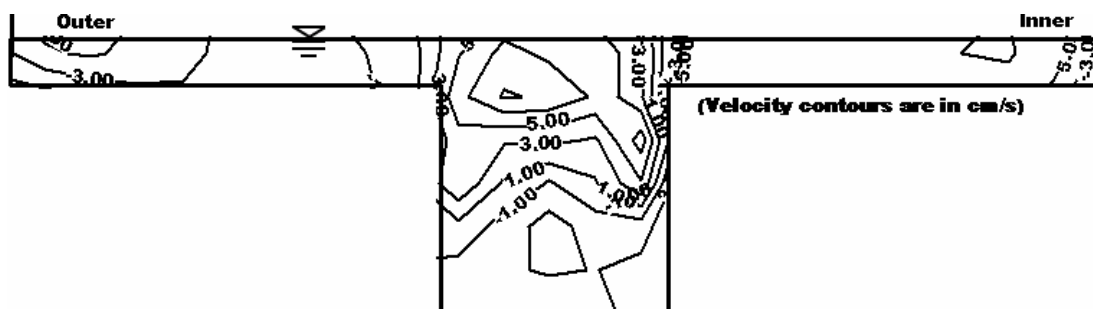**Fig. 4.16.7 Over-bank depth (*H- h*) = 1.68 cm (Type-II channel at cross over BB)**
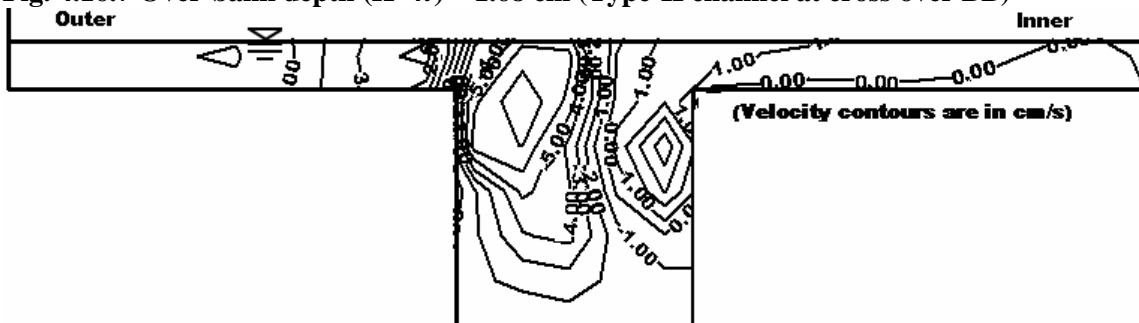
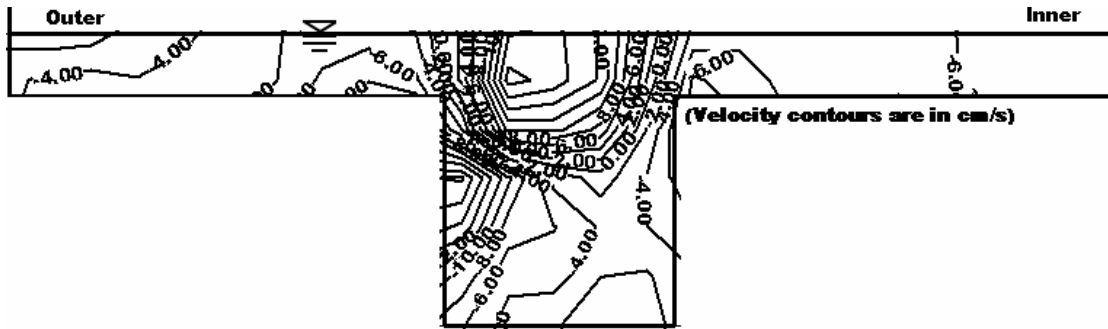**Fig. 4.16.8 Over-bank depth (*H- h*) = 2.42 cm (Type-II channel at cross over BB)**
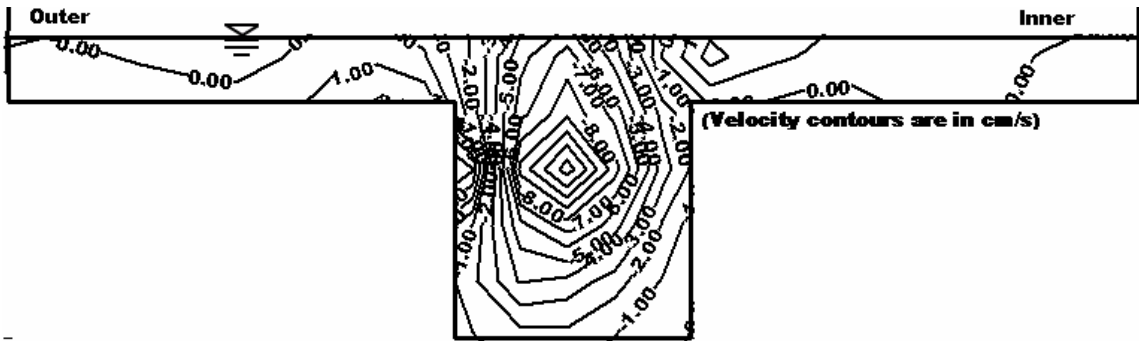
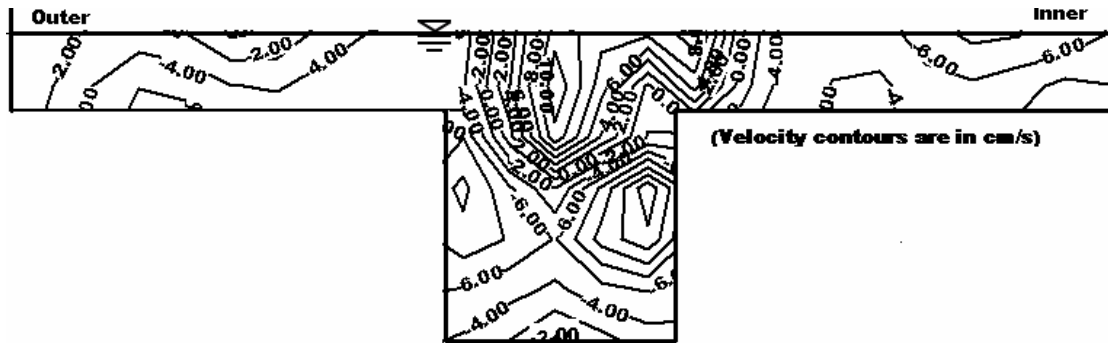**Fig. 4.16.9 Over-bank depth** $(H- h)$ = **3.28 cm (Type-II channel at cross over BB)**
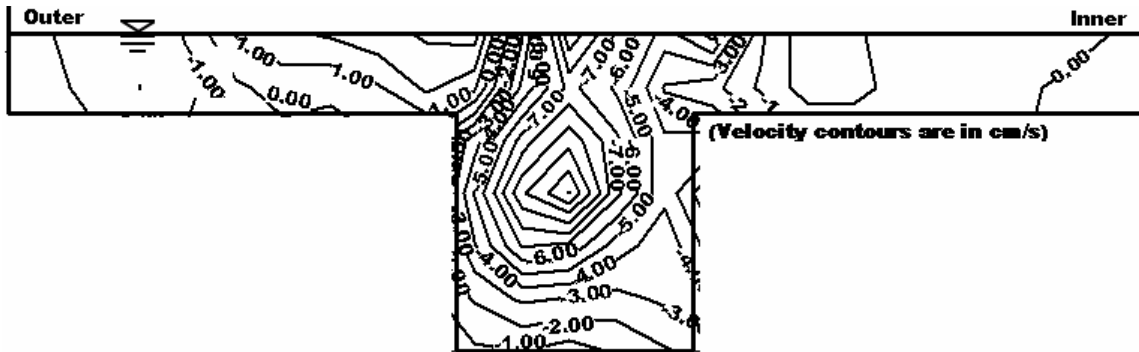
Fig. 4.16.10 Over-bank depth $(H- h)$ = **4.08 cm (Type-II channel at cross over BB)**
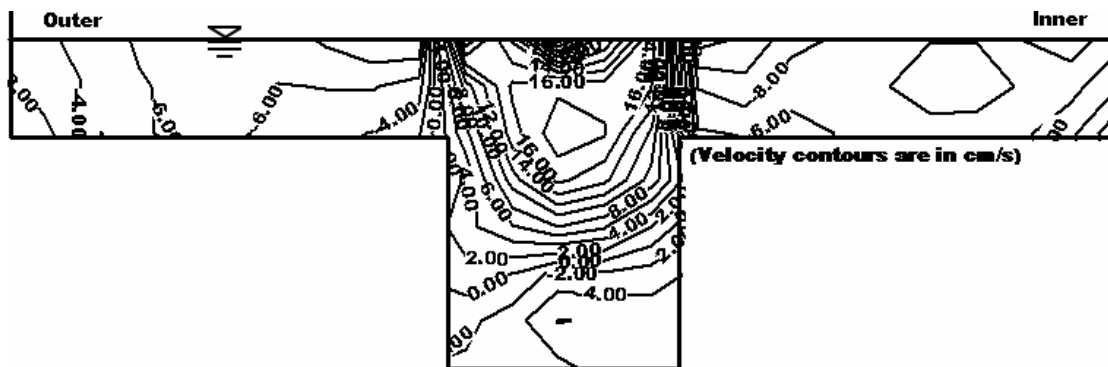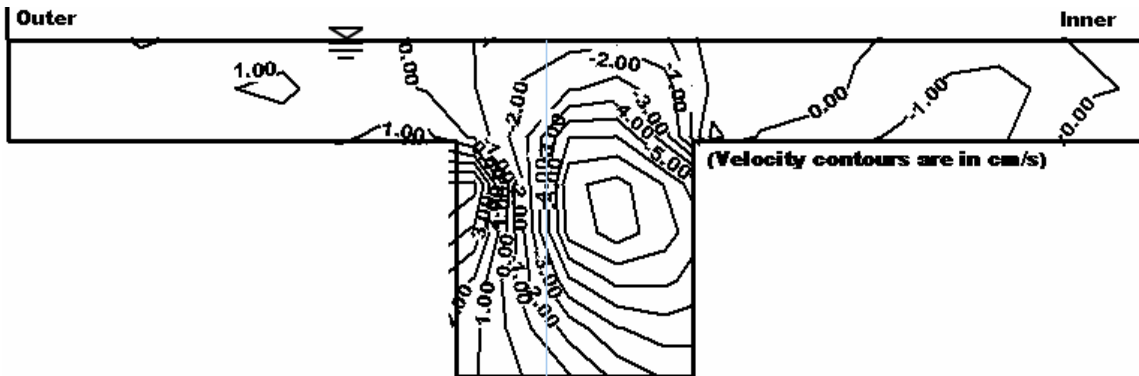

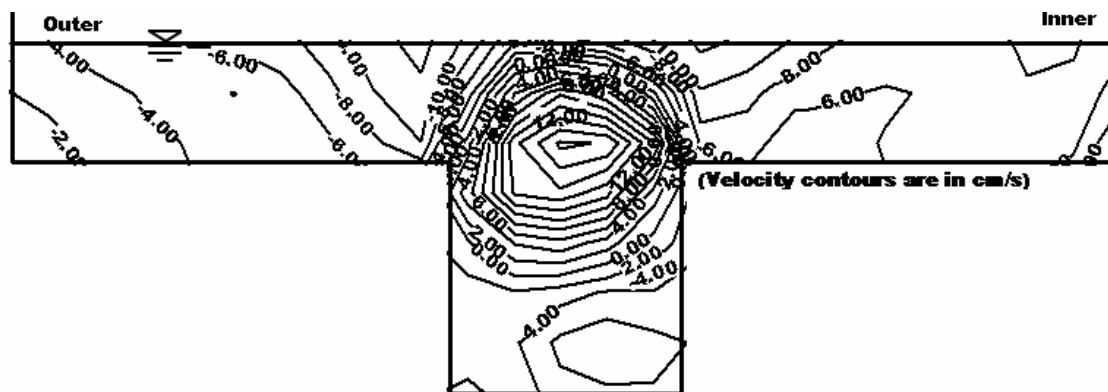**Fig. 4.16.11 Over-bank depth** *(H- h)* = **5.10 cm (Type-II channel at cross over BB)**
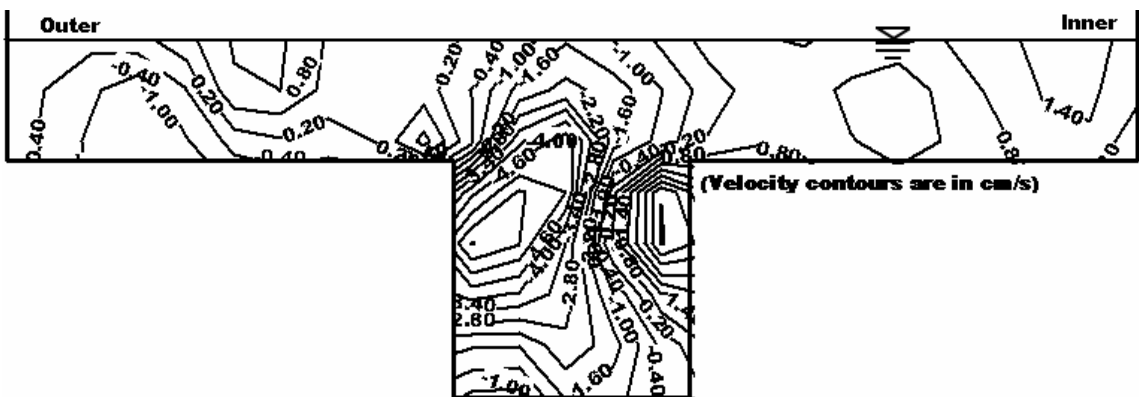
Fig. 4.16.12 Over-bank depth $(H- h)$ = **6.15 cm (Type-II channel at cross over BB)**

Fig.4.16.7-Fig.4.16.12 Contours showing the distribution of vertical velocity at geometrical cross-over of (Type-II) meandering compound channels.

Fig. 4.17.1 Over-bank depth (*H- h*) = 0.74 cm (Type-III meandering compound channel at bend apex AA)

Fig. 4.17.2 Over-bank depth (*H- h*) = 1.74 cm (Type-III meandering compound channel at bend apex AA)

Fig. 4.17.3 Over-bank depth (*H- h*) =1.92 cm (Type-III meandering compound channel at bend apex AA)
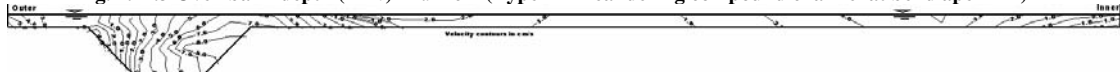
Fig. 4.17.4 Over-bank depth (*H- h*) = 2.17 cm (Type-III meandering compound channel at bend apex AA)
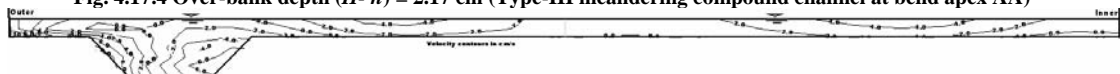
Fig. 4.17.5 Over-bank depth (*H- h*) = 2.93 cm (Type-III meandering compound channel at bend apex AA)
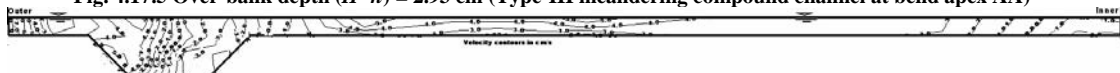
Fig. 4.17.6 Over-bank depth (*H- h*) = 3.01 cm (Type-III meandering compound channel at bend apex AA)

Fig.4.17.1-4.17.6 Contours showing the distribution of vertical velocity at bend-apex of (Type-III) meandering compound channels.
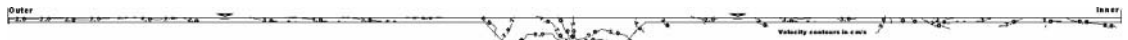
Fig. 4.17.7 Over-bank depth (*H- h*) = 0.74 cm (Type-III meandering compound channel at cross-over BB)
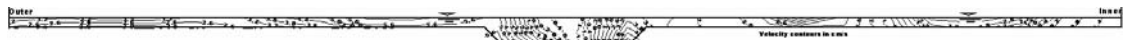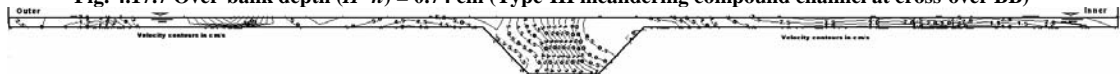

Fig. 4.17.8 Over-bank depth (*H- h*) = 1.74 cm (Type-III meandering compound channel at cross-over BB)

Fig. 4.17.9 Over-bank depth (*H- h*) = 1.92 cm (Type-III meandering compound channel at cross-over BB)

Fig. 4.17.10 Over-bank depth (*H- h*) = 2.17 cm (Type-III meandering compound channel at cross-over BB)

Fig. 4.17.11 Over-bank depth (*H- h*) = 2.93 cm (Type-III meandering compound channel at cross-over BB)
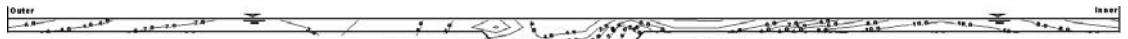

Fig. 4.17.12 Over-bank depth (*H- h*) = 3.01 cm (Type-III meandering compound channel at cross-over BB)

Fig.4.17.7-4.17.12 Contours showing the distribution of vertical velocity at geometrical cross-over of (Type-III) meandering compound channels.

4.7.2   MEANDER CHANNEL WITH FLOODPLAIN

From the vertical velocity contours (Figs. 4.16.1-Figs. 4.16.12 and Figs. 4.17.1-Figs. 4.17.12) for meander channel with floodplains corresponding to Type-II and Type-III channels respectively, the following features can be observed.

(i)   At the bend-apex for meandering compound channel of Type-II, the direction of vertical components are upward in outer region and down-ward at inner regions of the main channel.

(ii)   At the bend-apex of the Type-III meandering compound channel, the direction of vertical velocity are upward at the outer region, both for floodplain and main channel with higher contours appearing near the outer wall of floodplain. The down ward velocity contours are at the inner regions of floodplain with large contours appearing at the central region of inner floodplain.

(iii)   At the geometrical cross-over regions of meandering compound channels of Type-III, the direction of vertical components are mostly upward except small value looking vertical velocity contours down-ward near the wall of inner floodplain. Down ward velocity components are observed at both floodplains. For low depths of flow over floodplain, the velocity components in floodplain is found to be down ward direction but at higher over-bank depths, the velocity components in floodplain region are found to be upward.

(iv)   The threads of upward vertical velocity are found near the inner wall and down ward components are found near the outer wall of the main channel.

(v)   The magnitudes of vertical velocity in the floodplain regions are observed to be less than the main channel area at the bend-apex as well as at the geometrical cross-over.
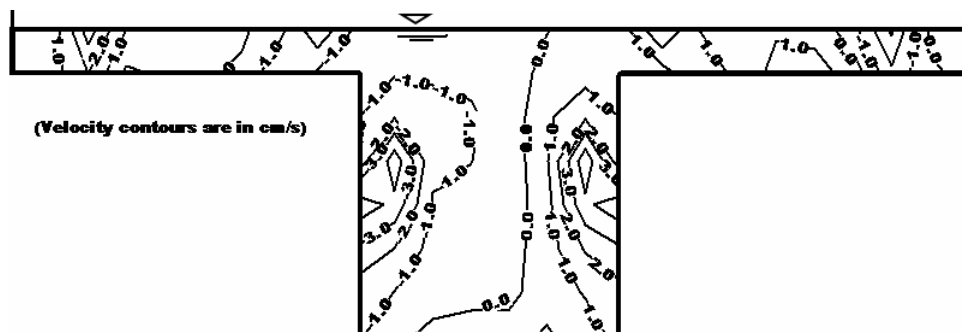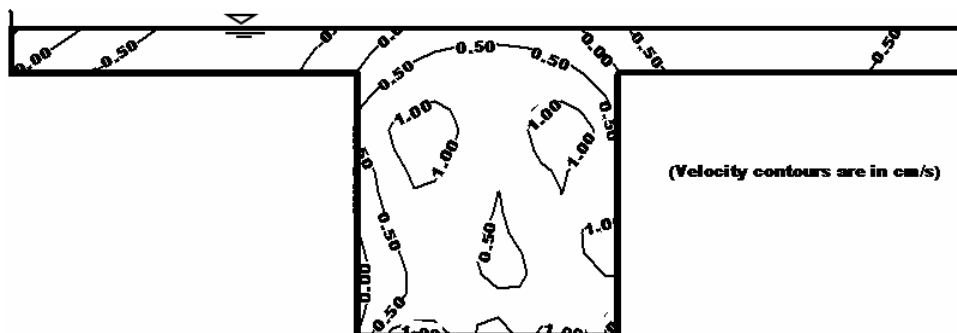

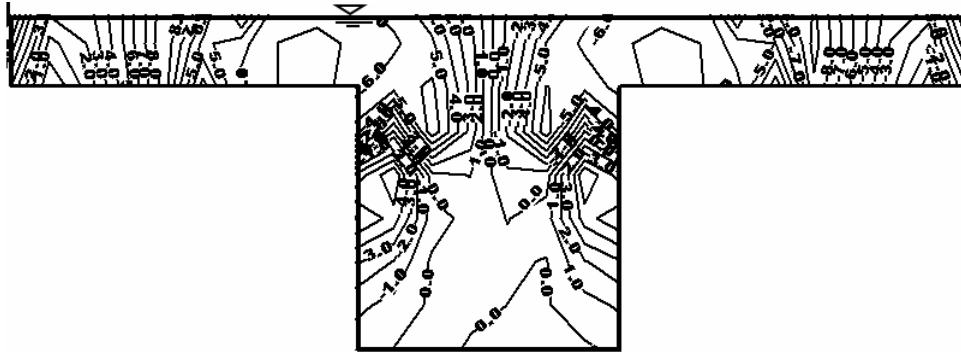**Fig. 4.18.1 Over-bank depth (H- h) = 2.12 cm (Type-I compound channel)**
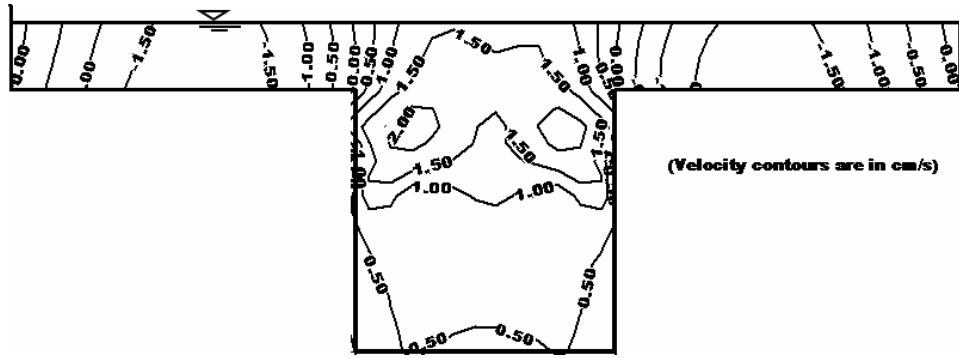
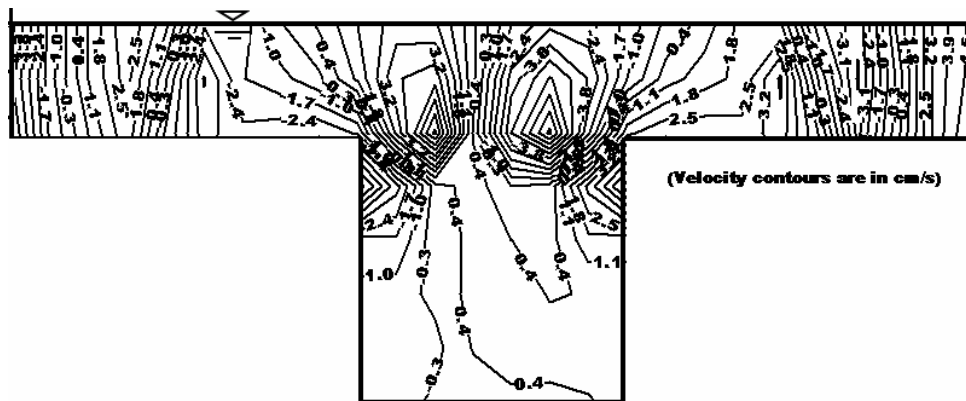**Fig. 4.18.2 Over-bank depth (*H- h*) = 3.15 cm (Type-I compound channel)**
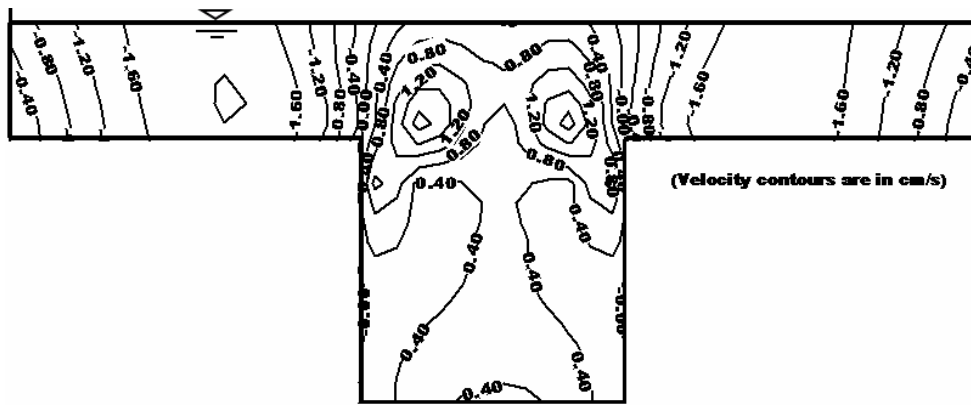
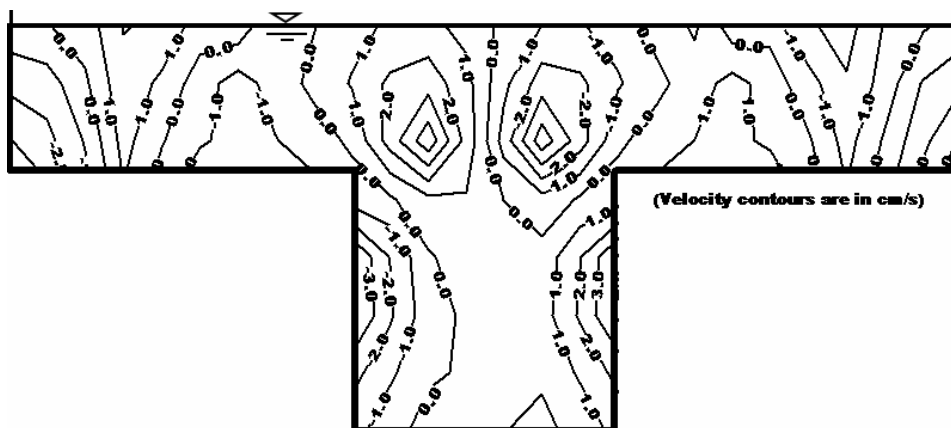**Fig. 4.18.3 Over-bank depth (*H- h*) = 5.25 cm (Type-I compound channel)**

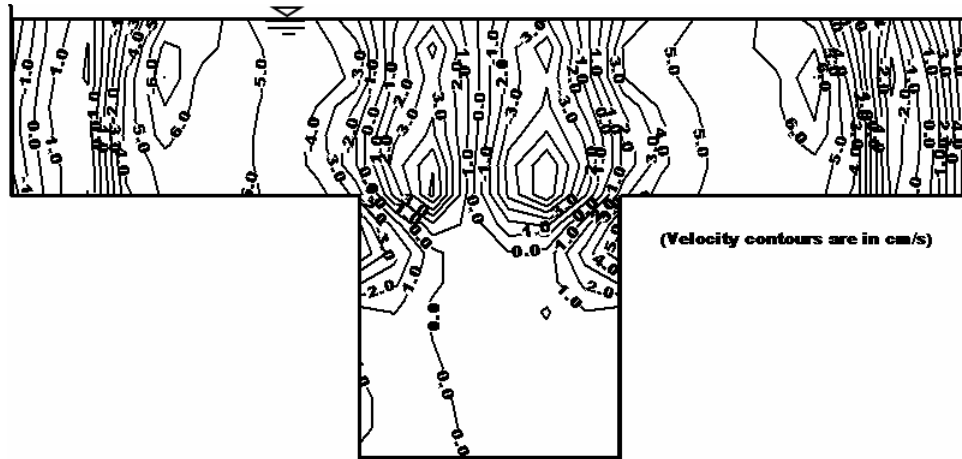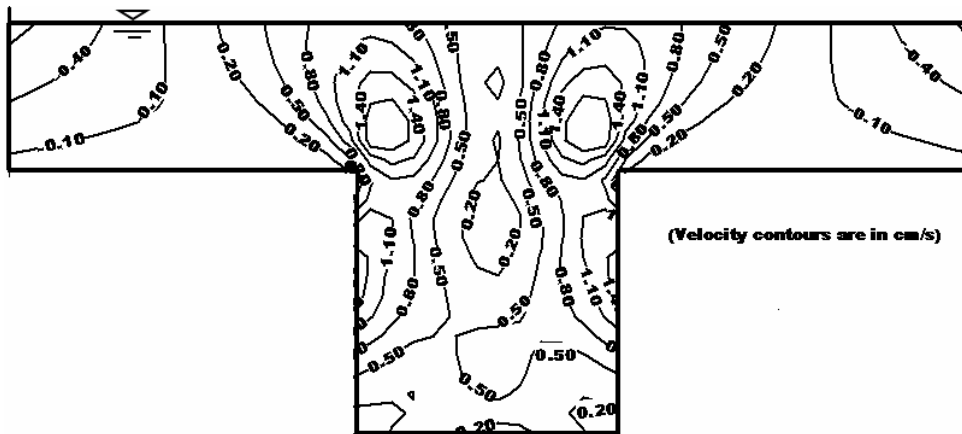**Fig. 4.18.4 Over-bank depth (*H- h*) = 6.75 cm (Type-I compound channel)**
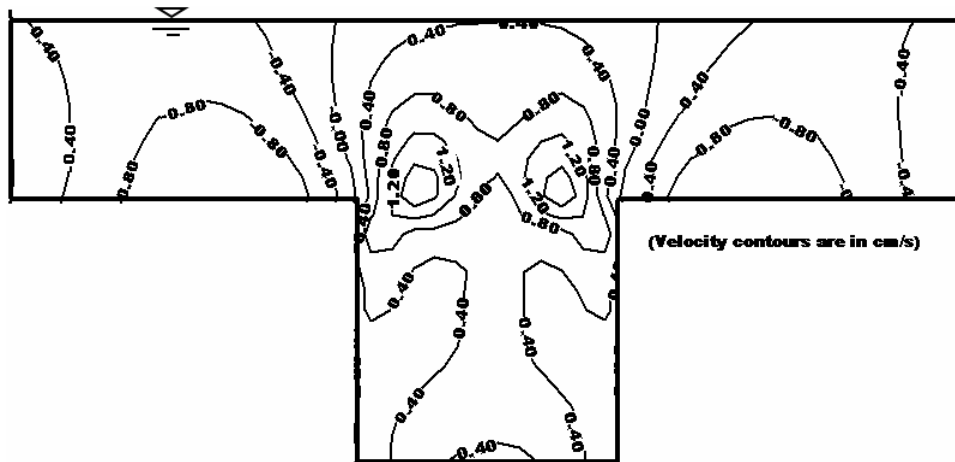
Fig. 4.18.5 Over-bank depth (*H- h*) = 8.21 cm (Type-I compound channel)

Fig.4.18.1-Fig.4.18.5 Contours showing the distribution of vertical velocity of Type-I straight compound channels.

4.7.3 STRAIGHT COMPOUND CHANNEL

From the isovels of vertical velocity for the straight compound channel geometry (Type-I), the following features can be noted (Figs. 4.18.1-Fig. 4.18.5).

(i)   The magnitude of vertical velocity is less when compared to the tangential velocity. The vertical component of velocity is found to be of the order of around 25% when compared to the transverse velocity at lower depths over floodplain (Fig.4.13.1-Fig.4.18.1) and 20 % at higher depths over floodplain (Fig.4.13.5–Fig.4.18.5).

(ii)   At lower over-bank depths, upward positive velocity components are found in the main channel region and down-ward velocity components are found at the flood plain regions.

(iii)   For lower over-bank depths, higher upward vertical velocity are observed at the junction between main channel and flood plain and the magnitude reduces with increase in depth over floodplain.

*****

ANALYSIS AND DISCUSSION OF THE RESULTS

5.1 GENERAL

The results of the experimental runs involving flow in simple meander channels, straight compound channel, and meander channel - floodplain geometry are analysed. Basing on the experimental data, discussion on the variation of channel resistance with depth of flow, the boundary shear force distribution, and analysis of momentum transfer are made. From the model out puts, the location of interface plain with zero shear for separating compound channel section into zones for discharge calculation using divided channel method is proposed. Various 1D discharge predictive models for straight and compound meandering channels are analysed and tested with the experimental data. Better alternative approaches to predict discharge in over-bank flow are suggested. Division of flow between main channel, lower main channel, and floodplain are attempted. The discharge adjustment factor-coherence relationships and the evaluation of interaction lengths at different interface plains are discussed. The experimental and computed parameters concerning the flow in simple straight channels (Type-I, runs S_1 to S_{11}), mildly meander channel (Type-II, runs MM_1 to MM_{15}) and for high meandering and wide channels (Type-III, runs HM_1 to HM_{15}) are given in Table 5.1. Similarly for over bank conditions, the corresponding data for Type-I (runs S_{12} to S_{21}), Type-II (runs from MM_{16} to MM_{27}), and for Type-III (runs HM_{16} to HM_{27}) channels are given in Table 5.2.

5.2 VARIATION OF REACH AVERAGED LONGITUDINAL VELOCITY U WITH DEPTH OF FLOW

Plots between the reach averaged velocity U and non-dimensional flow depth for all the experimental channels from in-bank to over-bank conditions for all the three types of channels are shown in Fig.5.1. From the figure it can be seen that for all the compound channels, the increase in the reach averaged longitudinal velocity of flow is nearly in accordance with the increase in depth of flow. The outflow of water to the floodplain above the bank full stage causes a sudden drop in the reach averaged

velocity. The drop is mainly due to the interaction between the main channel and floodplain flows resulting from the change of hydraulic radius. Due to flow interaction, there is an increased resistance to the flow, a large portion of which is from the additional loss of energy in the system.
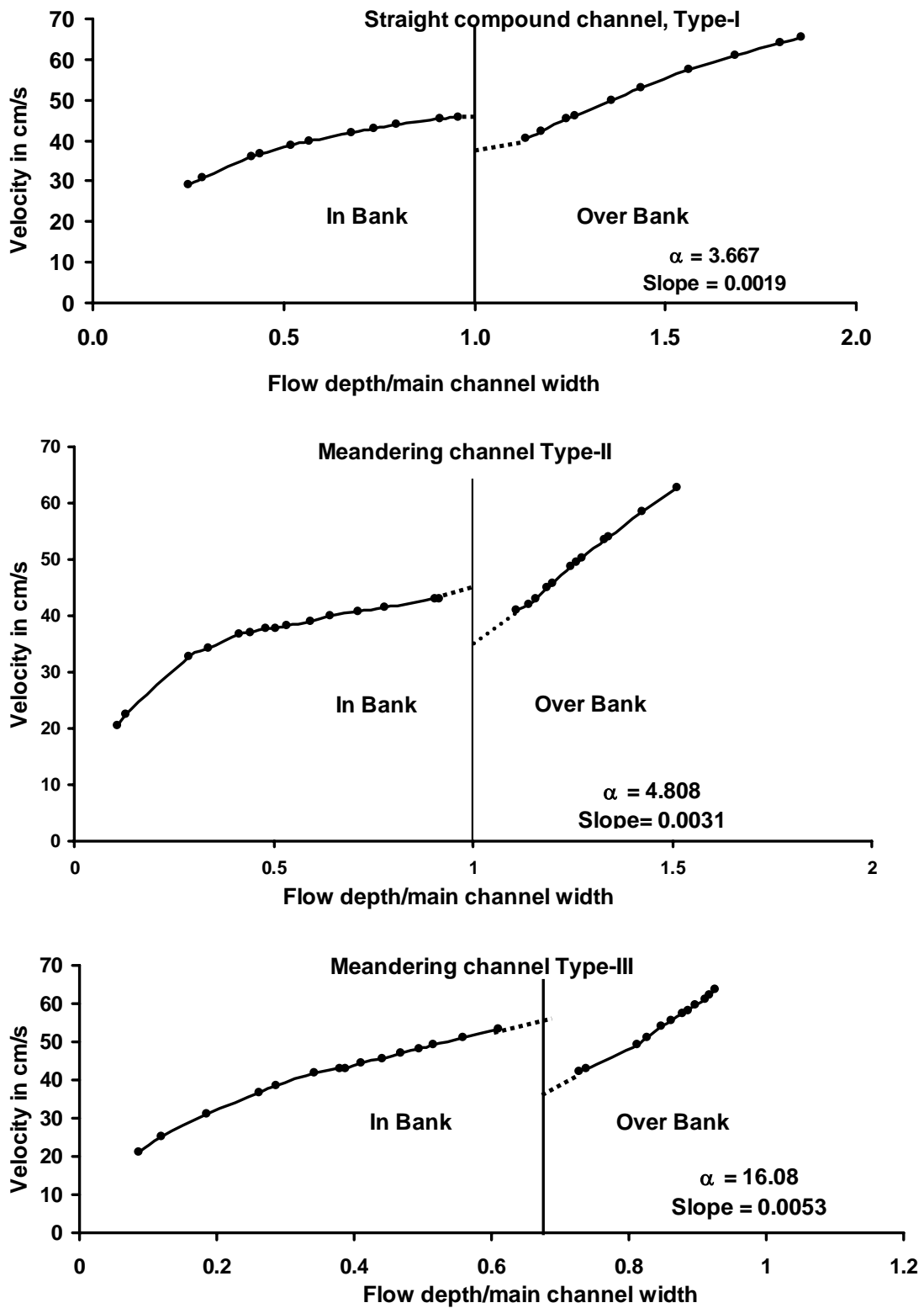
Fig 5.1 Reach Averaged Velocity Against Flow Depth/ Main Channel Width

The drop in the reach averaged velocity is higher for type-III channel. This may be due to spreading of water to a wider section for Type-III channel than Type-I and Type-II channel sections, ($\alpha = 3.667$ for Type-I, $\alpha = 4.808$ for Type-II, and $\alpha = 16.08$ for Type-III), resulting additional resistance to flow. As the depth of flow in the floodplain increases, the effect of flow interaction reduces. This is manifested in the form of increase in the section mean velocity of the compound channel with increase in flow depth in the floodplains. Both for in-bank and over-bank flow conditions, the rate of increase of velocity with flow depth is higher for the sinus channel of Type-III and lower for straight compound channel of Type-I. This is mainly due to their large differences in the longitudinal bed slopes. The slope of the channel is an important parameter influencing the desired driving force.

5.3 RESISTANCE FACTORS IN THE CHANNEL FLOW

Distribution of energy in a channel section is an important aspect that needs to be addressed properly. While using Manning's equation, selection of a suitable value of n is the single most important parameter for the proper estimation of velocity in an open channel. Major factors affecting Manning's roughness coefficient are the (i) surface roughness, (ii) vegetation, (iii) channel irregularity, (iv) channel alignment, (v) silting and scouring, (vi) shape and size of a channel, and (vii) stage-discharge relationship. Assuming the flow to be uniform and neglecting all non-friction losses, the energy gradient slope can be considered equal to the average longitudinal bed slope S of a channel. Under steady and uniform flow conditions, we use the equations proposed by Chezy's (1770), Darcy-Weisbach's (1857), or Manning's (1891) to compute the section mean velocity carried by a channel section proposed as

Manning's equation $\quad V = \dfrac{1}{n} R^{2/3} S^{1/2}$ (5.1)

Chezy's equation $\quad V = C \sqrt{RS}$ (5.2)

Darcy-Weisbach's equation $\quad Q = \left(\dfrac{8g}{f} \right)^{\frac{1}{2}} \sqrt{RS}$ (5.3)

where A = the channel cross-sectional area, g = gravitational acceleration, R = the hydraulic mean radius of the channel section, f = the friction factor used, n = Manning's resistive coefficient, and C = Chezy's channel coefficient.

Pang (1998), and Willets and Hardwick (1993), Patra (1999), Patra and Kar (2000) have shown that the roughness coefficient like Manning's *n* not only denotes the roughness characteristics of a channel but also the energy loss in the flow. The influences of all the forces that resist the flow in an open channel are assumed to have been lumped to a single coefficient *n*.

Table 5.1 Summary of Experimental Results for In-bank Flows

Channel Type	Run No	Discharge (cm³/s)	Flow Depth (cm)	Channel Width (cm)	Cross Section Area (cm²)	Wetted Perimeter (cm)	Average Velocity (cm/s)	Overall Mean shear (N/m²)	Manning's Roughness *n*	$\sqrt{S}/n$	Chezy's *C*	Friction Factor *f*
(1)	(2)	(3)	(4)	(5)	(6)	(7)	(8)	(9)	(10)	(11)	(12)	(13)
Type-I Straight channel	S1	1061	3.02	12	36.24	18.04	29.28	0.37	0.01100	3.96	47.39	0.035
	S2	1280	3.44	12	41.28	18.88	31.01	0.41	0.01099	3.97	48.11	0.034
	S3	2148	4.98	12	59.76	21.96	35.94	0.51	0.01097	3.97	49.99	0.031
	S4	2307	5.24	12	62.88	22.48	36.69	0.52	0.01095	3.98	50.33	0.031
	S5	2902	6.21	12	74.52	24.42	38.94	0.57	0.01093	3.99	51.14	0.030
	S6	3249	6.80	12	81.60	25.6	39.82	0.59	0.01098	3.96	51.16	0.030
	S7	4117	8.15	12	97.80	28.3	42.10	0.64	0.01099	3.97	51.95	0.029
	S8	4548	8.82	12	105.8	29.64	42.97	0.67	0.01100	3.96	52.17	0.029
	S9	5058	9.55	12	114.60	31.10	44.14	0.69	0.01094	3.99	52.75	0.028
	S10	5947	10.92	12	131.00	33.84	45.38	0.72	0.01090	3.96	52.91	0.028
	S11	6312	11.48	12	137.70	34.96	45.82	0.73	0.01102	3.96	52.95	0.028
Type-II Mildly Meandering Channel	MM1	316	1.29	12	15.48	14.58	20.41	0.32	0.01097	5.07	42.69	0.062
	MM2	426	1.57	12	18.84	15.14	22.61	0.37	0.0110	5.05	43.71	0.0592
	MM3	1347	3.44	12	41.28	18.88	32.63	0.66	0.0111	5.01	47.56	0.0500
	MM4	1669	4.05	12	48.60	20.1	34.34	0.73	0.0113	4.93	47.59	0.0499
	MM5	2200	4.98	12	59.76	21.96	36.81	0.82	0.0114	4.88	48.10	0.0488
	MM6	2357	5.31	12	63.72	22.62	36.99	0.85	0.0116	4.79	47.50	0.0501
	MM7	2619	5.78	12	69.36	23.56	37.76	0.89	0.0117	4.75	47.43	0.0502
	MM8	2757	6.08	12	72.96	24.16	37.79	0.91	0.0119	4.68	46.87	0.0515
	MM9	2946	6.41	12	76.92	24.82	38.31	0.94	0.0120	4.66	46.90	0.0514
	MM10	3338	7.11	12	85.32	26.22	39.12	0.98	0.0121	4.61	46.74	0.0517
	MM11	3698	7.7	12	92.40	27.40	40.02	1.02	0.0121	4.60	46.97	0.0512
	MM12	4191	8.55	12	102.60	29.10	40.84	1.07	0.0122	4.56	46.88	0.0514
	MM13	4656	9.34	12	112.08	30.68	41.54	1.11	0.0123	4.53	46.85	0.0515
	MM14	5596	10.9	12	130.32	33.72	42.94	1.17	0.0124	4.51	47.08	0.0510
	MM15	5680	11.01	12	132.12	34.02	42.99	1.18	0.0124	4.50	47.02	0.0511
Type-III Highly Meandering channel	HM1	287	1.05	12	13.70	14.97	20.94	0.05	0.0110	6.62	36.09	0.087
	HM2	484	1.44	12	19.35	16.07	25.01	0.06	0.0111	6.58	37.57	0.080
	HM3	987	2.22	12	31.57	18.28	31.28	0.09	0.0113	6.47	39.23	0.073
	HM4	1742	3.13	12	47.36	20.85	36.78	0.12	0.0115	6.34	40.23	0.070
	HM5	2048	3.44	12	53.11	21.73	38.55	0.13	0.0115	6.33	40.65	0.068
	HM6	2757	4.1	12	66.01	23.59	41.77	0.15	0.0116	6.26	41.16	0.067
	HM7	3224	4.55	12	75.30	24.87	42.81	0.16	0.0120	6.09	40.55	0.069
	HM8	3338	4.65	12	77.42	25.15	43.11	0.16	0.0120	6.07	40.50	0.069
	HM9	3698	4.93	12	83.46	25.94	44.30	0.17	0.0120	6.05	40.71	0.068
	HM10	4191	5.3	12	91.69	26.99	45.70	0.18	0.0121	6.02	40.87	0.068
	HM11	4656	5.62	12	99.02	27.89	47.02	0.18	0.0121	6.02	41.13	0.067
	HM12	5122	5.93	12	106.32	28.77	48.17	0.19	0.0121	6.00	41.30	0.066
	HM13	5515	6.18	12	112.35	29.48	49.09	0.20	0.0122	5.99	41.44	0.066
	HM14	6396	6.71	12	125.54	30.98	50.95	0.21	0.0122	5.97	41.71	0.065
	HM15	7545	7.33	12	141.69	32.73	53.25	0.22	0.0122	5.97	42.19	0.064

Table 5.2 Summary of Experimental Runs for Over-bank Flow Observed at Bend Apex

Channel Type	Run No	Discharge (cm³/sec)	Flow Depth (cm)	Flood Plain Width (cm)	Total Area (cm²)	Total Wetted Perimeter (cm)	Average Velocity (cm/sec)	Overall Mean shear (N/m²)	Manning's Roughness n	$\sqrt{S}/n$	Chezy's C	Friction Factor f
(1)	(2)	(3)	(4)	(5)	(6)	(7)	(8)	(9)	(10)	(11)	(12)	(13)
Type-I Straight channel	S12	8726	13.62	32	215.28	71.24	40.53	0.56	0.0104	4.17	53.49	0.0274
	S13	10007	14.12	32	237.32	72.242	42.16	0.61	0.0106	4.11	53.37	0.0275
	S14	12245	14.88	32	270.72	73.76	45.23	0.68	0.0106	4.09	54.16	0.0267
	S15	13004	15.15	32	282.60	74.3	46.01	0.71	0.0107	4.06	54.13	0.0267
	S16	16706	16.32	32	334.08	76.64	50.00	0.81	0.0108	4.03	54.94	0.0259
	S17	19861	17.25	32	375.11	78.50	52.96	0.89	0.0108	4.02	55.59	0.0254
	S18	25329	18.75	32	440.96	81.50	57.43	1.00	0.0108	4.01	56.64	0.0244
	S19	30844	20.21	32	505.24	84.42	61.04	1.11	0.0109	3.98	57.24	0.0239
	S20	36275	21.62	32	567.28	87.24	63.94	1.21	0.0110	3.95	57.52	0.0237
	S21	39071	22.28	32	596.32	88.56	65.52	1.26	0.0110	3.95	57.92	0.0234
Type-II Mildly Meandering Channel	MM16	9006	13.32	45.7	220.16	84.34	40.90	0.78	0.0119	4.64	45.47	0.0379
	MM17	10107	13.68	45.7	240.93	85.06	41.95	0.84	0.0123	4.51	44.76	0.0391
	MM18	10898	13.89	45.7	253.05	85.48	43.06	1.27	0.0123	4.50	44.95	0.0387
	MM19	12245	14.23	45.7	272.67	86.16	44.90	1.36	0.0124	4.48	45.34	0.0381
	MM20	13005	14.42	45.7	283.63	86.54	45.85	1.48	0.0124	4.47	45.48	0.0378
	MM21	15289	14.95	45.7	314.21	87.61	48.66	1.55	0.0124	4.47	46.14	0.0368
	MM22	15998	15.11	45.7	323.44	87.92	49.46	1.65	0.0124	4.47	46.31	0.0365
	MM23	16762	15.28	45.7	333.25	88.26	50.29	1.70	0.0124	4.46	46.49	0.0362
	MM24	19866	15.94	45.7	371.33	89.58	53.50	1.76	0.0124	4.46	47.19	0.0351
	MM25	20523	16.08	45.7	379.41	89.86	54.09	1.84	0.0124	4.46	47.28	0.0350
	MM26	25661	17.10	45.7	438.27	91.91	58.55	1.87	0.0125	4.45	48.15	0.0338
	MM27	31358	18.15	45.7	498.85	94.04	62.85	1.92	0.0125	4.45	49.01	0.0326
Type-III Highly Meandering channel	HM16	12757	8.74	165	302.82	201.10	42.12	0.79	0.0105	6.91	56.58	0.0352
	HM17	13974	8.86	165	325.98	201.34	42.86	0.86	0.0108	6.69	55.53	0.0366
	HM18	24487	9.74	165	495.82	203.10	49.38	0.90	0.0124	5.86	52.10	0.0416
	HM19	27185	9.92	165	530.56	203.46	51.23	0.96	0.0125	5.82	52.30	0.0413
	HM20	31299	10.17	165	578.81	203.96	54.07	1.00	0.0125	5.81	52.91	0.0403
	HM21	33817	10.33	165	609.69	204.28	55.46	1.09	0.0126	5.76	52.92	0.0403
	HM22	37173	10.53	165	648.29	204.68	57.34	1.12	0.0127	5.72	53.10	0.0400
	HM23	39048	10.65	165	671.45	204.92	58.15	1.15	0.0128	5.67	52.95	0.0402
	HM24	41416	10.76	165	692.68	205.14	59.79	1.26	0.0127	5.72	53.63	0.0392
	HM25	44412	10.93	165	725.49	205.48	61.21	1.28	0.0127	5.68	53.70	0.0391
	HM26	46014	11.01	165	740.93	205.64	62.10	1.45	0.0127	5.69	53.92	0.0388
	HM27	48474	11.11	165	760.23	205.84	63.76	1.61	0.0126	5.74	54.68	0.0377

5.3.1 VARIATION OF MANNING'S n WITH DEPTH OF FLOW FOR SIMPLE MEANDER CHANNEL

Experimental results for Manning's n with depth of flow for simple meander channels are plotted in Fig. 5.2. With the exception of Type-I straight channel, the plot indicates that the value of n increases as the flow depth increases. It is observed from the figure that the higher sinus channels consume more energy than low sinus channel for the same depth of flow. It is clear from Fig.5.2 that Manning's roughness coefficient not only denotes the characteristics of channel roughness but also the influence of the energy loss in the flow. It can be also observed from Fig.

5.2 that steeper channels consume more energy than flatter channels. The results are in line with earlier reports given by Bhattacharya (1995), Patra (2000), Sellin et al. (1993), Pang (1998), and Willetts and Hardwick (1993).
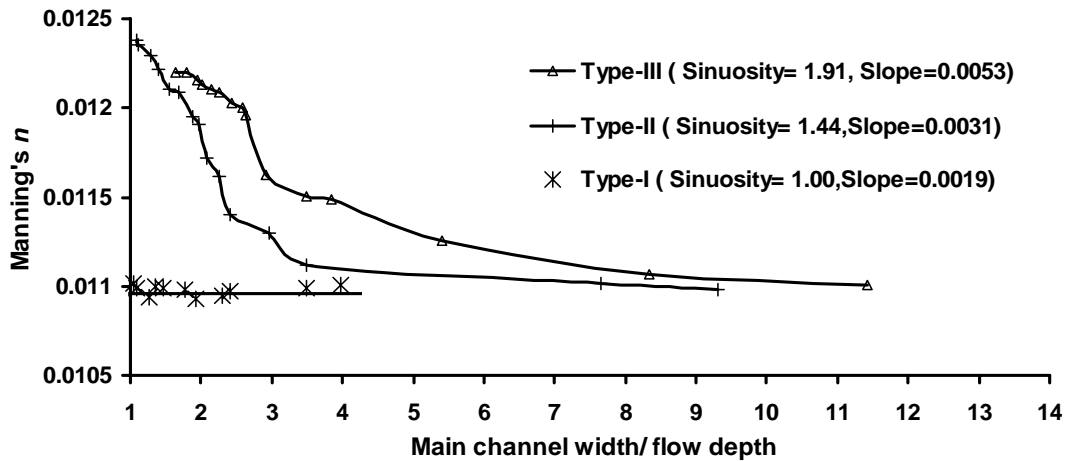
Fig. 5.2 Variation of Manning's *n* with Depth of Flow for Inbank Flows

5.3.2 VARIATION OF ENERGY ($\sqrt{S}/n$) WITH DEPTH OF FLOW FOR STRAIGHT AND MEANDERING COMPOUND SECTIONS

To understand the energy loss that are due to more potent flow exchange mechanism in meander channel floodplain geometry, the stage-discharge data are analysed using the standard resistance equations and the single channel method. Sellin et.al (1993) observed that for smooth floodplains, the flow resistance coefficient of Manning's *n*, when plotted against the relative depths of flow in the channel, showed a sharp change in the *n* values, particularly when the channel is highly sinuous. Pang (1998) had also reported that Manning's roughness coefficient not only denotes the characteristics of channel roughness, but also the influence of the energy loss of flow. The larger the value of *n*, the more is the energy loss in the flow. Willetts and Hardwick (1993) studied four types of sinuous channels having the same cross section and reported that the value of Manning's *n* for a 8 mm depth of water over the floodplain could vary from 0.01 (for their straight channel) to 0.018 for the channel with sinuosity of 2.06. The variation of *n* for a floodplain water depth of 40 mm ranged from 0.0026 (for straight channel) to 0.0199 for the same channel section with sinuosity of 2.06. For highly sinuous channels the values of *n* becomes large indicating that the energy loss is more for such channels.

For the present compound channels the values of $\sqrt{S}/n$, where *S* is the channel slope are plotted against the relative depth β in Fig. 5.3. It can be seen from Fig.5.3

that the value of $\sqrt{S}/n$ is the largest for Type-III and the least for Type-I channel. This may be due to higher longitudinal slope and floodplain width of Type-III channel when compared to Type-I channel. For all the three types of channel, there is a decrease in the values of $\sqrt{S}/n$ after the immediate bank full depth. For type-I channel and Type-II channel, the rate of decrease is less than the Type-III channel. Type-III channel is more sinuous and therefore meandering causes an additional loss of energy.
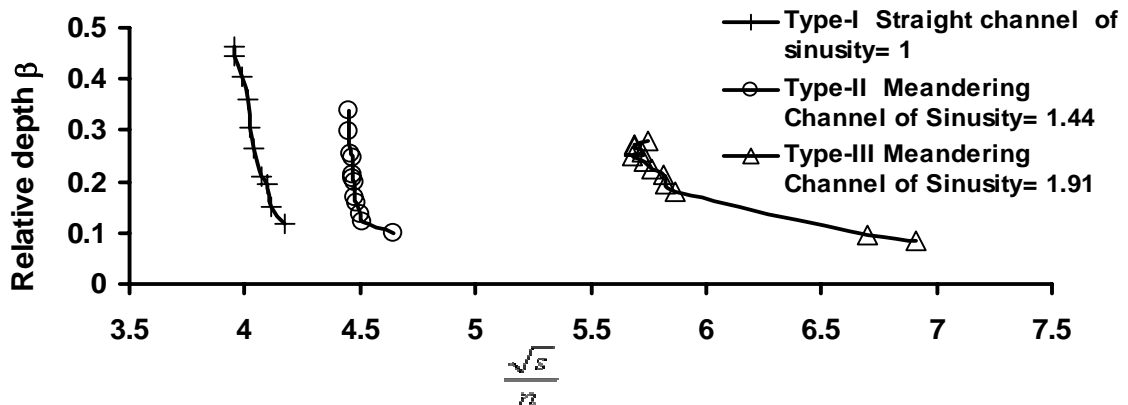
Fig.5.3 Variation of $\sqrt{S}/n$ with Relative Over-bank Depth of Flow β

5.3.3 VARIATION OF RESISTANCE FACTORS WITH DEPTH OF FLOW FROM SIMPLE TO COMPOUND SECTIONS

Due to flow interaction between the main channel and floodplain, the flow in a compound section consumes more energy than a channel with simple section carrying the same flow and having the same type of channel surface. The energy loss is manifested in the form of variation of resistance coefficients of the channel with depth of flow. The variation of Manning's roughness coefficient n, Chezy's C and Darcy - Weisbach friction factor f with depths of flow ranging from in-bank channel to the over-bank stage are discussed for the three different types of channel with different geometry and sinuosity. All the channel surfaces are kept smooth to give better insight into the problem. The variation of roughness coefficients are discussed with a greater detail on the Manning's n. The experimental results along with the computed values of n, C, and f for in-bank and over-bank flow conditions are given in Table.5.1 and 5.2 respectively.

5.3.3.1 VARIATION OF MANNING'S n WITH DEPTH OF FLOW

The variation of Manning's n with depth of flow ranging from in-bank to over-bank flow conditions for all the three types of channels investigated is shown in Fig. 5.4.

For the Type-I channel (straight) the value of n remains nearly constant. At just over bank condition a sudden fall in Manning's n is noticed. This is due to sudden decrease of the hydraulic radius at just over bank condition. At further increase of the depth of flow in the floodplain, the results of Type-I channel show a slow increase of the value of n. The results of this investigation are similar to the straight compound channel data reported by Knight and Demetriou (1983).
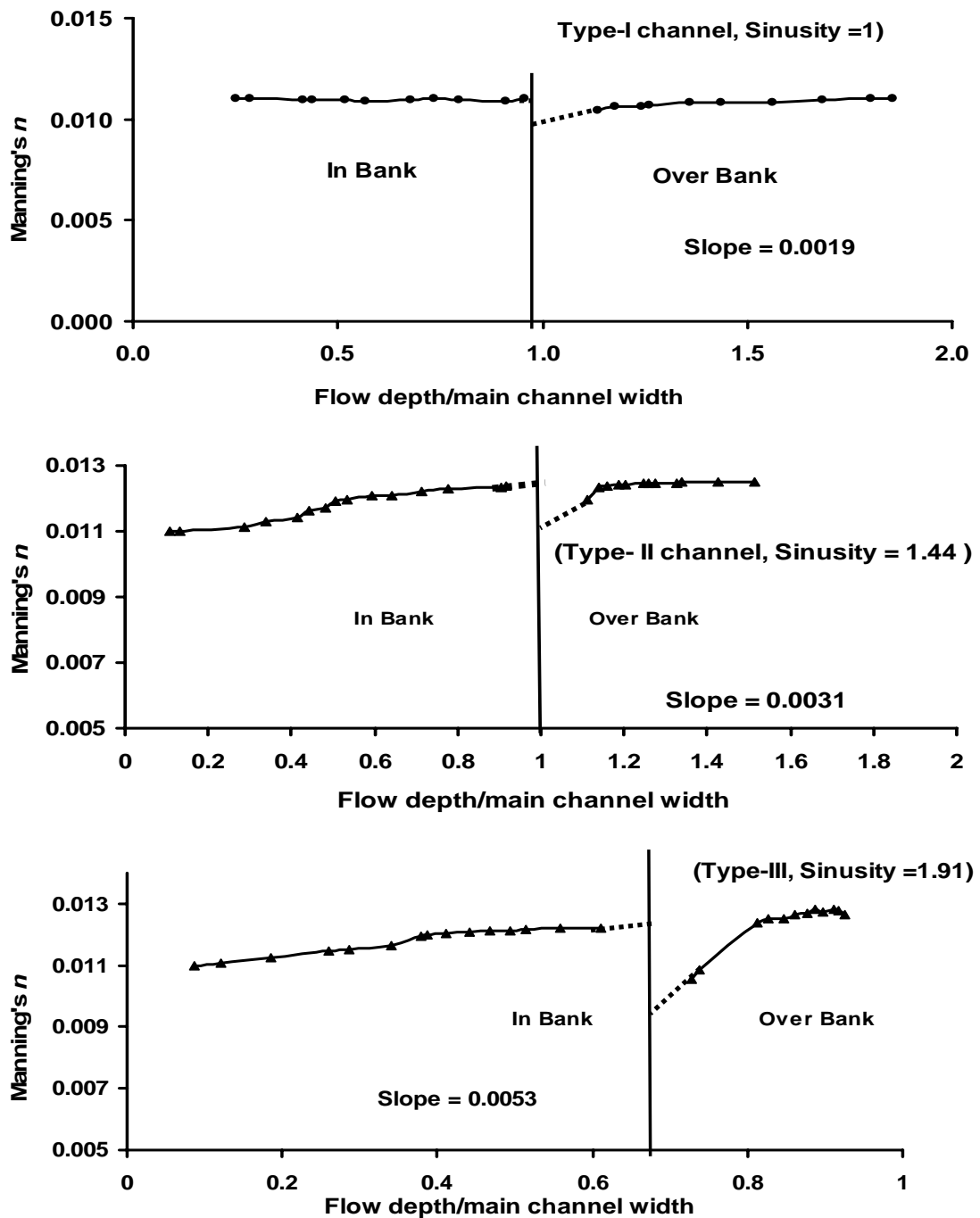
Fig. 5.4 Variation of Manning's n with Depth of Flow from In-bank to Over-bank

The values of Manning's *n* for Type-II and Type III channels exhibit a higher increasing trend than Type-I channel. For the simple meandering channel flow, the increase in Manning's *n* is mainly due to the increase in the strength of secondary flow induced by curvature resulting higher loss of energy. This increase in the value of *n* continues for the ranges of flow depths investigated. The increase is more in Type-III than Type-II channels mainly due to its higher sinuosity. In both types of channels a sudden fall in the value of Manning's *n* is noticed at just over-bank flow conditions. With further increase in over-bank flow depth, the value of Manning's *n* increases more steeply for Type-III channel than Type-II, except for the highest depth for Type-III channel. This is mainly due to a greater energy loss resulting from the flow interaction between the channel and the floodplain flows with sinuosity. At still higher over-bank depths, the value of *n* is expected to attain a constant value. The results are similar to the smooth trapezoidal channels of FCF, UK reported by Sellin et al. (1993) and the channel of Bhattacharya (1995).

5.3.3.2 VARIATION OF CHEZY'S *C* WITH DEPTH OF FLOW

The variation of Chezy's *C* with depth of flow for the three types of channels investigated is shown in Fig. 5.5. For Type-II and Type-III channels when the flow is confined to meandering section only, a gradual increase in the value of *C* with the flow depth is observed. Since it is very difficult to observe the flow parameters at just over-bank flow condition, interpretation of the data between in-bank to over-bank flow is the only alternative option. A sudden change in the value of *C* is expected to take place for Type-I and II channel when the water spreads to the floodplain which could not be recorded. However for Type-III channel, there is a jump in the value of *C* at just over bank condition. This may be due to critical combination of higher slope, sinuosity and the flow geometry (large flood plain width) of Type-III channel. With further increase in the depth of flow over floodplain there is an immediate decrease in the value of *C* that tries to increase and attain a steady state with further increase in its flow depth. As the depth of flow in the floodplain further increases, the value of *C* also increases for all types of channels investigated. The channels are expected to give a steady value of *C* at still higher depths of flow in the floodplain.

5.3.3.3 VARIATION OF DARCY-WEISBACH FRICTION FACTOR f WITH DEPTH OF FLOW

The variation of the Darcy-Weisbach's friction term f with depth of flow for the Type-I, Type-II, and Type-III channel is shown in Fig.5.6. The behavioral trend of friction factor f is nearly similar to that of the variation of Manning's n reported earlier.
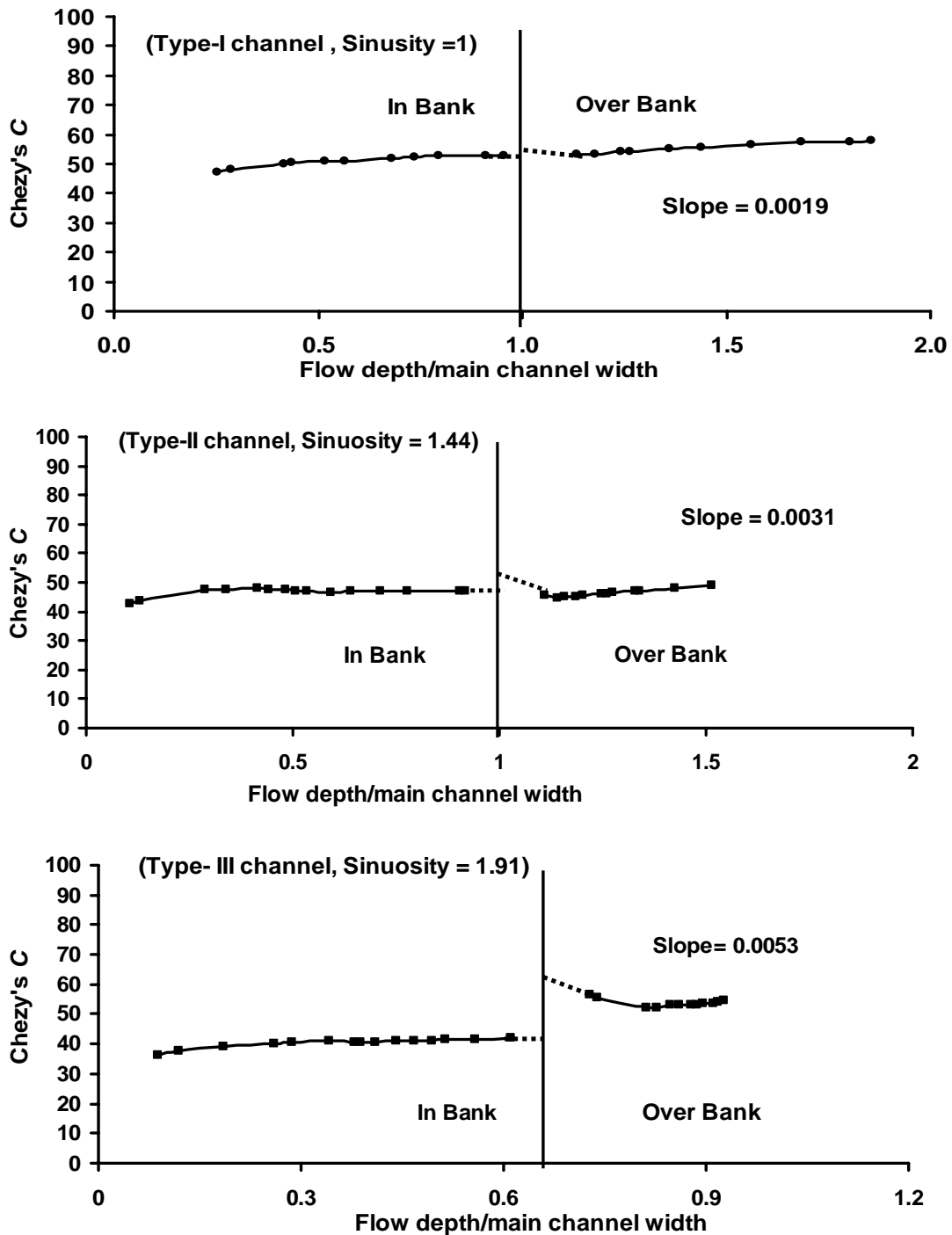
Fig. 5.5 Variation of Chezy's C with Depth of Flow from In-bank to Over-bank
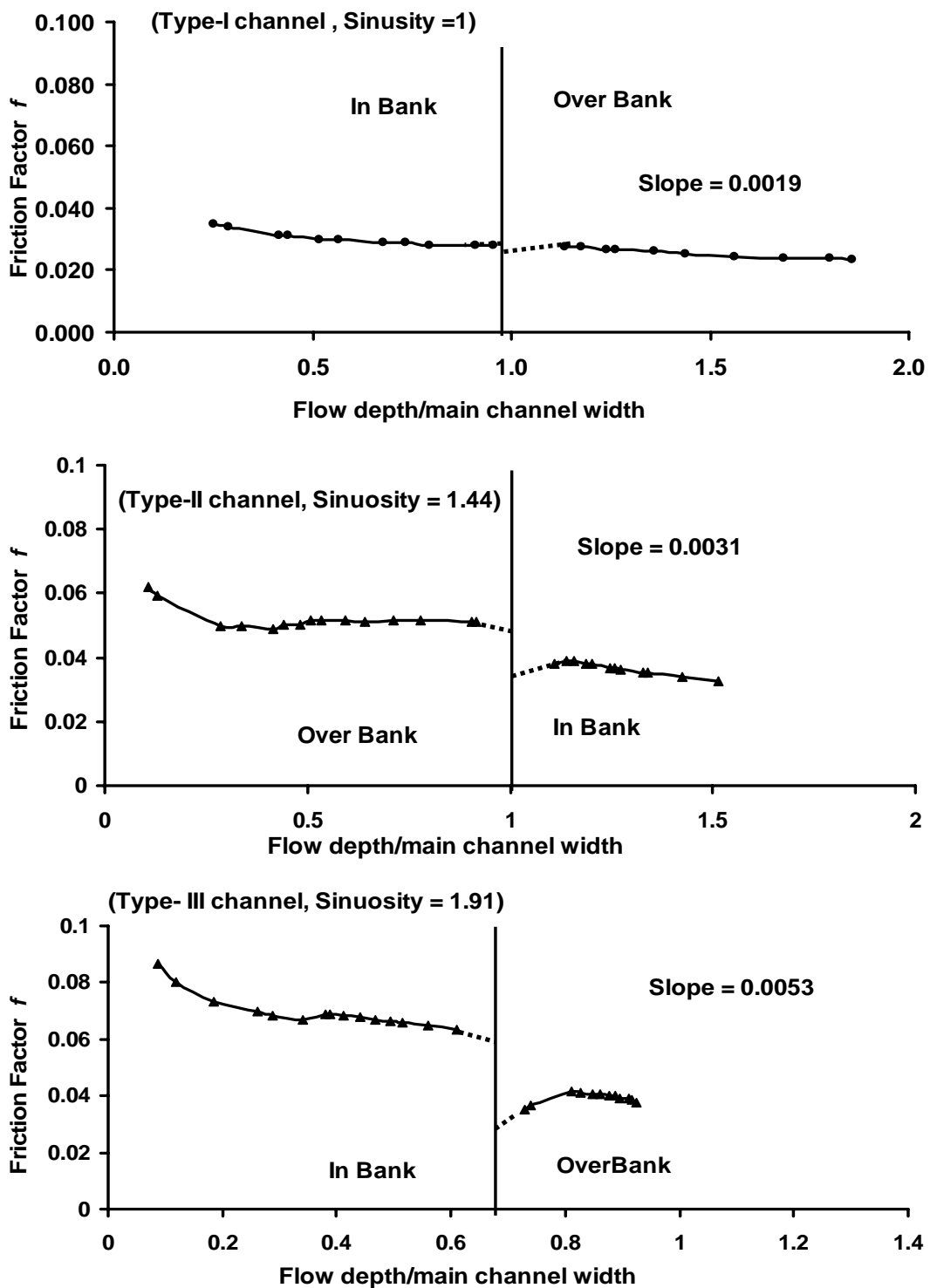
Fig. 5.6 Variation of Darcy-Weisbach Factor *f* with Depth of Flow from In-bank to Over-bank

5.4. ZONAL VARIATION OF MANNING'S *n* FOR MAIN CHANNEL AND FLOODPLAIN SUB-SECTIONS

At just over-bank flow condition, there is an abrupt change in the prevailing hydraulic condition of a compound channel. This gives rise to a sudden change in

the resistance to the flow of a channel. At over-bank flow, the mean velocity in the main channel sub-section and that in the floodplain sub-section are different. The channel section becomes compound and the flow structure for such section is characterized by large shear layers generated due to the difference of sub-area mean velocity between the main channel and floodplain flow. Under such a condition, Knight et al. (1989), Knight and Shino (1996) have shown that there is a large difference in the Manning's n between the main channel and floodplain to that when the channel is composite (reported for the River Severn). For the present experimental channels, the variation of Manning's n with depth of flow for the main channel and floodplain of the compound section is plotted in Fig. 5.7. The variation of Manning's n of main channel and flood plain separately under isolated condition and under interacting conditions is shown in the same figure.

It is seen from Fig.5.7 that for all the channels, the floodplain values of n decreases with depth of flow just after bank full depth, attains a minimum value, and then increases gradually back to the composite value of the compound channel. Similarly, the n values of main channel increases with depth of flow at just above the bank full stage, attains a maximum value, and then decreases gradually back to the composite value of the compound channel. The reason of decrease of the value of n in the floodplain sub-area for low over-bank depth is mainly due to (i) decrease in hydraulic radius, (ii) gain of large amount of momentum from main channel. At the stage of the minimum value of n of the floodplain the momentum transfer from main channel to floodplain is the maximum and its increase to the composite value of the compound section is the indication of the completion of momentum transfer process. A similar mirror reverse effect follows for the cases of the main channel sub-area. At still higher over-bank depths, the momentum transfer process is likely to be completed. At certain stage, the mean velocity of both main channel and floodplain sub sections become equal. At this over-bank stage, the value of n for both main channel and flood plain should reach the composite n. The diverse behavior of n should be considered, while computing discharge in the main channel and floodplain, else there may be errors between the actual and the computed values of discharge rate in a compound section.
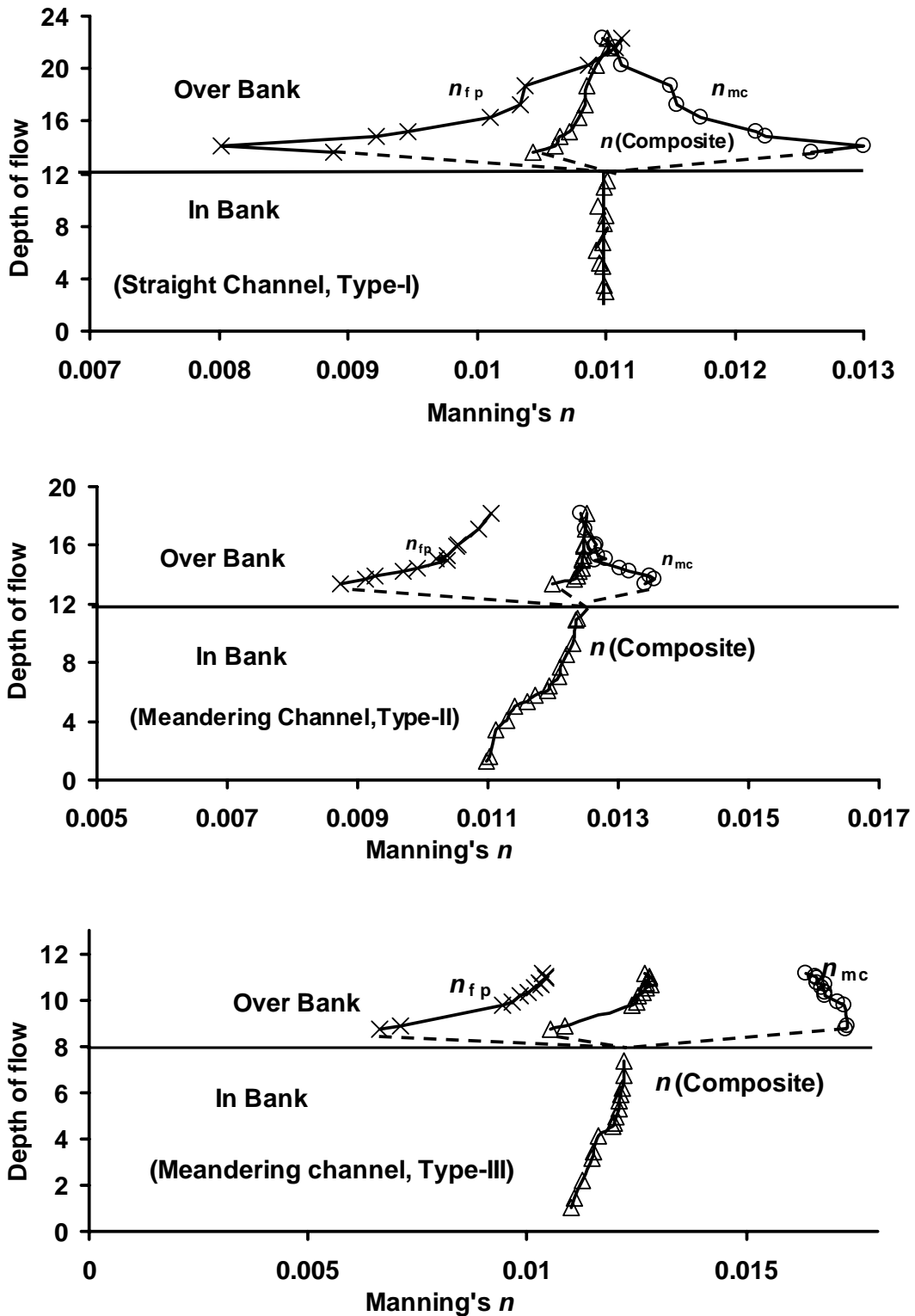
Fig. 5.7 Variation of Manning's *n* for Main channel and Floodplain Subsections for Experimental Channels

5.5 BOUNDARY SHEAR DISTRIBUTION IN COMPOUND CHANNELS

5.5.1 GENERAL

Information regarding the nature of boundary shear stress distribution is needed to solve a variety of river hydraulics and engineering problems such as to give a basic understanding of the flow resistance relationship, to understand the mechanism of sediment transport, to design stable channels, revetments etc. During floods, part of the discharge of a river is carried by the simple main channel and the rest are carried by the floodplains located to its sides. For such compound channels, the flow structure is complex due to the transfer of momentum between the main channel and the adjoining floodplains which magnificently affects the shear stress distribution in flood plain and main channel sub-sections. More-over, knowledge of momentum transfer at the various assumed interfaces originating from the junction between main channel and flood plain can be acquired if the distribution of boundary shear between them is known. Distributions of shear stress along the boundary of meandering and straight compound channel cross section have been investigated (Wright and Carstens 1970, Ghosh and Jena 1971, Myers and Elsawy 1975, Knight 1981, Rhodos and Knight 1994, Knight and Cao 1994, Kar 1977, Bhattacharya 1995, Patra 1999, Patra and Kar 2000). Distribution of boundary shear mainly depends upon the shape of the cross section and the structure of the secondary flow cells. However, for straight compound channel and compound channel with meandering main channel plan form, there is wide variation in the local shear stress distribution from point to point along the wetted perimeter. Therefore, there is a need to evaluate the boundary shear stress carried by the main channel and floodplain walls at various locations of meander path. An investigation is also made to describe the effect of the interaction mechanism on the basis of shear stress distribution in compound channel sections.

5.5.2 BOUNDARY SHEAR FORCE RESULTS

The results of boundary shear stress distributions for in-bank conditions of meandering channels of Type-II and Type-III are shown in Figs. 4.3.1 to Fig.4.3.6 and Figs.4.4.1 to Fig. 4.4.6 respectively. The boundary shear stress distributions for

over-bank conditions of Type-I, Type-II and Type-III channels are shown in Figs. 4.7.1 to 4.7.5, Figs. 4.5.1 to Fig.4.5.6 and Figs.4.6.1 to Fig.4.6.5 respectively. The section mean shear stresses for each run of the three channels for in-bank and over-bank flows are given in col. 9 of Table 5.1 and Table 5.2 respectively.

For the compound channels, the various boundary elements comprising the wetted parameters are labeled as (1), (2), (3) and (4) as shown in Fig. 5.8. Label (1) denotes the vertical wall(s) of floodplain of length $[2(H - h)]$, and (2) denotes floodplain beds of length $(B - b)$. Label (3) denotes the two main channel walls of length $(2h)$ and the bed of the main channel of length b are represented by label (4). Experimental shear stress distributions at each point of the wetted perimeter are numerically integrated over the respective sub-lengths of each boundary element (1), (2), (3), and (4) to obtain the respective boundary shear force per unit length for each element. Sum of the boundary shear forces for all the beds and walls of the compound channel is used as a divisor to calculate the shear force percentages carried by the boundary elements. Percentage of shear force carried by floodplains comprising elements (1) and (2) is represented as $(\%S_{fp})$ and for the main channel [(3) plus (4)] it can be taken as $(\%S_{mc})$. The lumped effect of momentum transfer between the main channel and floodplain, the surface resistance, meandering, and other flow properties are manifested in the form of boundary shear distribution in the walls and beds of the channel section. Therefore, the boundary shear distribution also helps to investigate the momentum transfer in terms of apparent shear at the assumed interfaces in a compound section. The results of the apparent shear are useful to select the sub-division lines for separating a compound channel into sub-sections for discharge assessment using Divided Channel Method (DCM).
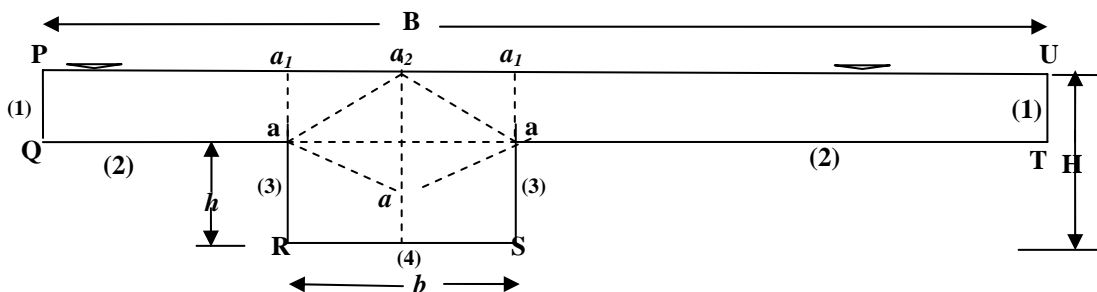
Fig.5.8 Compound channel with floodplain on both sides

Summary of the flow and boundary shear distribution in the sub-sections of a compound channel observed from the experimental runs for the three types of

compound channels are given in Table 5.3. The observed shear force percentages carried by the floodplains $(\%S_{fp})$ with depth ratio $[\beta = (H - h)/H]$ for the compound channels for the three channels (α = 3.67, 4.81, and 16.08) are given in col.5 of Table 5.3. It can be seen from the table that the values of mean shear stress increases with depth of flow in the channels. The published straight compound channel data of Knight and Demetrious (1983) for smooth surface are used along with the data of Type-I straight channel for the present analysis. Knight and Demetrious (1983) provided shear force data of three types of straight compound channel having symmetrical floodplains on both sides of main channel with width ratio α = 2, 3 and 4 respectively. Now, for the four types of straight compound channels, the variation of floodplain shear with relative depths are shown in Fig.5.9 (a) and the variation of the floodplain shear with different width ratio are shown in Fig.5.9 (b). From Figs.5.9 (a,b) it is clear that floodplain shear increases with channel width ratio (B/b $=\alpha$) and with relative depth $[H - h)/H = \beta]$, which are the most significant parameter influencing the flow interaction mechanism of compound channels.

Table 5.3 Sub-section flow and boundary shear distribution for over bank flow condition observed at bend apex of experimental channels.

Channel type	Run No.	Relative depth (β)	Total discharge (cm³/s)	Observed % of boundary shear in floodplain wetted perimeter	Flow in main channel (Q_{mc}) (cm³/s)	% of Flow in main channel (% Q_{mc})	Flow in lower main channel (Q_{lmc}) (cm³/s)	% of flow in lower main channel (% Q_{lmc})
(1)	(2)	(3)	(4)	(5)	(6)	(7)	(8)	(9)
Type-I Straight channel (α = 3.666)	S13	0.15	10007	42.10	7305	73	5885	58.81
	S15	0.21	13004	47.64	8805	67.71	6853	52.7
	S17	0.30	19861	53.70	12318	62.02	8560	43.1
	S18	0.36	25329	59.70	13151	51.92	9017	35.6
	S19	0.41	30844	61.10	17131	55.54	9932	32.2
Type-II Sinuous channel (α = 4.808)	MM17	0.12	10107	45.73	7105	70.30	6157	60.92
	MM20	0.17	13005	52.80	8036	61.79	6640	51.06
	MM23	0.21	16762	59.80	9225	55.035	7131	42.54
	MM25	0.25	20523	63.63	10356	50.46	7585	36.96
	MM26	0.30	25661	67.25	11714	45.65	8073	31.46
	MM27	0.34	31358	70.21	13255	42.27	8511	27.14
Type-III Highly Sinuous & Trapezoidal channel (α = 16.083)	HM16	0.08	12757	54.47	7832	61.39	6858	53.76
	HM18	0.18	24487	71.52	10147	41.44	7566	30.90
	HM19	0.19	27185	72.89	10700	39.36	7748	28.50
	HM20	0.21	31299	74.91	11556	36.92	8025	25.64
	HM25	0.27	44412	78.99	14039	31.61	8718	19.63
	HM27	0.28	48474	79.76	14838	30.61	8953	18.47
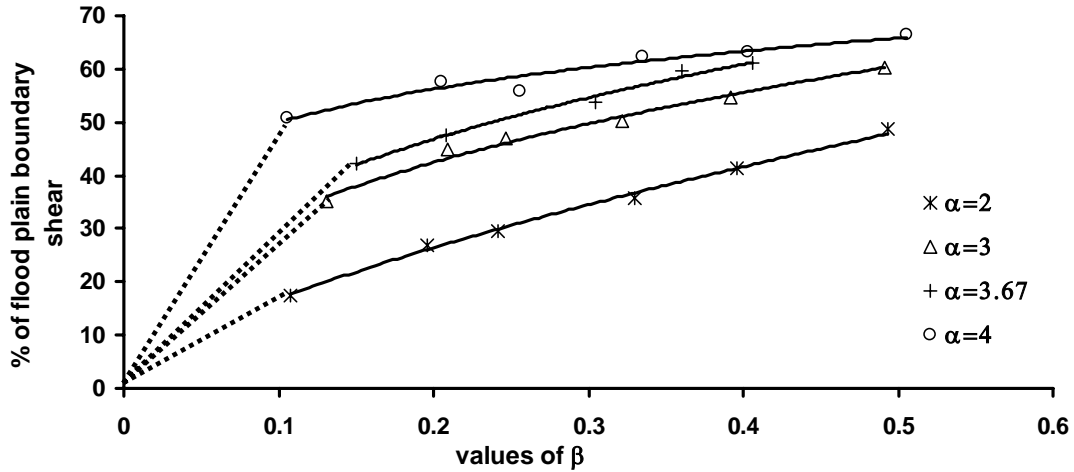
FIG. 5.9(a) Variation of percentages of flood plain shear with relative depth of straight compound channels
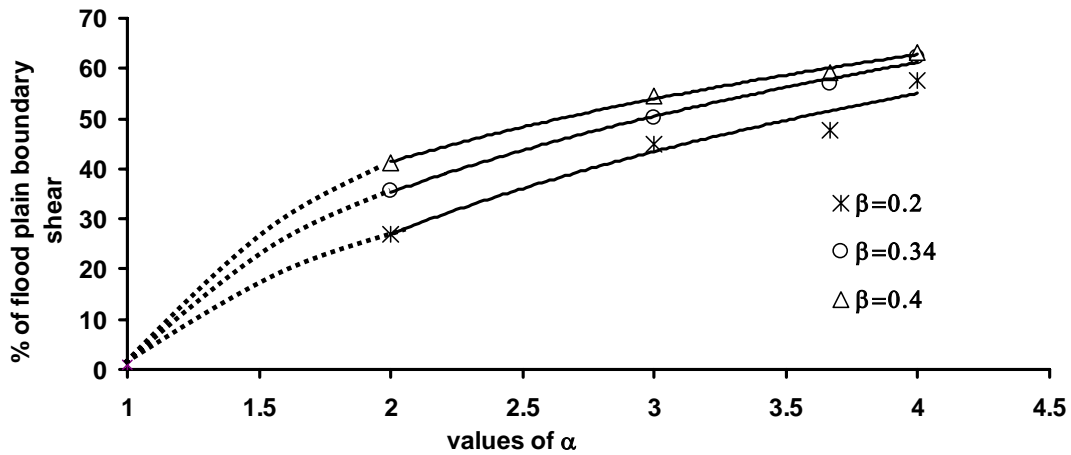
Fig. 5.9(b) Variation of percentage of flood plain shear with width ratio of straight compound channels

Similarly the shear force percentages carried by the floodplains (*%S$_{fp}$*) for the meandering compound channels (Type-II and Type-III) are plotted against width ratio (*B/b =α*) and depth ratio [(*H – h*)/*H =β*] in Fig.5.10. Along with this, two other types of published meandering compound channel data of Patra and Kar (2000) having width ratio *α* = 3.14 and 5.25 are plotted in the same figure. These two channels are smooth, having flood plains on both sides of the main channel so have the similarity with the present Type-II and Type-III meandering channels. Now, for the total four types of meandering compound channels the variation of the floodplain shear with relative depths are shown in Fig.5.10 (a) and the variation of the floodplain shear with different width ratios are shown in Fig.5.10 (b). The increase of floodplain shear is at uniform rate for straight channels when compared

to that of meandering channels. It is clear from Figs.5.9 and 5.10 that the percentage of total shear force carried by the floodplain beds and walls (%S_{fp}) increases with increase in relative depth β, the channel width ratio α, and decreases with sinuosity S_r (=length along channel center/ straight valley length)
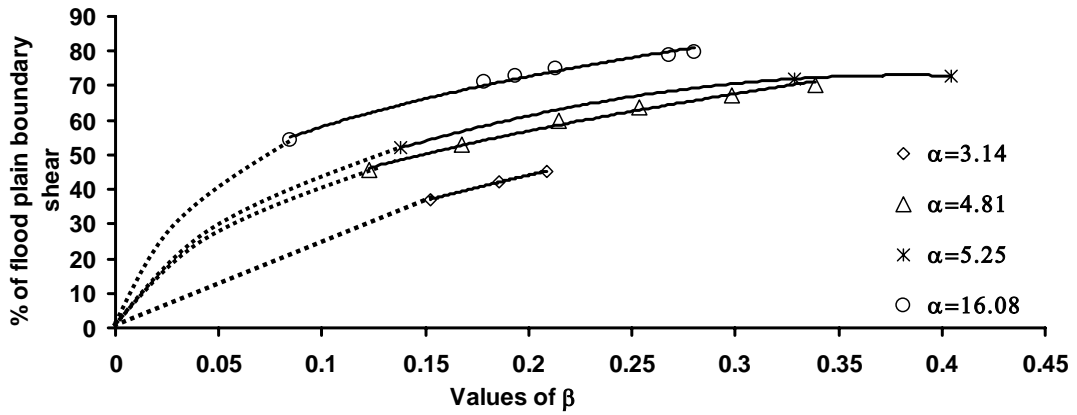
FIG. 5.10 (a) Variation of percentages of flood plain shear with relative depth for   meandering compound channels
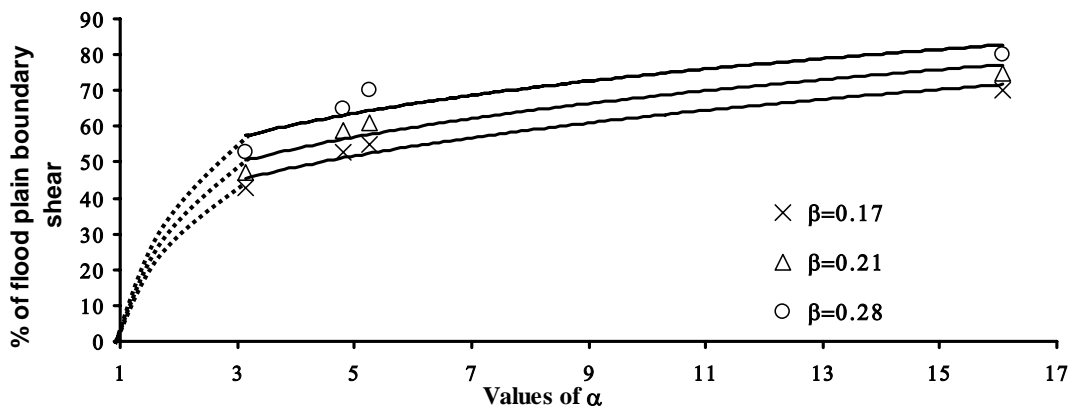
FIG. 5.10 (b) Variation of flood plain shear with width ratio for meandering compound channels

5.5.3 DEVELOPMENT OF THE BOUNDARY SHEAR DISTRIBUTION MODEL

Knight and Hamed (1984) improved the equation of Knight and Demetriou (1983) for straight and smooth compound channels and proposed equation for the percentage of total shear force carried by the floodplain as

$$\%S_{fp} = 48(\alpha - 0.8)^{0.289}(2\beta)^{m} \tag{5.4}$$

and the exponent *m* can be evaluated from the relation as

$$m = 1 / \left[0.75\, e^{0.38\,\alpha} \right] \tag{5.5}$$

Patra and Kar (2000) extended (5.5) and proposed equation for the percentage of total shear force carried by the floodplain of meandering compound channels as

$$\% S_{fp} = 48(\alpha - 0.8)^{0.289} (2\beta)^m \left[1 + \alpha \, \text{Re}^{-13.25\beta\delta} \right] \qquad (5.6a)$$

in which the exponent m can be calculated from the relation

$$m = 1 / \left[0.75 e^{0.38(\alpha - R)} \right] \qquad (5.6b)$$

where R = ratio of the amplitude of the meandering channel to the top width B of the compound section, δ = aspect ratio of the main channel b/h, b = width of main channel, and h = bank full depth of main channel. Equation (5.6) is valid for meandering compound section with smooth boundaries. For compound channel with different roughness in its floodplain and in the main channel Patra and Kar (2000) further modified (5.6) and proposed a general equation as

$$\% S_{fp} = 48(\alpha - 0.8)^{0.289} (2\beta)^m \left(1 + \alpha \, \text{Re}^{-13.25\beta\delta} \right) \left(1 + 1.02\sqrt{\beta} \log \gamma \right) \qquad (5.7)$$

where γ = the ratio of Manning's roughness n of the floodplain to that for the main channel. The authors have proved the adequacy of equations for the narrow channels having width ratio of α up to 5.25 and sinuosity (S_r) up to 1.22. Equation (5.7) when applied to the present wider channel of width ratio of $\alpha = 16.08$ and higher sinuosity of $S_r = 1.91$, gives the floodplain shear values much different when compared to the corresponding observed values. Equations 5.6 and 5.7 are therefore not suitable for wide flood plain channels. Using equation 5.6, the percentage of floodplain shear force ($\% S_{fp}$) for the Type-III channel is found to be more than 100% for all the over bank flow depths. Similar observation is recorded when equation (5.4) and (5.5) of Knight and Demetriou (1983) for straight compound channel is applied to very wide flood plain compound sections. For larger value of 'α' the equation is found to give percentage of shear force of floodplain more than 100% which is impossible. To overcome the difficulties, further analysis is made in this study to obtain a simple but more reliable general equation to predict the percentage of floodplain shear for channels having very wide floodplains which is true for most of the river geometry during high floods.

Due to transfer of momentum between floodplain and main channel in a compound channel, the percentage of shear carried by the main channel does not follow linearity with area ratios $\% A_{fp}$, where $\% A_{fp}$ is the percentage of area of

floodplain obtained by a vertical interface. To know the dependency of $\%S_{fp}$ with the floodplain area ratio $\%A_{fp}$ for straight compound channels, the variation of $\%S_{fp}$ with the area ratio $\%A_{fp}$ for the present straight compound channel (Type-I) along with the straight channel of Knight and Demetrious (1983) is plotted in Fig.5.11. From the plot the best fit function for percentage of shear carried by floodplain for a straight compound channel is obtained as

$$\%S_{fp} = 3.4817\left(\%A_{fp}\right)^{0.7317} \tag{5.8a}$$

Since for a rectangular main channel $\dfrac{A_{fp}}{A} = \dfrac{\beta(\alpha-1)}{1+(\alpha-1)\beta}$, equation(5.8a) is

rewritten as $\qquad \%S_{fp} = 3.4817\left[\dfrac{100\ \beta(\alpha-1)}{1+\beta(\alpha-1)}\right]^{0.7317} \tag{5.8b}$
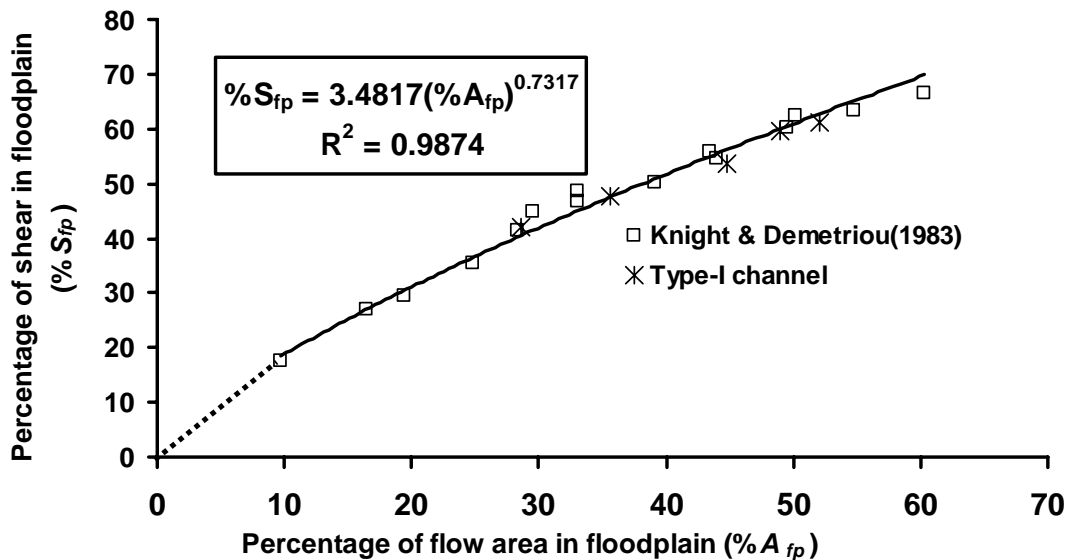
Fig. 5.11 Variation between % of shear in flood plain perimeter and the area in floodplain for straight compound channel

Table-5.4 Percentages of shear force in floodplain of Type-II and Type-III channels with and with out meandering effect.

Type-II	β	0.1228	0.1678	0.2146	0.2537	0.298	0.338
Sinuosity $(S_r = 1.44)$	$\%S_{fp}$(using equation 5.8)	43.83	50.80	56.40	60.18	63.76	66.51
	$\%S_{fp}$(Actual)	45.73	52.80	59.80	63.63	67.25	70.21
Type-III	β	0.0846	0.178	0.193	0.2133	0.268	0.28
Sinuosity $(S_r = 1.91)$	$\%S_{fp}$(using equation 5.8)	52.1	67.8	69.4	71.2	75.2	75.9
	$\%S_{fp}$(Actual)	54.47	71.52	72.89	74.91	78.99	79.76

For meandering channel with floodplain the distribution is further complicated and modified due to meandering effect. For Type-II and Type-III channels, the

percentage of floodplain shear is calculated using (5.8) and is compared with the actual value given in Table 5.4. From the table it can be seen that due to meandering effect the $(\%S_{fp})$ slightly increases with sinuosity. Therefore, the difference factor due to sinuosity is found out and the variation of this difference factor for the two present meandering channels and the test channels of Patra and Kar (2000) with the parameters of relative depth(β), sinuosity(S_r), and with width ratio (α) are plotted in Fig.5.12 (a, b and c) respectively. The best fit functional relationships of the (difference factor) with these parameters are obtained from the plots and given as

$$Difference\ factor = F_1(\beta^{0.404})\ ,\ F_2(\alpha^{0.306})\ and\ F_3(Ln(S_r)) + 0.0667 \qquad (5.9a)$$
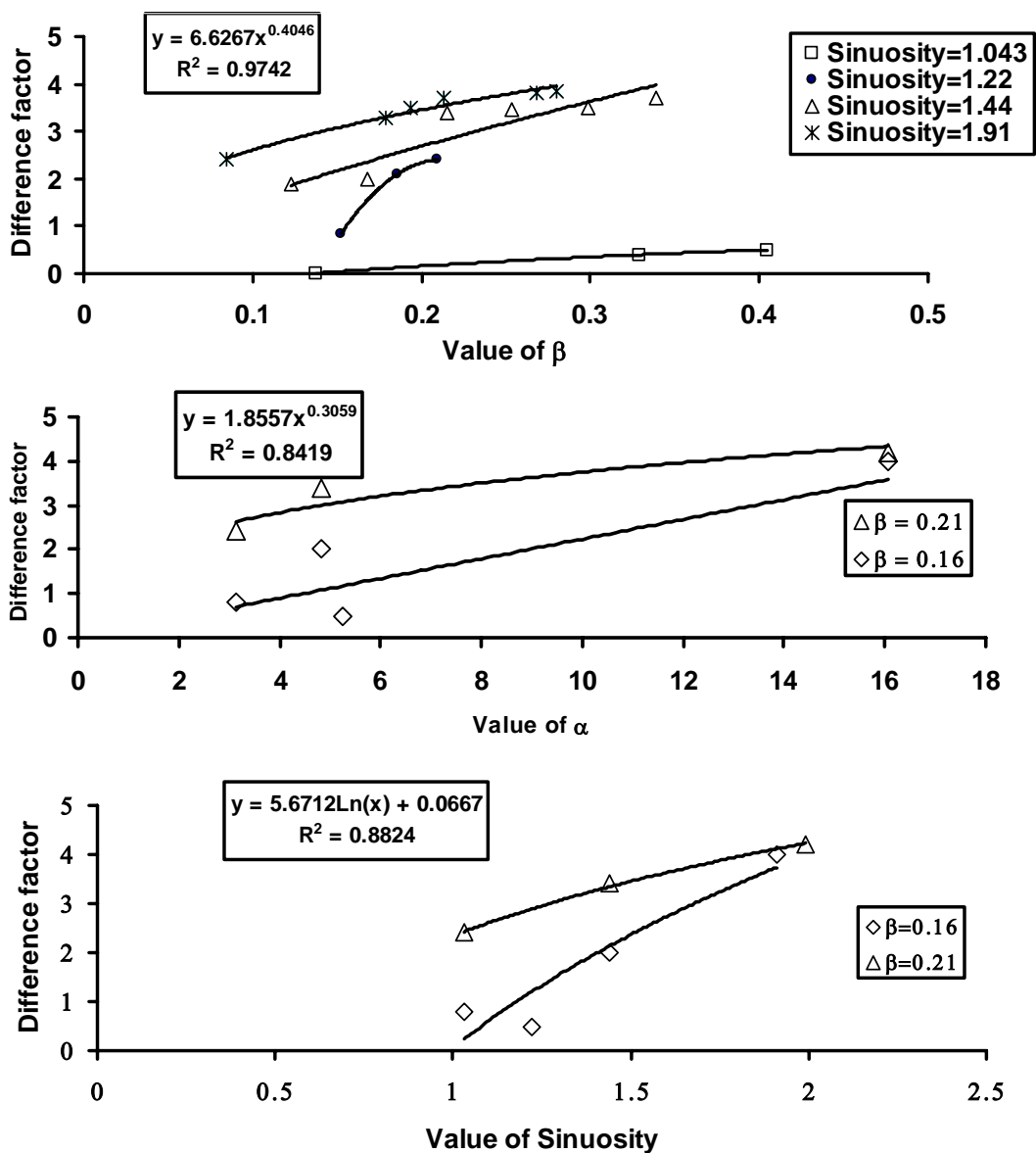
Fig.5.12 (a,b, and c) Variation of the difference factor for shear with relative depth (β), sinuosity(S_r), and width ratio (α)

Combining all the dependable parameters the difference factor is composited as

$$Difference\,factor = F\left[\beta^{0.404}\alpha^{0.306}Ln(1.06S_r)\right] = 5.22\,\beta^{0.404}\alpha^{0.306}Ln(1.06S_r) \qquad (5.9b)$$

Therefore, equation (5.8) is further modified for meandering compound channel and is written as

$$\%S_{fp} = 3.4817\left[\frac{100\,\beta(\alpha-1)}{1+\beta(\alpha-1)}\right]^{0.7317} + 5.22\,\beta^{0.306}\alpha^{0.404}Ln(1.06S_r) \qquad (5.10)$$

The results of equation (5.10) are interpolated down to in-bank stage (i.e. β =0) at which stage the floodplain shear force must be zero. For a straight compound channel, the sinuosity (S_r) becomes unity. Substituting the value of $S_r = 1$ in equation (5.10) we get the equation (5.8b). Equation (5.10) is valid for meandering compound channels with smooth surfaces only. For different roughness in main channel and flood plain surface, equation (5.10) is further improved and a general model to represent the percentage of shear force ($\%S_{fp}$) carried by floodplain of meandering compound channel is written as

$$\%S_{fp} = \left[3.4202\left\{\frac{100\,\beta(\alpha-1)}{1+\beta(\alpha-1)}\right\}^{0.7362} + 5.22\,\beta^{0.306}\alpha^{0.404}Ln(1.06S_r)\right]\{1+1.02\sqrt{\beta}\log\gamma\} \qquad (5.11)$$

The variation of computed percentage of shear force of floodplain wetted perimeter with the observed value of Type-I and that of Knight and Demetrious (1983) is shown in Fig. 5.13 (a). The variation of computed percentage of shear force of flood plain wetted perimeter with the observed value for Type-II and Type-III meandering compound channels and the compound meandering channels of Patra and Kar (2000) is plotted in Fig. 5.13 (b). Fig. 5.13 shows the adequacy of equation 5.10.
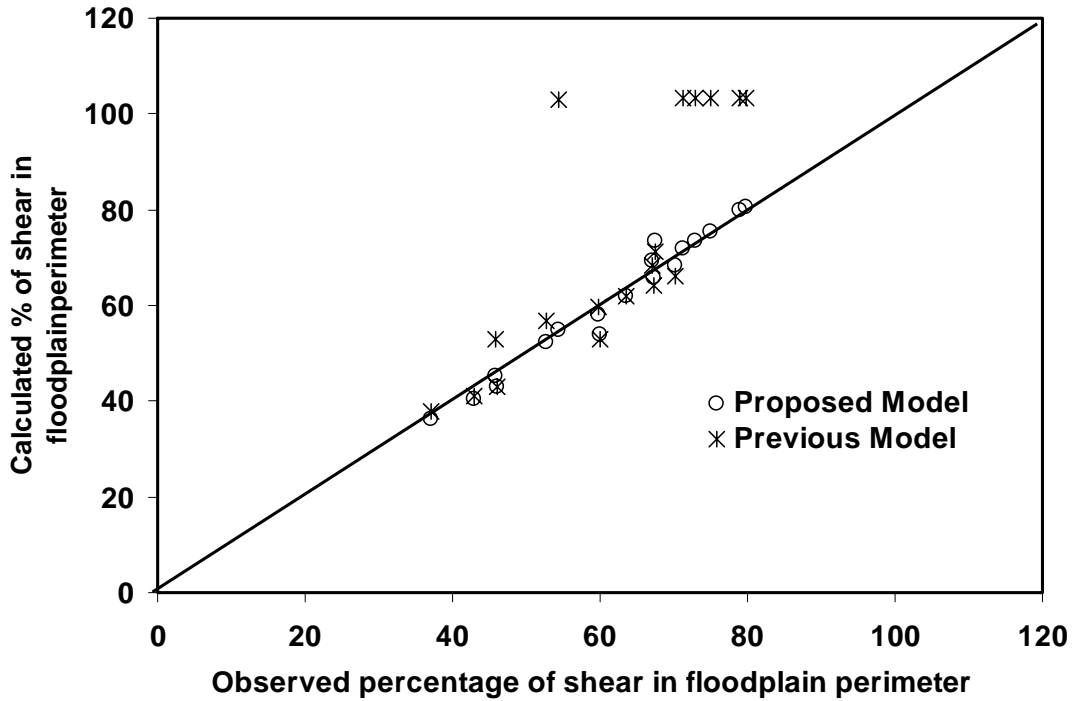
Fig. 5.13 (a) Variation between calculated and observed value of shear in floodplain for straight compound channels
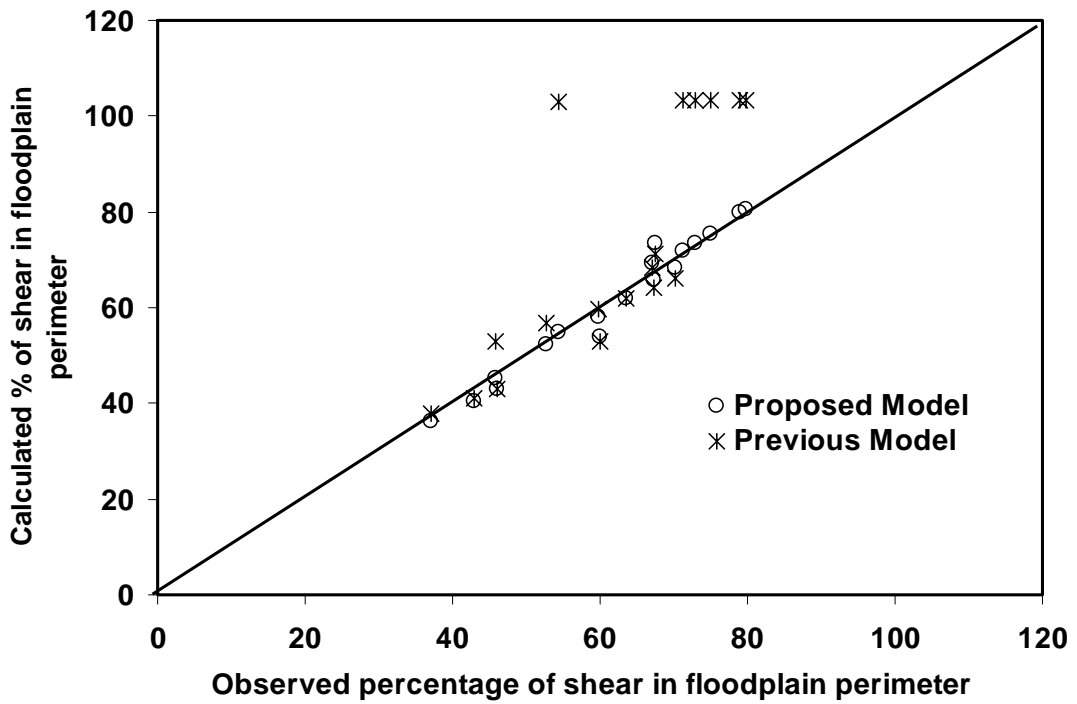
Fig.5.13 (b) Variation between calculated and observed value of shear in floodplain for meandering compound channels

5.6 HYDRAULICS OF A TWO STAGE COMPOUND CHANNEL

Once a river stage overtops its banks, the cross sectional geometry of flow undergoes a steep change. The channel section becomes compound and the flow structure for such section is characterized by large shear layers generated by the difference of mean velocity between the main channel and the adjoining floodplain subsection flows resulting from the different hydraulic conditions prevailing in the two sub-section. Just above the bank-full stage, the flow in the main channel exerts a pulling or accelerating force on the flow over floodplains, which naturally generates a dragging or retarding force on the flow through the main channel. This leads to the transfer of momentum between the channel section and the floodplain shown schematically in Fig 5.14 The interaction effect is very strong at just above bank full stage and decreases with increase in the depth of flow over floodplain. The relative "pull" and "drag" of the flow between faster and slower moving sections of compound section, complicates the flow process. Failure to understand this process may either overestimate or underestimate the discharge leading to the faulty design of a channel section. This causes frequent flooding at its lower reaches.
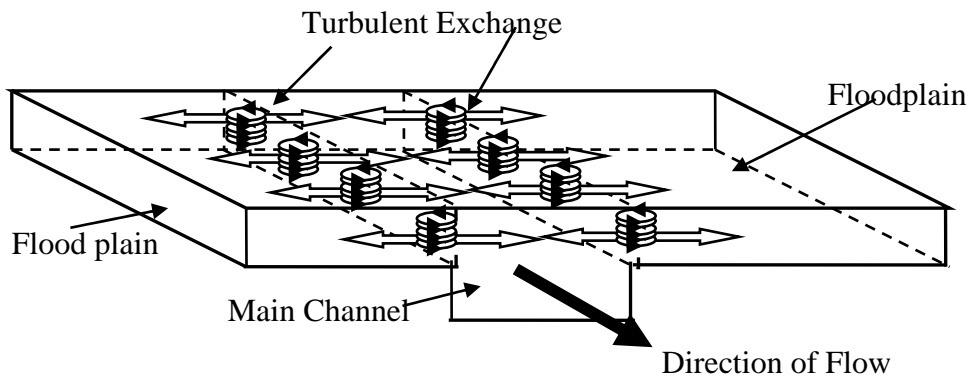
Fig.5.14 Schematic view of momentum transfer between main channel and floodplain of a two stage compound channel section

At the junction region between the main channel and that of the floodplain, Sellin (1964) and Knight and Demetriou (1983) indicated the presence of artificial banks made of vortices, which acted as a medium for transfer of momentum. At low depths over floodplain, transfer of momentum takes place from the main channel flow to the

floodplain leading to the decrease in the main channel velocity and discharge, while its floodplain components are increased. As the depth of flow in the floodplain increases beyond a limiting depth, transfer of momentum does not takes place between the main channel and the floodplain. And at still higher depths over floodplains the process of momentum transfer reverses, the floodplain supplies momentum to the main channel. Due to the continuous stream wise variation of radius of curvature, the velocity and flow parameters are considerably more complex in a meandering compound channel than in a straight channel of same geometry in cross section. Since a major length of any river course is in meander, knowledge on the hydraulics of flow in a meandering compound channel is a must for all Engineers dealing with the river works.

5.7 APPARENT SHEAR FORCE ON VARIOUS INTERFACES

A conventional method of calculation of discharge in a compound channel is to divide the section into hydraulically homogeneous regions by plane originating from the junction of the floodplain and main channel so that the floodplain region can be considered as moving separately from the main channel. The assumed plane may be: (1) vertical interface, (2) horizontal interface, or (3) diagonal interface. Once the shear force carried by the floodplain is known, the apparent shear force acting on the imaginary interface of the compound section can be calculated. The apparent shear force at the assumed interface plane gives an insight into the magnitude of flow interaction between the main channel and the adjacent floodplains basing on which the merits of the selection of the interface plains for discharge estimation can be decided. For any regular prismatic channel under uniform flow conditions the sum of boundary shear forces acting on the main channel wall and bed together with an ''apparent shear force'' acting on the interface plane between main channel and floodplain must be equal to the resolved weight force along the main channel given as.

$$\rho g A_{mc} S = \int_{mc} \tau dp + ASF_{ip} \quad \text{or} \quad ASF_{ip} = \rho g A_{mc} S - \int_{mc} \tau dp \qquad (5.12)$$

in which g = gravitational acceleration, ρ = density of flowing fluid, S = slope of the energy line, A_{mc} = area of the main channel defined by the interface plane, $\int_{mc} \tau dp$ = shear force on the surfaces of the main channel consisting of two vertical walls and bed, and

ASF_{ip} = apparent shear force of the imaginary interface plane. Prinos and Townsend (1984) proposed an empirical equation for the apparent shear stress (τ) in N/m^{2}given as

$$\tau = 0.874 \, (\Delta V)^{0.92} \, (\beta)^{-1.129} \, (\alpha)^{-0.514} \tag{5.13}$$

where ΔV is the difference of section mean velocity between the main channel and floodplain in m/s. This equation, proposed for straight compound channels was found to apply the results of Wormeleaton (1982), and Knight and Demetriou (1983) only. For the present meandering compound channels, further analysis are made to derive a general simple expression for the apparent shear at any interface plane, for both, straight and compound sections.

Due to main channel and floodplain interaction, the main channel boundary shear increases and the floodplain shear decreases (Myer and Elsawy 1975). Wormelaton et. al. (1982) have shown that the total dragging force on the main channel due to floodplain at the interfaces must be equal to the accelerating force on floodplain due to the main channel. Therefore, the wetted perimeter of the main channel needs to be increased suitably to take care of the net dragging force on the main channel. Similarly the wetted perimeter of the floodplain needs to be decreased by subtracting a suitable length of interface to account for the accelerating force on the floodplain due to the pulling of the main channel water. Net force at the assumed interface should balance each other. Let an arbitrary interface *op* in Fig.5.15 divides a compound channel into main channel and floodplain sub-sections. Let X_{mc} be the interface length for inclusion in the main channel wetted perimeter and X_{fp} the length of interface to be subtracted from the wetted perimeter of floodplain. By assuming the channel to be regular, prismatic and flow under uniform conditions, the sum of the boundary shear forces acting on the main channel plus the shear force on the assumed interface must be equal to the weight component of water of the main channel and is written as

$$(P_{mc}\tau_{mc} + X_{mc}\tau_{mc}) = \rho g A_{mc} S \tag{5.14}$$

Similarly for the floodplain equation (5.14) is written as

$$(P_{fp}\tau_{fp} + X_{fp}\tau_{fp}) = \rho g A_{fp} S \tag{5.15}$$

where P_{mc}, P_{fp} = the wetted perimeter of the main channel and floodplain respectively, A_{mc} and A_{fp} = the area of cross sections of main channel and floodplain subsections respectively, τ_{mc}, τ_{fp} = the mean boundary shear stress in main channel and floodplain per its unit length written as $\tau_{mc} = \int_{mc} \tau dp / P_{mc}$, $\tau_{fp} = \int_{fp} \tau dp / P_{fp}$ respectively, S = the longitudinal slope of the channel, ρ = the density of water, and g = the gravitational acceleration.
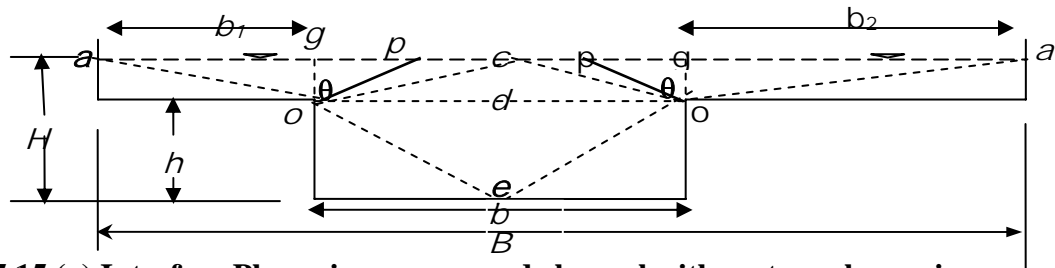
Fig.5.15 (a) Interface Planes in a compound channel with rectangular main channel
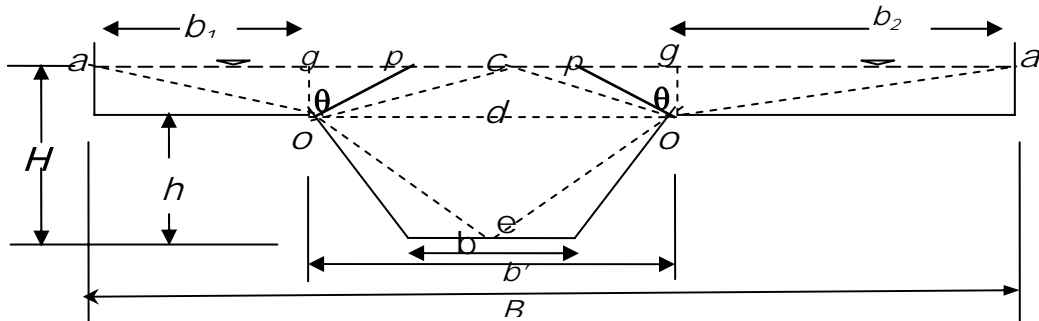
Fig.5.15 (b) Interface planes in a compound channel with trapezoidal main channel section

Again for the total compound section the boundary shear must be equal to the weight component of flowing fluid along longitudinal direction and is written as

$$(P_{mc}\tau_{mc} + P_{fp}\tau_{fp}) = \rho g A S \tag{5.16}$$

where A = the area of cross section of the compound channel section (= A_{mc} + A_{fp}). Since $\rho g A_{mc} S + \rho g A_{fp} S = \rho g A S$, the sum of weight components represented by equations (5.14, and 5.15) must be equal to the weight component represented by (5.16) from which we get $\qquad X_{mc} \tau_{mc} = -X_{fp} \tau_{fp} \tag{5.17}$

- 114 -

Equation (5.17) shows that the shear force on the main channel arising out of the assumed interface *op* must be equal and opposite to that considered for the floodplain by the divided channel approach. For that interface plane the term $X_{mc}\tau_{mc}$ or $-X_{fp}\tau_{fp}$ is taken as the apparent shear force ASF_{ip}. Now from equation (5.17) and (5.14) a general expression for X_{mc} for any interface is written as

$$X_{mc}\left(=\frac{ASF_{ip}}{\tau_{mc}}\right) = \frac{\rho\, gA_{mc}\, S - \tau_{mc}\, P_{mc}}{\tau_{mc}} \qquad (5.18a)$$

which is simplified to $\quad X_{mc} = P_{mc}\left[\frac{100}{(100 - \%\, S_{fp})}\frac{A_{mc}}{A} - 1\right]$ \hfill (5.18b)

Similarly for floodplain, the expression for $X_{fp}\left(=\dfrac{ASF_{ip}}{\tau_{fp}}\right)$ can be derived as

$$X_{fp} = P_{fp}\left[\frac{100}{\%\, S_{fp}}\left(\frac{A_{mc}}{A} - 1\right) + 1\right] \qquad (5.19)$$

From the lengths of X_{mc} and X_{fp} computed through the equations (5.18) and (5.19) an idea of the magnitude of shear force at the assumed interface plains of separation of a compound channel can be obtained. The strength of apparent shear forces is related to the quantum of momentum transfer between main channel and floodplain of a compound channel. In Fig.5.15 (a, b) the lines *oa* and *oe* are the extreme cases of assumed interface plains that can be used to separate a compound section into subsections for discharge estimations. Let us take an arbitrary interface *op*, between line *oa* to *oe* making an angle θ with vertical line at the junctions in Fig.5.15. The intensity of momentum exchange in terms of apparent shear length at different imaginary interface plains originating from the main channel and floodplain junction can now be calculated using the observed data. The convention for θ is 0 for vertical interface (*og*), positive if the interface lies in the main channel and negative, if the interface lies to the floodplain side with respect to the vertical interface. Two situations of locations of interface plains are discussed below.

Case-1 (When interface *op* lies between *oa* to *oc*)

This case is assumed when the interface line *op* is located between *oa* and *oc* (Fig.5.15) such that the angle θ can be defined as $\quad Tan\ \theta \le \dfrac{b}{2(H - h)}\quad$ and $\quad Tan\ (-\theta) \le \dfrac{b_1}{(H - h)}$

or $\dfrac{b_2}{(H-h)}$. The area of a rectangular main channel is given as $A_{m\theta}=bH-(H-h)^2 Tan\,\theta$, where b_1 and b_2 are the lengths of flood plain bed at both sides measured from vertical interface. For symmetrical compound channel $b_1=b_2=(B-b)/2$. The total area of cross section of channel is $A=bH+(B-b)(H-h)$. By substituting the expression of interface length X_{mc} for Type-I and Type-II compound channel is

$$X_{m\theta} = P_{mc}\left[\left(\frac{100}{100-\%S_{fp}}\right)\frac{(\delta-\beta^2 Tan\theta)}{\delta\{1+(\alpha-1)\beta\}}-1\right]\tag{5.20}$$

Similarly for the trapezoidal main channel section of Type-III, the area of main channel is written as $A_{m\theta}=b'H-(b'-b)h/2-(H-h)^2 Tan\theta$ and total area is $A=b'H+(B-b)(H-h)-(b'-b)h/2$. For this channel the value of $X_{m\theta}$ for the interface can be estimated directly using 5.18.

Case-II (When interface *op* lies between *oc* to *oe*)

This is considered when the interface line *op* lies between *oc* and *oe*. The angle θ can be calculated from the relations given as $Tan\,\theta \leq \dfrac{2h}{b}$ and $Tan\,\theta \geq \dfrac{b}{2(H-h)}$. For the rectangular main channel of Type-I and Type-II, the area of main channel can be calculated from the relations, $A_{mc}=bh+\dfrac{b^2}{4}Tan\theta$ and that for whole compound channel is $A = b\,H + (B-b)(H-h)$ Substituting the value of A_{mc} in (5.18) and simplifying we get

$$X_{m\theta} = P_{mc}\left[\left(\frac{100}{100-\%S_{fp}}\right)\left\{\frac{\delta\cot\theta-4\beta+4}{4\{1+(\alpha-1)\beta\}}\right\}-1\right]\tag{5.21}$$

Again for the Type-III trapezoidal main channel, the area of main channel section is calculated from the relation $A_{m\theta}=b'H-\dfrac{(b'-b)h}{2}-\dfrac{b^2}{4}\cot\theta$ and the total cross section area as $A=b'H+(B-b)(H-h)-(b'-b)h/2$. The value of X_{mc} can be calculated from equation (5.18b). From equation 5.18b and 5.19 a relation between X_{fp} and X_{mc} is given as

$$X_{f\theta} = X_{m\theta}\left(\frac{p_{fp}}{p_{mc}}\right)\left(\frac{100-\%S_{fp}}{\%S_{fp}}\right)\quad \text{Or}\quad X_{fp} = C'X_{mc}\tag{5.22}$$

where C' is a constant for a given flow depth as the values $\dfrac{p_{fp}}{p_{mc}}$ and $\dfrac{100 - \% S_{fp}}{\% S_{fp}}$ are constant for a flow depth in a channel. It shows that the apparent shear per unit average boundary shear stress per unit length $X_{m\theta}$ and $X_{f\theta}$ are proportional to each other and are the apparent shear per unit average boundary shear stress of main channel and floodplain per unit length of channel respectively termed as interaction length. By multiplying $\dfrac{\tau_{mc} \times 100}{\rho gAS}$ to X_{mc} or $\dfrac{\tau_{fp} \times 100}{\rho gAS}$ to X_{fp}, the percentage of apparent shear is obtained for any interfaces, where τ_{mc} and τ_{fp} = average boundary shear of main channel and floodplain respectively.

For example for vertical interface (og) the value of $\theta = 0^0$, for this situation of the interface (og) lies falls in case (i). Therefore using the case (i) equation i.e. equation (5.20), putting the value of $\theta = 0^0$ and multiplying the term $\dfrac{\tau_{mc} \times 100}{\rho gAS}$ the percentages of apparent shear for the horizontal ($\%ASF_V$) is obtained and simplified as

$$\% \ ASF_V = \frac{50}{[(\alpha - 1)\beta + 1]} - \frac{1}{2}\{100 - \% \ S_{fp}\} \tag{5.23a}$$

Percentages of apparent shear for horizontal interface can be obtained by putting the value $\theta = 90^0$ to the equation 5.21 [as the interface lies between oc and oe of case (ii)] and multiplying the term $\dfrac{\tau_{mc} \times 100}{\rho gAS}$ the percentages of apparent shear for vertical interface is obtained as

$$\% \ ASF_H = \frac{100 \ (1 - \beta)}{[(\alpha - 1)\beta + 1]} - \{100 - \% \ S_{fp}\} \tag{5.23b}$$

Similarly the percentages of apparent shear for diagonal interface ($\%ASF_D$) is obtained by putting the value of θ such that and $tan\theta = b/2h$ to (5.20) or (5.21) and multiplying the term $\dfrac{\tau_{mc} \times 100}{\rho gAS}$ is given as

$$\% \ ASF_D = \frac{25 \ (2 - \beta)}{[(\alpha - 1)\beta + 1]} - \frac{1}{2}\{100 - \% \ S_{fp}\} \tag{5.23c}$$

Same procedure can be followed to evaluate the percentages of apparent shear for any other assumed interfaces.
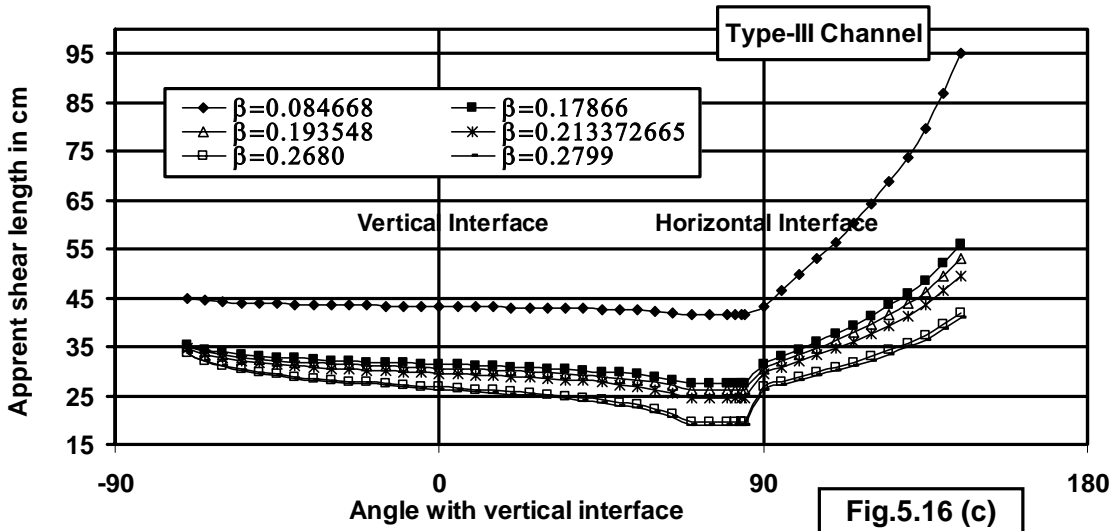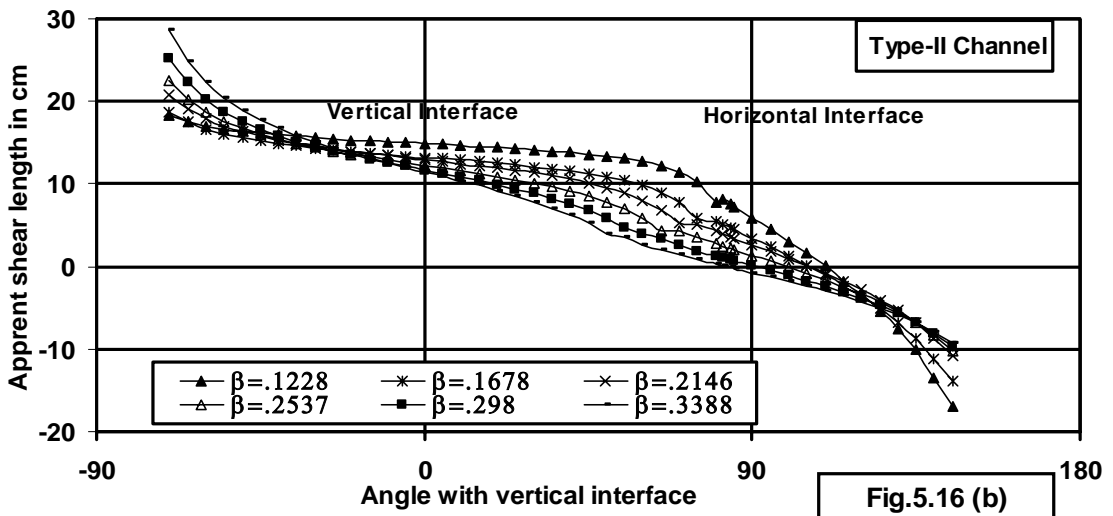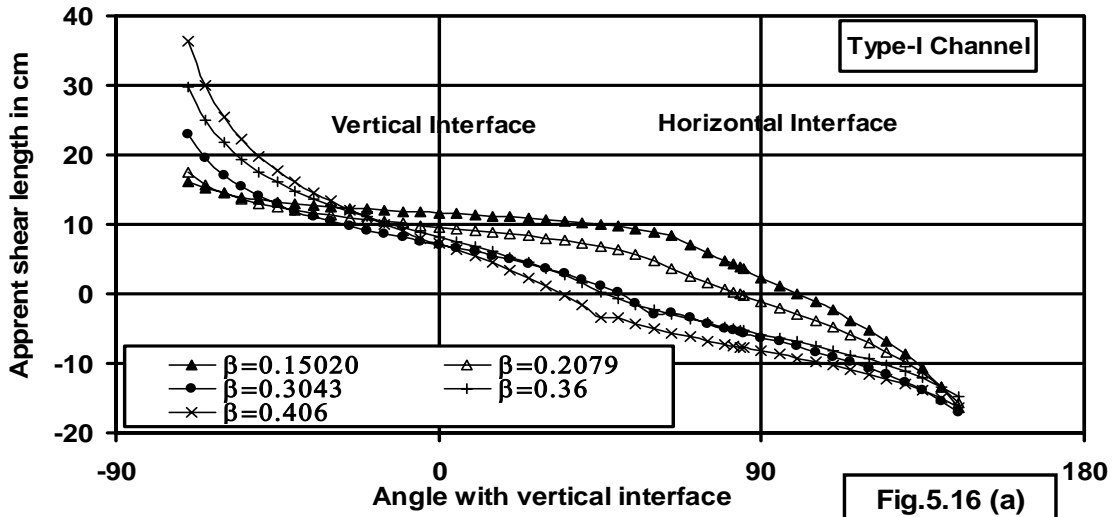
Fig.5.16 (a, b, and c) Variation of apparent shear along various planes of separations of compound channels into different sub-sections.

For other types of geometry the apparent shear may be calculated directly by (5.18b) with multiplication of $\dfrac{\tau_{mc} \times 100}{\rho gAS}$. The value of apparent interface length gives the magnitude of apparent shear, which in turn is related to the intensity of momentum transfer along the interface originating from the main channel-floodplain junction. Later in this chapter the values of apparent shear are quantified in terms of the length of interface. The quantity of apparent shear in terms of apparent shear length for the three types of channels are calculated at various interfaces and shown in Fig.5.16. The apparent shear at the interfaces for each over-bank depths are plotted between the region *oa* to *oe* of the compound channel at 5^0 intervals.

When we separate main channel from floodplain of the compound channels of Type-I and Type-II using interface plains, it is seen that the maximum positive apparent shear occurs along the extreme interface *oa* and the apparent shear gradually decreases as the interface moves to the channel centre. After reaching the interface plane of zero shear, the apparent shear at the planes becomes negative with maximum negative occurring at the other extreme interface *oe*. This concludes that for any over-bank depth, maximum positive momentum transfer takes place from main channel to floodplain if we consider the interface *oa* and the highest maximum negative momentum from floodplain to main channel takes place if we consider the interface *oe*.

For lower over-bank of Type-I channel, the interface plain of zero shear is found near the horizontal interfaces (approximately at $\theta = 99^0$ for the lowest over bank depth) and for higher over-bank depths, the interface plane of zero apparent shear is observed near a diagonal line of separation (approximately at $\theta = 40^0$) for the highest overbank). Similarly for Type-II channel the interface plane of zero shear lies at around ($\theta = 109^0$) that is with respect to horizontal line ($\theta = 19^0$) and is located towards lower main channel. For the highest over bank depth the interface of zero shear lies close to the vertical interface.

It can be seen that nature and quantity of momentum transfer occurs at the various assumed interface plains for Type-I and Type-II channels are almost same; varying from a high positive value across the assumed interface *oa* (Fig.5.15), decreasing gradually through the vertical, going negative at around the horizontal and

further negative if the assumed interface of separation of main channel and floodplain is assumed at still inside the main channel (Fig.5.16 a and b). The figure is extremely useful in selecting an interface plain for straight and mildly meandering compound channels into zones or sub-areas for discharge calculations using divided channel approach.

For Type-III meandering compound channel the apparent shear is found to be always positive for the ranges of over-bank depths investigated showing the momentum transfer is always from main channel to the floodplains for any interfaces between *oa* and *oe*(Fig.5.15). This may be due to very wide flood plain of Type-III channel having width ratio (α =16.08). Interface plane of zero shear for Type-III is not located for the interfaces between *oa* to *oe* for all flow depths. From the plot it clearly indicates that interface plain of zero shear is not possible for a very wide flood plains. However near a horizontal fluid boundary interface may be selected as a division line of the compound channel into sub-areas or zones for discharge estimation for very wide channels.

For three types of channel investigated, the apparent shear along the most commonly used interfaces such as vertical, diagonal or horizontal is never zero or equal to the average shear of the main channel/flood plain wetted perimeter. The apparent shear is found to vary with over-bank depths and from interfaces to interfaces. For over bank flows, we use the conventional approach of simple addition or deletion of interface length to the wetted perimeter for discharge evaluation through Manning's equation using Divided Channel Method (DCM). Therefore the approaches either over-estimate or under-estimate the compound channel discharge that have been demonstrated by several authors (Wormleaton et. al. 1982, Wormleaton et. al.1985, Knight and Demetriou 1983, Knight and Hamed 1984, Greenhill and Sellin (1993), Patra and Kar 2000), Ozbek et.al 2003). Use of the conventional interface method with the proper addition of interface length to the wetted perimeter of main channel subsection and subtraction of the proportionate length of interface from the flood plain wetted perimeter is expected to give the best discharge results using divided channel method. For the present test channels and the test channels of other investigators, it is demonstrated that proposed modification to the conventional methods give better results for both straight and meandering compound sections.

5.8 ZONAL FLOW DISTRIBUTION IN COMPOUND CHANNEL

5.8.1 GENERAL

Discharge carried by the main channel separated from the compound section by vertical fluid boundary is obtained by numerically integrating the area–velocity results from the isovel plots. Due to transfer of momentum between floodplain and main channel, the percentage of flow carried by the main channel with depth does not follow simple area ratios. At lower depths of flow over floodplain, the difference between percentage of flow in main channel and percentage of area of main channel is positive indicating that the main channel carries a greater percentage of flow than the simple area percentage. As the depth of flow over floodplain increases, the percentage of flow in main channel reduces. The flow and velocity distribution in compound sections have been investigated by many investigators (Knight and Demetriou 1983, Myer 1984, Kar 1977, Bhattacharya 1995, Patra 1999, Patra and Kar 2000, Patra and Kar 2004). The zonal or sub-area flow distributions in the main channel and floodplain of compound channel mainly depend on the channel geometry and flow parameters. An investigation is made to obtain the flow distribution between main channel, lower main channel, and floodplain for both straight and meandering compound sections.

5.8.2 DISHARGE DISTRIBUTION RESULTS

The results of velocity distributions for Type-I, Type-II, and Type-III channel are presented in chapter-4. Plots of the isovels for the longitudinal velocities are used to obtain the area-velocity distributions that are subsequently integrated to get the discharge of the main channel and floodplains sub-areas separated by various assumed interface planes. The total discharge of the compound channel is used as a divisor to calculate the percentages of discharge carried by the main channel and floodplain sub areas or zones. When a vertical interface is used, the area of main channel is denoted by the area a_1aRSaa_1 (Fig.5.8). The flow carried by the area is represented as *$\%Q_{mc}$*. Similarly when a horizontal interface divides a channel into the zones, the percentages of flow carried by the lower main channel area aRSa in Fig.5.8 is represented as *$\%Q_{lmc}$*. The flow percentages carried by the main channel and lower main channel with depth

ratio [$\beta = (H - h)/H)$] for the compound channels for varying geometry ($\alpha = 3.67$, 4.81 and 16.08) are given in Table 5.3. The three straight compound channel data of Knight and Demetrious (1983) are also used along with the data of present Type-I channel for the analysis of flow distribution.

For the four types of straight compound channels [$\alpha = 2$, 3 and 4 of Knight and Demetriou (1983) and the present Type-I experimental channel $\alpha = 3.67$ for the variation of the percentage of flow in main channel with relative depths for different width ratios are shown in Fig.5.17 (a) and the corresponding values for lower main channel is shown in Fig. 5.17 (b). From Fig.5.17 it is clear that main channel and lower main channel zonal discharges decrease with channel width ratio ($B/b = \alpha$) and also with relative depth [$(H - h)/H = \beta$] for straight compound channels.
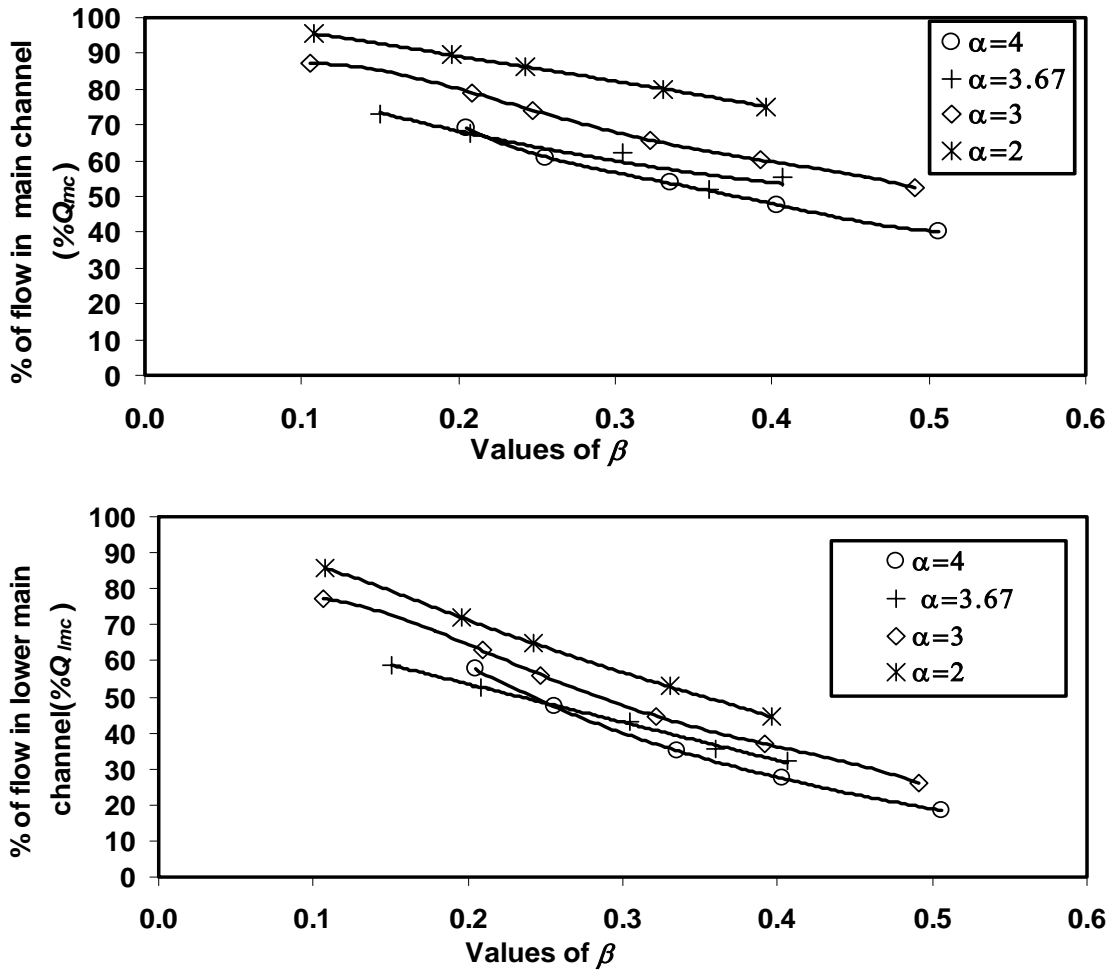
Fig.5.17 (a, b) Variation of percentage of flow in main channel and lower main channel with relative depth for straight compound channels

- 122 -

Similarly for the present meandering compound channels (Type-II and Type-III) the values of *%Q mc* and *%Q lmc* are also plotted against depth ratio $[H - h)/H = \beta]$ for different width ratios (*B/b = α*) in Fig.5.18. Two other types of meandering compound channel data of Patra and Kar (2000) having width ratio *α* = 3.14 and 5.25 are also plotted in the same figure for comparison. From Figs. 5.17 and 5.18 it can be seen that the main channel and lower main channel discharges decrease with the geometrical parameter of depth ratio and width ratio (for straight compound channel) while the increase of sinuosity (S_r) decreases the percentage of flow in main channel and lower main channels.
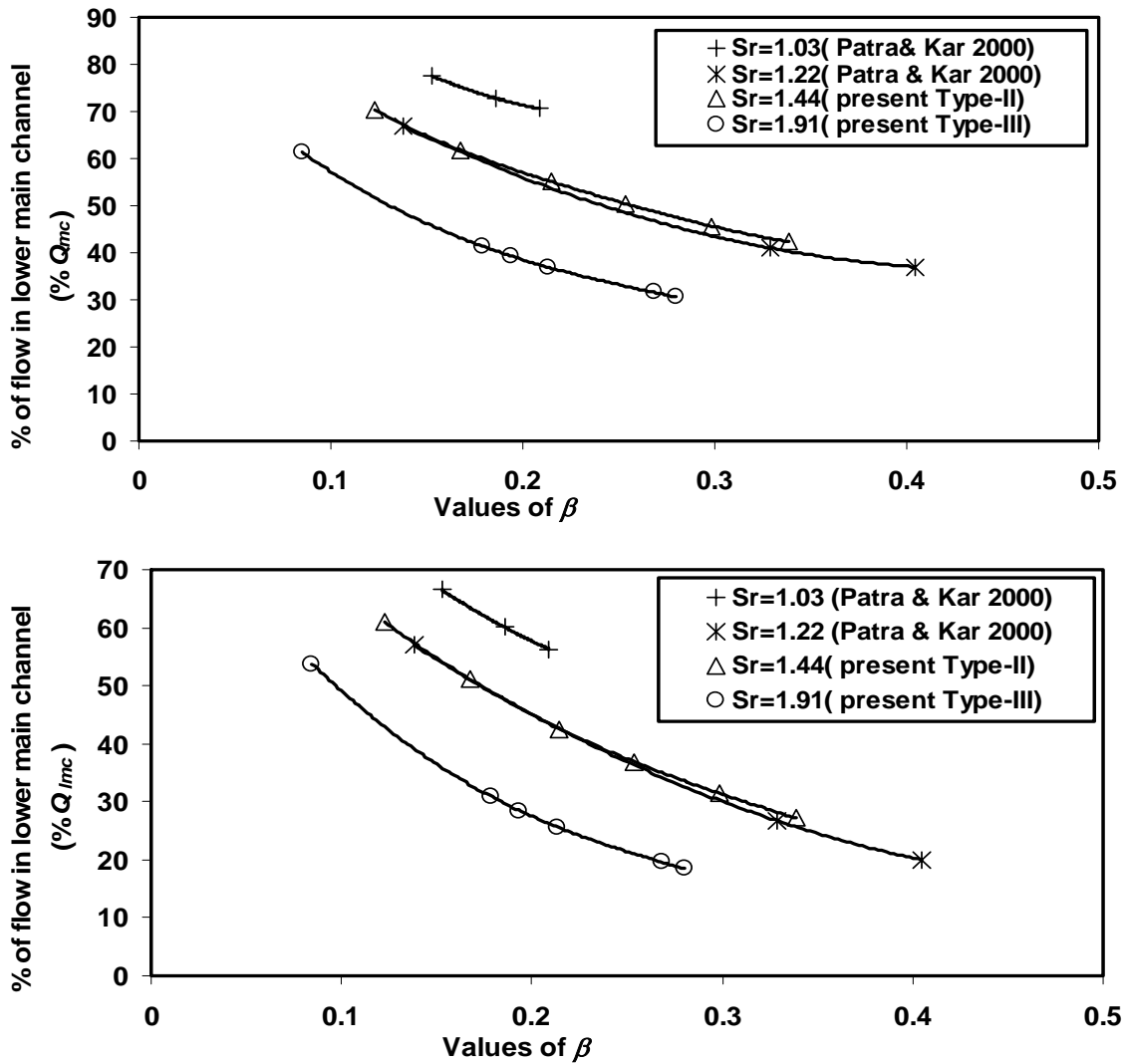
Fig.5.18 (a and b) Variation of percentage of flow in main channel and lower main channel with relative depth for meandering compound channel

5.8.3 THEORITICAL ANALYSIS OF THE FLOW DISTRIBUTION IN COMPOUND CHANNEL

Dimensional analysis is made to know the channel flow and resistance relationships leading to the carrying capacity of a compound section. Parameters governing resistance to flow in a straight compound channel having all smooth surfaces under uniform flow conditions can be functionally expressed as

$$\phi(F_m, \rho, \mu, V_{mc}, V_{fp}, R_{mc}, R_{fp}, g) = 0 \qquad (5.24)$$

where F_m = flow resistance in the main channel due to momentum transfer and other factors, ρ = density of water, μ = dynamic viscosity of water, V_{mc} and V_{fp} = the mean velocities of main channel and flood plain sub areas respectively, R_{mc} and R_{fp} = the hydraulic radius of main channel and flood plain sub-sections respectively, g = acceleration due to gravity.

For uniform flow condition, since the total gravitational force is equal to the total resisting force, the term g is excluded. Re-arranging the terms and applying Buckingham Π theorem, we can express (5.24) in a non-dimensional term as

$$\frac{F_m}{\rho V_{mc}^2} = \phi \left(\frac{\mu}{\rho V_{mc} R_{mc}}, \frac{V_{fp}}{V_{mc}}, \frac{R_{fp}}{R_{fmc}} \right) \qquad (5.25a)$$

where $\dfrac{F_m}{\rho V_{mc}^2}$ is the resistance coefficient (f_{mc}) of main channel sub-section. If N_{mc} and N_{fp} are taken as the Reynolds's number of main channel and flood plain sub-sections respectively, and by denoting N_r as the Reynolds number ratio ($N_r = N_{fp} / N_{mc}$), equation (5.25a) is simplified as

$$f_{mc} = \phi(N_{mc}, \frac{N_{fp}}{N_{mc}}) \text{ or } f_{mc} = \phi(N_{mc}, N_r) \qquad (5.25b)$$

Similar dimensional analysis can be made to show that the resistance coefficient of floodplain sub-area (f_{fp}) and for total cross section of the compound channel (f) are also function of respective Reynolds's number and Reynolds's number ratio and can be expressed as

$$f_{mc} = \phi(N_{mc}, N_r), \ f_{fp} = \phi(N_{fp}, N_r) \text{ and } f = \phi(N, N_r) \qquad (5.25c)$$

where N is the Reynolds's number of compound section. Reynolds number ratio (N_r) is a significant parameter that influences the flow resistance and therefore the carrying capacity for smooth compound sections. Experimental observations by Myer (1987) show that the Reynolds number of a channel, its floodplain, and the Reynolds's number ratio are independent of channel slopes and depends only on the channel geometry. Hence the carrying capacity of main channel, flood plain subsection, and the total carrying capacity of the compound channels are the functions of channel geometry only. Therefore the ratio of carrying capacities of main channel or floodplain subsection to the total is proportional to the dimensionless compound channel geometry. In a compound channel, the two significant dimensionless channel geometries are the width ratio (α) and the relative depth (β). Finally for a straight compound channel with smooth surfaces under uniform conditions, the percentages of ratio of flow in main channel to the total flow can be written as

$$\% Q_{mc} = \phi(\alpha, \beta) \text{ and} \% Q_{lmc} = \phi(\alpha, \beta) \tag{5.26}$$

where $\%Q_{mc}$ and $\%Q_{lmc}$ = the percentage of flow in the main channel and lower main channel subsections respectively of a compound channel obtained by the imaginary vertical and horizontal interface plains of separation. Knight and Demetrious (1983) for their straight channel data have presented an empirical equation for flow carried by the main channel ($\%Q_{mc}$) of a compound section separated by vertical interface plane as

$$\% Q_{mc} = \frac{100}{[(\alpha - 1)\beta + 1]} + 108 \left(\frac{\alpha - 1}{\alpha}\right)^{\frac{1}{4}} (3.3\beta)^{\frac{4}{\alpha}} e^{-9.9\beta} \tag{5.27a}$$

where α and β have their usual meanings defined before. Similarly for the lower main channel separated from the compound section by a horizontal interface plain at the level of floodplain, the flow $\%Q_{lmc}$ proposed by Knight and Demetriou (1983) is written as

$$\% Q_{lmc} = \frac{100(1 - \beta)}{[(\alpha - 1)\beta + 1]} + 300 \left(\frac{\alpha - 1}{\alpha}\right)^{1.25} (5.3\beta)^2 e^{-15.9\beta} \tag{5.27b}$$

Patra and Kar (2000) modified equation (5.27 a and b) for their meandering compound channel and proposed $\%Q_{mc}$ as

$$\% Q_{mc} = \frac{100}{(\alpha - 1)(\beta - 1)} + 108 \left(\frac{\alpha - 1}{\alpha}\right)^{\frac{1}{4}} (3.3\beta)^{\frac{4}{\alpha}} e^{-9.9\beta} [1 + 36\beta Ln(S_r)/\delta] \tag{5.28a}$$

where S_r = the sinuosity of the meandering channels and δ = the aspect ratio of main channel = b/h, b = width of main channel and h = bank full depth of main channel. Similarly equations representing the percentage of discharges in the lower main channel presented by Patra and Kar (2000) is given as

$$\%Q_{lmc} = \frac{100(1-\beta)}{[(\alpha-1)\beta+1]} + 300\left(\frac{\alpha-1}{\alpha}\right)^{1.25}(5.3\beta)^2 e^{-15.9\beta}\left[1+36\beta Ln(S_r)/\delta\right] \qquad (5.28b)$$

Adequacy of equations (5.27 and 5.28) for flow distribution in straight and meandering compound channel for the range of α up to 5.25 and for sinuosity (S_r) up to 1.22 are discussed by the respective authors. For the present Type-III channel having width ratio α = 16.08 and sinuosity Sr = 1.91, equation (5.28) gives higher percentages of error between observed and calculated discharges. Though the equation gives satisfactory results for Type-I channel and lesser satisfactory for Type-II channel, it gives very large error for $\%Q_{mc}$ and $\%Q_{lmc}$ for Type-III channel. Therefore, the models developed by previous investigators are not valid for channels having very wide floodplain (α = 16.08). Using the present compound channel data, further analysis is made here to improve equation (5.28) for better generalization of equations to predict the zonal sub-section discharges.

The equations developed by Knight and Demetriou (1983) and Patra and Kar (2000) shows that the percentage of flow carried by the main channel and lower main channel follow linearly to the simple area ratios ($\%A_{mc}$) and ($\%A_{lmc}$) respectively. To know the dependency of ($\%Q_{mc}$) with the area ratio ($\%A_{mc}$) for straight compound channels, the variation of ($\%Q_{mc}$) with the area ratio ($\%A_{mc}$) for the present straight compound channel Type-I and the straight channel of Knight and Demetrious (1983) are plotted in Fig.5.19 (a). From these plots the best fit power function is found instead of a linear function. The equation for $\%Q_{mc}$ for a straight compound channel is therefore modeled as

$$\%Q_{mc} = 1.2338(\%A_{mc})^{0.9643} \qquad (5.29a)$$

Since for a rectangular main channel $\dfrac{A_{mc}}{A} = \dfrac{1}{(\alpha-1)\beta+1}$ substituting in (5.29a) we get

$$\%Q_{mc} = 1.2338\left[\frac{100}{\{(\alpha-1)\beta+1\}}\right]^{0.9643} \qquad (5.29b)$$

- 126 -

Similarly for lower main channel the best fit power function between $\%Q_{lmc}$ and the area ratio $\%A_{lmc}$ is obtained from Fig.5.19 (b) as

$$\%Q_{lmc} = 1.0277\left(\%A_{mc}\right)^{1.0067} \tag{5.30a}$$

for a rectangular lower main channel $\dfrac{A_{lmc}}{A} = \dfrac{1-\beta}{(\alpha-1)\beta+1}$ substituting in (5.30a) we get

$$\% Q_{lmc} = 1.0277\left[\dfrac{100\ (1-\beta)}{\{(\alpha-1)\beta+1\}}\right]^{1.0067} \tag{5.30b}$$
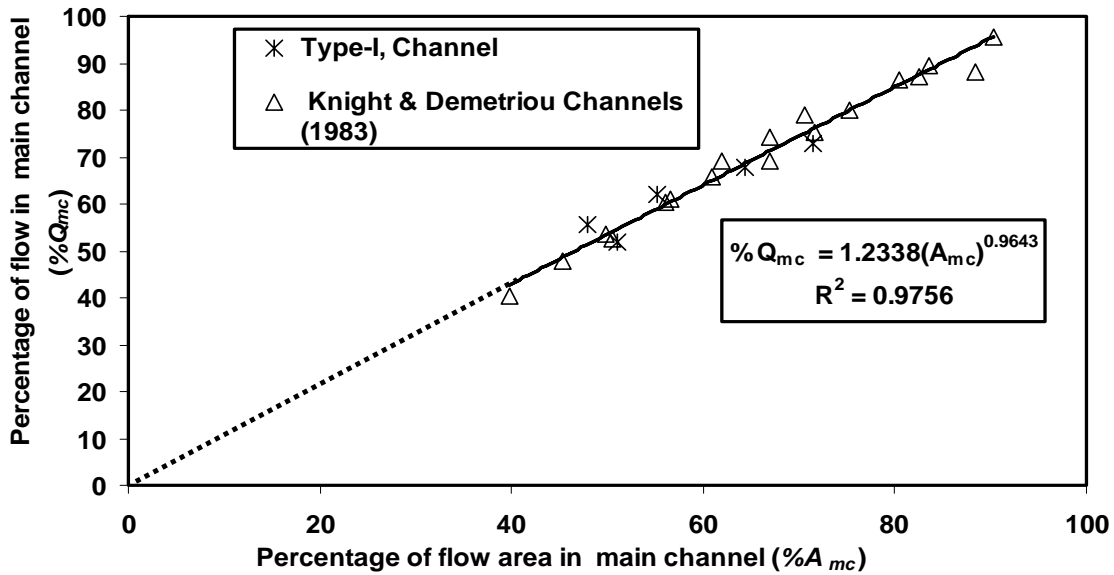
Fig. 5.19 (a) Variation of percentage of flow in main channel ($\%Q_{mc}$) against corresponding area of main channel for straight compound channels
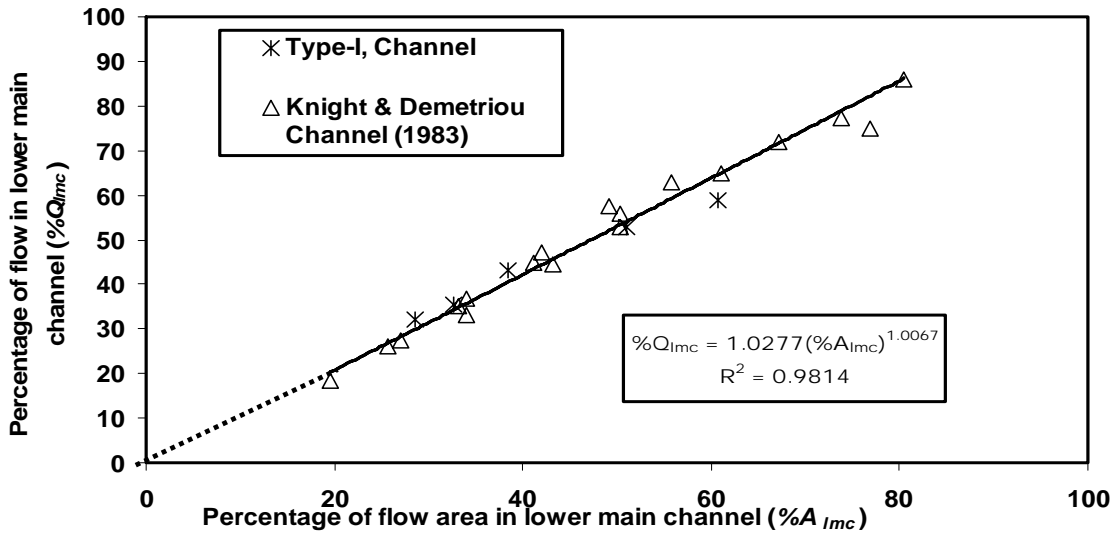
Fig. 5.19 (b) Variation of percentage of flow in lower main channel ($\%Q_{lmc}$) against corresponding area of lower main channel for straight compound channels
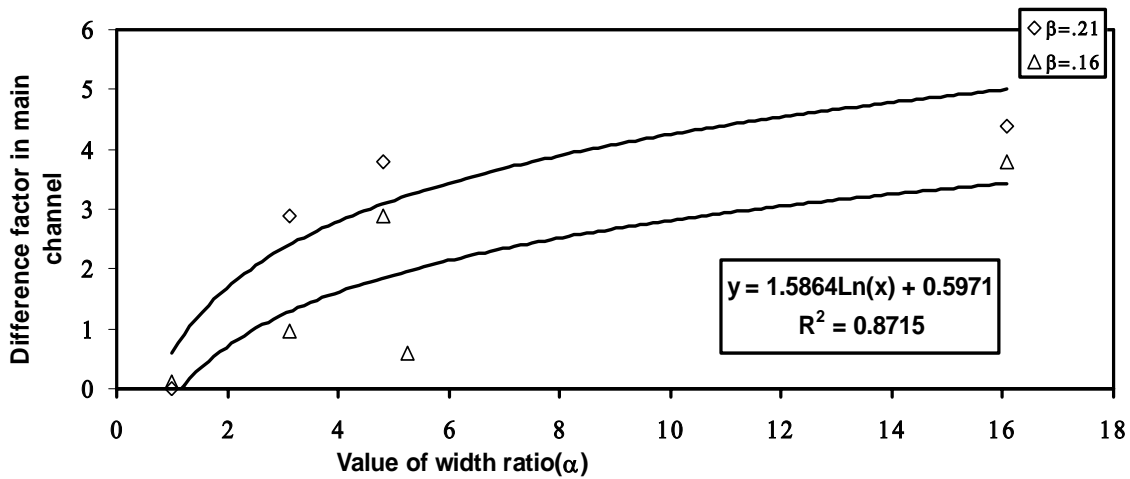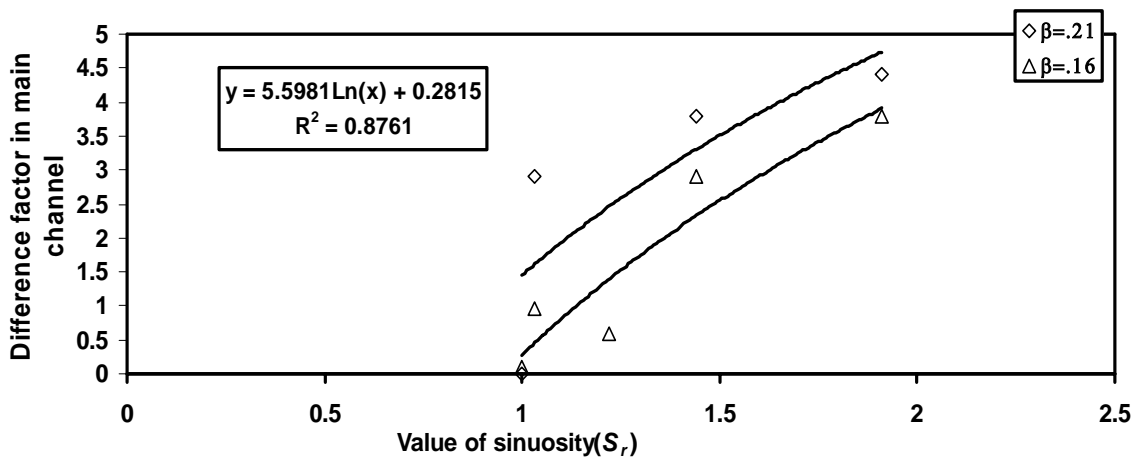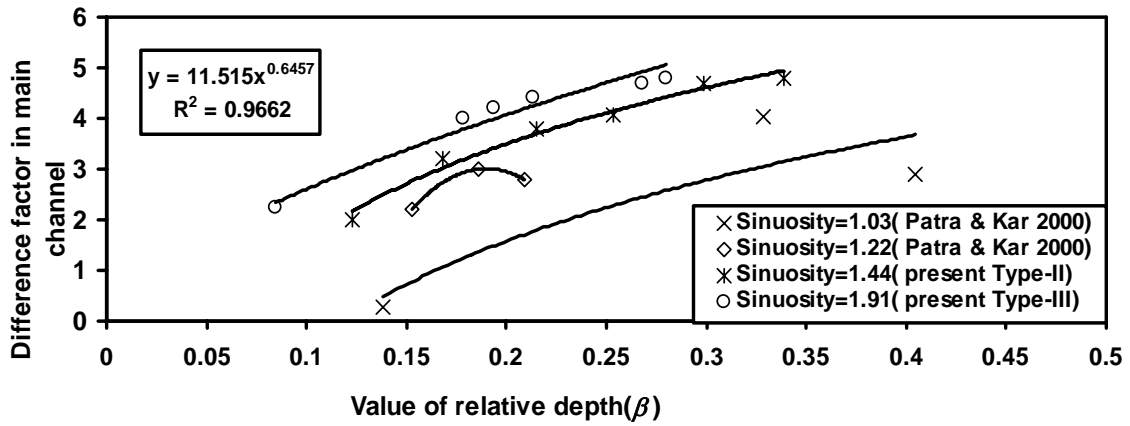
Fig.5.20 (a,b and c) Variation of the difference factor for flow in main channel with relative depth(β), sinuosity(S_r) and width ratio(α)
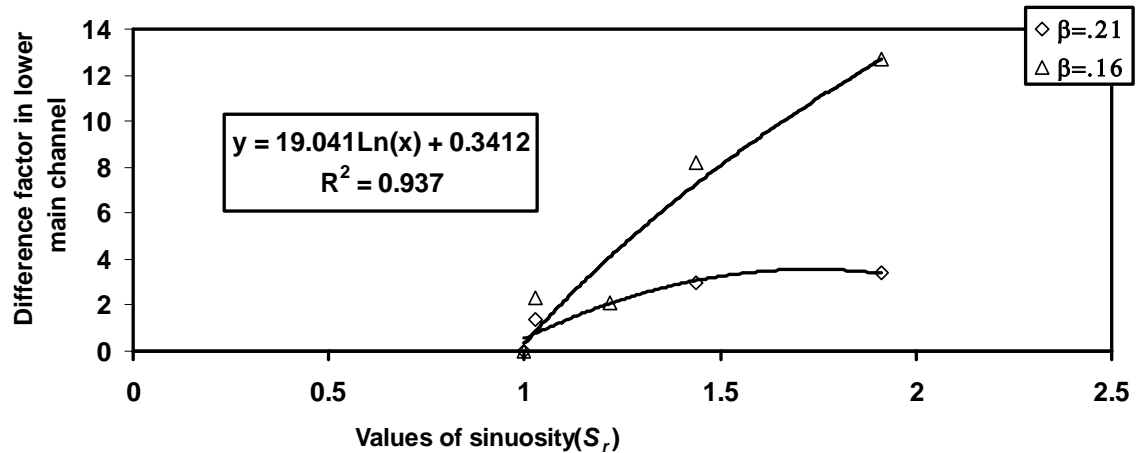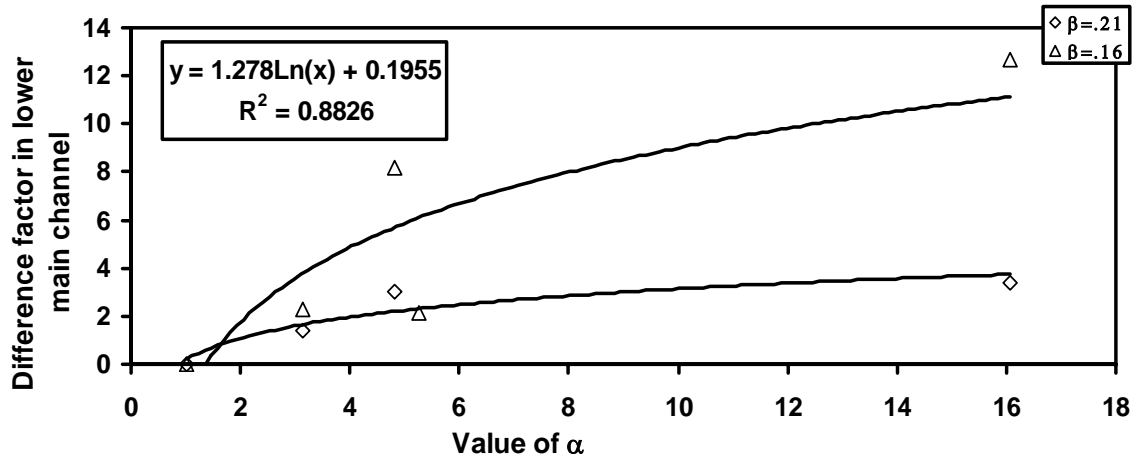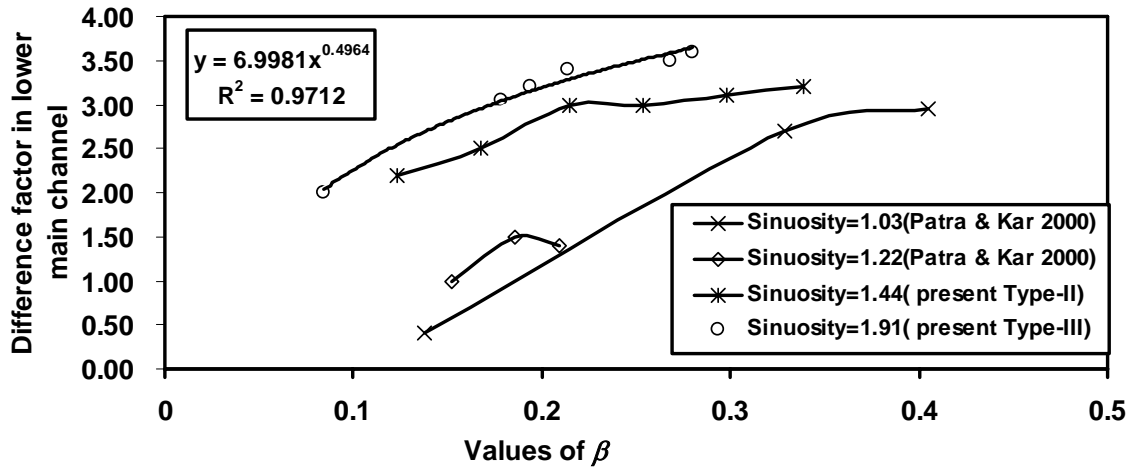
Fig.5.21 (a,b and c) Variation of the difference factor for flow in lower main channel with relative depth(β), sinuosity(S_r) and width ratio(α)

Distribution of zonal flow in a meandering compound channel is further affected by sinuosity. The $\%Q_{mc}$ and $\%Q_{lmc}$ of Type-II and Type-III channels is calculated using (5.30a) and (5.30b) and is compared with the observed values given in Table 5.5. From the table, it is seen that due to meandering effect the $\%Q_{mc}$ and $\%Q_{lmc}$ decreases with sinuosity. The difference factor due to sinuosity is found out and the variation of this difference factor with relative depth (β), sinuosity (S_r), and with width ratio (α) for $\%Q_{mc}$ and $\%Q_{lmc}$ are plotted in Fig.5.20 (a, b, and c), and Fig.5.21 (a, b, and c) respectively. The best fitted functional relationships for $\%Q_{mc}$ and $\%Q_{lmc}$ with the parameters are obtained and given as

Difference factor for $\%Q_{mc} = F_1(\beta^{0.6457})$, $F_2\{Ln(1.82\alpha)\}$ and $F_3\{Ln(1.32S_r)\}$

Difference factor for $\%Q_{lmc} = F_1'(\beta^{0.4964})$, $F_1'\{Ln(1.4\alpha)\}$ and $F_3'\{Ln(1.21S_r)\}$

Table-5.5   Comparison of percentage of flow in main channel and lower main channel of Type-II and Type-III channels with and with out meandering effect

Type-II Sinuosity (S_r =1.44)	β	0.1228	0.1678	0.2146	0.2537	0.298	0.338
	$\%Q_{mc}$ (With out meandering)	72.30	64.99	58.83	54.53	50.35	47.07
	$\%Q_{mc}$ (Actual)	70.30	61.79	55.04	50.46	45.65	42.27
	$\%Q_{lmc}$ (With out meandering)	63.13	53.56	45.54	39.96	34.57	30.34
	$\%Q_{lmc}$ (Actual)	60.93	51.07	42.54	36.97	31.47	27.14
Type-III Sinuosity (S_r =1.91)	β	0.0846	0.178	0.193	0.2133	0.268	0.28
	$\%Q_{mc}$ (With out meandering)	63.63	45.44	43.56	41.32	36.32	35.41
	$\%Q_{mc}$ (Actual)	61.39	41.44	39.36	36.92	31.62	30.61
	$\%Q_{lmc}$ (With out meandering)	55.76	33.94	31.71	29.01	23.14	22.1
	$\%Q_{lmc}$ (Actual)	53.76	30.91	28.51	25.65	19.64	18.48

Combining all the parameters the difference factor for $\%Q_{mc}$ is written as

$$\text{Difference factor} = F[\beta^{0.6457}Ln(1.82\alpha)Ln(1.32S_r)] = 5.05\beta^{0.6457}Ln(1.82\alpha)Ln(1.32S_r) \qquad (5.31)$$

Similarly the difference factor for $\%Q_{lmc}$ is written as

$$\text{Difference factor} = F[\beta^{0.4964}Ln(1.4\alpha)Ln(1.216S_r)] = 2.11[\beta^{0.4964}Ln(1.4\alpha)Ln(1.216S_r)] \qquad (5.32)$$

Now the equation for the percentage of flow in main channel is written as

$$\%Q_{mc} = 1.2338\left[\frac{100}{\{(\alpha-1)\beta+1\}}\right]^{0.9643} - 5.05\beta^{0.6457}Ln(1.82\alpha)Ln(1.32S_r) \qquad (5.33)$$

and the percentages of flow carried by lower main channel for meandering compound channel is obtained as

$$\%Q_{lmc} = 1.0277 \left[\frac{100(1-\beta)}{\{(\alpha-1)\beta+1\}} \right]^{1.0067} - 2.11\beta^{0.4964} Ln(1.4\alpha) Ln(1.216S_r) \qquad (5.34)$$

Using (5.33) and 5.34 the value of $\%Q_{mc}$ and $\%Q_{lmc}$ for meandering compound channels can be evaluated.
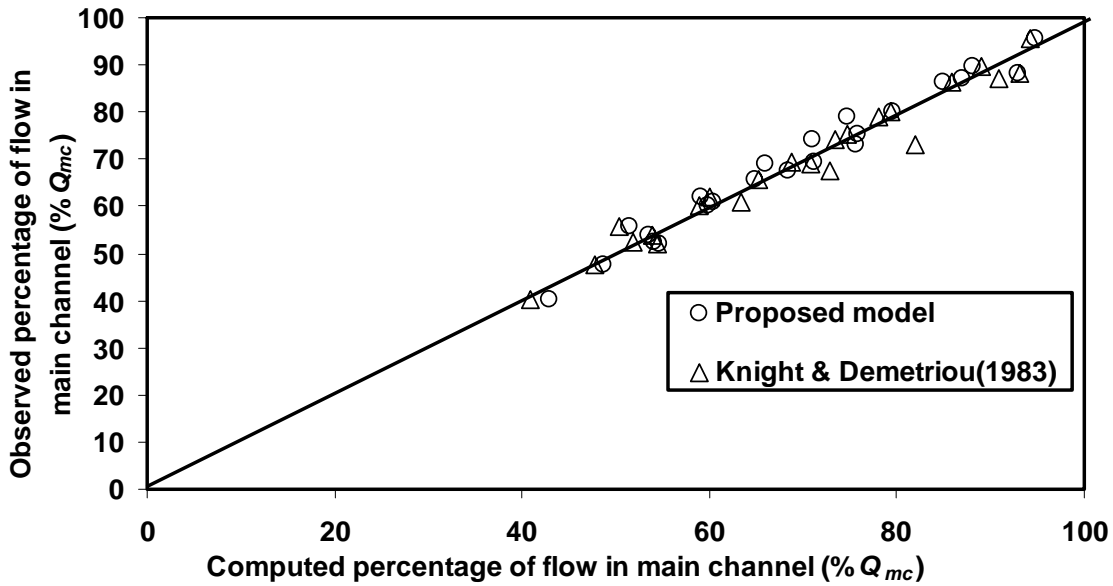
Fig. 5.22 (a) Variation of calculated verses observed value of flow distribution in main channel ($\%Q_{mc}$) for straight compound section
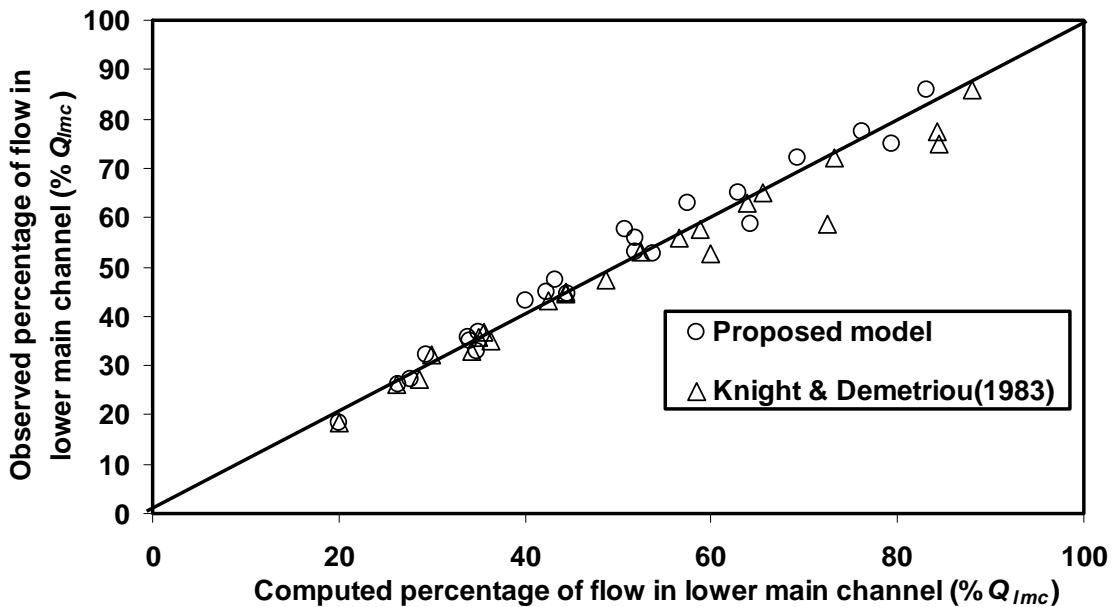
Fig. 5.22 (b) Variation of calculated verses observed value of flow distribution in Lower main channel ($\%Q_{lmc}$) for straight compound section

The variation of computed percentage of flow in main channel and lower main channel with the observed value of Type-I along with channels of Knight and Demetrious (1983) is shown in Fig. 5.22 (a) and Fig. 5.22 (b) respectively. Similarly the variation between computed and observed values for Type-II and Type-III meandering compound channels along with results of compound meandering channels of Patra and Kar (2000) is plotted in Fig. 5.23 (a) and Fig. 5.23 (b) respectively. Fig. 5.22 and Fig. 5.23 show the adequacy of equation (5.33 and 5.34) for straight and meandering compound channels for the evaluation of $\%Q_{mc}$ and $\%Q_{lmc}$ respectively.
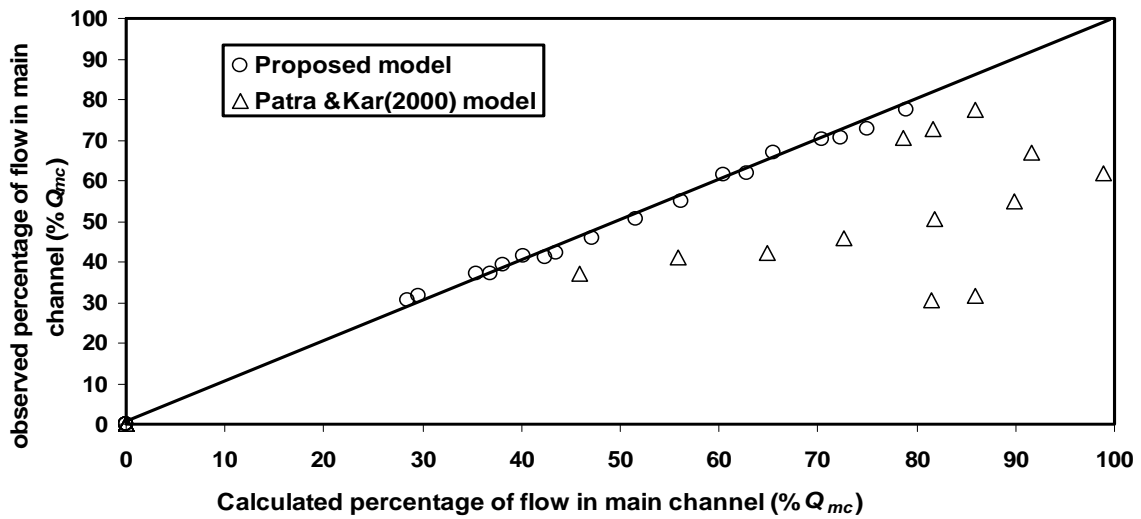
Fig. 5.23 (a) Variation of calculated verses observed value of flow distribution in main channel ($\%Q_{mc}$) for meandering compound sections
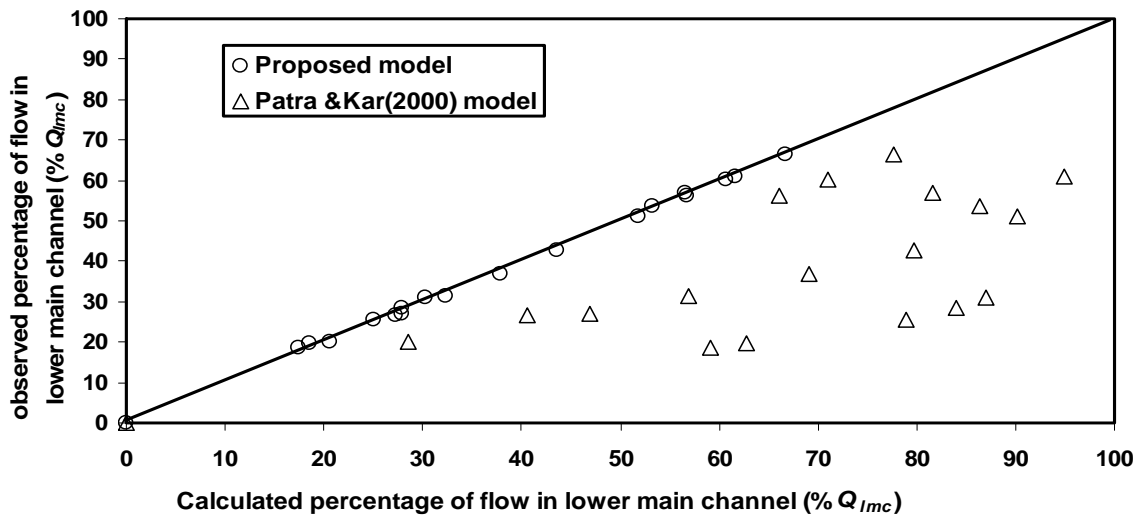
Fig. 5.23 (b) Variation of calculated verses observed value of flow distribution in lower main channel ($\%Q_{lmc}$) for meandering compound sections

- 132 -

5.9 ONE DIMENSIONAL SOLUTIONS FOR DISCHARGE ASSESSMENT IN TWO STAGE COMPOUND CHANNELS

During floods the river water often overtops the banks of the natural channels and inundates its floodplains. These floodplains provide the required extra storage capacity to attenuate the flood peak and to facilitate the transmission of the floodwaters down the river corridors (Fig.5.24). A major area of uncertainty in river channel analysis is the accuracy in predicting the discharge carrying capability of a channel with floodplains commonly known as compound section. Natural channels are never straight, they meander. For a meandering compound channel, the flow mechanism is more complicated due to the three-dimensional (3D) nature of flow and the momentum transfer involved in the system. Accurate assessment of discharge capacity for meandering and straight compound channels is essential for flood warning, determining the development of flood-risk areas, long-term management of rivers in controlling floods, and in designing artificial waterways. Different approaches for prediction of discharge in a straight and meandering compound channels with the proposed approaches are discussed in this section. The approaches are analysed using the present experimental channels.
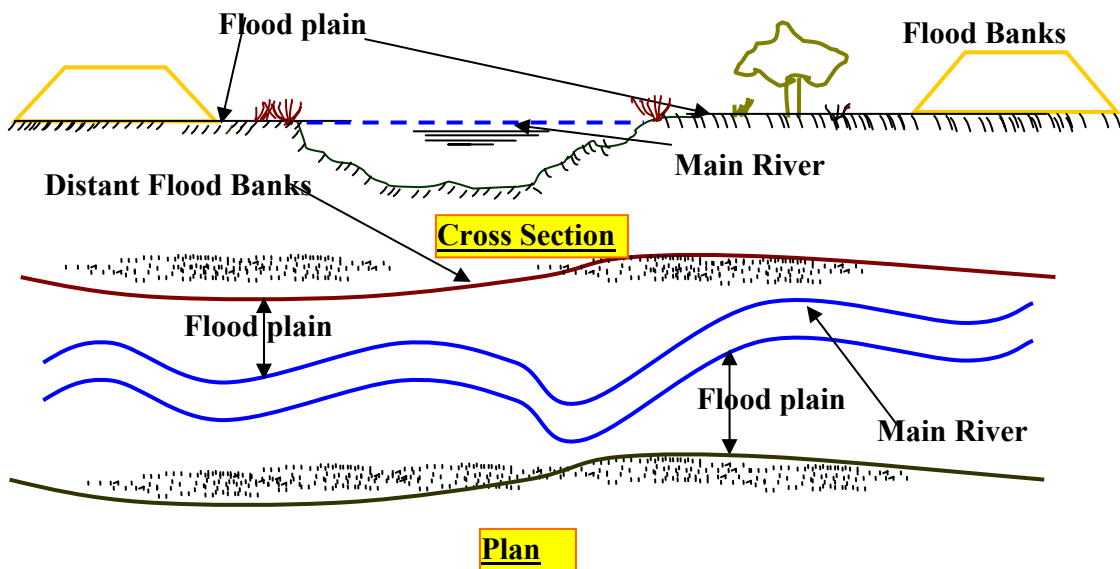
Fig. 5.24   Plan and cross section of a two-stage compound channel

5.9.1 ANALYSIS OF DATA USING SINGLE CHANNEL METHOD (SCM)

At low depths when the flow is confined to the main channel only, the conventional Manning's, Chezy's or Darcy-Weisbach equation may be used to assess the discharge capacity. However, during over-bank flows, the channel section becomes compound. Consideration of the whole channel as a single section and use of these classical formulas to the entire compound section is known as single channel method (*SCM*) which generally under estimates the actual discharge. At this stage the single channel method suffers from a sudden reduction in the hydraulic radius at just above bank full stage. The under-estimation is more at low over bank depths and gradually decreases as the flow depth over floodplain increases. The composite roughness method given by Chow (1959) is also essentially flawed when applied to the flow estimation of compound sections. Using the flood channel facility (FCF) data from the Wallingford UK, Greenhill and Sellin (1993) reported that when a compound section is analyzed as a single channel, the Manning's equation yields errors up to 30 percent between the observed and computed discharges. This is mainly due to the three-dimensional (3D) mixing of flow between the main channel and floodplain. Using SCM, the error between the observed and computed discharges for the three types of present experimental channels are shown as curve *SCM* in Figs.5.25 (a, b and c). It can be seen from the figures that for all the three test channels, the discharge is under-estimated. This is in line with the earlier reports of Greenhill and Sellin (1993). The channel discharge using SCM are tabulated in col.4 of Table 5.6 and in col.5 of Table 5.7.
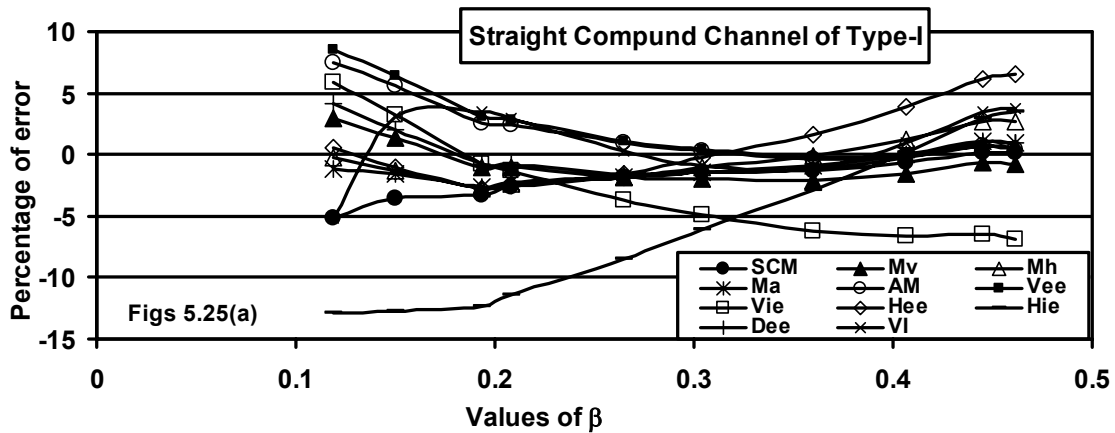
Fig. 5.25 (a) Variation of percentage of error between calculated and observed discharge with relative depth by different approaches for the straight Type-I Compound channel.
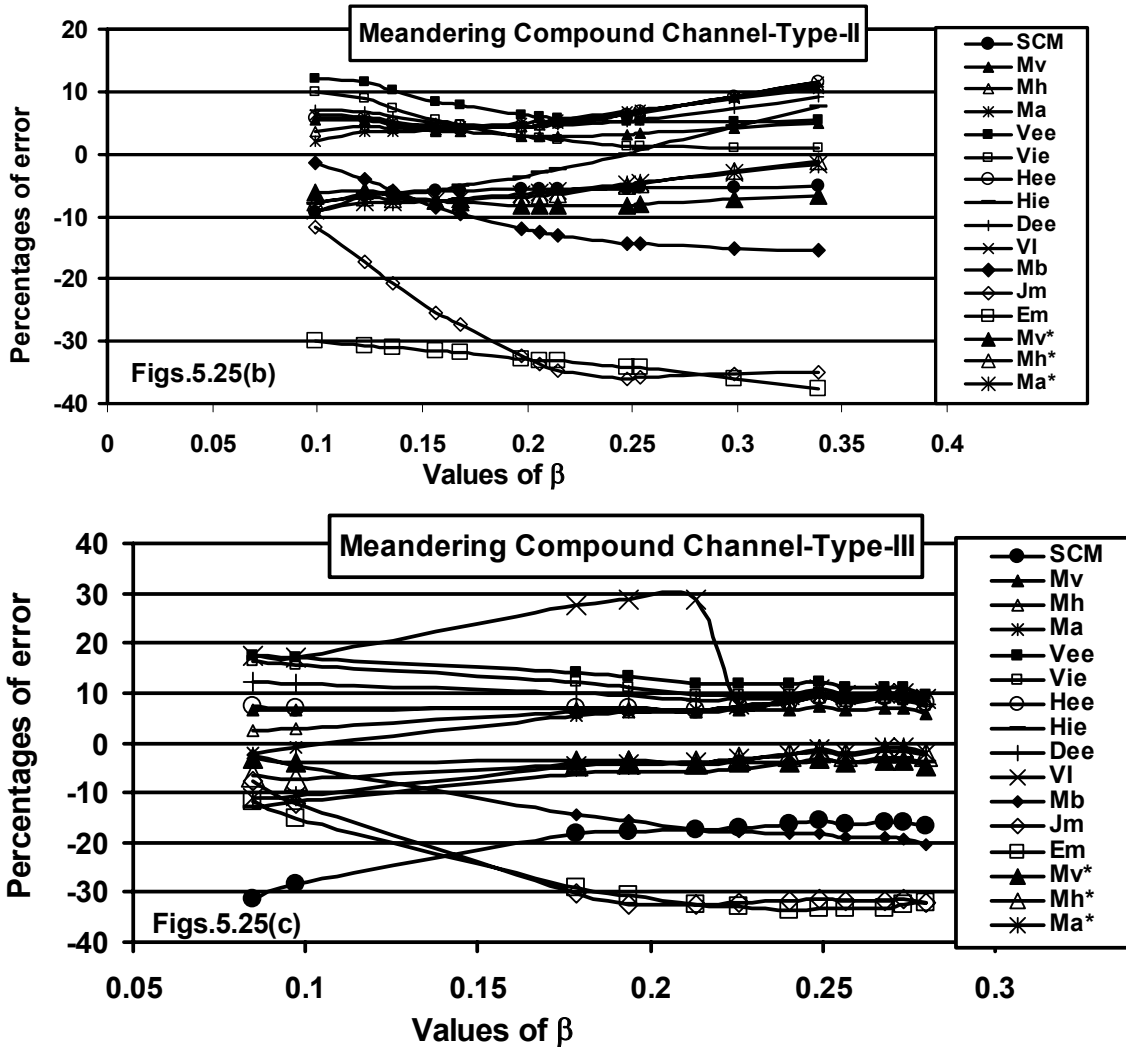
Fig. 5.25 (b and c) Variation of percentage of error between calculated and observed discharge with relative depth by different approaches for Type-II and Type-II Meandering channels

[SCM-Single channel method, Vee - (VDM-1), Vie - (VDM-1I), Hee - (HDM-1), Hie - (HDM-1I), Dee - DDM, AM - Area method, Mv*- Proposed Vertical method (VDM-III), Mh*- Proposed horizontal method (HDM-III), Ma*- Proposed area method, VI - Variable Inclined plain method, Jm - James & Wark method, Em - Ervine & Ellis method, Mb-Meander belt method]

5.9.2   DIVIDED CHANNEL METHOD (DCM)

A classical approach of discharge estimation by the river engineers follow is to decompose a compound channel section into reasonable homogeneous subsections by considering imaginary interface plains originating from the main channel and floodplain

junctions in such a way that the velocity field in each subsection is taken as uniform. The total discharge is the sum of the sub-area discharges given as

$$Q = \sum_{i=1}^{n} \frac{A_i R_i^{2/3}}{n_i} S^{1/2} \qquad (5.35)$$

where Q = total discharge, A_i = sub-area cross section area, R_i = sub-area hydraulic radius, n_i = sub-area channel roughness, S = the channel slope, and the subscript i stands for each sub- area. This is popularly known as divided channel method (DCM) and it gives us an option to select a division line in the form of a vertical, horizontal or a diagonal plane drawn from the junction between the main channel and the floodplains (Fig.5.26). Since in SCM for a compound channel it is difficult to assign a single Manning's n for the whole channel, the problem can be overcome by DCM and therefore the method gives better discharge results then SCM. Selection of the interface plane for the separation of the compound section to sub-areas can be made using the value of the apparent shear at the assumed interface plane (Knight and Demetriou1983). Nevertheless, the DCM is still deficit as the method does not take care of the turbulent interaction of the flow between the main channel and the floodplain leading to the momentum transfer between the deep and shallow sections and the 3D mixing of the flow, more importantly for meandering compound channels (Ervine et. al 2001).
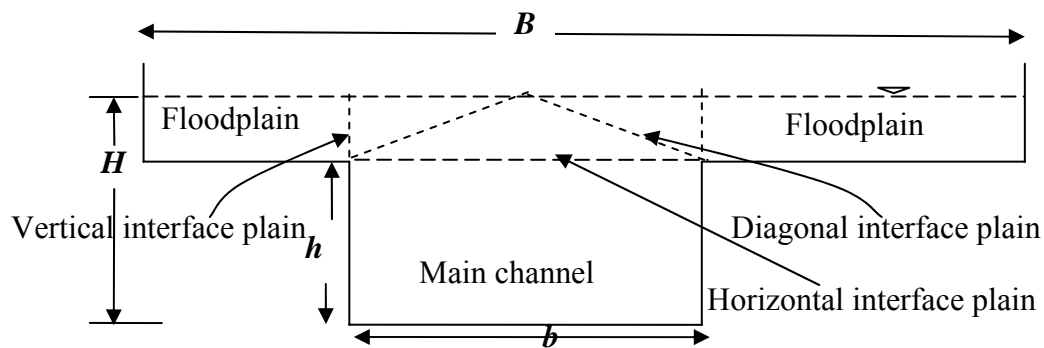
Fig. 5.26 Division of a compound section into sub areas using horizontal, vertical and diagonal interface planes

Proper selection of the interface plane is therefore important for separating a compound channel section into sub-areas for discharge estimation. Due to interaction mechanism, a bank of vortices is created originating from the main channel - floodplain junctions. The strength of vortices at the shearing zone is manifested as the shear force at the interface plane. At low depths of flow over floodplain, the shear force at this

apparent plane of separation is very much higher than the average bed shear force and gradually decreases as the depth of flow over flood plain increases. By including a length equal to ($H–h$) for vertical, b for horizontal, or $\sqrt{(H-h)^2+b^2}$ for a diagonal interface to the wetted perimeter of the main channel only, we are incorporating a share drag of magnitude equal to the interface length times the average boundary shear only and not the full shear generated due to the resultant dragging-pulling of water by the main channel-floodplain geometry. Therefore, these lengths need to be modified to take care of the interaction affect. This gives rise to a number of alternatives in the selection of interface plane for separation of a compound channel into sub-areas for discharge assessment using DCM. In the light of the knowledge gained about flow structure in compound channels, a number of methods can be proposed as to how these divided channel methods might be modified to simulate the interaction process in compound channels more accurately (Lambert and Myers, 1998). Using the present experimental channel results along with earlier reported data, the best selection of interface plane for discharge estimation using the "divided channel method" are discussed.

5.9.2.1 METHODS BASED ON ALTERING SUBSECTION WETTED PERIMETER

Vertical Division Method (VDM)

Several approaches on the vertical division method based on altering the wetted perimeter of the subsection area to account for the effect of interaction are proposed. A vertical division line for a compound channel is shown in Fig.5.26.

VDM - I

As the first approach, the length of interface ($H–h$) is not included both to the main channel and to the floodplain sub areas. The approach assumes zero apparent shear stress at the vertical interface and therefore does not take care of the interaction effect. The interaction affect is manifested indirectly in terms of error in the estimated discharge of the sub-areas due to the neglect of shear at the division interface. This is because, for any channel resistance-discharge equation, the magnitude of perimeter offering resistance or shear is very strongly related to the velocity flowing through the

area. For the present three experimental (straight and meandering) compound channels, the resulting section discharges are given in col.5 of Table 5.6 and col.6 of Table 5.7. It can be seen that the calculated discharges are different from the corresponding observed values. The percentage of error between the observed and calculated discharges for all types of channel is shown as the curve V_{ee} in Fig 5.25. Maximum error is noticed at the just over bank flow after which it decreases gradually to a minimum at higher over bank depths. It shows that for Type-II channels, momentum transfer is maximum at just over bank flow and the transfer across the vertical boundary is complete at around $\beta \approx 0.25$. At still higher over bank depths ($\beta > 0.25$) the percentage of error of discharge increases slowly. For Type-III channel, the errors of discharge continuously and gradually decreases with flow depth over floodplain for the ranges of the stages investigated. It is expected that the error curve to show to be nearly flat at still higher depths of flow. Excluding the interface length to the wetted perimeter always overestimates the discharge capacity of a compound channel. This is quite in agreement with the results given by Wormleaton and Hadjipanos (1982). Though this method gives good discharge results at certain relative flow depths of β around 0.25 for Type-II channel but the approach can not be accepted for all over bank flow depths and to all channel geometry because of its ineffectiveness to take care of the interaction results between main channel and its adjoining floodplain.

Table 5.6   Discharge results using various 1D approaches for straight Type-I compound channel

Experiment Series	Depth over Flood Plain (*H-h*) (cm)	Observed discharge Q (cm³/s)	Q-SCM (cm³/s)	VDM –I (Q-V_{ee}) (cm³/s)	VDM –II (Q-V_{ie}) (cm³/s)	VDM –III (Proposed VDM) Q-M_V (cm³/s)	HDM –I (Q-H_{ee}) (cm³/s)	HDM –II (Q-Hie) (cm³/s)	(Proposed HDM) Q-M_H (cm³/s)	ZASIM 1-(DDM) Q-D_{ee} (cm³/s)	Variable Inclined Plain method (Q-VI) (cm³/s)	Area Method (Q-AM) (cm³/s)	Proposed Area Method (Q-M_a) (cm³/s)
(1)	(2)	(3)	(4)	(5)	(6)	(7)	(8)	(9)	(10)	(11)	(12)	(13)	(14)
S12	1.62	8726	8276	9476	9237	8987	8771	7606	8709	9084	8280	9373	8632
S13	2.12	*10007*	9646	10651	10323	10149	9899	8734	9879	10212	10322	10569	9852
S14	2.88	12245	11848	12625	12147	12120	11898	10734	11906	12153	12670	12564	11921
S15	3.15	*13004*	12665	13377	12841	12872	12683	11518	12690	12903	13396	13322	12711
S16	4.32	16706	16397	16893	16082	16398	16452	15287	16397	16452	16763	16856	16397
S17	5.25	*19861*	19564	19946	18885	19459	19808	18644	19641	19568	19692	19917	19583
S18	6.75	25329	25001	25264	23744	24786	25754	24589	25307	25031	25035	25245	25099
S19	8.21	30844	30633	30833	28795	30351	32042	30878	31229	30767	31136	30817	30833
S20	9.62	36275	36350	36517	33916	36019	38488	37324	37247	36623	37555	36504	36650
S21	10.28	39071	39111	39269	36381	38760	41611	40447	40148	39454	40560	39256	39453

Table 5.7 Discharge results using various 1D approaches for Type-II and Type-III meandering compound channels

Ch. Type	Experiment Series	Depth Over Flood Plain (H-h) (cm)	Observed discharge Q (cm³/s)	SCM (cm³/s)	VDM–I (Q-Vee) (cm³/s)	VDM–II (Q-Vie) (cm³/s)	VDM–III (Proposed VDM) Q-Mv (cm³/s)	HDM–I (Q-Hee) (cm³/s)	HDM–II (Q-Hie) (cm³/s)	(Proposed HDM) (Q-MH) (cm³/s)	ZASIM 1-(DDM) (Q-Dee) (cm³/s)	Proposed Area Method (Q-Ma) (cm³/s)	Ervine and Ellis (Q-EM) (cm³/s)	James and Wark (Q-JM) (cm³/s)	Greenhill and Sellin (Q-MB) (cm³/s)	Patra and Kar (Q-VI) (cm³/s)
(1)	(2)	(3)	(4)	(5)	(6)	(7)	(8)	(9)	(10)	(11)	(12)	(13)	(14)	(15)	(16)	(17)
Type-II	MM16	1.32	9007	8172	10097	9896	8571	9527	8287	8387	9649	8283	4665	7960	8874	9581
	MM17	1.68	10108	9443	11269	11005	9628	10690	9450	9467	10804	9411	6185	8363	9710	10725
	MM18	1.89	10899	10215	12007	11703	10297	11443	10203	10158	11546	10123	7129	8639	10249	11469
	MM19	2.23	12246	11507	13279	12908	11452	12769	11529	11362	12845	11350	8712	9128	11193	12782
	MM20	2.42	13005	12253	14029	13619	12134	13563	12324	12077	13621	12073	9625	9448	11756	13571
	MM21	2.95	15290	14415	16256	15732	14161	15966	14675	14217	15954	14213	12271	10343	13449	15961
	MM22	3.11	15999	15091	16965	16405	14806	16742	15502	14902	16705	14893	13106	10629	13993	16734
	MM23	3.28	16762	15821	17737	17137	15508	17590	16350	15648	17525	15630	14009	10941	14586	17580
	MM24	3.94	19867	18761	20895	20132	18379	21102	19863	18713	20909	18637	17602	12718	17030	21085
	MM25	4.08	20524	19406	21596	20797	19016	21890	20650	19395	21666	19303	18404	13169	17575	21871
	MM26	5.1	25662	24311	27005	25921	23923	28025	26786	24665	27547	24407	24380	16597	21798	28001
	MM27	6.15	31358	29716	33068	31655	29411	34992	33753	30576	34201	30083	30971	20381	26546	34966
Type-III	HM16	0.74	12757	8763	15001	14834	12699	13704	11092	12167	14318	11804	93118	11790	12463	14966
	HM17	0.86	13974	9991	16379	16177	13801	14951	12311	13233	15619	12932	111179	12287	13342	16356
	HM18	1.74	24487	19981	27949	27455	24223	26206	22934	23636	26908	23648	232260	17121	20979	31280
	HM19	1.92	27185	22343	30795	30230	26800	29092	25576	26254	29739	26296	264116	18390	22928	34968
	HM20	2.17	31299	25788	34992	34322	30602	33397	29485	30137	33937	30203	308288	21170	25830	40348
	HM21	2.33	33817	28093	37822	37080	33167	36325	32128	32765	36780	32837	342409	23020	27801	36401
	HM22	2.53	37173	31078	41512	40677	36513	40170	35579	36204	40499	36270	385578	25364	30385	40711
	HM23	2.65	39048	32925	43805	42911	38593	42573	37728	38345	42816	38403	419862	26757	31997	43157
	HM24	2.76	*41416*	34654	45958	45009	40546	44837	39747	40359	44995	40406	456182	28200	33515	45399
	HM25	2.93	44412	37391	49379	48343	43650	48449	42960	43566	48465	43588	507166	30297	35934	48912
	HM26	3.01	46014	38707	51029	49949	45146	50195	44510	45113	50139	45121	548081	31528	37103	50593
	HM27	3.11	*48474*	40375	53125	51990	47048	52420	46481	47081	52270	47069	599253	32955	38590	52722

VDM - II

Typically, the length of vertical division lines between the main channel and the floodplain originating from the main channel-flood plain junction is included to the wetted perimeter of main channel only for discharge estimation by divided channel method. This is intended to take care of the effect of retarding the flow of main channel. Using the approach, the resulting discharge for the compound channels are given in col.6 of Table.5.6 and col.7 of Table.5.7 and the discharge errors are shown as curves V_{ie} in Fig.5.25. At low depths of flow over floodplain this approach gives better results than VDM-I but at higher floodplain depths the approach tends to underestimate the discharge capacity for Type-I and Type-II channel. This may be because at higher depths of flow over floodplain, the momentum transfer is reversed, that is, the floodplain supplies momentum to the main channel and therefore the interface length may not be required to be included to the wetted perimeter of the main channel. For

Type-III channel it still shows positive error of discharge even at the highest observed β.

To further improve the VDM-II, and to calculate the discharge of the present compound channels close to the observed values by divided channel method, the length of the vertical interface is increased suitably and added to the main channel perimeter. The extra length of interface added to the main channel may be termed as interaction length and is found to be many times higher than the flow depth ($H-h$) at low depths of flow over floodplain and gradually reduces to ($H-h$) as the depth of flow increases. This shows that the interaction is intense at low depths of flow over floodplain and reduces gradually as the depth increases. A graph between β verses ($H-h$) times the length of interface that is added to the main channels are plotted in Fig.5.27.
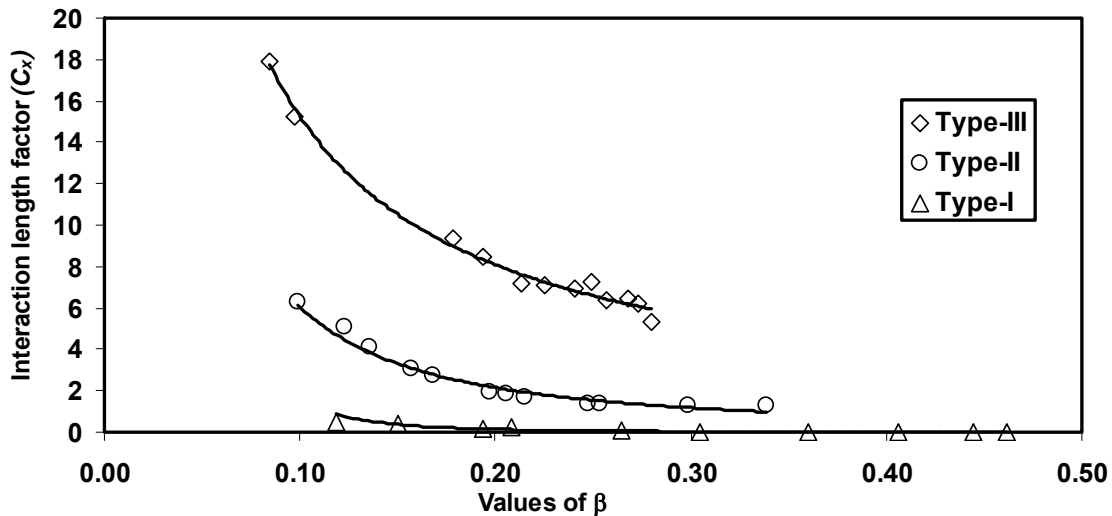
Fig. 5.27 Variation of interaction length factor C_x in a vertical interface division with relative depth to obtain the actual over all discharge

The values of C_x for various channels are given in Table 5.8. The computed discharge of the compound channel is found to be close to the observed values and therefore there is zero error between the observed and computed discharges. Using the method the discharges for main channel and floodplain sub-areas are found to be different from their actual values. By adding the extra length of the interface to the main channel, the overestimation of the main channel discharge is reduced. From Fig.5.27, a relation between β verses ($H-h$) times C_x, where C_x is a factor representing the length of

- 140 -

interface $(H–h)$ times that is to be added to the main channel perimeter only, is obtained from the best fit power function given as

for Type-I $\qquad\qquad C_x = 0.0306\ \beta^{-1.2752}$ $\qquad\qquad$ (5.36a)

for Type-II $\qquad\qquad C_x = 0.1945\ \beta^{-1.4932}$ $\qquad\qquad$ (5.36b)

and for Type-III $\qquad\qquad C_x = 1.7818\ \beta^{-0.9425}$ $\qquad\qquad$ (5.36c)

It can be seen from the table that the magnitude of C_x decreases with increase in β. The method is simple, straight forward and can easily be adoptable to any compound channel with the only disadvantage being that the observed and calculated sub-area discharges do not match.

VDM - III **(Proposed Modified Interface Method)**

This method is an improvement to the conventional divided channel method. From the values of apparent shear at vertical interface in Fig.5.16 (a,b, and c), it can be seen that the plane is neither shear free nor the apparent shear at this surface is equal to boundary shear of main channel or the floodplain surfaces. It requires that the main channel boundary shear to be increased suitably and that of floodplain decreased due to main channel and floodplain flow interaction (Myer and Elsawy 1975). Wormelaton et. Al. (1982) have shown that the total dragging force on the main channel due to floodplain at the interfaces must be equal to the accelerating force on floodplain due to the main channel. Net force at the assumed vertical interface should balance each other. The interaction lengths for main channel X_{mc} and floodplain X_{fp} can be derived using equations 5.18 and 5.19 respectively. If a vertical interface is selected than the proposed interaction lengths is simplified as

$$X_{mcV} = \frac{100\ P_{mc}}{(100\ -\ \%\ S_{fp})\{1\ +\ (\alpha\ -\ 1)\beta\ \}} - P_{mc} \qquad\qquad (5.37)$$

where $X_{mcv}=$ the length of vertical interface to be included to the wetted perimeter of main channel sub-area, $P_{mc} =$ wetted perimeter of main channel, $\alpha =$ width ratio B/b and $\beta =$ relative depth $(H-h)/H$. Similarly, the equivalent decrease in the length of floodplain wetted perimeter for a for vertical interface is written as

$$X_{fpV} = P_{fp} - \frac{100\ (\alpha\ -\ 1)\beta}{(\%\ S_{fp})\{1\ +\ (\alpha\ -\ 1)\beta\}}\ P_{fp} \qquad\qquad (5.38)$$

where $X_{fpv} =$ the length of vertical interface to be deducted from the wetted perimeter of floodplain sub-section and $P_{fp} =$ wetted perimeter of the floodplain sub-area. The

percentage of shear force, $\%S_{fp}$ carried by the floodplain walls and bed can be calculated from equation (5.10). Knowing $\%S_{fp}$ and channel geometry, the interface lengths X_{mcV} and X_{fpV} are evaluated. Next, the discharge for main channel and floodplain are calculated using Manning's equation given as

$$Q = \frac{\sqrt{S}}{n}\left\{A_{mc}^{5/3}(P_{mc} + X_{mcv})^{-2/3} + A_{fp}^{5/3}(P_{fp} - X_{fpv})^{-2/3}\right\} \qquad (5.39)$$

For the present compound channels the percentage of error between calculated and observed discharges using equation (5.39) is shown as curves M_v^* in Fig. 5.25. The standard error of estimate between observed and calculated discharge are found to be 1.68, 7.3, and 3.8 for Type-I, Type-II and Type-III channels respectively for all the over-bank flow depths taken together.
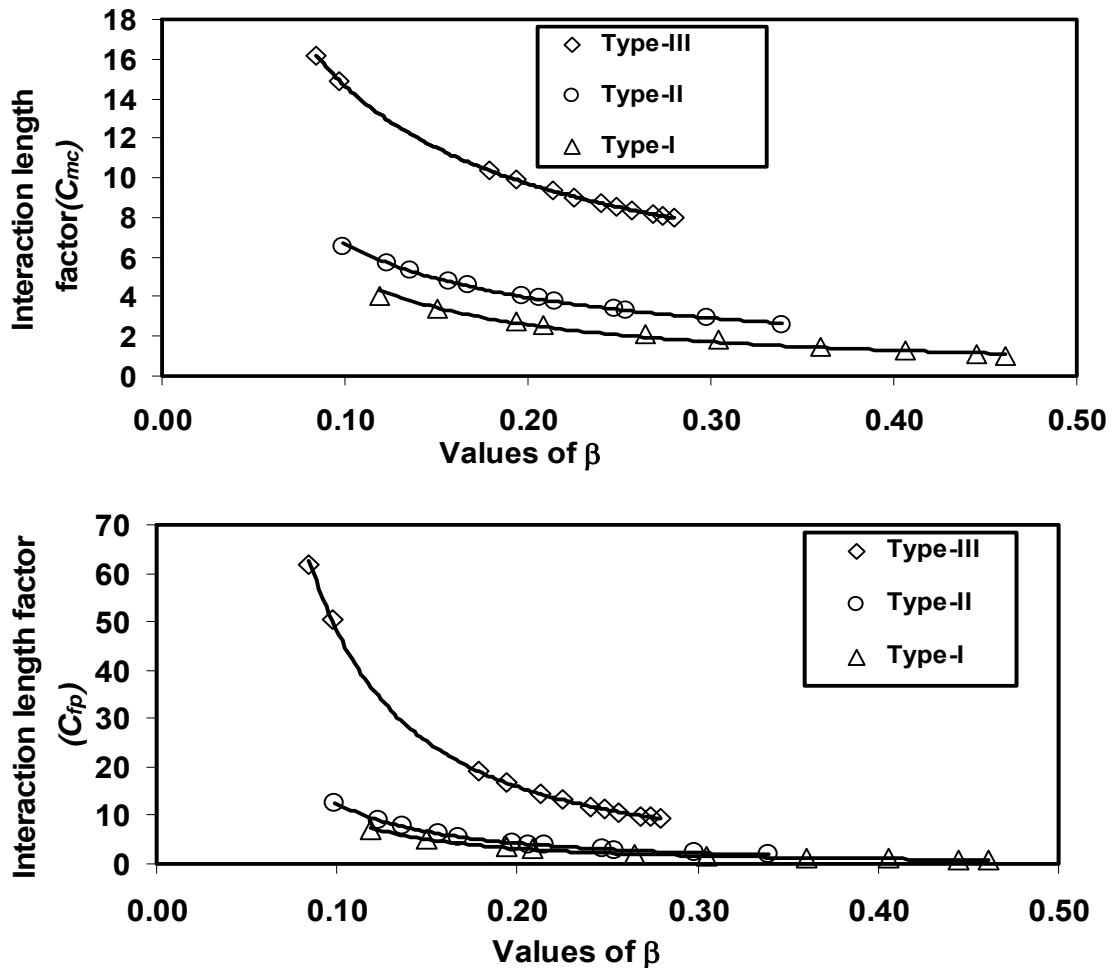
Fig.5.28 (a and b) Variation of interaction length factor C_{mc} for main channel and C_{fp} for floodplain perimeter with relative depth obtained from the proposed modified vertical method

From VDM-III, the length of interface X_{mcv} to be added to the wetted perimeter of the main channel and interface length X_{fpv} subtracted to be from the floodplain perimeter for calculation of discharge using divided channel method are given in terms of factors C_{mc} and C_{fp} in Table 5.8, where $C_{mc} = X_{mcv}/(H-h)$ and $C_{fp} = X_{fpv}/(H-h)$. Variation of the interaction length factors C_{mc} and C_{fp} with relative depth β are shown in Fig. 5.28 (a and b) respectively. From the plots, the best fit power function of the factors C_{mc} and C_{fp} are modeled as

For Type-I channel $C_{mc} = 0.5164\,\beta^{-1.0012}$ and $C_{fp} = 0.2373\,\beta^{-1.6119}$ (5.40a)

For Type-II channel $C_{mc} = 1.1769\,\beta^{-0.754}$ and $C_{fp} = 0.3384\,\beta^{-1.5684}$ (5.40b)

For Type-III channel $C_{mc} = 3.7481\,\beta^{-0.5916}$ and $C_{fp} = 1.224\,\beta^{-1.5936}$ (5.40c)

Table 5.8 Interaction length factor for vertical and horizontal division lines for the experimental channels

Channel Type	Run no.	ß	Vertical interface division (VDM)					Horizontal interface division (HDM)				
			C_x	C_{mc}	C_{fp}	C'_{mc}	C'_{fp}	C_x	C_{mc}	C_{fp}	C'_{mc}	C'_{fp}
Type-I	S12	0.12	0.46	4.02	7.08	----	----	0.03	0.90	1.58	----	----
	S13	0.15	0.36	3.39	5.02	4.15	5.36	0.01	0.33	0.49	0.18	0.45
	S14	0.19	0.19	2.77	3.41	----	----	0.02	-0.19	-0.23	----	----
	S15	0.21	0.24	2.60	3.05	1.88	2.46	0.10	-0.32	-0.37	-0.20	0.00
	S16	0.26	0.08	2.07	2.07	----	----	0.20	-0.68	-0.68	----	----
	S17	0.30	0.03	1.79	1.65	0.44	0.61	0.30	-0.84	-0.77	-0.72	-0.60
	S18	0.36	0.02	1.47	1.24	0.11	0.22	0.40	-0.98	-0.82	-0.99	-0.87
	S19	0.41	0.01	1.26	1.01	0.00	0.01	1.03	-1.03	-0.83	-1.16	-1.10
	S20	0.44	0.01	1.11	0.86	----	----	2.50	-1.05	-0.82	----	----
	S21	0.46	0.01	1.05	0.81	----	----	3.17	-1.05	-0.81	----	----
Type-II	MM16	0.10	6.30	6.53	12.39	----	----	0.37	0.35	0.66	----	----
	MM17	0.12	5.06	5.68	9.04	8.21	7.86	0.42	0.33	0.52	0.65	0.45
	MM18	0.14	4.13	5.31	7.75	----	----	0.38	0.31	0.46	----	----
	MM19	0.16	3.09	4.81	6.25	----	----	0.37	0.28	0.37	----	----
	MM20	0.17	2.76	4.58	5.62	4.30	3.03	0.40	0.27	0.33	0.24	0.21
	MM21	0.20	1.97	4.06	4.36	----	----	0.49	0.21	0.23	----	---
	MM22	0.21	1.83	3.93	4.08	----	----	0.54	0.19	0.20	----	---
	MM23	0.21	1.71	3.81	3.82	2.23	0.83	0.63	0.17	0.17	-0.13	0.74
	MM24	0.25	1.40	3.40	3.04	----	----	1.01	0.10	0.09		
	MM25	0.25	1.41	3.33	2.92	1.30	-0.12	1.15	0.08	0.07	-0.38	1.12
	MM26	0.30	1.27	2.89	2.23	0.69	-0.67	2.53	-0.03	-0.02	-0.62	1.50
	MM27	0.34	1.25	2.57	1.80	0.36	-0.93	5.87	-0.14	-0.10	-0.81	1.81
Type-III	HM16	0.08	17.91	16.15	61.92	44.11	121.2	0.48	0.24	0.91	0.84	3.93
	HM17	0.10	15.28	14.90	50.31	----	----	0.47	0.24	0.80	----	----
	HM18	0.18	9.34	10.38	19.32	19.15	19.97	0.58	0.21	0.38	0.53	2.44
	HM19	0.19	8.45	9.90	16.97	16.83	15.75	0.58	0.20	0.34	0.46	2.31
	HM20	0.21	7.15	9.35	14.48	14.15	12.03	0.56	0.18	0.29	0.36	2.19
	HM21	0.23	7.11	9.04	13.21	----	----	0.59	0.18	0.26	----	----
	HM22	0.24	6.91	8.71	11.90	----	----	0.63	0.17	0.23	----	----
	HM23	0.25	7.26	8.54	11.23	----	----	0.69	0.16	0.21	----	----
	HM24	0.26	6.33	8.38	10.67	----	----	0.62	0.15	0.20	----	----
	HM25	0.27	6.47	8.17	9.91	9.77	4.37	0.68	0.15	0.18	0.14	1.80
	HM26	0.27	6.24	8.07	9.58	----	----	0.67	0.14	0.17	----	----
	HM27	0.28	5.29	7.96	9.21	9.08	4.74	0.59	0.14	0.16	0.10	1.84

VDM - IV

Wormeleaton et.al. (1985) on the basis of their experimental results concluded that though a model may be good in predicting the over all discharge of a compound section, that can badly predict the sub-section discharges. It is seen that though the proposed VDM-III gives a reasonably good estimate of the total discharge of a compound channel, the sub-area discharges of the main channel and floodplain are found to be different from their observed values. To overcome this, further modification to the VDM-III has been carried out. The sub-area discharge of the main channel is made equal to the observed value by adding a suitable length of vertical interface line C'_{mc} (H-h) to the main channel only. Similarly the sub-area discharge of floodplain is made equal to its observed value by subtracting a suitable vertical length of interface C'_{fp} (H-h) from the floodplain, where C'_{mc}, and C'_{fp} are the length factors of interface to be added to main channel and subtracted from floodplain respectively. With this, though the sub-area discharges are made equal to the respective observed values, the length of interfaces added to the main channel perimeter and subtracted from the floodplain perimeter are found to be slightly different from each other (Table 5.8). Plots between β verses (H-h) times C'_{mc}, and β vrs. (H-h) times C'_{fp}, respectively are shown in Fig. 5.29 (a) and Fig. 5.29 (b).
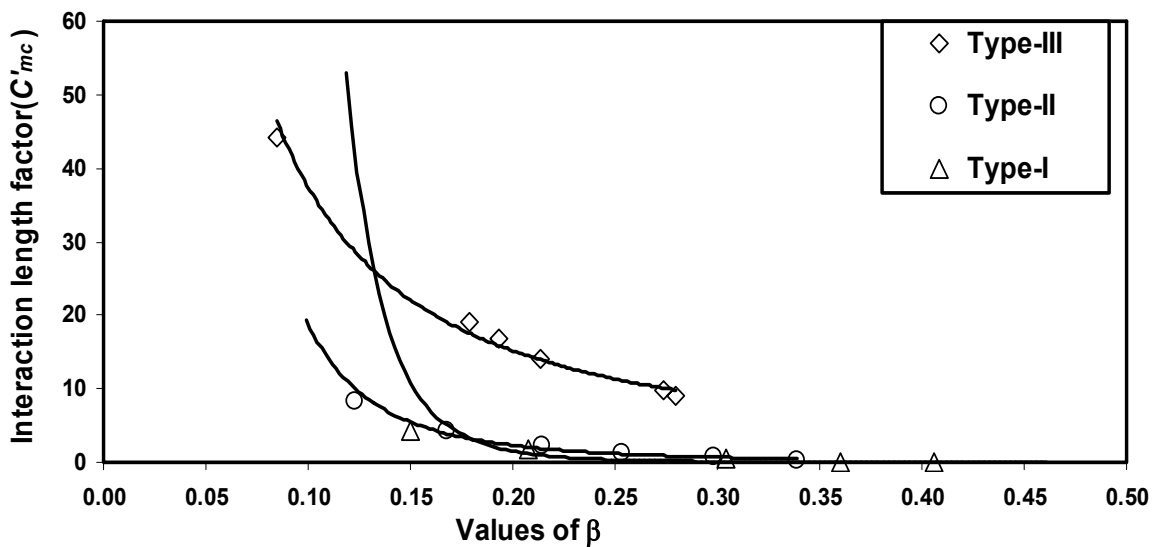
Fig. 5.29(a) Variation of interaction length ratio C'_{mc} for main channel with relative depth to obtain the actual discharge in the main channel sub-section
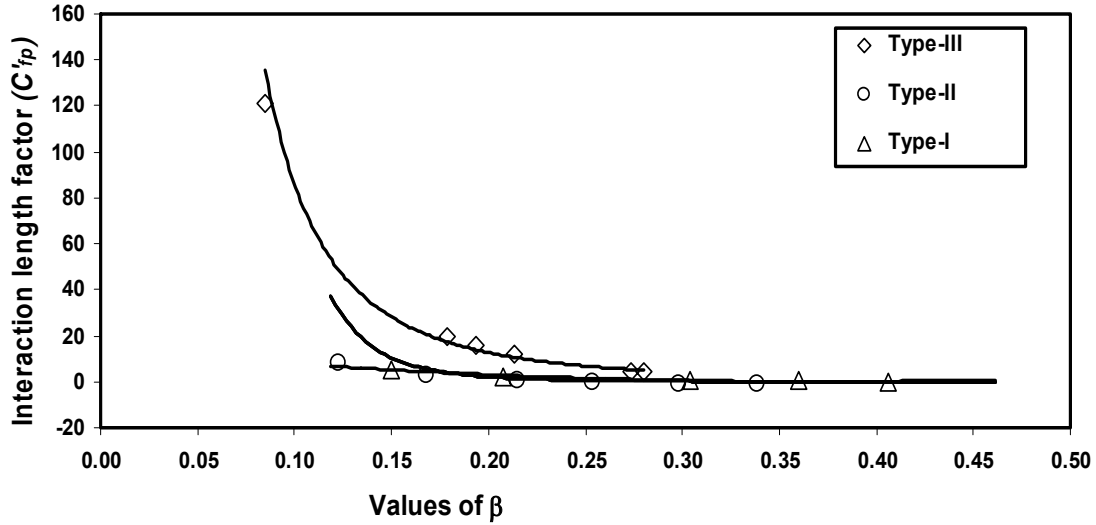
Fig. 5.29(b) Variation of interaction length ratio C'_{fp} for floodplain with relative depth to obtain the actual discharge in the floodplain sub-section

From the plots the best fit power function for the length factors are obtained as

For Type-I channel $C'_{mc} = 0.00003\beta^{-6.8239}$ and $C'_{fp} = 0.0003\beta^{-5.505}$ (5.41a)

For Type-II channel $C'_{mc} = 0.0173\beta^{-3.0334}$ and $C'_{fp} = 0.00003\beta^{-6.8746}$ (5.41b)

For Type-III channel $C'_{mc} = 1.8614\beta^{-1.3037}$ and $C'_{fp} = 0.00003\beta^{-6.6432}$ (5.41c)

This approach gives zero error of discharge. Once the stage- discharge relationship in terms of C'_{mc} and C'_{fp} are evaluated and validated for a compound channel from the available historical records, the modified wetted perimeters of main channel and floodplain sub areas can be evaluated by taking

$P_{mcv} = P_{mc} + C'_{mc} \times (H-h)$ and $P_{fpv} = P_{fp} + C'_{fp} \times (H-h)$ (5.42)

where P_{mcv} and P_{fpv} = the modified main channel and floodplain wetted perimeters respectively using vertical subdivisions. Using Manning's equation for the main channel and floodplain separately, the discharge flowing through each sub area can be evaluated and added up to get the total discharge carried by a compound section.

Horizontal Division Method (HDM)

Toebes and Sooky (1967) carried out laboratory experiments on a two stage composite channel section and showed that a nearly horizontal fluid boundary located at the junction between the main channel and floodplain would be more realistic than a vertical fluid boundary in dividing a compound channel for discharge calculation. Using

a horizontal interface (Fig.5.26), a compound section is divided into two sub-areas. Discharge for the upper and lower main channel sub areas are calculated separately and added to get the total discharge of the compound section. Following the same method of vertical division, using horizontal interfaces discharges are calculated as *HDM-I*, *HDM-II* and *HDM-III* respectively and the results are given in cols. 8,9,and 10 at Table 5.6 for Type-I channel and in cols. 9,10,11 at Table 5.7 for Type-II and Type-III channels respectively. The variation of discharge error with β by excluding the interface length from the wetted perimeter of both main channel and floodplain is shown in Fig. 5.25 as curves H_{ee}. This approach gives better results than the vertical interface method for low depths of flow over floodplain but gives large discharge error at higher depths.

Further, by including the horizontal interface plane to the main channel and excluding from floodplain, the discharge for each sub-area are calculated again and added to get the section discharge of the compound channel. Following this approach, the percentages of error between the calculated and observed discharges are plotted as curve H_{ie} in Fig. 5.25. The results show that the method under-estimates for all types of channel where as H_{ee} over estimates the discharge values.

The method is again not found to be suitable for all depths of flow over flood plain. Like the VDM-IV, a modified horizontal interface plain method is tried. Discharges in each sub-area are calculated using the modified interface lengths for main channel and flood plains respectively and added to get the total section discharge. The error percentages of discharge are plotted as curve M_h^* in Fig.5.25. The nature of the curve M_h^* can be seen as similar to that of M_v^* and also gives less errors. The standard error of estimate between observed and calculated percentages of discharge for all the over-bank flow depths investigated are found to be 1.9, 6.2, and 3.9 respectively for Type-I, Type-II, and Type-III channels respectively. As a parallel analysis to vertical interface plane, the interaction lengths for a horizontal sub-division are also evaluated and given in Table 5.8.

5.9.2.2 METHODS BASED ON ZERO APPARENT SHEAR AT THE INTERFACE PLANES (ZASIM)

In this approach it is required to specify the division lines between sub-areas of a compound channel along which zero shear stress can be assumed. However, due to the

3-D nature of velocity field in the channels, it is almost impossible to generalize the position of these division lines for all types of channel shapes, flow depths, and roughness configuration. Moreover, it is known from the three dimensional turbulence considerations that orthogonal lines to the isovels do not necessarily imply lines of zero shear stress. Methods under this approach are discussed below.

ZASIM - I: The Diagonal Division Method (DDM)

Yen and Overtone (1973) observed that the line of zero shear stress between the main channel and flood plains can take the shape along a line commencing from the bank at intersection and inclined towards the center of main channel surface. These lines are referred as diagonal interface. Wormeleaton et.al. (1982) attempted to measure the apparent shear stress along this interface and found it to be negligible and ASSR (Apparent Shear Stress Ratio= ratio between apparent shear to the average boundary shear) = 0.4. Experimental results demonstrate that the shear stress along a diagonal division line is negligible except for small depths of flow over floodplain (Wormleaton et. al. 1982; Knight and Hamed 1984) that are commonly experienced when a river just goes over bank. Therefore, it is assumed here that there is zero-shear along the diagonal lines that originates from the main channel-flood plain junction and is inclined towards center of the main channel water surface, separating the main channel from its floodplains. The total discharge is than obtained by summing up the discharges obtained for each of the three individual sub-zones (Fig.5.26). Using the diagonal interface, discharge of compound channel is calculated and is given at col. 11 of Table 5.6 for Type-I channel and col.12 of Table 5.7 for Type-II and Type-III channels. The error between the observed and calculated discharges is shown as curves D_{ee} in Fig. 5.25. This is a better approach when compared to other divided channel methods as it gives less error between observed and computed discharge of the compound channels. Since, the shear along a diagonal interface is assumed to be negligible, the length of interface is not included to the main channel or to the floodplain perimeters while calculating discharge of the respective sub areas. It is seen from Figs. 5.15(a, b and c) that though the apparent shear is less along the diagonal line for straight compound channel of Type-I, it is not so for meandering compound channels of Type-II and Type-III.

Therefore, this method is found to give erroneous results for meandering compound channels for all depths of flow over floodplain.

ZASIM - II: The Area Method

For straight compound channels Stephenson and Kolovopoulos (1990) developed a method by extending the DCM. They assumed a zero shear stress line along a curved interface planes marked as a_1-a_o in Fig.5.30. Let A_{mc} and A_{fp} are the modified area of main channel and floodplain respectively after separation by the curved interface plain of zero shear. If A_{mv} the area of main channel and A_{fv} the area of floodplain subsection when a vertical interface separates the main channel from floodplain than we can write

$$A_{mc} = A_{mv} - (\Delta A) \text{ and } A_{fp} = A_{fv} + (\Delta A) \tag{5.43}$$

where ΔA = the additional area that is required to be added to the floodplain area and subtracted from the main channel area to get the modified area of the floodplain and main channel respectively in equation (5.43).
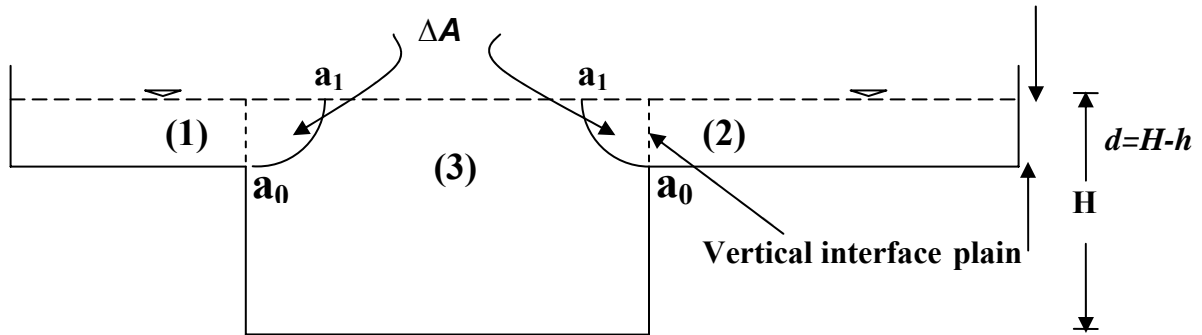
Fig. 5.30 The area method of separation of a compound channel

Assuming the channel to be regular, prismatic, and flow under uniform conditions the boundary shear forces acting on the wetted perimeter of floodplain minus the apparent shear force on the assumed vertical interface must be equal to the weight component of water of the floodplain. For equilibrium condition this is written as

$$P_{fp}\, \tau_{fp} = \rho g A_{fv}\, S + \tau_v d \tag{5.44}$$

where $P_{fp}\, \tau_{fp}$ = the shear force on wetted perimeter of floodplain per unit stream wise length, τ_v = the apparent shear stress on vertical interface, d = the depth of flow over floodplain = $(H-h)$, S = the longitudinal slope of the channel, P_{fp} = the wetted perimeter

of the floodplain, τ_{fp} = the mean boundary shear stress in floodplain, A_{fv} = the area of floodplain for vertical subdivision, and g = the acceleration due to gravity. If at the curved interface plane a zero shear is assumed then

$$P_{fp}\tau_{fp} = \rho g(A_{fv} + \Delta A)S \tag{5.45}$$

By combining equation (5.44) and (5.45) we have

$$\Delta A = \frac{\tau_v}{\rho g S}d = \frac{\tau_v}{\rho g S d}d^2 = \tau_r d^2 \tag{5.46}$$

where τ_r = the relative apparent shear stress and is given by Prinos-Townsend empirical formula (1984) as

$$\tau_r = \frac{1}{11.213\ dS}(\Delta V)^{0.92}(\beta)^{-1.129}(\alpha)^{-0.514} \tag{5.47}$$

where α and β = the width and depth ratios respectively, and ΔV = the difference of mean velocity between main channel and floodplain. It should be noted that equation (5.47) has been verified for the symmetrical straight compound channel data of Wormealeaton et.al. (1982) and Knight and Demetriou (1983). This method is generally found to be not applicable to the data of other investigators. Using this method, the discharges for Type-I channel are calculated and given in col. 13 of Table 5.6. The percentage of error between the observed and calculated discharges is shown as curve AM in Fig. 5.25(a).

ZASIM - III: Proposed Area Method

Assuming the compound channel to be regular, prismatic, and flow under uniform conditions, the total boundary shear must be equal to the weight component of flowing fluid along longitudinal direction and is written as

$$(P_{mc}\tau_{mc} + P_{fp}\tau_{fp}) = \rho g A S \tag{5.48}$$

where P_{mc} = the wetted perimeter of the main channel and τ_{mc} = the mean boundary shear stress in main channel. By dividing total weight of compound channel $\rho g A S$ to both sides of equation (5.48) and by denoting the percentage of shear force carried by the floodplains as ($\%S_{fp}$) and the percentage of shear force carried by the main channel as ($\%S_{mc}$) we have

$$\%S_{fp} = 100 \times \frac{P_{fp}\tau_{fp}}{\rho g A S}, \quad \%S_{mc} = 100 \times \frac{P_{mc}\tau_{mc}}{\rho g A S} \quad \text{and} \quad \%S_{fp} + \%S_{mc} = 100\% \tag{5.49}$$

The curved interface plain of zero shears in Fig.5.30 divides the compound channel into two sub-sections where the modified area of main channel becomes $A_{mv} - \Delta A$ and the modified area of flood plain is $A_{fv} + \Delta A$. The boundary shear forces due to the modified main channel perimeter must be equal to the weight component of water of the main channel and is written as

$$\rho g (A_{mv} - \Delta A) S = P_{mc}\tau_{mc} \tag{5.50}$$

Dividing total weight of compound channel $\rho g A S$ to both sides of equation (5.50) and taking the percentages it becomes $100\frac{(A_{mv} - \Delta A)}{A} = \%S_{mc} = 100 - \%S_{fp}$ (5.51)

For a rectangular main channel, $100\frac{A_{mv}}{A} = \frac{100}{\{(\alpha - 1)\beta + 1\}}$ by substituting in equation 5.51 and further simplifying, the additional area, ΔA is obtained as

$$\Delta A = \left[\frac{\%S_f}{100} - \frac{(\alpha - 1)\beta}{1 + (\alpha - 1)\beta} \right] A \tag{5.52}$$

Having computed $\%S_{fp}$ from equation (5.11) and knowing the channel geometry parameters, the area ΔA can easily be calculated from (5.52). Next, the discharge for main channel plus floodplain are calculated using Manning's equation as

$$Q = \frac{\sqrt{S_f}}{n} \left[A_{mc}^{5/3} \left(P_{mc} \right)^{-2/3} + A_{fp}^{5/3} (P_{fp})^{-2/3} \right] \tag{5.53}$$

Using the proposed modified area method of zero shear, discharge for the compound section is calculated and given in col.14 of Table.5.6 and in col.13 of Table.5.7. The error percentages of discharge are plotted as curve M_a^* in Fig.5.25. This method is also found to give less error between calculated and observed discharges. The standard error of estimate between observed and calculated discharge are found to be 1.5, 6.3, and 5.1 respectively for Type-I, Type-II, and Type-III channels respectively by considering all the flow depths.

ZASIM - IV: The Variable Interface Method

Patra and Kar (2000) extended DCM and proposed a variable inclined interface plane of zero shear to separate meandering section from the floodplains of a compound channel.

Patra, Kar, and Bhattacharya (2004) further modeled the depth averaged subsection velocity, discharge, and point velocity involving the process of locating the interface of zero shear in the compound channels. They tried to locate the interface planes of zero shear in the fluid from the isovel plots and found that the angle of inclination of this plane to the vertical line drawn from main channel - floodplain junction decreases with depth over the floodplain. The equation of the angle θ to locate the plane with reference to the vertical line (Fig. 5.14) is given as

$$\theta = (\alpha - R_o \beta)\,(1 - \beta)^{\beta}\,(5.25\,\beta)^{0.075}\,\mathrm{e}^{-\beta(\alpha - R_o)} \tag{5.54}$$

where α = the width ratio B/b, β = the relative depth $=[(H-h)/H]$, and R_o = the ratio of the amplitude ε of the meandering channel to its top width B. The apparent shear force percentage of this plane is obtained from the relation given as

$$\%\,ASF_{VI} = \frac{100\,A_{mc}}{bH\,[(\alpha - 1)\beta + 1]} - \{100 - \%\,S_{fp}\} \tag{5.55}$$

where $\%ASF_{VI}$ = the apparent shear force on the variable inclined interface as percentage of total, $\%S_{fp}$ = the shear force in floodplain boundary that can be calculated from equation (5.11), A_{mc} = the area of main channel separated by the variable inclined plain. Using the method, the discharge for the experimental channels are calculated and given in col.12 of Table.5.6 for Type-I channel and in col.17 of Table.5.7 for Type-II and Type-III channels. The percentage of error between calculated and observed value of the discharge is shown as curve VI in Fig.5.25.

5.9.3 APPLICATION OF OTHER APPROACHES TO THE PRESENT CHANNELS

Meandering and the flow interaction between main channel and its adjoining floodplains are those natural processes that have not been fully understood. Prediction of discharge is therefore difficult for over bank flows. Some published approaches of discharge estimation for meandering over-bank flow are discussed and applied to the experimental data of the present very wide and highly sinuous channels to know their suitability for such geometry.

Ervine and Ellis method

The method proposed by Ervine and Ellis (1987) is based on finding the energy loss coefficients of different sub-sections of a meandering compound channel. A compound section may be divided into three distinct subsections or zones as shown in Fig.5.31. Discharge for each zone is calculated separately and added to get the total sectional discharge. The different zones are (1) The main channel below bank full depth (lower main channel), (2) Floodplain within meander belt, and (3) Floodplain outside the meander belt. In this approach the turbulent shear at the horizontal interfaces are ignored. The energy loss coefficients are obtained empirically for each zone that are related to zonal velocities and the sub-section discharges are computed. The steps followed are described as follows:

Plan   **Sectional elevation**
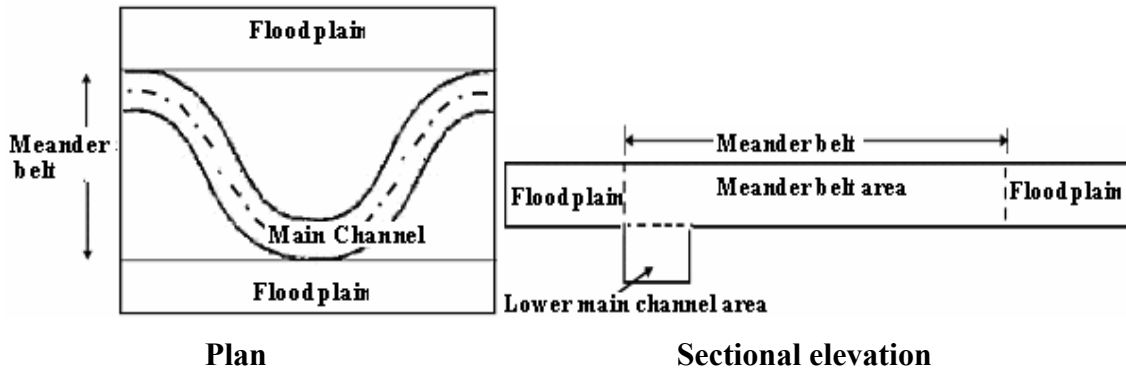
Fig. 5.31(a) Plan and sectional elevation of the three zones considered at bend apex of a meandering compound channel by Ervine and Ellis (1987)

(1) The lower main channel zone is obtained when a horizontal interface line is drawn at the bank full level in Fig.5.31 (a). For this zone the energy equations are written

in the following forms

$$k_{bf}\frac{V_a^2}{2g} + k_{sf}\frac{V_a^2}{2g} = \frac{S_o}{S}$$

(5.56)

where V_a = the sectional mean velocity of this zone, S_o = the valley slope and S_r = the sinuosity, k_{bf} and k_{sf} = the dimensionless energy coefficients in (m^{-1}) due to boundary friction and secondary flow respectively and are represented

as $k_{bf} = \dfrac{f}{4R}$ and, $k_{sf} = \left(\dfrac{2.07f + 2.86\sqrt{f}}{0.565 + \sqrt{f}}\right)\left(\dfrac{h}{r_c}\right)^2\left(\dfrac{1}{h}\right)$, f = the friction factor obtained

from Darcy-Weisbach equation for whole cross section using (5.3) and r_c = the bend radius, and h = the bank full depth.

(2) For the second zone (upper layer with in meander belt) , the energy equation is given as

$$k_{bf}\frac{V_b^2}{2g} + k_{ex}\frac{V_b^2}{2g} + k_{co}\frac{V_b^2}{2g} = S_o B_w L_w \tag{5.57}$$

where V_b = the sectional mean velocity of this zone, B_w = width of the meander belt, L_w = one wave length of the meander channel, k_{bf}, k_{ex} and k_{co} = the dimensionless energy coefficients in (m^{-1}) due to boundary friction, expansion, and contraction respectively represented as $k_{bf} = \frac{f}{4(H-h)}(1 - S_r\frac{b'}{B_w})$, $k_{ex} = (1-\beta)^2\frac{S_r(\sin\theta')^2}{B_w}$, and

$k_{co} = K_c\frac{S_r(\sin\theta')^2}{B_w}$ where b' = the top width of main channel at bank full level, θ = the mean angle of incidence averaged over the meander wave length calculated from numerical integration(θ = 21.9^0, 38.9^0 and 45^0 for 30°, 60° and 90° bends respectively). K_c = given by a third order polynomial fit obtained from the Yen and Yen (1983) data, H and h = the total depth and the bank full depth of the channel.

(3) For the third zone (upper layer out side the meander belt) the boundary friction only is considered and is given as

$$k_{bf}\frac{V_c^2}{2g} = \frac{f}{4R}\frac{V_c^2}{2g} = S_o \tag{5.58}$$

where V_c = the sectional mean velocity of this zone. Knowing the sectional mean velocities of the three zones from equations (5.56, 5.57, and 5.58) discharges in each zones are calculated by multiplying them with sectional area of each zone respectively and added up to obtain the total channel discharge. However, the method follows many complex steps and is difficult for practical use by field engineers. Due to neglect of the turbulent interfacial shear, many investigators like Mc Keogh and Kiely (1989), Kiely (1990), and James and Wark (1992) have observed that this method over-predicts discharge at low over bank depth and under-predict at high over bank depths. Therefore, this method is generally not acceptable to solve the river problems. Using this method to the present Type-II and Type-III meandering experimental channels, the error in

discharge estimation is found to be large and the error curve E_m is shown in Fig 5.25 (b and c) respectively.

Shiono et.al. (1999) tested this method for their three types of experimental meandering compound channels with sinuosity 1.093, 1.37, and 1.571 respectively. The discharge errors in the lower main channel for the meandering compound channel with sinuosity 1.571 and 1.37 were found to be very large. The error percentages were 54% and 48.5% respectively for the relative depth of $\beta = 0.15$. They introduced an additional term for the turbulent energy loss to equation (5.56) for the lower main channel and a second term to equation (5.57) for turbulent shear in the upper layer. Shiono et.al. (1999) also found that by using the coefficients of Chang (1983) as used by Ervine and Ellis (1987) the value of the energy loss coefficients due to expansion (K_{ex}) and contraction (K_{co}) in equation (5.57) were found to be much different. Although the calculated discharges in upper layer (meander belt) agreed well with the measured value, the lower main channel discharge was found to be over-estimated for low over bank depth ($\beta = 0.15$) and under-estimated for high over bank flow depth ($\beta = 0.5$). They improved the magnitude of coefficients further but the error percentage was still found to be around 20%. This improved method of Ervine and Ellis (1987) were applied to the data of Shiono et, al. (1999) only. The improved method is still very difficult to apply to solve the river problems.

James and Wark Method

This empirical method developed by James and Wark (1992) is based on dividing a compound meandering channel section into either three or four zones. When the meandering compound channel is symmetrical with respect to the centerline of the main channel, three zones (Fig.5.31 a) are considered, while for non-symmetrical channels the compound section is split into four zones as shown in Fig.5.31 (b). The discharge for each zone is calculated separately and added to get the total sectional discharge.
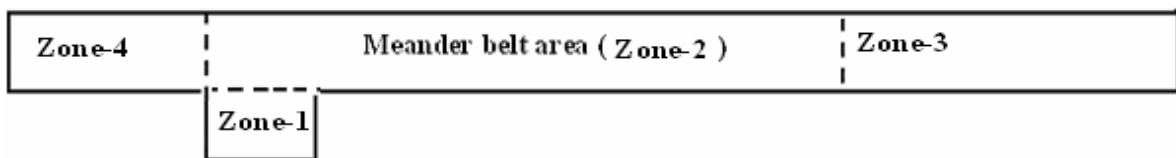
Fig. 5.31 (b)   The four zones considered by James and Wark

The developed empirical equations for calculating discharge by accounting different loss parameters in a meandering compound channels for each sub-area are as follows:

Zone 1: The discharge for this lower main channel zone in Fig.5.31 (b) is calculated by the relation given as
$$Q_1 = Q_{bf} C_1 \qquad (5.59a)$$
where Q_{bf} = the bank full discharge calculated using in bank method and then adjusted to account for the effect of over-bank secondary currents by an correction factor which is greater of the two
$$C_1 = 1.0 - 1.69y' \quad \text{or} \quad C_1 = m\,y' - K\,c \qquad (5.59b)$$
The empirical coefficients m, K, and c are based on geometry, sinuosity, and friction factor respectively and are represented as

m (Geometry factor) $\quad = \dfrac{0.0147 b'^2}{A_{lmc}} + 0.032 f' + 0.169,$

K (Friction factor) $= 1.14 - 0.136 f'$ and

c (Sinuosity factor) $= \dfrac{0.0132 b'^2}{A_{lmc}} - 0.302\,S_r + 0.851$, where b' = top width of main

channel, A_{lmc} = area of lower main channel (Zone-1), S_r = sinuosity of the channel, y' = dimensionless flow depth of floodplain = $[(H-h)/(A/B)]$, H = total depth of flow, h = the depth of lower main channel, and A = total cross sectional area.

Zone 2: The meander-belt area is marked as zone-2 in Fig.5.31 (b). An empirical adjustment factor is derived for expansion and contraction losses for this flow zone basing on the data of FCF and river Aberdeen. Discharge for zone-2 is given as
$$Q_2 = A_2\,V_2 \qquad (5.60)$$
The flow velocity (V_2) with interaction effect is given as
$$V_2 = \left[\frac{2gS_0 L}{\{f_2 L/(4R_2)\} + F_1 F_2 K_e} \right]^{1/2} \qquad (5.61)$$
where L = meander wave length factor for non friction loss due to main channel geometry $F_1 = \dfrac{0.1 b'^2}{A_{lmc}}$ for $\dfrac{b'^2}{A_{lmc}} < 10$ and $F_1 = 1$ for $\dfrac{b'^2}{A_{lmc}} \geq 10$

Factor for non friction loss due to main channel sinuosity $F_2 = \dfrac{S_r}{1.4}$

Factor for expansion and contraction loss in zone-2 is $K_e = C_{sl} C_{wd} \left[C_{sse}(1 - \beta^2) + C_{ssc} K_c \right]$

where length coefficient for expansion and contraction losses $C_{sl} = \dfrac{2(W_2 - b')}{W_2}$, W_2 =

the width of zone-2.

C_{wd} = Shape coefficient for expansion and contraction losses = $\dfrac{0.02b'^2}{A_{lmc}} + 0.69$, C_{sse} =

Side slope coefficient for expansion loss = $1.0 - S_s/5.7$ (but C_{sse} is not less than 0.1), C_{ssc}
= Side slope coefficient for contraction loss = $1.0 - S_s/2.5$ (but C_{ssc} is not less than 0.1)
S_s = the cotangent of main channel side slope, K_c = the contraction factor ranging
between 0 to 0.5 for the value of depth ratio $\beta = [(H-h)/H]$ varying between 0 to 1.0.

Zone 3 or zone 4 : For the outer two floodplain zones in Fig.5.31(b) which is solely
controlled by bed friction only, the Darcy-Weisbach resistance formula (5.3) is used
separately to the Zone 3 and zone 4 to get the respective discharge Q_3 and Q_4
respectively. Now, the total discharge Q is calculated by adding the zone discharges of
the sub-areas given as

$$Q = Q_1 + Q_2 + Q_3 + Q_4 \qquad\qquad (5.62)$$

Using the procedures outlined by James and Wark (1992), the discharge for the
present experimental meandering compound channel for Type-II and Type-III are
calculated and given in Table 5.7. The percentage of error between observed and
calculated discharges is shown as curve J_m in Fig.5.25 (b and c) for Type-II and Type-
III channels.

The Coherence Method (COHM)

The coherence method (*COHM*) is developed by Ackers (1992 and 1993 a and b).
Coherence (*COH*) is defined as the ratio of the basic conveyance calculated by treating
the channel as a single unit with perimeter weighting of the friction factor to that
calculated by summing the basic conveyances of the separate zones, and is given as

$$COH = \frac{\sum_{i=1}^{i=n} A_i \sqrt{\sum_{i=1}^{i=n} A_i \Big/ \sum_{i=1}^{i=n} (f_i P_i)}}{\sum_{i=1}^{i=n} \left[A_i \sqrt{A_i / (f_i P_i)} \right]} \qquad\qquad (5.63)$$

where i identifies each of the n flow zones (for example $n = 3$ in Fig.5.26 using a vertical division), A_i = the sub-area, P_i = the wetted perimeter of each sub-area, and f = the Darcy-Weisbach friction factor. COH is further simplified to

$$COH = \frac{\left(1 + A_*\right)\sqrt{\left(1 + A_*\right)/\left(1 + P_* f_*\right)}}{1 + A_* \sqrt{A_* /\left(P_* f_*\right)}}$$
(5.64)

where $A_* = N_f A_{fp}/A_{mc}$; $P_* = N_f P_{fp}/P_{cmc}$; $f_* = N_f f_{fp}/f_{mc}$, N_f is the number of floodplains, A_{fp} and A_{mc} = the area of cross section of floodplain and main channel respectively, P_{fp} and P_{mc} = the wetted perimeter of floodplain and main channel respectively. For a compound channel with smooth boundary, the floodplain friction factor term f_{fp} and main channel friction factor term f_{mc} are unity and therefore $f_* = 1$.

The value of COH is always less than unity. The closer to unity the coherence approaches, the more appropriate it is to treat the channel as a single unit, that is, the flow interaction is considered to be negligible. When the coherence is less than unity, estimation of a discharge adjustment factor (DISADF) is required in order to correct the individual discharges in each sub-area. Generally vertical division lines are used to separate a compound channel into zones (sub-areas). These division lines are not used as the wetted perimeters for any of the sub-areas. Each sub-area discharges are calculated from the conventional equations (5.1, 5.2 or 5.3) and added to obtain the 'basic' discharge (Q_{basic}), which is then adjusted to account for the effects of interaction between the main channel and the floodplain flows. DISADF is calculated as

$$DISADF = \frac{Actual \ conveyance}{sum \ of \ the \ conveyance \ calculated \ by \ using \ divided \ channel \ method}$$
(5.65)

The experimental evidence shows that

$$\left(COH = \frac{Q_{single}}{\sum Q_{zones}}\right) < \left(DISADF = \frac{Q_{actual}}{\sum Q_{zones}}\right) < 1.0$$
(5.66)

This implies that, for a given stage in a compound channel the actual discharge is usually somewhere between these two values.

$$Q_{single} \leq Q_{actual} \leq Q_{basic}$$
(5.67)

Coherence for a compound channel is a function of geometry only. This approach is useful for establishing stage-discharge relationships for over bank flows. From an established relationship between DISADF and COH, the DISADF can easily be known from the calculated COH values. For a compound channel, a validated

relationship between *DISADF* and *COH* can be effectively used as stage-discharge curve. Although the coherence method is developed from the laboratory data from the Flood Channel Facility, it has been applied successfully to a number of natural rivers. The *COH* method is more difficult to apply when the roughness of the main river bed varies with discharge, as is the case in sand bed rivers. From the present experimental data, the *DISADF* and *COH* for the three types of channels are calculated and plotted in Fig.5.32. From the plot, the best fit linear relationships are obtained as

For Type-I channel $\quad\quad DISADF = 0.6431(COH) +0.3611$ (5.68a)

For Type-II channel $\quad\quad DISADF = 0.7347(COH) +0.2883$ (5.68b)

For Type-III channel $\quad\quad DISADF=0.3068(COH) +0.6667$ (5.68c)
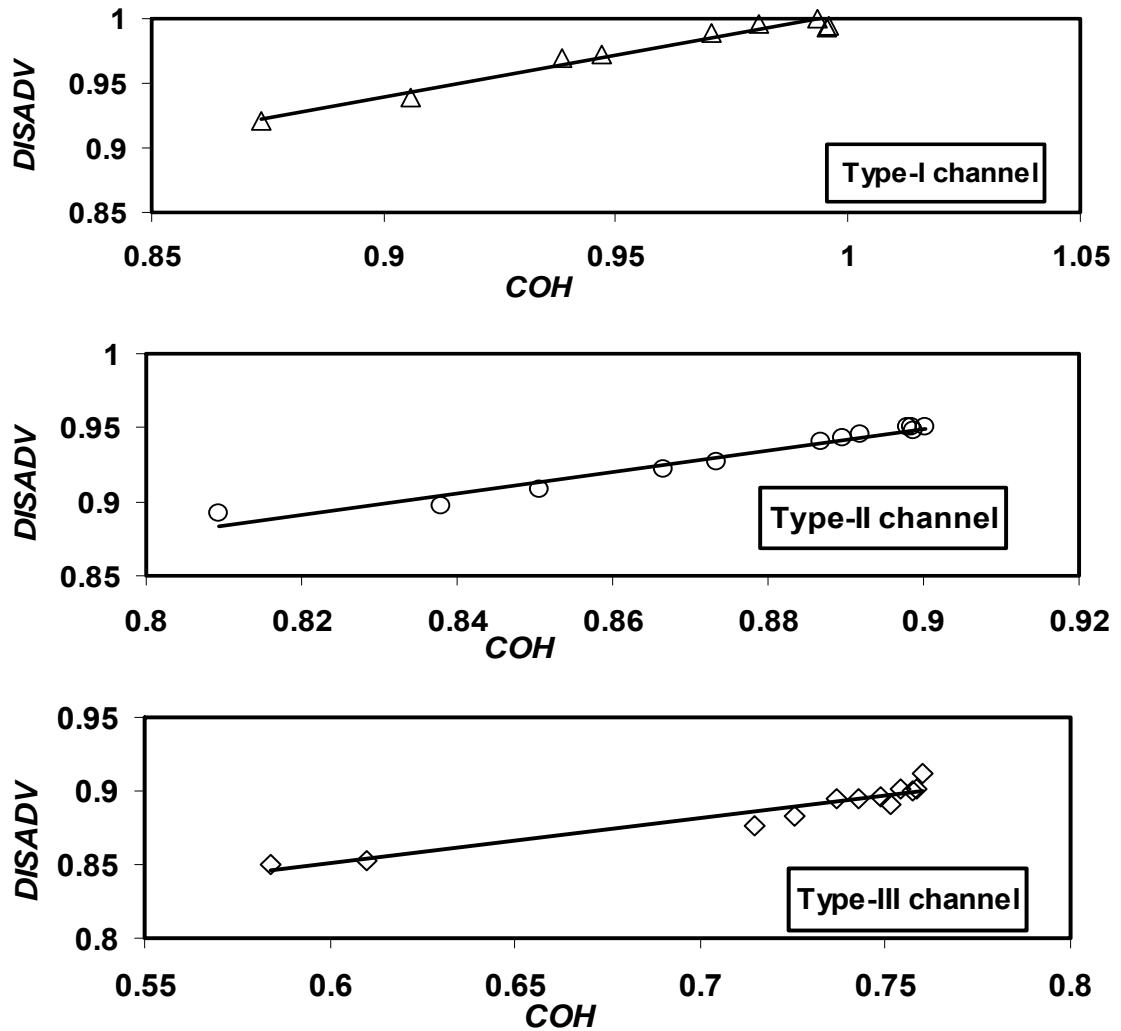
Fig.5.32 Discharge adjustment factor (DISADF) and coherence (COH) relationships for the experimental channels

Greenhill and Sellin Method

Using the FCF meandering channel data, Greenhill and Sellin (1993) extended the divided channel method (DCM) for discharge estimation by considering five alternative methods. The methods they proposed are (1) by considering the full channel as a single section where errors up to 30% are recorded; (2) by considering a horizontal subdivision line at the bank full stage, thus separating the section into two zones, the upper and the lower subsections, the discharge errors range between 8-20%; and (3) by dividing the compound section into three zones as shown in Fig.5.31(a), viz. (a) main channel within bank, (b) the floodplain within meandering belt, and (c) the floodplain outside the meandering belt. By further improving the method (3) in the form of changing the flood plain longitudinal slope to main channel slope for the central zone, and again by inclining the subdivision lines from vertical to 45°, two more methods of discharge are proposed as methods (4) and (5) respectively. With all these improvements discharge errors up to $\pm$ 3.5% still persisted for the FCF data. The method developed is generally known as meander belt method. One of the major disadvantages of this approach for its application to the natural river sections is the difficult to define the parameter such as meander belt width and the in-bank depth. Following the method, the present compound meandering channels are divided in to zones and the section discharges for Type-II and Type-III are calculated. The percentage of error between observed and calculated discharge is shown as curve M_b in Fig.5.25 (b and c).

5.9.4   SELECTION OF MANNING'S *n* FOR DISCHARGE ESTIMATION

Sellin et. al. Pang (1998), Willetts and Hardwick (1993), and Patra & Kar (2000) reported that the assumption of an average value of flow resistance coefficient in terms of Manning's *n* for all depths of flow may result in significant errors in discharge estimation. Keeping in view their reports the present experimental observations are also directed to study the variation of Manning's *n* with the flow depth ranging from in-bank to over-bank flows for the three different types of compound channels having smooth boundaries.

The experimental channel surfaces are made using perspex sheets representing smooth surface. For the straight simple channel (Type-I), the average value of Manning's n is found to be 0.01096. Since the same materials is used for making surfaces of all the three types of experimental channels, the value of $n = 0.01096$ is taken constant for the present channels. However, it is further seen that in simple meandering channels of Type-II and Type-III, the values of n when plotted against the flow depth shows a very significant variation. It continues to increase from 0.01098 at the in-bank depth of 12.9 mm to reach a value of 0.0123 at a depth of 110.1 mm for Type-II channel. Similarly for Type-III channel, the value of n increases from 0.011 at 10.5 mm depth to a value 0.0122 at in-bank depth of 73.3 mm. Increase of Manning's n for in-bank flow is found to be higher for Type-III channel than Type-II channel may be due to its higher sinuosity and trapezoidal geometry. In both meandering channels it is seen that the value of Manning's n reaches a maximum value at just below the bank full depth (Fig.5.3). In the over bank depth, the variation of n with flow depth is less when compared with the in-bank stages., Even though a sudden fall in the composite value of Manning's n is noticed for both the meandering channels at the beginning of over-bank stage, the values of n again increases at a slower rate. It is expected to attain a constant value at still higher over bank depth, close to the bank full value of n. This finding is similar to the earlier reports of Sellin (1993), Willet and Hard wick (1993), Bhattacharya,(1995), and Patra and Kar (2004). Therefore, for the present investigation, the bank full value of Manning's n is used for individual channels rather than that of the straight channel in discharge assessment.

In the present flow analysis for Type-II and Type-III meandering compound channels, the value of Manning's n is tested for two cases (i) Manning's $n = 0.01096$ obtained from straight channel of Type-I (with same materials used for the surfaces), and (ii) Manning's n obtained at the bank full level of each meandering compound channels separately, i.e. $n = 0.01234$ for Type-II channel and $n = 0.01225$ for Type-III channels. For the three proposed methods, (a) Modified Vertical Interface Method, (b) Modified Horizontal Interface Method, and (c) New Area Method, Type-II and Type-III meandering compound channels are tested for case (i) Manning's n and the discharge error curves are shown as M_v, M_h, M_a respectively in Fig.5.25 (b and c). Similarly the

proposed discharge methods are again tested to both the channels by using the value of Manning's n obtained from case (ii) which are shown curves as M_v*, M_h*, M_a* respectively in Fig.5.25 (b and c). By using the Manning's n for the case (ii) above value of Manning's n gives the least discharge error when compared to discharge error computed using the value of Manning's n of case (i). This is so because of incorporation of meandering effect of the full channel in the evaluation of Manning's n.

5.10 APPLICATION OF THE METHODS TO OTHER TEST CHANNELS

Since the proposed one dimensional discharge estimation models for compound channels are found to be quite adequate for the present wide and large sinuous experimental channels, analysis is further made to apply the three proposed methods (Modified Vertical Interface Method, Modified Horizontal Interface Method, and the New Area Method) for discharge prediction in straight and meandering compound channel using the reported data of other investigators.

5.10.1 STRAIGHT TEST CHANNELS OF KNIGHT AND DEMETRIOU

The proposed methods of discharge estimation are applied to the three types ($\alpha = 2, 3$ and 4) of straight compound channel data of Knight and Demetriou (1983). The compound channels are symmetrical about the centerline of main channel having longitudinal bed slope of 0.00096. The main channel was rectangular in shape of 152 mm wide and 76 mm deep. The width of flood plain was taken as 304 mm, 456 mm, and 608 mm respectively for the three types of channels to give rise to (α) = 2, 3 and 4 respectively. All the surfaces were smooth having Manning's n = 0.01, that was observed at their simple straight channel made of Perspex sheets. The Modified Vertical Interface Method, Modified Horizontal Interface Method, and the New Area Method are applied to the three experimental compound channels data reported by Knight and Demetriou (1983). The errors of discharge using the three proposed methods for the three types of channels are obtained and are plotted as curves M_v, M_h and M_a in Fig.5.33. The standard error of estimate between the observed and calculated

percentages of discharge for the three proposed methods is found to be 3.1, 3.9 and 3.6 respectively.

Fig.5.33 (a, b, and c) Variation of percentage of error between calculated and observed discharges by the proposed methods with relative depths applied to the three straight compound channel data of Knight and Demetriou

5.10.2 DEEP CHANNELS DATA OF PATRA AND KAR

The proposed methods of discharge calculations are applied to the deep meandering channel data reported by Patra and Kar (2000) for their two test series (A and I). The

channels have sinuosity of 1.22 and 1.03 and width ratio of $\alpha = 3.14$ and $\alpha = 5.25$ respectively. The meandering channel is rectangular with smooth boundaries. The main channel of series-A is 100 mm wide and 100 mm deep with unequal flood plains having top width of 525 mm. The width of main channel for series-I is 440 mm and depth of 250 mm having equal flood plains on both sides. Total top width of series-I is 1380 mm. For both series of channels, the proposed methods are applied. The errors of discharge between calculated and observed values are shown as curves M_v^*, M_h^*, and M_a^* for the methods of Modified Vertical Interface Method, Modified Horizontal Interface Method and the New Area Method respectively in Fig.5.34. The standard error of estimate between observed and calculated percentages of discharge for the three proposed three methods are found to be 7.4, 6.4 and 6.8 respectively.
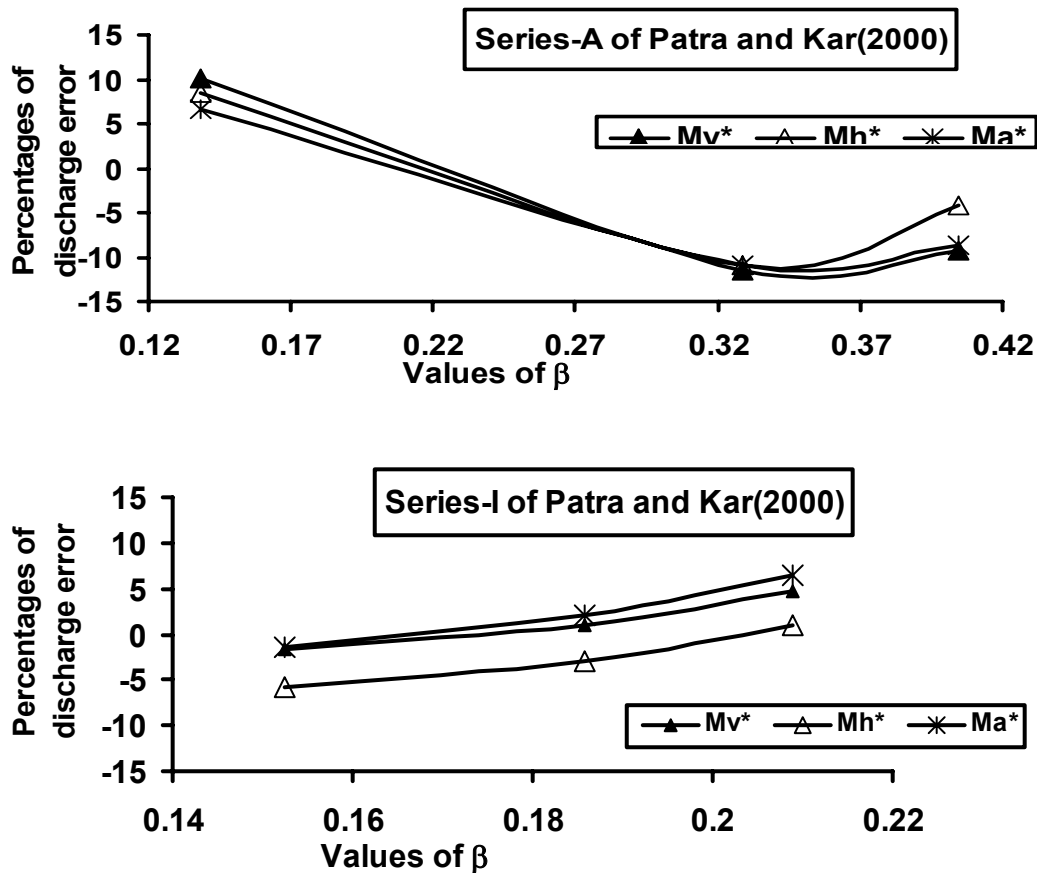
Fig.5.34 (a and b) Variation of percentage of error between calculated and observed discharges by the proposed methods with relative depths applied to the two channels of Patra and Kar

5.10.3 HIGHER SINUS CHANNEL DATA OF WILLET AND HARDWICK

The Type-II and Type-III meandering channels considered for the present experimental analysis are having sinuosity of 1.44 and 1.91 respectively. Therefore proposed models are applied to a higher sinus channels data (sinuosity = 2.06) reported by Willets and Hardwick (1993). The channel has the similar geometry with the present experimental channels. Like the present Type-III channel, the Willets and Hardwick (1993) meandering channel is trapezoidal having the top and bottom channel widths of 174 mm and 139 mm respectively. All the surfaces of the channels are smooth. The bank full depth of main channel is 50 mm. The top width of meandering compound section is 1200 mm. From the reported stage-discharge curves of Willets and Hardwick (1993), the discharges corresponding to the various stages for the over-bank flow are scaled from the figures by computer. The discharge data are applied to the present analysis and the error between calculated and observed discharge for the three methods are plotted as curves M_v*, M_h* and M_a* respectively in Fig.5.35. It can be seen from the figure that the proposed methods gives better results to this test channels. The standard errors of estimate between the observed and calculated percentages of discharge for the three proposed methods are found to be 7.3, 7.7, and 7.8 respectively.
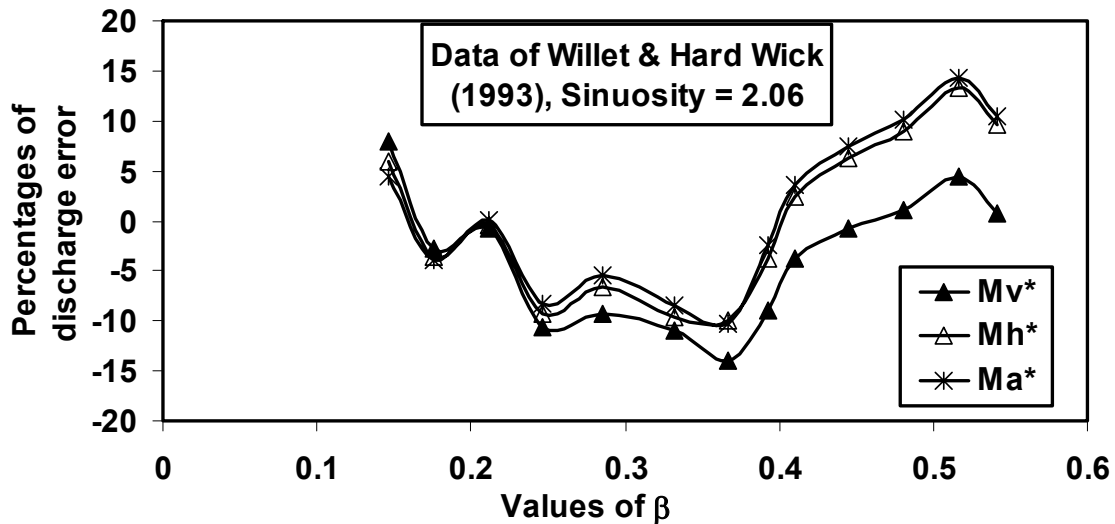
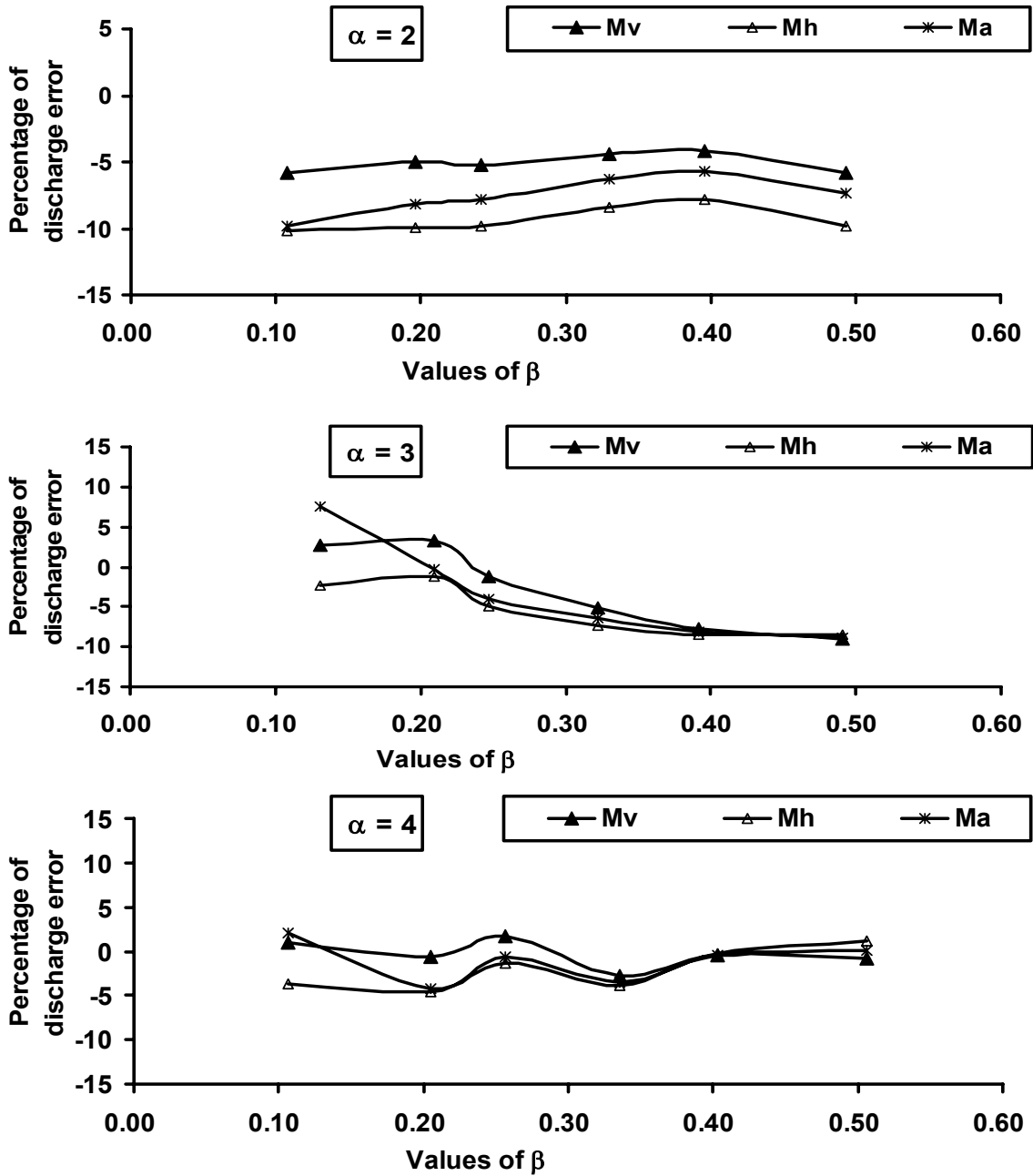**Fig.5.35 Variation of percentage of error between calculated and observed discharges by the proposed methods with relative depths applied to the higher sinus data of Willet and Hardwick**

5.10.3 LARGE SCALE CHANNEL DATA OF (FCF)

The proposed methods of discharge estimations are also applied to the Series B channel data of Flood Channel Facility (FCF) observed at Wallingford UK. This channel has smooth surfaces and having flood plains at both sides of the meandering main channel. The FCF is a 50 m long and 10 m wide flume. The main channel is sinusoidal and has four meanders contained within a total length of 48 m giving rise to a meander wavelength of 12 m each. The main channel is 150 mm deep and trapezoidal in section with a top width of 1200 mm and a 45° bank slope. The main channel is 60 degree meander giving sinuosity =1.374 and the flood plain has a slope of 0.000996. Each floodplain has a maximum width of 6.855 m and a minimum width of 1.945 m.
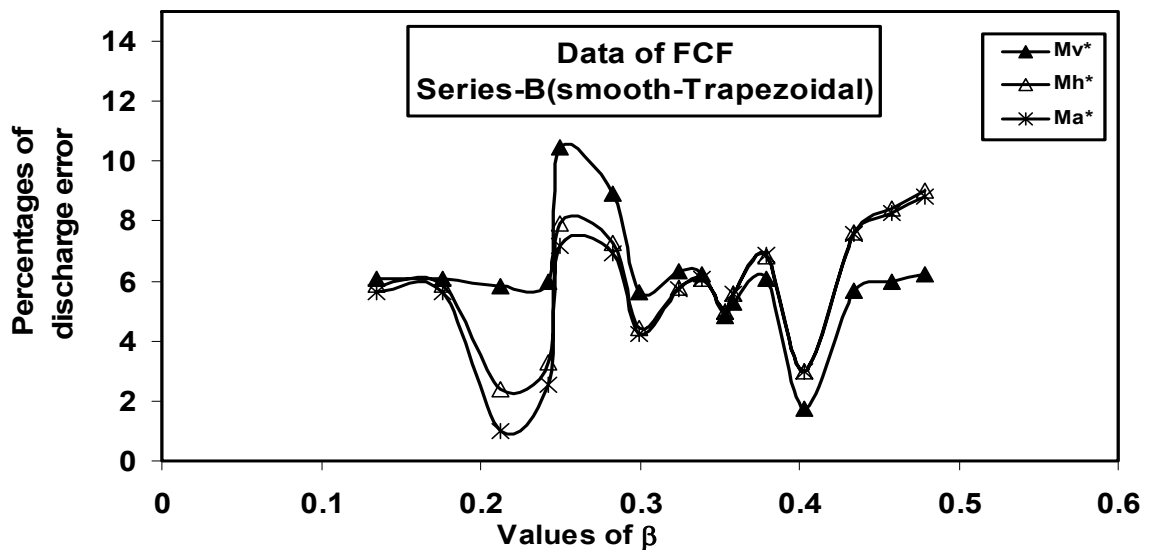
Fig.5.36 Variation of percentage of error between calculated and observed discharges by the proposed methods with relative depths for FCF data

The proposed discharge prediction approaches of Modified Vertical Interface Method, Modified Horizontal Interface Method, and the New Area Method are applied to this large scale channel data. The percentages of error for the three methods are obtained and plotted against the relative depth β as curves M_v^*, M_h^*, and M_a^* respectively in Fig. 5.36. The adequacy of the methods can be seen from the figures for the above applications. The standard error of estimate between observed and calculated percentages of discharge for the three proposed methods are found to be 6.3, 6.1, and 5.8 respectively.

*****

- 165 -

CONCLUSIONS

The present theoretical investigation supported by experimental observation is made for straight and meandering channels with and without floodplains having different geometries and sinuosity. On the basis of the investigations concerning flow, energy loss aspects, and boundary shear stress distribution in deep and rigid channels, the following conclusions are drawn.

- ❖ For the meandering channels, the contours of tangential velocity distribution indicate that the velocity patterns are skewed with curvature. Maximum skewing of the longitudinal velocity can be observed at the point of minimum radius of curvature (bend apex) and minimum skewing of the velocity occurs at the geometrical cross over. At the bend apex of meandering compound channels, the maximum velocity contours are found near the inner wall junction for low over bank depth and at the inner wall of flood plain for higher over bank depth. At low over bank depths of straight compound channels, the thread of maximum velocity contour lies in the upper main channel layer near the free surface and for higher over bank depths, the thread of maximum velocity occurs at two regions in the main channel.

- ❖ For simple meander channels, there is an increase in the reach averaged tangential velocity with the depth of flow. With the outflow of water into the floodplain, a sudden drop in the section mean velocity is recorded. The drop is found to be higher for channels with wider floodplains than the channels with the narrow floodplains. At low over bank depths, the section mean velocity in the floodplain is found to be less than the main channel. As the depth of flow in the floodplain increases, the section mean velocity in the floodplain also increases. At the highest depth of flow in the floodplain, the section mean velocity of the floodplain is found to be higher than the section mean velocity of the main channel. Again the mean velocity in the inner floodplain is observed to be higher than the outer floodplain at all depths at the bend apex.

- ❖ The boundary shear stress distribution in meandering channels is asymmetrical especially where there is predominant curvature effect. For higher depths over floodplain in the meandering compound channels, the maximum bed shears is

located in the floodplain region. For low over bank depths, the maximum bed shear lies close to near the inner bed of the main channel. Low magnitude of boundary shear is found at the outer wall when compared to the inner wall. The boundary shear at the main channel-floodplain junctions of the straight compound channel is generally found to be higher when compared to other points of the wetted perimeter. Though the general pattern of shear distribution is rather unaffected by the over bank flow depths, the width of floodplain and sinuosity are found to affect the nature of distribution to some extent.

❖ At bend-apex, the radial velocity is found to be mostly negative indicating that the velocity is in the inward direction. Higher velocity contours are seen near the inner bank and lower contours at the outer banks. At the geometrical cross-over region, the radial component are directed in-ward with lesser magnitude when compared to that at the bend-apex, indicating a phase lag between channel cross-over and flow cross over. The radial velocity components at the geometrical cross over region of Type-III meandering compound channel are found to be more than that at bend-apex showing almost 90^0 phase lag between channel geometry and flow geometry. The radial component of velocity for straight compound channel is observed to be the less when compared to that of meandering over bank flow for nearly the same depth ratio.

❖ The magnitudes of vertical velocity components of meandering channels are found to be the order of around 1.4% of longitudinal velocity for type-III channel and as high as 14% for type-II channel. The maximum upward vertical components are found at outer wall and maximum down-ward components are found at inner wall. With increase in flow depths, the values of vertical velocity are found to decrease. At the geometrical cross-over region, the vertical components of velocity are mostly in down-ward direction. With increase in flow depth, the magnitude of vertical velocity decreases. The magnitudes of the vertical velocity component in the floodplain regions of meandering compound channels are observed to be less when compared with the main channel area at the bend-apex as well as at the geometrical cross-over. The threads of higher upward vertical velocity are found near to the inner wall and down ward components are found near to the outer wall of the main channel.

❖ For straight compound channel the magnitude of vertical component of velocity is of the order of around 25% when compared to the transverse velocity at lower depths over floodplain and 20 % at higher depths over floodplain. At low over bank depths, higher upward vertical velocity are found at the junction between main channel and flood plain and the magnitude reduces with increase in depth over floodplain.

❖ The variation of Manning's n , Chezy C, and Darcy-Wieshbach friction factor f with the depth of flow ranging from in-bank to the over bank flow indicate the amount of energy loss in carrying the flow in the channels. The variation of the roughness coefficient is found to be dependant on the sinuosity, bed slope, and the geometry of the channel section.

❖ The diverse behaviors of Manning's n for main channel and floodplain sub-areas have been investigated for the experimental channels. Just after bank full depth, the floodplain values of n decreases with depth of flow, attains a minimum value and then increases gradually back to the composite value of the compound channel. Similarly, the n values of main channel increases with depth of flow just above the bank full stage, attains a maximum value, and then decreases gradually back to the composite value of the compound channel.

❖ The percentage of shear carried by flood plain region is found to be more when compared with the straight compound channel. The equations developed by previous investigators to estimate the percentage of total shear carried by the flood plain of the compound channels give results more than 100% for channels having high width ratio and sinuosity. Equations are developed to predict the percentage of total shear carried by the floodplain using the present experimental data of high width ratio (α = 16.08) and high sinuosity (S_r = 1.91) and is shown to be dependant on four dimensionless channel parameters. These equations are validated for other channel data. The proposed equation is shown to represent this adequately.

❖ For the purpose of discharge calculation, a compound channel is divided into zones by assuming a vertical, horizontal, diagonal or other assumed fluid boundary. Equations are presented to evaluate the amount of momentum transfer in terms of interaction lengths for any location of interface in a compound channel. Percentage of apparent shear at these interfaces can be

calculated using the proposed model. The percentage of apparent shear are dependant on the over bank depth, width ratio, and sinuosity of the channel.

❖ For any over-bank depth of Type-I and Type-II compound channels, the maximum positive momentum transfer takes place from main channel to floodplain if we consider the interface *oa* (Fig.5.15) lying in the floodplain region and the highest maximum negative momentum transfer from floodplain to main channel takes place if we consider the interface *oe* (Fig.5.15) lying in the lower main channel region.

❖ At lower over-bank the straight Type-I channel ($\alpha = 3.66$), the zero apparent shear is found near the assumed horizontal interfaces. For higher over-bank depths, the interface plane of zero apparent shear is observed near diagonal line, that is originating from the main channel and floodplain junctions and radial to the channel center. Similarly, for Type-II meandering channel ($\alpha = 4.81$) the interface plane of zero shear at low over bank depth, lies at around 19^0 with respect to the horizontal line and towards the lower main channel. For higher over bank depth, the interface of zero shear lies near to the vertical interface. Interface plane of zero shear for Type-III meandering channels could not be located at all the over-bank depths investigated. For this wide channel of ($\alpha = 16.08$) the apparent shear is found to be always positive, showing the momentum transfer always taking place from main channel to the floodplains across the interfaces and for all the ranges of depths investigated.

❖ It is found from the experimental channels that the apparent shear along the most commonly used interfaces such as vertical, diagonal, and horizontal is never zero or equal to the average shear of the main channel or flood plain wetted perimeter. The apparent shear has been found to vary with over-bank depths and from interface to interface.

❖ Discharge carried by main channel lower main channel of meandering and straight compound channel sections always differ from simple area ratios. The equations presented by previous investigators to estimate the zonal discharges are valid for the compound channels of low width ratio and low sinuosity. Equations to predict the zonal flow distribution in main channel, lower main channels, and floodplain sub-areas are presented. These equations are modeled using the compound channel data of high width ratio and sinuosity. The proposed equations are validated using data from other experimental channels.

- ❖ A number of modified interface plain methods of separation of compound channel into sub-areas for discharge calculation are proposed. An area method of separation of a compound channel by zero shear interfaces is also presented. These methods give the most satisfactory discharge results for all types of straight and meandering compound channel geometry investigated.

- ❖ Methods of discharge prediction for both meandering and straight compound channels proposed by the other investigators are applied to the present experimental channels. The results of the proposed (i) Modified vertical interface method, (ii) Modified horizontal interface method, and (iii) New area methods give the least error between observed and computed discharges when compared to other models.

- ❖ The proposed methods of discharge estimation have also been applied to the well published data of other investigators. Using the present methods, the error estimation between the observed and calculated discharge are also found to be less for the three types of straight compound channels of knight and Demetriou (1983), higher sinuosity channel of Willets and Hardwick (1993), meandering channel data of Patra and Kar (2000) and large scale data of FCF at Walling Ford, U.K.

SCOPE FOR FUTURE WORK

The present work leaves a wide scope for future investigators to explore many other aspects of compound channel analysis. Evaluation of flow, energy loss aspects, momentum transfer, and boundary shear stress distribution have been performed for the meandering and straight compound channels using limited data. The equations developed may be improved by incorporating more data from channels of different geometries and sinuosity. Further investigation is required to study the flow properties and develop models to predict the boundary shear, zonal flow distribution, and energy loss aspects of having different geometry in the main channel and floodplain. The channels here are rigid. Further investigation for the flow processes may also be carried out for mobile and of meandering compound channels of different geometry and sinuosity.

<center>*****</center>

REFERENCES

Ackers, P. (1992). "Hydraulic Design of Two Stage Channels." *Proceedings of the Institution of Civil Engineers, Water, Maritime and Energy,* December, Paper No. 9988, pp. 247-257.

Ackers, P. (1993a). "Stage-Discharge Functions for Two-Stage Channels." The Impact of New Research", *Journal of Institution of Water & Environmental Management,* Vol. 7, No. 1, February, pp. 52-61.

Ackers, P. (1993b). "Flow Formulae for Straight Two-Stage Channels", *Journal of Hydraulic Research,* IAHR, Vol. 31, No.4, pp. 509-531.

Bhattacharya, A. K. (1995). "Mathematical Model of Flow in Meandering Channel." *PhD Thesis* Presented to the IIT, Kharagpur, India.

Bousamar, D. Zech, Y. (1999). "Momentum Transfer for Practical Flow Computation in Compound Channels." *Journal of Hydraulics Division, ASCE,* Vol25, No.7, Paper No. 18224.

Chang, H.H. (1983). "Energy Expenditure in Curved Open Channels." *Journal of Hydraulics Engineering, ASCE,* Vol.109, No.7, pp. 1012-1022.

Chow,V.T.(1959)."Open-Channel Hydraulics."New York, McGraw- Hill Book Co.

Das,A.K. (1984).''A study of River Floodplain and Boundary Shear Stress Distribution in Meander Channels with One side Flood plains.'' *PhD Thesis* Presented to the IIT, Kharagpur, India.

Ervine, D.A., and Ellis, J. (1987). "Experimental and Computational Aspects of Overbank Flood-Plain Flow."*Trans. Royl. Society Edinburgh,* Series A, Vol. 78, pp. 315-325.

Ervine, D.A., Willetts, B.B., Sellin, R.H.J. and Lorena, M. (1993). "Factors Affecting Conveyance in Meandering Compound Flows." *Journal of Hydraulics Engineering, ASCE,* Vol., 119, No.12, pp. 383-1399.

Ervine D. A., Koopaei K.B., and Sellin R. H.. J. (2000)." Two-Dimensional Solution for Straight and Meandering Over-bank Flows." *Journal of Hydraulic Engineering*, ASCE, Vol. 126, No. 9, September, paper No.22144, 653-669.

Ghosh, S.N., and Jena, S.B.(1971). "Boundary Shear Distribution in Open Channel Compound." *Proceedings of the Institution of Civil Engineers, London,* Vol.49, August, pp. 417-430.

Ghosh, S.N., and Kar, S.K. (1975). "River Flood Plain Interaction and Distribution of Boundary Shear in a Meander Channel with Flood Plain." *Proc. of the Inst. of Civil Engineers, London,* Vol.59, Part 2, December, 1975.

Greenhill, R.K. & Sellin, R.H.J. (1993). "Development of a Simple Method to Predict Discharge in Compound Meandering Channels." *Proceedings of the Institution of Civil Engineers, Wat., Merit and Energy,*101, March, 37-44.

Guide for Selecting Roughness Coefficient *n* Values for Channels. (1963). *Soil Conservation Services*, U.S. Department of Agriculture, Washington,D.C.

Inglis, C.C.(1947). "Meander and Their Bering on River Training." *Proceedings of the Institution of Civil Engineers, Maritime and Waterways Engineering Div., Meeting, 1947.*

James, C. S., and Wark, J. B. (1992). "Conveyance Estimation for Meandering Channels." *Rep. SR 329*, HR Wallingford, Wallingford, U.K.Dec.

James C. S. (1994)."Evaluation of Methods for Predicting Bend Loss in Meandering Channels." *Journal of Hydraulic Engineering, ASCE,* Vol. 120, No. 2, February, 1994.

Johannesson,H.,and Parker,G. (1989)."Velocity Distribution in Meandering Rivers." *Journal of Hydraulic Engineering, ASCE,* Vol. 115, No. 8, pp. 1019-1039.

Kar, S.K. (1977). "A Study of Distribution of Boundary Shear in Meander Channel with and without Floodplain and River Floodplain Interaction." *PhD Thesis* Presented to the IIT, Kharagpur, India.

Kiely, G. (1990). "Overbank Flow in Meandering Channels the Important Mechanisms." *Proceedings of the Institution Conference on River Flood Hydraulics*, W. R. White, ed., Wiley, Chichester, U.K., pp. 207–217.

Knight, D.W. (1981). "Boundary Shear in Smooth and Rough Channels." *Journal of Hydraulic Engineering, ASCE,* Vol. 107, No.7, pp. 839-851.

Knight, D.W., and Abril, B.(1996). "Refined Calibration of a Depth-averaged Model for Turbulent Flow in a Compound Channel." *Proceedings of the Institution of Civil Engineers, Maritime and Energy Div., London,* Sept, Vol-118, No.11017.

Knight, D.W., and Demetriou, J.D. (1983). "Floodplain and Main Channel Flow Interaction." *Journal of Hydraulic Engineering, ASCE* Vol.109, No.8, pp. 1073-1092.

Knight, D.W., and Hamed, M.E.(1984), "Boundary Shear in Symmetrical Compound Channels." *Journal of Hydraulic Engineering, ASCE,* Vol.110, Paper 19217, pp.1412-1430.

Knight,D.W.,Yuan,Y.M.,and Fares,Y.R..(1992). "Boundary shear in meandering channels." *Proceedings of the Institution Symposium on Hydraulic research in nature and laboratory,* Wuhan, China (1992) Paper No.11017, Vol. 118, Sept., pp. 151-159.

Knight, D.W. (1989). "Hydraulics of Flood Channels In: Floods: Hydrological Sedimento-Logical and Geo-Morphological Implications." K. Beven (Ed.) Wiley, Chichester, 83 -105.

Knight, D.W., and Cao, S. (1994). "Boundary Shear in The Vicinity of River Banks." *Proceedings National Conference of Hydraulic Engineering., ASCE,* Bualo, USA, 1994.

Knight, D.W., and Shino, K. (1996). "River Channel and Floodplain Hydraulics." Floodplain Processes.,Edited by M.G.Anderson,Des E.Walling and Paul D., 1996.

Lambert, M.F., and Myers, W.R. (1998). "Estimating the Discharge Capacity in Straight Compound Channels." *Proceedings of the Institution of Civil Engineers, Water, Maritime and Energy,No.*130, pp. 84-94.

Leliavsky, S.(1955). "An Introduction to Fluvial Hydraulics."Constable, London.

Lotter, G.K.(1933). "Consideration in Hydraulic Design on Channels with Different Roughness on Walls." *Trans. All Union Scientific Research, Institution Hydraulic Research ,* Leningrad, pp. 238-241.

Mc Keogh, E.J. and Kiley, G.K. (1989). "Experimental Study of Mechanism of Flood Flow in Meandering Channels.*" Proceeding of 23rd IAHR congress, Ottawa, Canada,* Vol-B, pp.491-498.

Maria, A.A, and DaSilva A. F.(1999). "Friction Factor of Meandering Flows." *Journal of Hydraulic Engineerin, ASCE,* Vol.125, No.7, pp. 779-783.

Morvan ,H., Pender G. ,Wright N. G. , and Ervine D. A.(2003). "Three-Dimensional Hydrodynamics of Meandering Compound Channels." *journal of hydrologic engineering © asce / march/april 2003 / 99*

Myers,W.R.C.,andElsawy (1975). "Boundary Shear in Channel with Floodplain." *Journal of Hydraulic Engineering, ASCE*, Vol.101, HY7, pp. 933-946.

Myers, W.R.C. (1987). "Velocity and Discharge in Compound Channels." *Journal of Hydraulic Engineering, ASCE*, Vol.113, No.6, pp. 753-766.

Myer, W.R.C., and Lyness, J.F., (1997). "Discharge Ratios in Smooth and Rough Compound Channels," *Journal of Hydraulic Engineering, ASCE*, Vol.123, No.3, pp.182-188.

Myer, W.R.C., and Lyness, J.F., and Cassells, J., (2001). "Influence of Boundary Roughness on Velocity and Discharge in Compound River Channels," *Journal of Hydraulic Engineering, ASCE*, Vol.39, No.3.

Ozbek , T .,and Cebe ,K.(2003). "Comparison of Methods for Predicting Discharge in Straight Compound Channels Using the Apparent Shear Stress Concepts." *Tr. Journal of Engineering and Environmental Science,* Tubitak, pp. 101-109

Pang, B. (1998). "River Flood Flow and its Energy Loss." *Journal of Hydraulic Engineering, ASCE*, Vol. 124, No.2, pp. 228-231.

Patra,K.C (1999). "Flow interaction of Meandering River with Flood plains." *PhD Thesis* Presented to the IIT, Kharagpur, India.

Patra,K.C.,Kar,S.K.(2000). "Flow interaction of Meandering River with Flood plains." *Journal of Hydraulic Engineering, ASCE*, Vol., 126, No.8, pp. 593-603.

Patra, K.C., and Kar, S.K., Bhattacharya.A.K. (2004). "Flow and Velocity Distribution in Meandering Compound Channels." *Journal of Hydraulic Engineering*, *ASCE*, Vol. 130, No. 5. 398-411.

Prinnos, P., and Townsend, R. D.(1984). "Comparison of Methods of Predicting Discharge in Compound Open Channels." *Advances in Water Res*. Vol.7 (12), pp. 180–187.

Proust. S; Rivière. N., Bousmar. D; Paquier. A, Zech., Y and Morel. R. (2006). "Flow in Compound Channel with Abrupt Floodplain Contraction." *Journal of Hydraulic Engineering*, *ASCE*, Vol. 132, No. 9, September 1.

Rajaratnam, N., and Ahmadi, R.M. (1979). "Interaction between Main Channel and Flood Plain Flows." *Journal of Hydraulic Division*, *ASCE,* Vol..105, No. HY5, pp. 573-588.

Rhodes, D.G., and Knight, D.W.(1994). "Distribution of Shear Force on the Boundary of a Smooth Rectangular Duct." *Journal of Hydraulics Engineering, ASCE* , Vol.120, No.7, pp. 787-807.

Rozovskii, I.L.(1957). "Flow of Water in Bends of Open Channels." *Academy of Science of Ukranian SSR, Kiev,1957,* Translated by Prushansky, Y., The Israel Program for Scientific Translation, 1961.

Sellin, R.H.J.(1964). "A Laboratory Investigation into the Interaction between Flow in the Channel of a River and that of its Flood Plain." *La. Houille Blanche*, No.7, pp. 793-801.

Sellin, R.H.J., Ervine, D.A., and Willetts B.B.(1993). "Behavior of Meandering Two stage Channels." *Proceedings of the Institution of Civil Engineers, Water, Maritime and Energy,* June, Vol.101, paper No.10106, pp. 99-111.

Shiono, K., Al-Romaih, J.S., and Knight, D.W.(1999). "Stage-Discharge Assessment in Compound Meandering Channels." *Journal of Hydraulic Engineering, ASCE,* Vol.125, No.1, pp. 66-77.

Shiono, K., Knight, D.W.(1988). "Refined Modelling and Turbulance Measurements." *Proceedings of 3rd International Symposium, IAHR, Tokyo, Japan*, 26-28, July-1988.

Shiono, K., Lin, B.(1992). "Three Dimensional Numerical Model for Two Stage Open Channel Flow." *Hydro.Comp.92, Budapest, Hungary, May, 25-29,* pp. 123-130.

Shiono, K., Muto, Y., Knight, D.W. & Hyde, A.F.L.(1999). "Energy Losses due to Secondary Flow and Turbulence in Meandering Channels with Overbank Flow." *Journal of Hydraulic Research*, IAHR, Vol. 37, No. 5, pp. 641-664.

Stephenson, D., and Kolovopoulos, P. (1990). "Effects of Momentum Transfer in Compound Channels." *Journal of Hydraulic Engineering, ASCE*, Vol.116, No.HY12, Paper No.25343, pp. 1512-1522.

Toebes, G.H., and Sooky, A.A.(1967). "Hydraulics of Meandering Rivers with Floodplains." *Journal of the waterways and Harbor Division, Proceedings of ASCE*, Vol.93, No.WW2, May, pp. 213-236.

Tominaga,A., Knight., D.W. (2004). *"Numerical Evaluation of Secondary Flow Effects on Lateral Momentum Transfer in Overbank Flows." River Flow-2004, Taylor and Francies Group, London*

Wark, J.B., and James, C.S.(1994). "An Application of New Procedure for Estimating Discharge in Meandering Overbank Flows to Field Data." *2nd Intl. Conf. on River Flood Hydraulics,* 22-25, March, Published by John Wiley & Sons Ltd, pp. 405-414.

Willetts, B.B., and Hardwick, R.I.(1993). "Stage Dependency for Over Bank Flow in Meandering Channels." *Proceedings of the Institution of Civil Engineers, Water, Maritime and Energy,* March, Vol.101, paper No.10049, 45-54.

Wormleaton, P.R., Allen, J.,and Hadjipanos, P.(1982). "Discharge Assessment in Compound Channel Flow." *Journal of Hydraulic Engineering, ASCE*, Vol.108, No.HY9, pp. 975-994.

Wormleaton, and Hadjipanos,P.(1985). "Flow Distribution in Compound Channels." *Journal of Hydraulic Engineering, ASCE*, Vol.111, No.7, pp. 1099-1104.

Yen, C.L., and Overton, D.E. (1973). "Shape Effects on Resistance in Floodplain Channels." *Journal of Hydraulic Division, ASCE,* Vol.99, No.1, pp. 219-238.

Yen, B.C.,and Yen, C.L. (1983)."Flood FLow Over Meandering Channels." *River Meandering(ed. C. M. Elliott),* 554-561.

Younis, B.A. (1996). "Turbulance Modelling for Open Channel Flows in Flood plain Processes." [Eds M.G..Anderson, D.E.Walling and P.D.Bates]., Chapter 9, Journals of Wiley, pp. 581-608.

Zarrati, A.R., Tamai, N., and Jin, Y.C.(2005). "Mathematical Modeling of Meandering Channels with a Generalized Depth Averaged Model." *Journal of Hydraulic Engineering, ASCE,* Vol.131, No.6, pp. 467-475.

Zheleznyakov, G.V.(1965). "Interaction of Channel and Floodplain Streams." *Proc. 14th Congress of IAHR,* 5, Paris, France, pp. 144-148.

*****

Publications from the Work

A: Published

1. *"Energy loss in two stage meandering and straight compound channels"* Presented and Published in the national symposium of **Hydro-2005,** December.2005, at Tumkur, Karnataka, India

2. *"Selection of Interface Plane in the Assessment of Discharge in Two Stage Meandering and Straight Compound Channels"* Published in the proceedings of International Conference on Fluvial Hydraulics (***IAHR***) *September 6-8, 2006*-(**River Flow-2006),** Lisbon,

3. *"Boundary shear stress distribution in compound channel flow"* The Paper is Presented and Published in the proceedings of **Hydro-2006,** December.2006, at Pune, India

4. *"Energy Loss and Discharge Estimation in Two Stage Meandering and Straight Compound Channel".* Presented and published in the proceedings of International *Perspective on Environmental & Water Resources*–Dec. 2006,at New Delhi, India held by **EWRI** of American Society of Civil Engineers (*ASCE*) and **IIT Kanpur**.

5. *"River and Flood plain Hydraulics"* Published in Annual session of Institution of Engineers India (IEI), India- Jan.2007, Orissa state center, (<u>**Obtained gold medal for the best paper**</u>)

6. *"Roughness characteristics in two stage meandering and straight compound channels" "* Published in the Conference proceeding on **CEAC-2007**, 9-11, march,2007, M.M. Engineering College Mullana, Ambala

7. *"Boundary shear stress distribution in meandering compound channel flow"* Paper is reviewed and published in the **5th Australian Stream Management** Conference to be held in Albury, NSW, Ausralia on 22-25 May 2007.

B: Accepted for Publication

8. *"Boundary shear stress distribution in compound channel flow"* Accepted for publication in the Journal of Indian Society for Hydraulics (***ISH***), 2007.

9. *"Discharge Assessment in Two Stage Straight Compound Channels"* Review is complete and sent for publication in the Journal of Hydraulic Engineering, Journal of International Association of Hydraulic Research (***IAHR***), 2007.

10. *"One dimensional solution for Predicting Discharge in Two Stage Meandering Compound Channels"* Review is complete and sent for publication in the Journal of Hydraulic Engineering, American Society of Civil Engineers (***ASCE***), 2007

11. *"Interaction of flow between meandering and straight channel within flood plains"* The final Paper is reviewed and was accepted for publication in the International Conference on **Water Resources Management**, May 21-23,-2007, KOS,Greece.

12. *"Flow distribution in meandering compound channel flow"*. The Paper is accepted for publication in the proceedings of International Conference on Water, Environment, and Energy & Society 18-21 December, 2007, at New Delhi.

C: Communicated

13. *"Momentum transfer between river channel and flood plains"* The Paper is communicated for publication in the journal of International Association of Hydraulic Research (**IAHR**).

14. *"Boundary shear in very wide compound channels"* The Paper is communicated for publication in the Journal of Hydraulic Engineering, American Society of Civil Engineers (**ASCE**).

15. *"Role of Interface Plane in the Assessment of Discharge in Compound Channel"*. The Paper is communicated for publication in the proceedings of International Conference Hydro-Vision, July 14-18, 2008, California,USA.

16. *"A practical method to predict flow for a compound river section"* The Paper is communicated to the national conference **Hydro-2006,** December.2007, at VNIT, Surat, India

*****

Brief Bio-Data of the Author

(i)   **Name** :   KISHANJIT KUMAR KHATUA

(ii)   **Date of Birth:**   April 04, 1969

(iii)   **Educational Qualification :**

Graduated in Civil Engineering from the University College of Engineering, Burla (Autonomous Institute) in 1990

Post graduated (with 1st position and Honors) in *Hydraulics and Irrigation Engineering* from the University College of Engineering, Burla (Autonomous Institute) in 1996

(iv)   **Present address   :**   Senior Lecturer,

Department of Civil Engineering

National Institute of Technology,

Rourkela, (Orissa), INDIA

Ph.91-661-246-2307(o), 2307®

Email: kkkhatua@nitrkl.ac.in

kkkhatua@yahoo.com

(v)   **Teaching Experience:**   16 years

(VI)   **Research Experience**:   10 years in Water Resources and Hydraulic Engineering.

*****